UAB
Universitat Autònoma de Barcelona

DNA repair in cancer therapeutics: developing a specific inhibitor for tumors and targeted therapies to treat solid tumors in rare diseases

Debora Cavero Moreno

ADVERTIMENT. L'accés als continguts d'aquesta tesi doctoral i la seva utilització ha de respectar els drets de la persona autora. Pot ser utilitzada per a consulta o estudi personal, així com en activitats o materials d'investigació i docència en els termes establerts a l'art. 32 del Text Refós de la Llei de Propietat Intel·lectual (RDL 1/1996). Per altres utilitzacions es requereix l'autorització prèvia i expressa de la persona autora. En qualsevol cas, en la utilització dels seus continguts caldrà indicar de forma clara el nom i cognoms de la persona autora i el títol de la tesi doctoral. No s'autoritza la seva reproducció o altres formes d'explotació efectuades amb finalitats de lucre ni la seva comunicació pública des d'un lloc aliè al servei TDX. Tampoc s'autoritza la presentació del seu contingut en una finestra o marc aliè a TDX (framing). Aquesta reserva de drets afecta tant als continguts de la tesi com als seus resums i índexs.

ADVERTENCIA. El acceso a los contenidos de esta tesis doctoral y su utilización debe respetar los derechos de la persona autora. Puede ser utilizada para consulta o estudio personal, así como en actividades o materiales de investigación y docencia en los términos establecidos en el art. 32 del Texto Refundido de la Ley de Propiedad Intelectual (RDL 1/1996). Para otros usos se requiere la autorización previa y expresa de la persona autora. En cualquier caso, en la utilización de sus contenidos se deberá indicar de forma clara el nombre y apellidos de la persona autora y el título de la tesis doctoral. No se autoriza su reproducción u otras formas de explotación efectuadas con fines lucrativos ni su comunicación pública desde un sitio ajeno al servicio TDR. Tampoco se autoriza la presentación de su contenido en una ventana o marco ajeno a TDR (framing). Esta reserva de derechos afecta tanto al contenido de la tesis como a sus resúmenes e índices.

WARNING. The access to the contents of this doctoral thesis and its use must respect the rights of the author. It can be used for reference or private study, as well as research and learning activities or materials in the terms established by the 32nd article of the Spanish Consolidated Copyright Act (RDL 1/1996). Express and previous authorization of the author is required for any other uses. In any case, when using its content, full name of the author and title of the thesis must be clearly indicated. Reproduction or other forms of for profit use or public communication from outside TDX service is not allowed. Presentation of its content in a window or frame external to TDX (framing) is not authorized either. These rights affect both the content of the thesis and its abstracts and indexes.

Universitat Autònoma de Barcelona

Institut de Recerca de l'Hospital de la Santa Creu i Sant Pau
Unitat Mixta de Recerca en Medicina Genòmica UAB - IR Sant Pau
Genome Instability and DNA Repair Syndromes group

DNA repair in cancer therapeutics: developing a specific inhibitor for tumors and targeted therapies to treat solid tumors in rare diseases

PhD thesis
Doctoral program in Genetics

Debora Cavero Moreno

Directors

Dr. Jordi Surrallés Calonge **Dr. Jordi Minguillón Pedreño**

Tutor

Dr. Jordi Surrallés Calonge

PhD program coordinator: Francisco José Rodriguez-Trelles Astruga

Barcelona, 2024

Universitat Autònoma de Barcelona

Institut de Recerca de l'Hospital de la Santa Creu i Sant Pau
Unitat Mixta de Recerca en Medicina Genòmica UAB - IR Sant Pau
Genome Instability and DNA Repair Syndromes group

DNA repair in cancer therapeutics: developing a specific inhibitor for tumors and targeted therapies to treat solid tumors in rare diseases

PhD thesis
Doctoral program in Genetics

Debora Cavero Moreno

Thesis director	Thesis director	Thesis tutor	Author
Dr. Jordi Surrallés Calonge	Dr. Jordi Minguillón Pedreño	Dr. Jordi Surrallés Calonge	Debora Cavero Moreno

Para eso sirven los sueños, ¿no?

Para enseñarnos hasta donde podemos llegar.

Laura Gallego-García

Table of contents

Abbreviations **5**
Abstract **15**
1. Introduction **23**
1.1. DNA damage, replication stress and cancer 25
1.2. DNA repair mechanisms 26
1.3. Synthetic lethality 30
1.3.1. PARP inhibitors 31
1.4. DNA damage response to target cancer 34
1.4.1. DNA damage sensor proteins 35
1.4.2. DNA damage signaling proteins 36
1.4.3. DNA damage effector proteins 38
1.5. Protein-protein interactions 39
1.5.1. Small molecules as modulators in PPIs for cancer treatment 41
1.6. Fanconi anemia /BRCA pathway 43
1.6.1. The role of FA pathway in replicative stress 45
1.7. [redacted] 47
1.7.1. [redacted] 47
1.7.2. [redacted] 48
1.8. Fanconi anemia disease 55
1.8.1. Head and neck squamous cell carcinomas 59
1.9. Target therapies in HNSCC 61
1.9.1. ERBB receptor family inhibition 61
1.9.2. Alternative therapies 67
1.9.3. HNSCC treatment in FA patients 69
2. Objectives **71**
3. Materials and methods **75**
3.1. [redacted] developing inhibitors of DNA damage repair for cancer therapy 77
3.1.1. Cell lines 77
3.1.2. Virtual screening of First-In-Class specific inhibitors [redacted] 77
3.1.3. Surface Plasmon Resonance (SPR) assay 79
3.1.4. Western blot (WB) 82
3.1.5. [redacted] 84
3.1.6. [redacted] 84
3.1.7. Immunofluorescence analysis [redacted] 84
3.1.8. Clonogenic assay 85
3.1.9. [redacted] 85

3.2. Obtaining and characterization of afatinib-resistant HNSCC cell lines 87
3.2.1. Cell lines 87
3.2.2. Cell line correction 87
3.2.3. DEB survival assay 88
3.2.4. Afatinib survival assay 88
3.2.5. Gefitinib survival assay 88
3.2.6. Cetuximab survival assay 88
3.2.7. Human Phospho-RTK array dot blot 89
3.2.8. Cell membrane marker's expression 89
3.2.9. Multiplex Ligation-dependent Probe Amplification (MLPA) assay 90
3.2.10. RNA sequencing 90
4. Results 93
4.1. [redacted] developing inhibitors of DNA damage repair for cancer therapy 95
4.1.1. Virtual screening of First-In-Class specific inhibitors [redacted] and virtual screening (Fx and F2.x candidates) 95
4.1.2. Fx and F2.x candidates' validation 98
4.1.3. Virtual structural optimization of the candidates by Structure Activity Relationships (SAR) and medicinal chemistry (F3.x candidates) 99
4.1.4. F3.x candidates' validation 101
4.1.5. Second virtual structural optimization of the candidates by medicinal chemistry (F4.x candidates) 105
4.1.6. F4.x candidates' validation 106
4.1.7. Third virtual structural optimization of the candidates by molecular docking and medicinal chemistry (F5.x candidates) 113
4.1.8. F5.x candidates' validation 114
4.1.9. Forth virtual structural optimization of the candidates by virtual molecular docking and medicinal chemistry (F6.x candidates) 119
4.1.10. F6.x candidates' validation 120
4.1.11. De novo [redacted] inhibitors design and virtual screening by molecular docking and medicinal chemistry (2Fx candidates) 123
4.1.12. 2Fx candidates' validation 126
4.2. Obtaining and characterization of AR HNSCC cell lines 135
4.2.1. Generation of AR HNSCC cell lines 135
4.2.2. Gefitinib cytotoxicity in AR HNSCC cell lines 139
4.2.3. Cetuximab cytotoxicity in AR HNSCC cell lines 140
4.2.4. Tyrosine kinase receptors (RTKs) expression in AR HNSCC cell lines 141
4.2.5. ERBB family expression in AR FA HNSCC cell lines 146
4.2.6. CD44v6 expression in AR FA HNSCC cell lines 146
4.2.7. NKG2D ligands expression in AR FA HNSCC cell lines 147
4.2.8. Number of copies of ERBB receptors in AR HNSCC cell lines 149
4.2.9. RNA expression in AR HNSCC cell lines 150

5. Discussion 157
5.1. [redacted] developing inhibitors of DNA damage repair for cancer therapy 159
5.2. Obtaining and characterization of AR HNSCC cell lines 165
6. Conclusions 171
7. References 175
8. Supplementary data 197
8.1. Appendix 1 199
8.2. Appendix 2 229
Acknoledgments 259

Abbreviations

Abbreviations

Abbreviations	Meaning
ADP	Adenosine diphosphate
AG20	FANCA+FANCG+FAAP20
AKT	Protein kinase B
Alt-NHEJ	Alternative NHEJ
APC	Adenomatous polyposis coli protein
APE1	Apurinic/apyrimidinic endonuclease 1
APS	Ammonium persulphate
AR	Afatinib resistant
ATM	Ataxia-telangiectasia mutated
ATMi	ATM inhibitor
ATP	Adenosine triphosphate
ATR	Ataxia telangiectasia and Rad3 related
ATRi	ATR inhibitor
BER	Base excision repair
BL100	FANCB-FANCL-FAAP100 complex
BM	Bone marrow
BMF	Bone marrow failure
BMP4	Bone morphogenetic protein 4
BRCA1/2	Breast cancer gene 1/2
CAR	Chimeric antigen receptor
CDA	Confidentiality agreement (CDA/NDA)
CEF	FANC-FANCE-FANCF complex
CHI3L1	Chitinase 3-like 1 protein, also YKL-40
CIEMAT	Centro de Investigaciones Energéticas, Medioambientales y Tecnológicas

CNA	Copy number alteration
CNAG	Centro Nacional de Análisis Genómico
CPMs	Counts per million
CSC	Cancer stem cell
CSIC	Consejo Superior de Investigaciones Científicas
DAPI	4',6-diamidino-2-phenylindole
DDR	DNA damage response
DEB	Diepoxibutane/ 1,3-butadiene diepoxide
DMSO	Dimethyl sulfoxide
DNA	Deoxyribonucleic acid
DSB	Double strand break
DSBR	Double-strand break repair
dsDNA	Double strand DNA
E2	Ubiquitin-conjugase enzyme
E3	Ubiquitin-ligase enzyme
ECD	Extracellular domain
EGF	Epidermal growth factor
EGFR	Epidermal growth factor receptor
EMA	European Medicines Agency
ENCODE	Encyclopedia of DNA Elements
ERBB1-4	HER1 (EGFR)- HER4
F2.x	Second virtual screening
F3.x	First optimization screening
F4.x	Second optimization screening
F5.x	Third optimization screening
F6.x	Fourth optimization screening

FA	Fanconi anemia
FA/BRCA pathway	Fanconi anemia/BRCA pathway
FAAP10	Fanconi anemia-associated protein 10, also MHF2/CENPX/SRA13
FAAP16	Fanconi anemia-associated protein 16, also MHF1/CENPS/APITD1
FAAP20	Fanconi anemia-associated protein 20
FAAP24	Fanconi anemia-associated protein 24
FAN1	Fanconi anemia complementation group 1 protein
FANCA	Fanconi anemia group A protein
FANCB	Fanconi anemia group B protein
FANCC	Fanconi anemia group C protein
FANCD1	Fanconi anemia group D1 protein, also BRCA2
FANCD2	Fanconi anemia group D2 protein
FANCE	Fanconi anemia group E protein
FANCF	Fanconi anemia group F protein
FANCG	Fanconi anemia group G protein, also XRCC9
FANCI	Fanconi anemia group I protein
FANCJ	Fanconi anemia group J protein, also BRIP/BACH1
FANCL	Fanconi anemia group L protein
FANCM	Fanconi anemia group M protein
FANCN	Fanconi anemia group N protein, also PALB2
FANCO	Fanconi anemia group O protein, also RAD51C
FANCP	Fanconi anemia group P protein, also SLX4
FANCQ	Fanconi anemia group Q protein, also ERCC4/XPF
FANCR	Fanconi anemia group R protein, also RAD51
FANCS	Fanconi anemia group S protein, also BRCA1
FANCT	Fanconi anemia group T protein, also UBE2T

FANCU	Fanconi anemia group U protein, also XRCC2
FANCV	Fanconi anemia group V protein, also MAD2L2/REV7
FANCW	Fanconi anemia group W protein, also RFWD3
FANCY	Fanconi anemia group Y protein, also FAAP100
FARF	Fanconi Anemia Research Foundation, now Fanconi Cancer Foundation
FASTQ	A text format for storing DNA sequencing data
FBDD	Fragment-based drug design
FC	Fold change
FDA	Food and Drug Administration
FQ Prop.	Fit quality properties
FragPELE	Fragment-based Protein-Ligand Explorer (software)
Fx	First virtual screening
GVHD	Graft-versus-host disease
h	hours
HER1-4	Human epidermal growth factor receptor 1-4
hFIB	Human fibroblast
HNSCC	Head and neck squamous cell carcinoma
HPV	Human papillomavirus
HR	Homologous recombination
HRP	Horseradish peroxidase
HSC	Hematopoietic stem cell
HSCT	Hematopoietic stem cell transplantation
HSP60/90	Heat shock protein 60/90
HSPC	Hematopoietic stem and progenitor cell
HTS	High-throughput screening
HTVS	High-throughput virtual screening

HU	Hydroxyurea
ICIs	Immune checkpoint inhibitors
ICL	Interstrand crosslink
ID2	FANCI-FANCD2 complex
IF	Immunofluorescence
K_A	Association rate constant
K_D	Dissociation constant
K_{OFF}	Dissociation rate constant
K_{ON}	Association rate constant
M	Molar
mAbs	Monoclonal antibodies
MCS	Medicinal Chemistry & Syntesis (CSIC company)
MICA/B	MHC class I polypeptide–related sequence A/B
min	Minutes
miRNA	MicroRNA (small non-coding RNA)
mL	Mililiter
MLPA	Multiplex ligation-dependent probe amplification
MMC	Mitomycin C
MMR	Mismatch repair
MN	Micronucleous
MRN	MRE11-RAD50-NBS1 complex
mRNA	Messenger RNA
NBD	Nostrum Biodiscovery (in silico drug discovery CRO)
NER	Nucleotide excision repair
NHEJ	Non-homologous end joining
NHS	National Health Service

NK	Natural killer
NKG2D	Killer cell lectin-like receptor subfamily K member (KLRK1)
NKG2D-Ls	NKG2D ligands
NSCLC	Non-small cell lung cancer
OD	Optical density
OSCC	Oral squamous cell carcinoma
PAINS	Pan-assay interference compounds
PARP	Poly(ADP-ribose) polymerase
PARPi	PARP inhibitor
PBA/ PB-Azide	Phenylbenzoyl azide
PBS	Phosphate-buffered saline
PFS	Progression-free survival
PCNA	Proliferating cell nuclear antigen
PCR	Polymerase chain reaction
PD-1	Programmed cell death protein 1
PD-L1	Programmed cell death ligand 1
PDB	Protein Data Bank
Phospho-RTK	Phosphorylated receptor tyrosine kinase
PI3K	Phosphatidylinositol-3-kinase
PIK3CA	Phosphatidylinositol-4,5-bisphosphate 3-kinase catalytic subunit alpha
PKB/ PKC	Protein kinase B / Protein kinase C
Pol	Polymerase
PPI	Protein-protein interaction
Ref.	Reference
RNA	Ribonucleic acid
ROS	Reactive oxygen species

RPA	Replication protein A
RS	Replication stress
RSEM	RNA-Seq by Expectation Maximization (software)
RT	Reverse transcription
RTA	Real time analysis
RTK	Tyrosine kinase receptors
RU	Response unit
SALSA	Sequenced Amplification Ligation and Sequencing Assay
SAR	Structure-activity relationship
SBDD	Structure-based drug design
SBVS	Shape-based virtual screening
SCC	Squamous cell carcinoma
SCF	Skp1-Cullin-F-box complex
SCFR	Stem cell factor receptor
SD	Standard deviation
SDS	Sodium dodecyl sulfate (detergent)
SEM	Standard error of the mean
SFI	Specific fluorescence intensity
siRNAs	Small interfering RNAs
SL	Synthetic lethality
SNVs	Single nucleotide variants
SP	Standard precision (virtual screening)
SPR	Surface plasmon resonance
SRB	Sulforhodamine B
SSA	Single-strand annealing
SSB	Single strand break

SSBR	Single-strand break repair
ssDNA	Single strand DNA
STAT	Signal transducer and activator of transcription protein
SVI	St Vincent's Institute
T-cell	Lymphocyte T
TALEN	Transcription activator-like effector nuclease
TBST	Tris-buffered saline with Tween 20
TCA	Trichloroacetic acid
TCGLS	TCG Lifesciences (synthesis company)
TCR	T cell receptor
TKI	Tyrosine kinase inhibitor
TSCC	Tongue squamous cell carcinoma
UAB	Universitat Autònoma de Barcelona
Ub	Ubiquitination
UV	Ultraviolet
vs	Versus
WB	Western blot
WEE1	WEE1 G2 checkpoint kinase
WEE1i	WEE1 inhibitor
WHO	World Health Organization
WT	Wild type
YFP	Yellow fluorescent protein
γ-H2AX	Phosphorilated histone 2AX
µL	Microlitres
µM	Micromolar

Abstract

Abstract

[redacted] DNA repair is taking relevance as targeted therapy against cancer, offering an alternative to the conventional therapies. In this field, synthetic lethality, term used to refer the genetic relationship stablished between two genes in which the loss of function of both results in cell death, but the loss of one of either of the two genes does not, has been taking into consideration for some cancer therapeutic approaches. Such is the case of the PARP inhibitors, used in tumors with BRCA1/2 mutations, and approved to treat breast, ovarian, prostate and pancreas cancer.

This thesis is a continuation of a drug discovery project aimed in finding [redacted] inhibitor [redacted] that could be used for cancer treatment in presence of mutations that have synthetic lethal interactions [redacted] Our specific target [redacted]. At the beginning of the project, the 3D structure of both proteins was studied, as well as the amino-acids that compose [redacted] After the target characterization, a first virtual screening took place, starting from a compound library with 136 million of molecules (3D ZINC15 database). The library was filtered by multi-step docking and 39 out of the 57 potential candidates selected were bought and tested in U2OS and human fibroblasts cells. The interaction between the candidates and the target was measured by surface plasmon resonance (Camps-Fajol's thesis, 2022).

This first virtual screening (Fx) was followed by a second virtual screening (F2x) consisting of a fragment-based strategy, in which 24 candidates were validated (Camps-Fajol's thesis, 2022). After these validations, F27 and F2.14, the best candidates of the Fx and F2.x rounds were optimized in the F3.x round. Four optimization rounds (F3.x-F6.x) have been done in total, what comprises more than 50 new-synthetized candidates validated in both cell lines (*in vitro* validation), and with their interaction with the target (biochemical validation). Some candidates such as F3.6, F3.10, F3.14, F4.3, and F5.6 have shown good results [redacted] inhibition and in target affinity, but with toxicity at 6-8h and not good solubility. The last optimization round until now (F6.x) has demonstrated an improvement in comparison with the last rounds: hit F6.1 has good affinity for the target, good [redacted] inhibition, and non-toxic effects. In addition, a new virtual screening (2Fx) has been done in parallel with the last optimization round, starting from a compound library with 13 million of molecules (ZINC database filtered by compounds' molecular weight). From the 39 candidates selected in that round, 26 new candidates were bought and validated. In this case, 2F17 has also showed good results without toxicity in the treated cells. Although there are many steps to be done, the perspectives in view of our last results are promising for the future of our drug discovery project.

On the other hand, the lack of the FA/BRCA pathway is the origin of a rare genetic disorder characterized, mainly, by bone marrow failure, physical abnormalities and increased risk of cancer. The development of head and neck squamous cell carcinoma (HNSCC) in these patients is 500-800 fold higher than in general population, with the additional drawback that FA patients cannot deal with chemo- or radiotherapy, due to the lack of interstrand crosslinks repair pathway. On account of their intolerance to radio/chemotherapy, surgical resection remains the only approved therapy for these patients. However, a high content screening and preclinical validation published in 2020 by our team, identified the panERBB inhibitor afatinib as a promising non-genotoxic, anti-tumor agent for FA patients (Montanuy, Camps-Fajol, et al., 2020; Montanuy, Martínez-Barriocanal, et al., 2020). Additionally, EGFR amplification has been recently observed in FA-HNSCC (Webster et al., 2022). While our group is committed to demonstrate the efficacy and safety of afatinib in FA patients with HNSCC through a repurposing, multicenter and international clinical trial; and taking into consideration that tumors frequently develop resistance to these therapies, limiting their long-term efficacy, we also aim to identify new therapeutic targets for afatinib-resistant FA HNSCCs.

By long-term culture of up to 3 months with increasing doses of afatinib, afatinib-resistant cell lines, including sporadic (CAL 27, and CAL 33), FA (VU 1131, VU 1365, VU 1604, and OHSU 974), gene-edited FA-deleted ("fanconized" clones of CAL 27 and CAL 33), and FA-corrected

(corrected lines of VU 1131, VU 1365, VU 1604, and OHSU 974) HNSCC cell lines were developed. Considering that FA HNSCC cell lines exhibited 20-50 times lower resistance to afatinib than sporadic HNSCC cell lines (20-45-80 nM vs. 800-1,000 nM afatinib), we tried to stablish the main differential mechanisms between sporadic and FA HNSCC afatinib-resistant and non-resistant cell lines. A 49 phospho-receptor tyrosine kinases array was done to the main cell line pools, first, and to the independent cell lines later, but the results were unconclusive. In parallel, we explored the expression of targets for CAR-T cell therapies that are currently under preclinical and clinical development for sporadic HNSCC, such as ERBB, NKG2D-ligands and CD44v6 receptor, whose differential expression between AR and non-resistant cell lines was significant. In view of the results obtained, we studied the number of *ERBB* copies by a multiplex ligation dependent probe amplification, to verify that there were not duplications in the afatinib-resistant cells in comparison with the non-resistant. And lately, we analyzed the activation status of the most relevant RNA transcripts by RNA sequencing of the sporadic and FA-derived HNSCCs in comparison with resistant cell lines. From the obtained results, it was relevant the expression of 89 genes that were upregulated in afatinib-resistant FA HNSCC cell lines in comparison with sporadic HNSCC; as well as the expression of only 8 genes identified as common upregulated in all the afatinib-resistant cell lines. [redacted] were some of the genes upregulated in these FA HNSCC.

Although the low afatinib-resistance acquisition in FA HNSCC cell lines supports the use of this inhibitor in clinical trials, the identification of potential targets in the differential expression of transcriptomic data between cell lines, pave the way for new therapeutic strategies for FA HNSCC. Therefore, and considering the data obtained, further experiments must be done in order to propose a potential alternative therapy in this field.

Resumen

[redacted] La reparación del DNA es un objetivo importante en la terapia dirigida contra el cáncer, y supone una alternativa a las terapias convencionales. En este ámbito, la letalidad sintética, término usado para referirse a la relación genética que se establece entre dos genes cuya pérdida de función desemboca en la muerte celular, mientras que la pérdida de función de solo uno de ellos no, está siendo considerada para diferentes enfoques terapéuticos contra el cáncer. Un ejemplo de ello son los inhibidores de la PARP (PARPi), usados en tumores con mutaciones en BRCA1/2, y aprobados para el tratamiento de cáncer de mama, ovario, próstata o páncreas.

Esta tesis es continuación de un proyecto de descubrimiento de fármacos (*drug discovery*) cuyo objetivo es encontrar un inhibidor [redacted], que pueda ser usado para tratar tumores con mutaciones letales sintéticas con la ruta mencionada, [redacted] Nuestra diana específica [redacted]. La estructura 3D de ambas proteínas fue detenidamente estudiada al inicio del proyecto, así como los aminoácidos que componen [redacted] Después de esta caracterización, se llevó a cabo un primer cribado de compuestos a partir de una librería con 136 millones de moléculas (base de datos 3D ZINC15). Esta librería fue filtrada mediante un proceso de acoplamiento entre moléculas en varios pasos y 39 de los 57 potenciales candidatos que seleccionados, fueron comprados y validados en células U2OS y fibroblastos humanos. Además, la interacción de estos candidatos con la diana terapéutica fue probada y medida mediante la técnica de SPR *(surface plasmon resonance*) (Camps-Fajol's thesis, 2022).

A este primer cribado virtual (Fx) le siguió un segundo (F2.x), que consistió en una estrategia denominada *fragment-based strategy*, y del cual se obtuvieron 24 candidatos que fueron posteriormente validados (Camps-Fajol's thesis, 2022). Después de estas validaciones, los mejores candidatos de las rondas Fx y F2.x, F27 y F2.14, fueron optimizados en una tercera ronda (F3.x). En total se llevaron a cabo cuatro rondas de optimización de fármacos (F3.x-F6.x), que incluyeron más de 50 candidatos de nueva síntesis que fueron validados en ambas líneas celulares (validación *in vitro*), y cuya interacción con la diana fue medida mediante SPR (validación bioquímica). Algunos candidatos como F3.6, F3.14, F3.14, F4.3 y F5.6 mostraron buenos resultados en cuanto a inhibición [redacted] y afinidad con la diana, pero con toxicidad pasadas 6-8 horas, y mala solubilidad. La última ronda de optimización hasta ahora (F6.x) ha demostrado una mejora en comparación con las rondas anteriores: el candidato F6.1 presenta buena afinidad por la diana, buena inhibición [redacted], y no presenta toxicidad. Por otro lado, se ha llevado a cabo un nuevo cribado (2Fx) de manera paralela a esta última ronda de optimización, a partir de una base de datos con 13 millones de moléculas (ZINC *database* filtrada por el peso molecular de los compuestos). De los 39 candidatos seleccionados en esta ronda, 26 fueron comprados y validados. En este caso, el candidato 2F17 también ha mostrado buenos resultados sin presencia de toxicidad en las células tratadas. Para concluir, aunque todavía hay mucho por avanzar, las perspectivas de este proyecto en vistas a los últimos resultados resultan esperanzadoras.

Por otra parte, la falta de una ruta FA/BRCA funcional es el origen de un raro desorden genético caracterizado, principalmente por fallo de médula ósea, anomalías físicas y mayor riesgo de cáncer. De hecho, el desarrollo de carcinomas escamosos de cabeza y cuello (HNSCC) en pacientes con anemia de Fanconi es entre 500 y 800 veces mayor que en población general, a lo que se suma el inconveniente adicional de que estos pacientes no pueden someterse a quimio- o radioterapia debido a la pérdida del mecanismo de reparación de enlaces cruzados entre cadenas. A causa de esta intolerancia a la radio/quimioterapia, la resección quirúrgica es la única terapia aprobada para este tipo de tumores en pacientes Fanconi. Sin embargo, en 2020 se publicó un estudio hecho por nuestro grupo, en el que a partir de un cribado a gran escala (*high content screening*) se identificó a afatinib, inhibidor panERBB, como un prometedor agente antitumoral y no genotóxico para pacientes Fanconi (Montanuy, Camps-Fajol, et al., 2020; Montanuy, Martínez-Barriocanal, et al., 2020). Además, la amplificación de EGFR ha sido recientemente observada en FA HNSCC (Webster et al., 2022). Mientras nuestro grupo intenta

demostrar la eficacia y seguridad de afatinib en pacientes Fanconi con HNSCC a través de un ensayo clínico de reposicionamiento, multicéntrico e internacional; y teniendo en cuenta que los tumores suelen desarrollar resistencia a estos tipos de terapia, limitando su eficacia a largo plazo, nuestro objetivo se centró en identificar nuevas dianas terapéuticas para los tumores FA HNSCC resistentes a afatinib.

Las líneas celulares resistentes a afatinib se crearon a partir del cultivo de las líneas de tumores esporádicos (CAL 27 y CAL 33), Fanconi (VU 1131, VU 1365, VU 1604 y OHSU 974), los clones "fanconizados" a partir de las líneas esporádicas, y las líneas FA corregidas, sometidos a cultivo con dosis crecientes de afatinib durante más de 3 meses. Considerando que las líneas FA HNSCC exhibían 20-50 veces menos resistencia a afatinib que las líneas esporádicas (afatinib 20-45-80 nM vs. 800-1.000 nM), intentamos establecer los principales mecanismos diferenciales entre líneas esporádicas y Fanconi, resistentes y no resistentes a afatinib. En primer lugar, se llevó a cabo un *array* que contenía 49 fosfo-receptores tirosina-quinasa en los principales conjuntos de células, y más delante de manera independiente en cada línea celular, pero los resultados no fueron concluyentes. En paralelo se exploró la expresión de dianas comunes en diferentes terapias CAR-T, bajo actual desarrollo preclínico y clínico, como los ERBB, los ligandos de NKG2D o el receptor CD44v6., cuya expresión diferencial entre líneas resistentes y no resistentes a afatinib fue significativa. En vista de los resultados obtenidos, se estudió el número de copias de los genes codificantes para *ERBB* presentes en las líneas de HNSCC, mediante MLPA (*multiplex ligation dependent probe amplification*), para verificar que no había duplicaciones en las células resistentes a afatinib en comparación con las no resistentes. Y más tarde se analizaron también los tránscritos de RNA más relevantes en líneas esporádicas y FA HNSCC en comparación con las líneas resistentes. Dentro de los resultados obtenidos mediante este análisis de secuenciación del RNA, llama la atención la expresión diferencial de 89 genes, sobre-expresados en líneas Fanconi resistentes a afatinib; así como la sobreexpresión de 8 genes, identificados como comunes en todas las líneas resistentes (esporádicas y FA). [redacted] son algunos de los genes sobre-expresados en las líneas FA HNSCC resistentes a afatinib.

Aunque la baja adquisición de resistencia a afatinib en líneas FA HNSCC apoya el uso de este inhibidor en ensayos clínicos, la identificación de potenciales dianas terapéuticas con expresión diferencial en los datos de transcriptómica obtenidos abre la puerta a nuevas estrategias contra tumores HNSCC en pacientes Fanconi. Asimismo, y considerando los datos obtenidos, más experimentos deben ser hechos a la hora de poder proponer una potencial alternativa en este campo.

Resum

[redacted] La reparació del DNA és un objectiu important en la teràpia dirigida contra el càncer, i suposa una alternativa a las teràpies convencionals. Després del descobriment de la letalitat sintètica, mot utilitzat per a referir-se a la relació genètica establerta entre dos gens la pèrdua de funció dels quals desemboca en la mort cel·lular, mentre que la pèrdua de funció de tan sols un d'ells no, s'han desenvolupat diversos enfocaments terapèutics en base a aquesta relació. Un exemple en són els inhibidors de la PARP (PARPi), emprats en tumors amb mutacions en BRCA1/2, i aprovats per al tractament de càncer de mama, ovari, pròstata o pàncrees.

Aquesta tesi és la continuació d'un projecte de descobriment de fàrmacs (*drug discovery*) amb la finalitat de trobar un inhibidor [redacted] que pugui ser utilitzat per tractar tumors amb mutacions letals sintètiques amb la ruta esmentada, [redacted] El nostre objectiu específic [redacted]. L'estructura 3D d'ambdues proteïnes va ser estudiada detingudament a l'inici del projecte, com també ho van ser els aminoàcids que componen [redacted] Després d'aquesta caracterització, es va dur a terme un primer cribratge de compostos a partir d'una llibreria de 136 milions de molècules (base de dades 3D ZINC15). Aquesta llibreria fou filtrada mitjançant un procés d'acoblament entre molècules en diversos passos i se'n van comprar i validar en cèl·lules U2Os i fibroblasts humans 39 dels 57 candidats potencials seleccionades. A més, la interacció d'aquests candidats amb la diana terapèutica es va provar i mesurar mitjançant SPR *(surface plasmon resonance*) (Camps-Fajol's thesis, 2022).

A aquest primer cribratge virtual (Fx) s'hi va sumar un segon cribratge virtual (F2.x) que va consistir en una estratègia denominada *fragment-based strategy*, del qual es van obtenir 24 candidats que van ser validats posteriorment (Camps-Fajol's thesis, 2022). Després d'aquestes validacions, els millors candidats de les rondes Fx i F2.x, F27 i F2.14 van ser optimitzats en una tercera ronda (F3.x). En total, es van dur a terme quatre rondes d'optimització de fàrmacs (F3.x-F6.x), que van incloure més de 50 candidats de nova síntesi que van ser validats en les dues línies cel·lulars (validació *in vitro*), i la interacció dels quals amb la diana es va mesurar mitjançant SPR (validació bioquímica). Alguns candidats com F3.6, F3.14, F3.14, F4.3 i F5.6 van mostrar bons resultats quant a inhibició [redacted] i afinitat amb la diana, però amb toxicitat un cop passades 6-8 hores, i mala solubilitat. L'última ronda d'optimització fins ara (F6.x) ha demostrat una millora en comparació amb les rondes anteriors: el candidat F6.1 presenta bona afinitat amb la diana, bona inhibició [redacted] i no presenta toxicitat. Per altra banda, s'ha dut a terme un nou cribratge (F2.x) de manera paral·lela a aquesta darrera ronda d'optimització, a partir de d'una llibreria de 13 milions de molècules (ZINC *database* filtrada per peso molecular dels compostos). Dels 39 candidats seleccionats, 26 nous candidats van ser comprats i s'han validat. En aquest cas, el candidat 2F17 també ha mostrat bons resultats sense presència de toxicitat en les cèl·lules tractades. Finalment, malgrat que encara hi hagi molt de marge per avançar, les perspectives d'aquest projecte en base als darrers resultats resulten esperançadors.

Per altra banda, la manca d'una ruta FA/BRCA funcional és l'origen d'un desordre genètic minoritari caracteritzat, principalment, per fallada de medul·la òssia, anomalies físiques i un major risc de càncer. De fet, el desenvolupament de carcinomes escamosos de cap i coll (HNSCC) en pacients amb anèmia de Fanconi és entre 500 i 800 vegades més elevat que en població general, a la qual cosa s'hi suma l'inconvenient addicional que aquests pacients no es poden sotmetre a quimio- o radioteràpia degut a la pèrdua del mecanisme de reparació d'enllaços creuats entre cadenes. A causa d'aquesta intolerància a la radio-/quimioteràpia, la resecció quirúrgica és l'única teràpia aprovada per aquest tipus de tumors en pacients Fanconi. Tanmateix, el 2020 es va publicar un estudi fet por el nostre grup, a partir d'un cribratge a gran escala (*high content screening*) en el que es va identificar a afatinib, inhibidor panERBB, com a un agent tumoral prometedor i no genotòxic per a pacients Fanconi (Montanuy, Camps-Fajol, et al., 2020; Montanuy, Martínez-Barriocanal, et al., 2020). A més, l'amplificació d'EGFR ha estat recentment observada en FA HNSCC (Webster et al., 2022). Mentre el nostre grup intenta demostrar l'eficàcia

i seguretat d'afatinib en pacients Fanconi amb HNSCC a través d'un assaig clínic de reposicionament, multicèntric i internacional, i tenint en compte que els tumors acostumen a desenvolupar resistència a aquests tipus de teràpia limitant l'eficàcia a llarg termini, el nostre objectiu es va centrar en identificar nous dianas terapèuticas per als tumors FA HNSCC resistents a afatinib.

Les línies cel·lulars resistents a afatinib es van crear a partir del cultiu de les línies de tumors esporàdics (CAL 27 i CAL 33), Fanconi (VU 1131, VU 1365, VU 1604 i OHSU 974), els clons "fanconitzats" a partir de les línies esporàdiques, i les línies FA corregides, sotmesos a cultiu amb dosis creixents d'afatinib durant més de 3 mesos. Considerant que les línies FA HNSCC exhibien 20-50 vegades menys resistència a afatinib que les línies esporàdiques (afatinib 20-45-80 nM vs. 800-1.000 nM), vam intentar establir els principals mecanismes diferencials entre línies esporàdiques i Fanconi, resistents i no resistents a afatinib. En primer lloc, es va dur a terme un *array* que contenia 49 fosfo-receptors tirosina-quinasa en els principals conjunts de cèl·lules i, més endavant, de manera independent en cada línia cel·lular, però els resultats no van ser concloents. En paral·lel, es va explorar l'expressió de diverses teràpies CAR-T sota desenvolupament actual preclínic i clínic, com els ERBB, els lligands de NKG2D o bé el receptor CD44v6, culla expressió diferencial entre línies resistents i no resistents a afatinib és significativa. En vistes dels resultats obtinguts, es va estudiar el nombre de còpies dels gens codificadors per *ERBB* presents en les línies de HNSCC, mitjançant MLPA (*multiplex ligation dependent probe amplification*), para verificar que no hi havia duplicacions en las cèl·lules resistents a afatinib. I més tard, es van analitzar també els transcrits de RNA més rellevants en línies esporàdiques i FA HNSCC en comparació amb les línies resistents. Dins dels resultats obtinguts a través d'aquest anàlisi de seqüenciació de l'RNA, crida l'atenció l'expressió diferencial de 89 gens, sobreexpressats en línies Fanconi resistents a afatinib, així com la sobreexpressió de 8 gens, identificats com a comuns en totes les línies resistents (esporàdiques i FA): [redacted], [redacted] són alguns dels gens sobreexpressats en les línies FA i HNSCC resistents a afatinib.

Malgrat que la baixa adquisició de resistència a afatinib en línies FA HNSCC apuntala l'ús d'aquest inhibidor en assaigs clínics, la identificació de potencials dianes terapèutics amb expressió diferencial en les dades de transcriptòmica obtinguts obre camins a noves estratègies contra tumors HNSCC en pacients Fanconi. Així mateix, i considerant les dades obtingudes, cal dur a terme més experiments abans de proposar una potencial alternativa en aquest camp.

Introduction

1. Introduction

1.1. DNA damage, replication stress and cancer

The term of cancer embraces a complex and multifaceted disease, characterized by uncontrolled cell growth and proliferation. The World Health Organization (WHO) estimated that it was one of the main causes of death worldwide in 2020, accounted for 10 million deaths, about 2 million of them in USA and Europe (WHO, 2024). Because of its diverse nature, there are more than 100 different types, with different diagnosis and treatment. Given that DNA is a reactive molecule that compounds the fundamental unit of inheritance, it may be argued that a cancer tumor always begins with a DNA mutation (Chatterjee & Walker, 2017). In fact, cancer is fundamentally linked to genetic alterations that activate oncogenes and deactivate tumor-suppressor genes. These changes, accumulated over time, are driven by DNA damage and errors during replication, leading to genomic instability. Genome instability arises from various sources, including errors in DNA replication, exposure to genotoxic compounds, and damage from radiation. These factors collectively generate thousands of DNA lesions daily in mammalian cells, with reactive oxygen species being a significant contributor to endogenous DNA damage (Jackson, 2009; Gaillard et al., 2015) .

While environmental factors like UV radiation and certain chemicals contribute to DNA damage, internal factors such as metabolic byproducts also pose threats to DNA integrity. Various mechanisms have evolved to repair DNA damage and to promote telomere maintenance. Despite these protective systems, DNA damage can result in a range of adverse effects, from cell-cycle arrest to irreversible mutations that promote cancer development. Lesions can disrupt transcription and replication, triggering cell death or increasing the risk of oncogenesis. Moreover, DNA breaks, particularly double-strand breaks, are highly relevant to cancer development, as they can induce chromosomal aberrations and contribute to oncogenic translocations. Cells employ checkpoints throughout the cell cycle to detect and repair DNA damage, but if repair mechanisms fail, apoptosis may be initiated to prevent the propagation of damaged genetic material (Hoeijmakers, 2001; Gaillard et al., 2015).

During cell division, accurate replication of billions of nucleotides is crucial, but errors in DNA replication can cause mutations or blockages, leading to chromosome breakage, rearrangements, and missegregation (Gaillard et al., 2015). Replication begins at numerous replication origins, where initiation proteins prepare the chromatin for replication before DNA synthesis begins. Therefore, cells must balance accuracy, speed, and resource allocation to efficiently complete replication. Although its regulation is unclear, most replication origins remain inactive during normal replication and can be activated in response to stress to ensure DNA synthesis at stalled replication forks (Zeman & Cimprich, 2014). Replication stress (RS), characterized by slowed DNA synthesis or stalled replication forks, is a primary driver of genome instability. Sophisticated checkpoint pathways, particularly in the S phase of the cell cycle, monitor DNA replication and coordinate the DNA damage response (DDR) to prevent genome instability (Gaillard et al., 2015). However, oncogene expression disrupts cell cycle regulation, contributing to RS and DNA damage. Pre-cancerous lesions often exhibit constitutive activation of DNA damage signaling, which can delay or prevent tumorigenesis by inducing apoptosis or senescence. Accordingly, dysfunction in DDR exacerbates tumor progression under oncogene-induced RS, as evidenced by mutations in DDR factors frequently found in human cancers. Experimental evidence supports the link between RS and tumorigenesis: inhibition of DNA polymerases or depletion of nucleotides promotes the development of cancer-like mutations in both experimental models and human tumors. Taking that into account, understanding the molecular mechanisms underlying RS and its impact on genome instability and tumorigenesis is crucial for developing novel anticancer therapies (Hoeijmakers, 2001; Zeman & Cimprich, 2014).

1.2. DNA repair mechanisms

Although some DNA mutations are essential for evolution, there are repair mechanisms designed to correct DNA damage. DNA damage occurs continuously in cells exposed to exogenous or endogenous factors, such as UV light exposure, ionizing radiation (IR), chemical exposure, cellular metabolism, DNA RS or oxidative stress (Chatterjee & Walker, 2017). If the damage occurs in one of the DNA strands, it is referred to single-stranded DNA (ssDNA) breaks (single strand breaks, SSBs), whereas if the damage occurs in both strands it is called double-stranded DNA (dsDNA) breaks (double strand breaks, DSB). In addition, another type of damage recognized are base and sugar lesions, DNA interstrand crosslinks (ICLs), and clustered damage sites, consisting in multiple lesions (Jackson, 2009; Huang & Zhou, 2021).

Talking about DNA repair mechanisms, there are seven important pathways involved: mismatch repair (MMR), nucleotide excision repair (NER), base excision repair (BER), homologous recombination (HR), non-homologous end joining (NHEJ), single-strand annealing (SSA) and the Fanconi anemia (FA)/BRCA pathway (Figure 1) (Chatterjee & Walker, 2017).

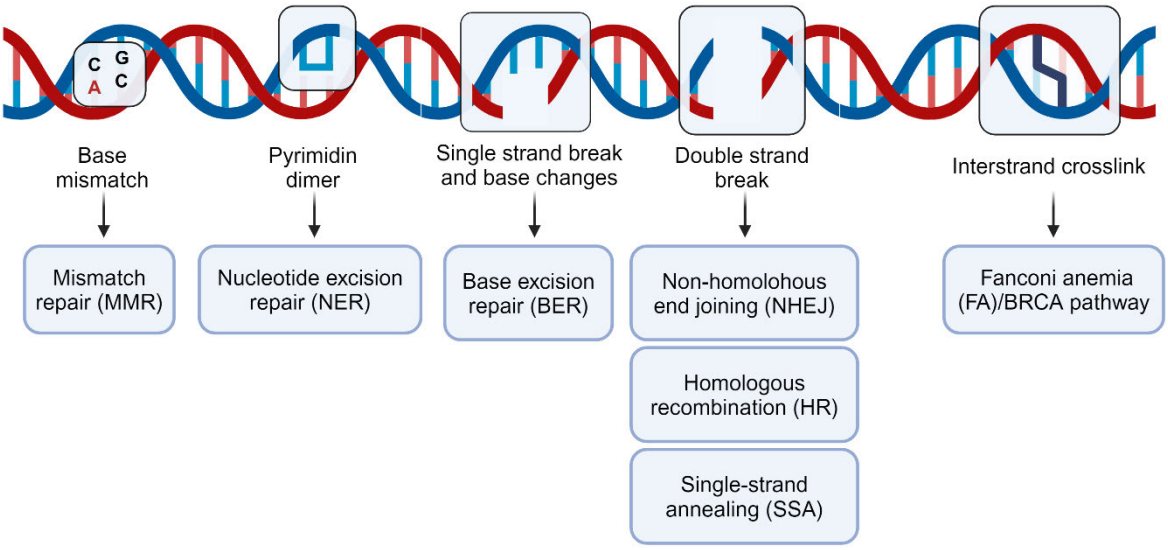


Figure 1. DNA damage repair pathways.

MMR pathway is called into action when a nucleotide misincorporation generates DNA base mismatches, small insertions, and deletion loops during DNA replication. After the recognition of the mismatch by MSH2-MSH6 (MutSα complex), MLH1-PMS2 (MutLα complex) are recruited and interact with proliferating cell nuclear antigen (PCNA) and exonuclease 1 (EXO1) to excise the error-containing DNA strand. Finally, DNA polymerase δ fills in the excised region, and DNA ligase I seals the final nick (Figure 2). The inactivation of MMR is associated with hereditary human cancers, and the increase of the incidence of sporadic tumors (Rahimian et al., 2020; Wang et al., 2021).

NER pathway is used by the cells to remove complicated lesions or structures, such as DNA adducts, pyrimidine dimers or cross-linking lesions; whereas BER is the main pathway used to repair SSB or base changes by the replacement of 1 to 10 nucleotides (Rahimian et al., 2020; Huang & Zhou, 2021; Wang et al., 2021). In NER, after the DNA damage recognition by the XPC-RAD23B complex, the helix opening takes place by the helicases XPB and XPD, that unwinds the DNA around the lesion. Then, the excision is done by the endonucleases XPG and XPF-ERCC1, on a short ssDNA that harbors the lesion. Afterwards, the new DNA synthesis is done by DNA polymerase δ, ε, or κ, which fills the gap copying the undamaged strand as a template. The DNA ligase I or III seals the nick of the strand at the end of the process (Figure 2) (Wang et al., 2021). Mutations in NER genes interfere with the capacity for DNA damage repair, resulting in

introduction of novel mutations. Previous research has shown that inadequate NER may contribute to the occurrence of xeroderma pigmentosum (XP), a rare disease that can enhance the predisposition risk of skin cancer (Zuo et al., 2022). Mutation in ERCC4, which is also a component of the NER pathway, is related not only to XP disease, but also with the segmental XFE progeroid syndrome and FA (Bogliolo et al., 2013; Zuo et al., 2022).

In BER, specific DNA glycosylases recognize and cut the damaged bases, which are substituted for a short or long-patch, depending on the number of nucleotides that need to be refilled. These DNA glycosylases create an abasic site (AP), which is a location in DNA that has neither a purine nor a pyrimidine base, that it is recognize and cut by AP endonuclease 1 (APE1). After the incise, DNA polymerase β inserts the correct nucleotide, and the nick is sealed by DNA ligase III in complex with XRCC1 (Figure 2) (Rahimian et al., 2020; Wang et al., 2021). In addition to base changes repair, BER pathway also operate in SSB, where poly (ADP-ribose) polymerase 1 (PARP1), is a key enzyme as damage sensor. It is linked to several molecular and cellular functions, including transcription, chromatin modification, and mitotic spindle formation. In addition to these roles, it also plays a crucial impact in tumorigenesis and progression; and expression abnormalities have been observed in many human malignancies such as colorectal or gastric cancer (Zhou et al., 2020).

The main differences between the HR and the NHEJ is that the first DNA repair mechanism occurs in S-phase and uses a homologous sequence in the genome as a template for DSB repair, meanwhile the NHEJ is described as an error-prone mechanism, because it does not use a DNA template as reference, and works in G1 (Mateos-Gomez et al., 2015; Ranjha et al., 2018; Rahimian et al., 2020; Wang et al., 2021). The HR pathway involves the MRN complex (MRE11-RAD50-NBS1) to detect DSBs. After the detection, protein kinase ataxia-telangiectasia mutated (ATM) is activated, and the resection is carried out by CtIP and the EXO1 and DNA2 nucleases, in cooperation with the helicase BLM. BRCA1, BRCA2, PALB2 and RAD51 mediate in the strand invasion. Finally, DNA polymerases extend the invading strand using homologous template, ensuring accurate repair (Figure 2). Given their role in DSB repair, germline mutations in these genes can give rise to cancer prone syndromes, like Nijmengen breakage syndrome, Seckel syndrome, Bloom syndrome, FA, or hereditary breast and ovarian cancer (Yata & Esashi, 2009; Ranjha et al., 2018; Yoon et al., 2023).

The NHEJ pathway relies on a heterodimer of Ku70/Ku80 and the DNA-dependent protein kinase (DNA-PKcs) catalytic subunit, which recognizes DSBs and activates downstream signaling factors such XRCC4, XLF, and DNA ligase IV (Figure 2) (Brochier & Langley, 2013; Wang et al., 2021). The classical NHEJ (c-NHEJ) and HR pathways are responsible for repairing DSBs of DNA, but an alternative-NHEJ (alt-NHEJ, alternative end joining, or microhomology-mediated end joining) is responsible for residual DSBs that could not be repaired by the other pathways (Huang & Zhou, 2021). The low-fidelity polymerase θ is a critical factor in alt-NHEJ pathway, and the depletion of the encoding gene of this polymerase has an impact on cell survival in absence of BRCA genes (Mateos-Gomez et al., 2015). The fidelity of alt-NHEJ is lower than the classical one, being highly error-prone due to the use of short single-strand microhomology sequences and resulting mutagenic in most of the cases (Mateos-Gomez et al., 2015; Rahimian et al., 2020; Wang et al., 2021; Zuo et al., 2022).

DSBs are, along with ICLs, the most deleterious kind of DNA damage, and may result in chromosome breaks leading to chromosomal translocation, production of fusion genes, often displaying oncogenic properties to fuel cancer transformation. Although in humans DSBs are repaired mainly by NHEJ and HR, SSA is also involved in DNA DSB repair (Figure 1). Though there are some molecular similarities, SSA is not an HR or NHEJ variation since it functions differently due to distinct proteins and metabolic events. Essentially, SSA is a DSB repair pathway that takes place when a DSB has at least two direct DNA repeats on both ends. Consequently, SSA does not require a donor sequence, in contrast to HR (Bhargava et al., 2016; Blasiak, 2021; Vu et al., 2022).

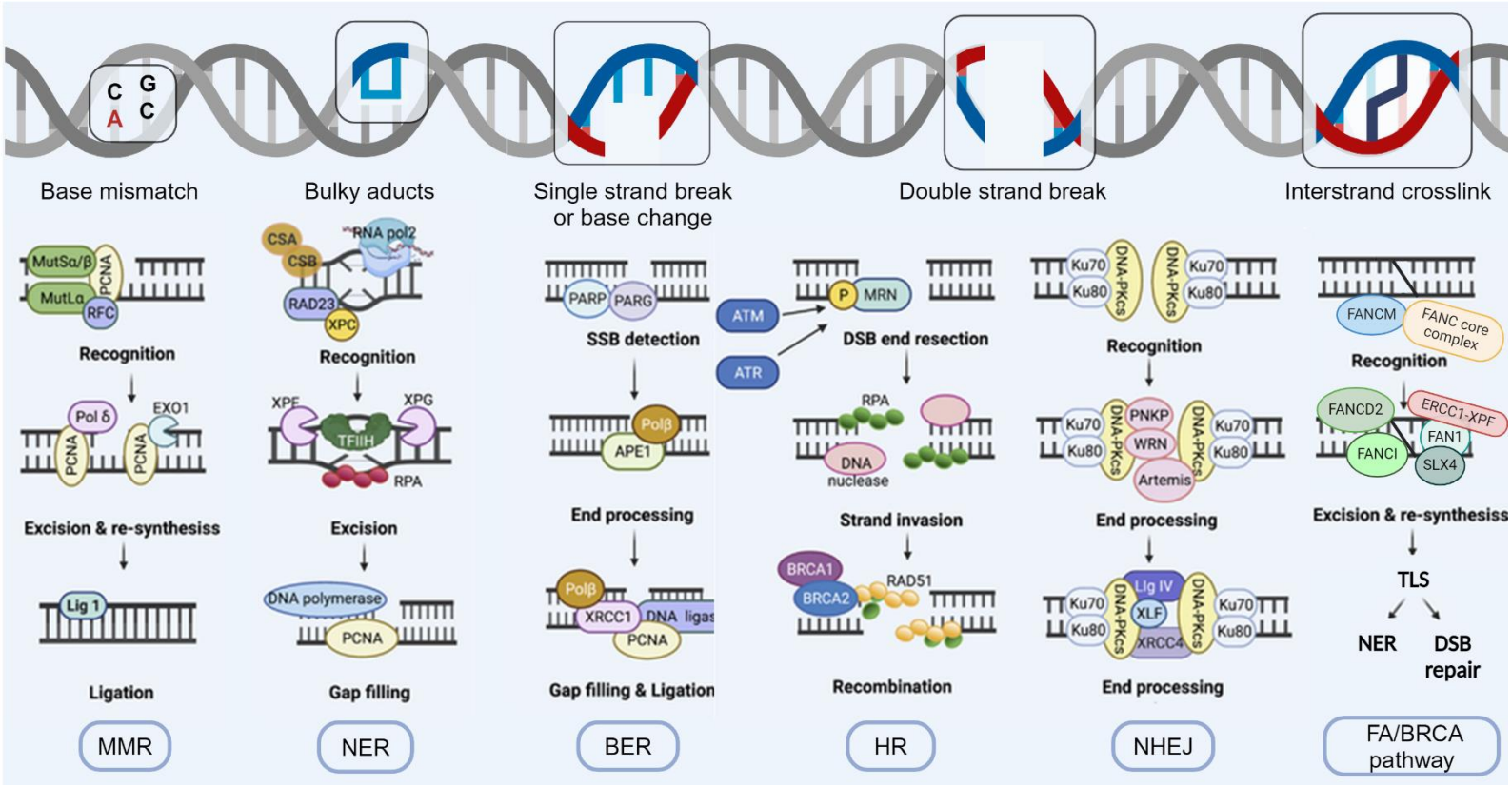


Figure 2. Overview of DNA damage repair (DDR) pathways. MMR pathway fixes mismatches, small insertions, and deletions during DNA replication. MutSα detects errors, MutLα, PCNA, and EXO1 excise the error, and DNA polymerase δ and DNA ligase I complete the repair. NER pathway removes bulky lesions like adducts and pyrimidine dimers. XPC-RAD23B detects damage, XPB and XPD unwind DNA, XPG and XPF-ERCC1 excise the damaged strand, and DNA polymerase δ, ε, or κ and DNA ligase I or III repair the gap. BER pathway fixes small lesions and single-strand breaks. After the lesion detection by PARP and PARG, DNA glycosylases remove damaged bases, APE1 cleaves the site, DNA polymerase β inserts the correct nucleotide, and DNA ligase III-XRCC1 seals the nick. HR pathway repairs double-strand breaks using a homologous sequence during S-phase. The MRN complex detects breaks, ATM is activated, resection is performed by CtIP, EXO1, DNA2, and helicase BLM, and BRCA1, BRCA2, PALB2, and RAD51 mediate repair. NHEJ pathway repairs double-strand breaks without a template, making it error-prone. Ku70/Ku80 and DNA-PKcs recognize breaks, and XRCC4, XLF, and DNA ligase IV complete the repair. Alt-NHEJ repairs residual breaks but is highly error-prone. FA/BRCA pathway repair ICLs. FA core complex activates FANCD2-FANCI, recruiting FAN1 and SLX4 to unhook crosslinks. Specialized polymerases perform translesion synthesis (TLS) or HR/NER fill the gap, with final ligation restoring DNA integrity. Figure edited and adapted from Wang et al., 2021.

ICL are lesions in which two bases from complementary strands are covalently linked due to crosslinking agents like platinum compounds (cisplatin, for example), mitomycin C (MMC), bi-alkylating agents, or aldehydes, among other agents, avoiding the complete separation of the two DNA strands (Chatterjee & Walker, 2017; Wang et al., 2021; Webster et al., 2022). These lesions are extremely toxic, and they are repaired by FA proteins and interacting partners, that constitute the FA/BRCA pathway (Figures 1, 2). After the recognition of the ICLs, in which several proteins are involved, the FA core complex binds to the DNA and activates the monoubiquitination of FANCD2-FANCI complex. Once recruited to the site of the ICL, the monoubiquitinated FANCD2-FANCI complex interacts with structure-specific endonucleases such as FAN1 and SLX4, which facilitate the unhooking of the crosslink. This process involves incising one of the DNA strands adjacent to the crosslink, creating a ssDNA gap with an unhooked crosslink intermediate. With the crosslink unhooked, specialized DNA polymerases, such as polymerase ζ, can bypass the lesion by inserting nucleotides opposite the unhooked crosslink. This process, known as translesion synthesis (TLS), allows replication to proceed past the lesion. Alternatively, the ssDNA gap created by the unhooking of the crosslink can be filled in by high-fidelity DNA polymerases, leading to repair synthesis. The remaining gap is typically filled in by either HR or NER, depending on the context and the cell cycle phase. Ultimately, the final steps of ICL repair involve ligation of the newly synthesized DNA strands and restoration of DNA integrity (Figure 2) (Sparkes, 1996; Kottemann & Smogorzewska, 2013; Cheung & Taniguchi, 2017; Niraj et al., 2019).

Cells that are unable to repair their ICLs are more vulnerable to DNA breakage and rearrangement, which increases the possibility of oncogene modification and tumor suppressor gene loss. Moreover, excess cytokine production, inflammasome activation, cell-cycle abnormalities, and heightened sensitivity to free radicals and aldehydes are all consequences of additional cellular dysregulation brought on by deficiencies in FANC proteins. Furthermore, the absence of a functional FA/BRCA pathway affects ICL repair, but also the mitochondrial function, provoking an increase of reactive oxygen species (ROS). For this reason, it is believed that the high incidence of hematologic illnesses and significantly cancer susceptibility in FA patients are caused by this constellation of genetic and cellular abnormalities (Minguillón y Surrallés, 2018; Cornwell et al., 2019; Lee et al., 2021; Wang et al., 2021; Webster et al., 2022).

In addition to the main repair pathways, there are some additional mechanisms that can be used by the cell to restart replication and maintain genomic stability, depending on the type of damage, availability of repair proteins, and genetic background. These mechanisms are called DNA damage tolerance (DDT) pathways and include homology-dependent repair (HDR), fork reversal, TLS, and fork repriming (Figure 3) (Sale, 2012; Khatib et al., 2024).

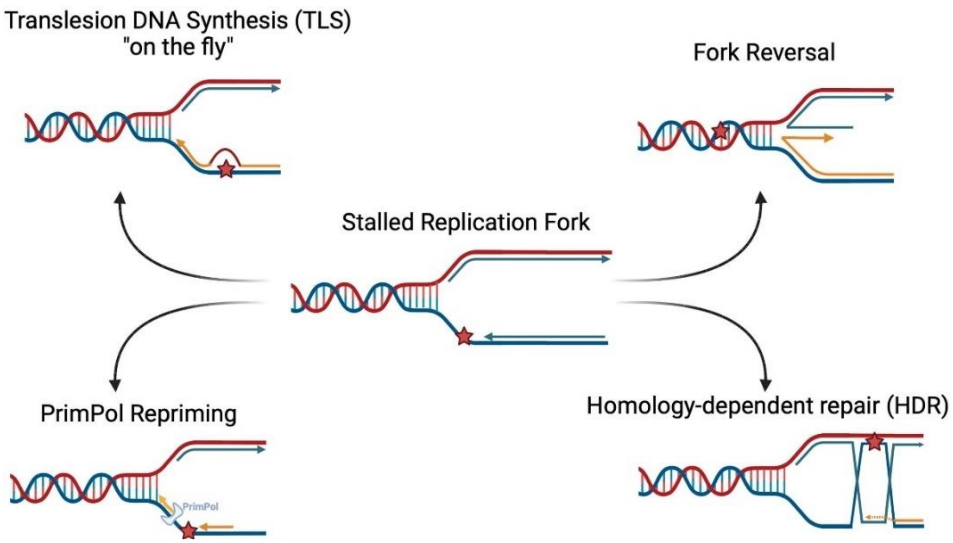


Figure 3. Mechanisms for DNA damage tolerance. Translesion synthesis (TLS), fork reversal, fork repriming (PrimPol repriming) and homology-dependent repair (HDR) are important to avoid the replication forks stop due to the replication stress and DNA-damaging chemicals. Figure extracted from Khatib et al., 2024.

HDR repair includes all repair mechanisms that rely on a homologous donor: strand transfer from the donor (HR) and template switch mechanisms, in which the information is copied from the donor (Adar et al., 2009). While HDR is an error-free repair, that includes BRCA pathway-dependent HR, TLS is an error-prone repair pathway, that employs low-fidelity polymerases to bypass replication when one of the two DNA strands is damaged or broken (Khatib et al., 2024). Specialized TLS polymerases are enlisted to mediate the replication through and past the lesion, for which they must interact with mono-ubiquitinated PCNA before nucleotides are inserted across the lesion (Quinet et al., 2018; Nayak et al., 2021).

Replication fork reversal is a variant of template switching (TS) in which the two newly manufactured DNA strands anneal, remodeling the replication fork into a four-way junction. Fork reversal generally moves the lesion ahead of the fork, giving repair additional time, allowing DNA replication to resume, and preventing fork collapse. It has been shown that ssDNA gaps can be healed post-replicative in the late S phase or G2 phase, even though lesion bypass may occur co-replication (Neelsen & Lopes, 2015; Khatib et al., 2024).

Fork repriming process is characterized by the replication of the DNA strand, leaving ssDNA gaps behind the replication. This repriming is mediated by the human primase and DNA directed polymerase (PrimPol), and after that, the ssDNA gaps are filled by the TS or TLS mechanisms. As in BRCA-deficient cells HR is not functional, cells adopt TLS as a compensatory route (Mourón et al., 2013; Khatib et al., 2024).

1.3. Synthetic lethality

Synthetic lethality (SL) is defined as a genetic relationship in which the loss of function of two genes results in cell death, but the loss of one of either of the two genes does not. It assumes two parallel pathways for performing the same function, so disrupting one of the pathways is viable while disrupting both pathways is lethal (Figure 4) (Bryant et al., 2005; Zinovyev et al., 2013).

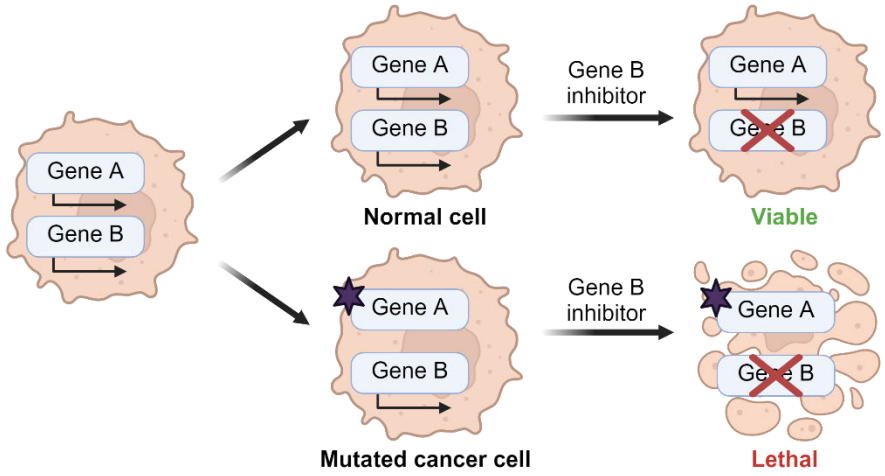


Figure 4. Synthetic lethality. This phenomenon is based on the presence of two parallel pathways that perform the same essential function; disrupting one pathway is survivable, but disrupting both is lethal. In normal cells, the inhibition of one of the genes is viable, meanwhile in cancer cells with mutations in gene A, the inhibition of gene B causes the cell death.

Some authors divided the concept of SL into synthetic dosage lethality and conditional SL. The first one is defined as a genetic interaction between two genes where the inhibition of gene/protein A combined with the overexpression of gene/protein B is lethal to cells. Meanwhile conditional SL depends on certain intrinsic conditions (genetic background, hypoxia or metabolic changes), or extrinsic conditions (DNA-damaging drugs) (Zinovyev et al., 2013; Zhu et al., 2020).

It wasn't until the 1940s that Dobzhansky discovered synthetic connections between two mutations in distinct genes in *Drosophila*; but nowadays SL has been applied as a therapeutic strategy in the treatment of cancer, combining pharmacological inhibition with loss-of-function mutations (Zinovyev et al., 2013).

1.3.1. PARP inhibitors

The initial model was established in tumor cells lacking BRCA1/2, which exhibit SL through inhibition of PARP (Bryant et al., 2005; Farmer et al., 2005). The PARP family is formed by 17 members, but as was explained before, PARP1 facilitates DNA repair by binding to DNA breaks and attracting DNA repair proteins to the site of damage in BER pathway. After binding to damage DNA, PARP1 forms a homodimer and catalyzes nicotinamide adenine dinucleotide (NAD^+) into nicotinamide and ADP-ribose. These components are then used to create branched-chain nucleic acid polymers, with poly ADP-ribose covalently attached to nuclear receptor proteins. Due to their negative charge, these ADP-ribose polymers, significantly impact the function of target proteins. This process is followed by a conformational change in PARP1, which recruits various DNA repair proteins to the damaged site, facilitating the repair. Ultimately, PARP1 undergoes molecular changes leading to reduced DNA affinity, followed by release from the lesion and returning to an inactive state (Murai et al., 2012; Zhu et al., 2020; Zimmermann et al., 2022; Zhu et al., 2023).

PARP-1 is also involved in the activation of ATM, which is essential for HR, and inactivating DNA-dependent protein kinases, which play an important role in NHEJ. Additionally, PARP1 plays a role in other cellular functions such chromatin structure regulation, transcriptional regulation, genomic stability maintenance and apoptosis. It is also involved in various diseases, including cancer and neurodegenerative disorders (Zhu et al., 2020; Zhu et al., 2023).

There are different forms of SL action models for PARP inhibitors (PARPis). As mentioned above, the most well-known mechanism of BER inhibition and PARPis is not the only explanation for SL. NHEJ inhibition has been linked to cell death because of HR-deficient cells that depend on NHEJ as a compensatory repair pathway. Regardless, clinical PARPis are usually NAD^+ analogs, which action mechanism is based on blocking the catalytic activity of PARP1 and PARP2 by competitively binding to the NAD^+-binding catalytic pocket of PARP enzymes. The binding of the PARPi avoids the formation of PAR-polymers and, consequently, it avoids the recruitment of DNA damage repair proteins (Zhu et al., 2023). Consequently, PARP1 has been identified as a promising target for anticancer therapy in order to accomplish DNA damage-induced cell death, and multiple generations of PARP1 inhibitors have been created and approved for use in clinical settings (Figure 5).

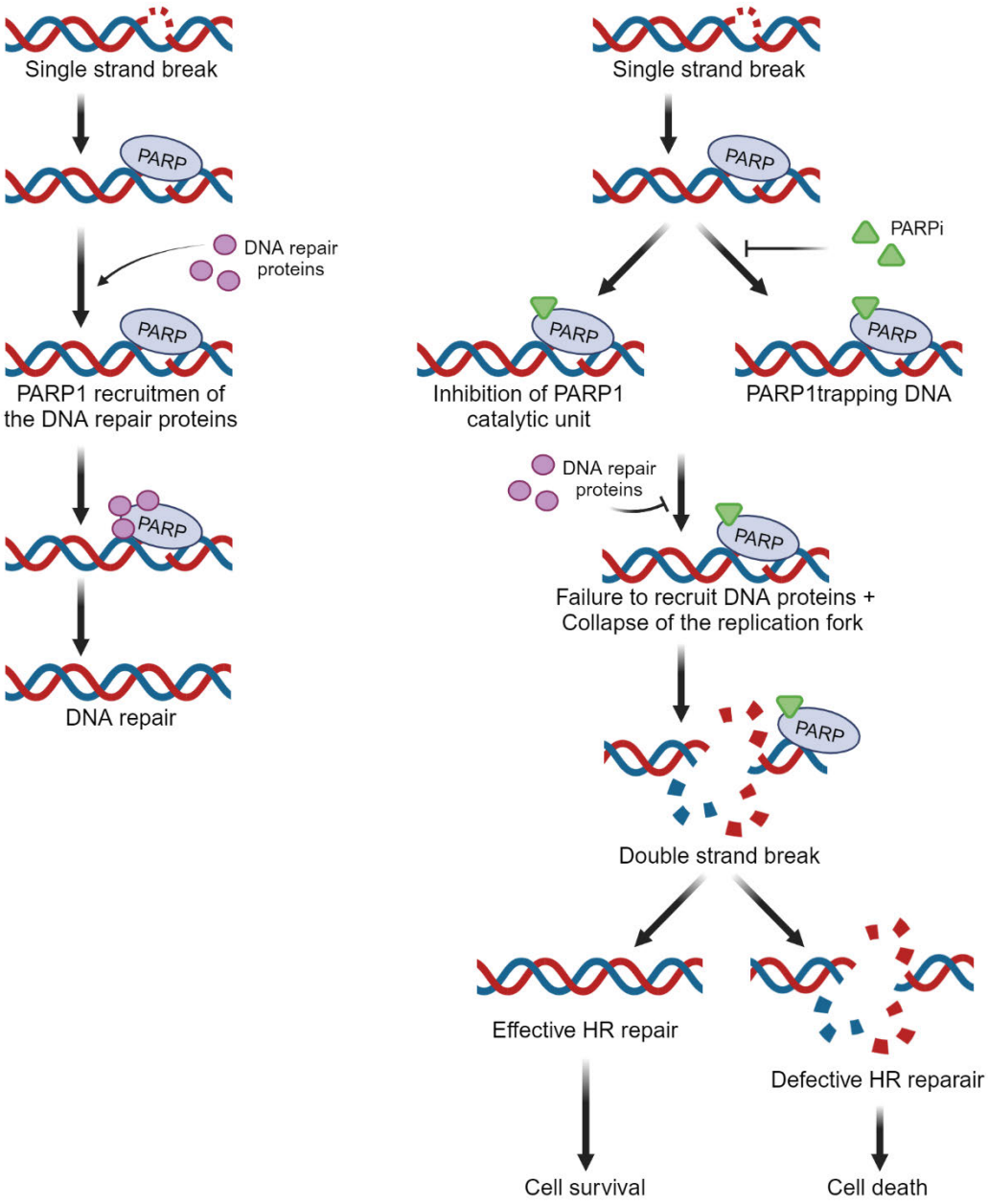


Figure 5. Schematic representation of the proposed mechanisms of action of PARP inhibitors. PARP inhibitors (PARPi) disrupt the normal function of PARP1, a protein involved in DNA repair. Under normal conditions, PARP1 detects DNA single strand breaks, leading to its activation, auto-PARylation, and recruitment of DNA repair proteins to facilitate DNA repair. However, when PARPi are present, they suppress PARP1 activity, preventing the recruitment of repair proteins and resulting in the persistence of single strand breaks. Additionally, PARPi can trap PARP1 at DNA lesions, forming cytotoxic complexes that cause the collapse of replication forks. This leads to the accumulation of persistent single strand breaks and ultimately the formation of DNA double strand breaks. In cells proficient in HR, double strand breaks can be efficiently repaired; meanwhile, in cells deficient in HR the inability to repair double strand breaks accurately leads to cell death. Figure based on Zhu et al., 2023.

Due to the induction of single strand DNA lesions by PARPis, which result in persistent SSBs that cannot be repaired by defective HR pathway, these inhibitors are lethal to BRCA1/2 mutated cancer cells (Figure 6). Taking into consideration this SL mechanism, several PARPi are being tested in clinical trials, and, nowadays, there are six FDA (Food and Drug Administration)-approved PARPis for anticancer treatment: olaparib (Deeks, 2015), talazoparib (Hoy, 2018), rucaparib (Anscher et al., 2021), fuzuloparib (A. Lee, 2021), pamiparib (Markham, 2021), and niraparib (Zhi et al., 2022). Moreover, PARPis have also been considered as a promising

therapeutic approach in some types of cancers in FA patients (Zhu et al., 2021; Zhu et al., 2023). Thus, in *clinicaltrials.gov* website there are now two clinical trials that accept FA patients with cervical cancer (NCT04483544) and metastatic biliary tract cancer (NCT04042831) to be treated with pembroluzimab and olaparib.

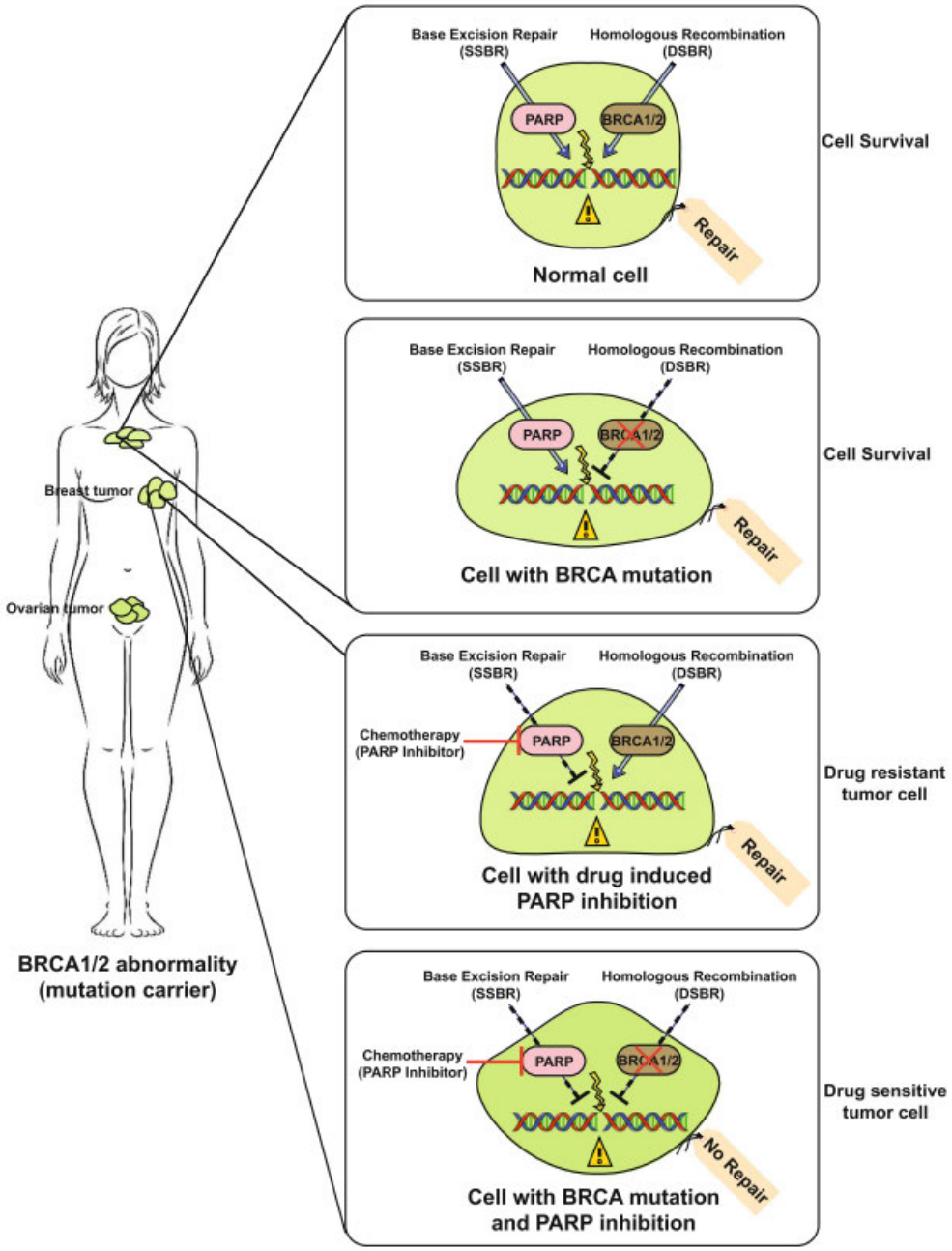


Figure 6. Model for synthetic lethality with PARP inhibitors: synthetic lethal interactions to find molecular targets for cancer therapy. When BRCA1/2 are mutated in breast/ovarian tumor cells, the cancer cell becomes susceptible to chemotherapy medicines that prevent SSBR. However, because they may use the DSBR pathway to repair the DNA damages, cells that have functional BRCA1/2 genes are spared. Tumor cell death is caused by a compromised BER pathway in conjunction with a defect in HR. Figure extracted from Bhattacharjee & Nandi, 2017.

Unfortunately, most patients often develop drug resistance to the PARPi after a period of treatment, contributing to the recurrence of the tumor. Mechanisms of resistance to PARPis include restoration of HR capacity because of BRCA reverse mutations, change in the miRNA environment, or increase of RAD51 protein. The stabilization of replication forks, the decrease of the PARP levels, reducing the DNA-bound of PARP1, and the reduction of the intracellular PARPi levels due to the P-glycoprotein-mediated drug efflux (also called multi-drug resistance protein 1, MDR1), are other mechanism that could explain the drug resistance (Zhu et al., 2020; Zhu et al., 2023). Combination PARPi therapies with other kinase or immune checkpoints blockers have been recognized as an efficient approach against this resistance. An example of that could be the use of PARPis in combination with atasia-telangiectasia and Rad3-related (ATR) kinase inhibitors (ATRis). Several ATRis are currently being clinically tested both alone and alongside PARPis. This combination has a solid molecular base due to these two types of inhibitors have complementary mechanisms: PARPis induce DNA damage, activating the ATR pathway, which facilitate cell survival by the coordination of the DDR in several ways. First, ATR activates a cell cycle checkpoint to pause mitosis until DNA damage is repaired. In order to prevent RS from spreading further, ATR also prevents dormant replication origins from firing. In addition, by activating the enzymes responsible for fork remodeling and HR for DNA repair, ATR facilitates the stability, repair, and restart of replication forks that have stalled. By this way, PARPis induce DNA damage during S-phase by trapping PARP enzymes on DNA, while ATRis prevent cells from recovering from PARPi treatment. This leads to rapid cell death due to premature entry into mitosis with unrepaired DNA damage and inflammatory signaling. As a result, combinations of ATRis and PARPis demonstrate synergistic cytotoxicity in laboratory studies and enhanced effectiveness in animal models with BRCA1/2 deficient tumors compared to either inhibitor alone (Zimmermann et al., 2022).

Understanding and applying SL would promote the development of new targeted drugs for cancer therapy. Although PARPi are the most common SL inhibitors in cancer treatment, other inhibitors are explained in the following section. ATRi, ATM inhibitors (ATMi), DNA-PK inhibitors (DNA-PKi), CHK1/2 inhibitors (CHKi), WEE1 inhibitors (WEE1i), POLQ inhibitors (POLQi), and USP1 inhibitors (USP1i) are other SL interaction targets examples.

1.4. DNA damage response to target cancer

DNA damage in cells could be manifested as neurodegeneration, infertility, immunodeficiencies, bone marrow failure and cancer susceptibility, among other characteristics. Due to the accumulation of oncogenic mutations when the DDR mechanisms failed, genome instability is recognized as a characteristic of cancer. Cancer are more vulnerable to RS and the accumulation of DNA damage. Moreover, they have a dysfunctional redox homeostasis because of their overproduction of ROS, their dysregulation in genes involved in redox regulation, and the tumor microenvironment low oxygen levels. Oxidative stress, telomere attrition, RS and other causes of DNA damage in cancer cells could be considered an advantage as a potential therapeutic opportunity. DDR, therefore, can be used as a target of anticancer drug treatments (Jackson, 2009; Brown et al., 2017; R. Huang & Zhou, 2021).

The identification of novel SL interactions within diverse DDR pathways, along with the effectiveness of PARPi, has led to a growing interest in exploring alternative DDR elements as targets for SL-based cancer treatments (Figure 7) (Brown et al., 2017).



Repair pathway	NHEJ	HR	alt-NHEJ/ MMEJ	SSA	ICL repair	SSB repair	BER	TLS	NER	MMR
Source of DNA damage	IR, radiomimetics, topo II inhibitors	X-linking agents, replication inhibitors, anti-metabolites, topo I inhibitors			X-linking agents	IR, ROS, radiomimetics topo I inhibitors H2O2, alkylating agents	Alkylating agents	UV, alkylating agents	Alkylating agents, X-linkers	DNA pol proofreading errors
Damage sensors	Ku70/Ku80	MRN	PARP	MRN	FA core complex (FANCA, B, C,E, F, G, L and M	PARP	DNA glycosylases, APE1	PCNA	XPC DDB2 CSA	MSH2, MSH3, MSH6, MLH1, PMS2
Signalling/ mediator proteins	DNAPK	MK2, CtIP, BRCA1,BRCA2, PALB2, RPA		CtIP	FANC1 (BRCA2), D2, I, J (BRIP1), N (PALB2), O (RAD51C), P (SLX4), T (UBE2T), RAD51, USP1, XPF			RAD6 RAD18	XPA, XPF, RPA	
Effector proteins	XRCC4 XLF LIG4 APLF Artemis PAXX WRN	RAD51 MUS81/EME1 SLX1/SLX4 RTEL1 BLM TOPOIII POLQ PARI RECQL5 FANCJ, BLM	XRCC1, LIG3, LIG1, CtIP, POLQ	RAD52	Shared with HR, TLS and NER.	XRCC1, PNKP, POLBeta, FEN1, TDP1, Aprataxin, LIG1, LIG3A	As SSB repair	REV1, POLH POLI, POLK.	XPG, ERCC1, POLE, POLD, LIG1, LIG3	EXO1, POLD, LIG1

Figure 7. Damage sensors, signaling proteins, and effector proteins implicated in repair pathways. Sensors, signaling and effector proteins implicated in the different repair pathways that could be targeted in cancer therapy. Proteins which drug inhibitors published are indicated in red. Figure adapted from Brown et al., 2017.

1.4.1. DNA damage sensor proteins

DDR sensor proteins identify the damaged DNA area and control the subsequent cellular reactions, activating the repair pathways. An example of SSBs sensor protein is, which is an essential endonuclease in the BER pathway, whose function is to removal 3' obstructive lesions in DNA (Brown et al., 2017).

For DSBs, Ku (Ku70/Ku80 protein heterodimer) and MRN are the principal sensor protein complexes. The first complex takes part in NHEJ pathway, participating in the recruitment of the repair proteins; meanwhile the MRN complex plays a role in the HR. Some of the FA proteins (FANCA, B, C, E, F, G, L and M), MMR proteins (MSH2, MSH3, MSH6, MLH1 and PMS2), and NER proteins (XPC, DDB2 and CSA) are also involved in the DNA-damage sensors group, apart from PARP proteins (Jackson, 2009; Brown et al., 2017).

As explained before, PARP is a recognized indicator of DNA damage, and the clinical development of PARPis has been a considerable advance in the cancer therapy field. For many of the current clinical methods targeting DNA repair/DDR, SL between repair pathways has offered a new perspective.

Several publications support the importance of MLH1 and PMS2 inhibition to delay or stop tumor growth in different cancers (Shinsato et al., 2013; Shinohara et al., 2016; Pitu et al., 2021; Liu & Weigelt, 2024). However, many DDR sensor proteins have been targeted for potential inhibitors during the last years. Thus, a MRN inhibitor was published in 2009 (Garner et al., 2009). In addition, a few months ago, Arvindh and coworkers, suggested that nimbolide, an anticancer

drug, could reduce the expression of the MRN complex, working as an DDR inhibitor in cellular and animal models (Arvindh et al., 2024).

A small molecule inhibitor of PCNA has also been published, where PCNA is a multifaceted protein that plays a crucial role in DNA replication and repair processes, mainly in TLS repair pathway. This protein serves as molecular scaffold, interacting with DNA polymerases and enhancing DNA synthesis (Srivastava et al., 2012; Gu et al., 2023).

Due to the important role of APE1 in the recognition of base changes in BER repair pathway, there are several studies about its inhibition. An example of that is a study published in 2012 where the authors demonstrated the biological evaluation and structure-activity relationships of new APE1 inhibitors (Rai et al., 2012; Kohl et al., 2019). Furthermore, mitotraxone, a clinical drug used for different cancer types, such as acute lymphoblastic leukemia, has recently demonstrated APE1 inhibitor effect (Minko et al., 2024).

Finally, after a high-throughput screening of 11,745 small molecule compounds, a novel Ku70/Ku80 inhibitor has been also discovered and published this year (Chen et al., 2024).

1.4.2. DNA damage signaling proteins

DDR signaling proteins play a crucial role amplifying the damage signal in the cell and coordinating the most appropriate cellular responses, as transcriptional modifications, cell cycle checkpoint activation, alternative splicing and DNA repair, or senescence or apoptotic cell pathways.

Two main signaling pathways control the DDR: the ATR-checkpoint kinase 1 (CHK1) pathway in response to DNA SSBs, and the ATM-checkpoint kinase 2 (CHK2) in response to DNA DSBs; and both are partially complementary (Figure 8) (Tozaki et al., 2023).

ATM is a DDR signaling protein that promotes DNA DSB repair, after its activation through interactions with NBS1 (MRN complex). ATM is the kinase responsible for histone H2AX phosphorylation (γH2AX), that binds to mediator of DNA damage checkpoint protein-1 (MDC1) potentiating the DNA damage signal. Taking into consideration that molecular biology techniques or gene mutations that inactivate ATM have demonstrated that ATM insufficiency makes cancer cells more susceptible to ionizing radiation and DNA-damaging chemotherapeutic drugs, the identification of ATM kinase's critical function made it an attractive target for cancer therapy. In fact, a number of small-molecule compounds have been identified and employed as molecular probes, and even with their restricted potency and selectivity, those initial inhibitors have contributed to the validation of the theory that suggests that short-term inhibition of ATM activity could enhance the anticancer effect of radiation therapy and drugs that induce DNA damage. The Zimmermann and coworkers' publication showed that two small ATM inhibitors (M3541 and M4076) have demonstrated efficacy in vitro and in vivo when they were combined with radiotherapy, chemotherapy, or a DNA-PK inhibitor (Zimmermann et al., 2022).

A well-known ATM substrate is CHK2, whose activity is crucial for the activation of the G1-S phase checkpoint. In the same way that CHK2 is an ATM substrate, CHK1 is the best described substrate of ATR. ATR is a DNA damage signaling protein that is activated by the replication protein A (RPA) in response to different types of DNA damage and genotoxic stress. ATR is recruited to RPA-ssDNA by ATRIP (ATR-interacting protein) and is activated by TOPBP1 (topoisomerase binding partner 1) in complex with various proteins. To this extent, CHK1 regulates the cell cycle progression by the inhibition of the cyclin-dependent kinase (CDK) activity (Sanjiv et al., 2016; Brown et al., 2017; Tozaki et al., 2023).

CHK1i drugs have been developed during the last years, where research has looked into the combination with other therapies. Despite the fact that numerous CHK1i medications have moved on to phase III testing and FDA approval, no one has reached phase III evaluation. The CHK1i AZD7762 clinical trial is an example of that because it was stopped due to several negative consequences, including cardiac toxicity. Furthermore, prior clinical trials indicate that the normal

tissue toxicities induced by combining a CHK1i with conventional cytotoxic DNA-damaging drugs outweigh the negligible increases in therapeutic efficacy. These results emphasize the necessity of therapeutic approaches that target cancer cells at reduced concentrations. In fact, since 2015 there is evidence of a SL relationship between ATR and CHK1 inhibition, which combined blockage causes ssDNA accumulation, replication collapse, replication fork arrest, and synergistic cell death in cancer cells (Sanjiv et al., 2016; Brown et al., 2017). The inhibition of ATM and CHK1 has been also demonstrated as a SL combination, and it has been demonstrated that when ATMi and CHK1i are combined, they work in concert to activate CDK1, causing apoptosis in cancer cells because of the acceleration of their cell cycle progression (Garrett & Collins, 2011; Matthews et al., 2013; Tozaki et al., 2023).

DNA-PK is another example of DDR signaling protein, whose activity is essential in the NHEJ pathway. The activity of this kinase is dependent of a serine/threonine catalytic unit (DNA-PKcs). When this protein binds to DNA, its autophosphorylation induces a structural alteration that disrupts the NHEJ core complex, allowing end-processing and ligation enzymes to reach the DNA ends for repair. This autophosphorylation also inactivates the kinase activity of the DNA-PK. DNA-PK mutants that missed kinase activity, or treatment of cells with small molecule inhibitors of DNA-PK kinase activity cause the latter to be stabilized on DNA ends, limiting NHEJ and most likely interfering with other repair processes, including HR by obstructing DNA end-resection. Despite the poor pharmacokinetic qualities that have made it difficult to produce DNA-PK inhibitors with high potency and selectivity, several new DNA-PK inhibitors have also been tested in clinical trials in the last years (Zhao et al., 2006; Brown et al., 2017).

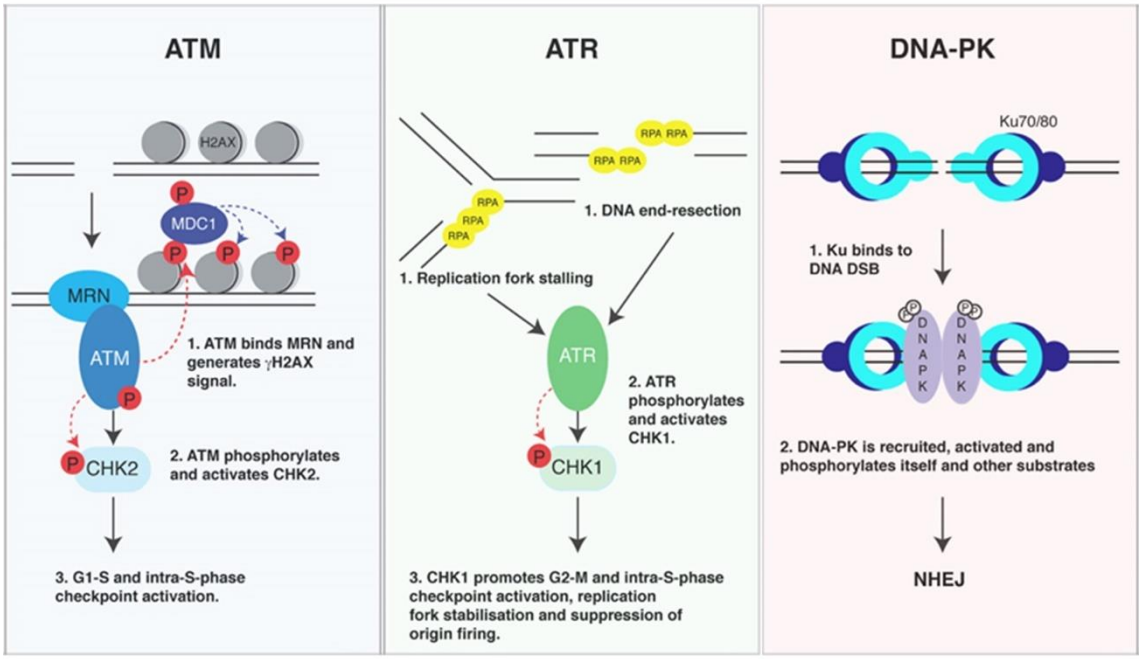


Figure 8. DNA damage signaling proteins. DDR signaling proteins amplify and diversify the damage signal within a cell and coordinate the most appropriate cellular responses. DNA DSB signaling events are largely coordinated DNA-PKcs, ATM, and ATR proteins. Figure adapted from Brown et al., 2017.

In recent years, multiple inhibitors targeting RPA (replication protein A) have been discovered, as it is the case of TDRL-505 and its derivatives, which inhibit the ssDNA binding activity of RPA, exhibiting cytotoxic effects both as monotherapies and in conjunction with other DNA-damaging agents. HAMNO is also a novel inhibitor that disrupts protein-protein interactions involving RPA. Specifically, HAMNO hinders the interaction between RPA70 and the ATR/ATRIP complex, thereby inhibiting checkpoint activation in response to RS. This inhibition is evidenced by an increase in γ-H2AX staining during the S phase, indicative of heightened RS. In addition, some studies have demonstrated that depletion of RPA activates the FA pathway to maintain genomic

stability, what suggests that FA-deficient cells would be hypersensitive to RPA inhibition, exhibiting selective cytotoxicity compared to FA-proficient cells. Jang and Kim findings confirmed that HAMNO-mediated RPA inhibition significantly compromises the maintenance and survival of FA-deficient cells; and when they used this RPA inhibitor in combination with cisplatin, HAMNO synergistically enhanced the cytotoxic effects of cisplatin in FA-deficient cells. Collectively, these results propose that targeting RPA inhibition may serve as an effective therapeutic strategy for tumors deficient in the FA pathway (Glanzer et al., 2014; Jang & Kim, 2022).

The XPF-ERCC1 heterodimer is another DDR signaling protein that has been highly studied during the last years. The importance of this protein inhibition lies in its relevant role in the repair of bulky DNA lesions and helix distortions induced by chemical agents or UV radiation; what explains that the inhibition of its activity has been shown to sensitize cancer cells to these agents (Jordheim et al., 2013; Elmenoufy et al., 2019, 2020).

In the context of cancer cells, which exhibit elevated levels of DNA damage and RS, CtIP is also a potential target for drugs that inhibit DNA repair proteins. Human CtIP facilitates homology-directed repair of DNA DSBs and safeguards stalled replication forks from nucleolytic degradation, what makes a promising candidate for targeted cancer therapy. In fact, in the study developed by Kuster and cowoekers, they suggest a peptide mimetic of the CtIP tetramerization motif as effective inhibitor of the CtIP activity (Kuster et al., 2021)

1.4.3. DNA damage effector proteins

To repair damaged double-stranded DNA ends, DNA ligase 4 (LIG4) is commonly recruited to sites of DNA damage along with XRCC4 and XLF. As DNA LIG4 plays a crucial role in the NHEJ repair pathway induced by radiation, its deficiency leads to a rare primary immunodeficiency disorder which renders individuals more susceptible to radiation-induced damage, neurological issues, bone marrow failure, and cancer. Research into LIG4 inhibitors holds promise for cancer treatment and some studies have shown that drugs like rabeprazole and U73122 can disrupt adenylate transfer, DNA re-linking, and impede the repair of DNA damage caused by ionizing radiation by selectively targeting LIG4. SCR7 has also been found to hinder LIG4-mediated DNA binding (Srivastava et al., 2012; Tseng et al., 2012; Tan et al., 2023).

The DNA ligase 1 (LIG1) has been also studied in this context. In fact, in ovarian cancer cell lines, depletion of LIG1 enhances platinum-induced cytotoxicity. In 2021 it was published a small molecule inhibitor called L82, that demonstrated SL in XRCC1-deficient ovarian cancer cells and 3D spheroids. Additionally, L82 exhibits selective toxicity in BRCA2-deficient and ATM-deficient cancer cells (Ali et al., 2021). Currently, this inhibitor is available for research uses (MedChemExpress).

Polθ (DNA polymerase theta, PolQ) is an effector protein on the HR and the alt-NHEJ pathway. The expression of this enzyme is highly coordinated, being upregulated in cancer cells in comparison with somatic non-cancerous cells. Accordingly, Polθ is an attractive SL drug target, mainly in HR deficient tumors. The development of inhibitors against this enzyme is a current goal, and ART558 is an example of small molecule inhibitor against BRCA-deficient tumors, whose use is also studied in PARPi resistant cases (Brown et al., 2017; Brambati et al., 2020; Zatreanu et al., 2021).

There are also current inhibitors that target the RAD51 recombinase family's protein-protein interactions. As its role is to facilitate the search of the homologous DNA sequences and to promote the strand exchanges between damaged and undamaged DNA molecules, an inhibitor of this protein may prevent RAD51-dependent HR in cells, leading to the accumulation of DNA damage and inducing cell death (Brown et al., 2017; Tan et al., 2023).

RAD52, a crucial component of the HR pathway, by its role in maintaining genome integrity, has been also study as a target in this field. Although single RAD52 mutations do not manifest notable phenotypes in mammals, their combination with mutations in genes associated with hereditary breast and ovarian cancers, such as BRCA1, BRCA2. Few years ago, small molecule inhibitors

of RAD52 were identify after conducted a high-throughput screen. Consequently, the compounds that specifically inhibit RAD52's biochemical activities, suppressed the growth of BRCA1 and BRCA2 deficient cells, and inhibited RAD52-dependent SSA in human cells. (Sullivan et al., 2015; Huang et al., 2016).

Flap endonuclease 1 (FEN1) is a crucial protein in the BER pathway and plays a significant role in Okazaki fragment maturation during DNA replication. Research has also implicated FEN1 in the regulation of other DNA repair pathways, such as HR and NHEJ. Abnormal expression or mutations in FEN1 can lead to a variety of pathological conditions, including cancers. Overexpression of FEN1 has been associated with drug resistance in several cancer types, suggesting that FEN1 is a promising therapeutic target for cancer treatment. In fact, several small-molecule inhibitors targeting FEN1 have been developed and shown to induce cancer regression, so targeting FEN1 has proven to be an effective strategy in both monotherapy and combination therapy for cancer (Yang et al., 2022).

1.5. Protein-protein interactions

The term protein-protein interactions (PPIs) refers to the physical contacts, either permanent or temporary, that arise from biomolecular forces between two or more proteins. It is estimated that there are between 130,000 and 650,000 different types of PPIs, which form a complex network called "interactome". Studies suggest that 15–40% of the human interactome is comprised of protein-peptide interactions. PPIs are highly specific although their binding affinity strength could vary. Due to their dynamic nature, PPIs can be regulated in response to cellular or environmental changes. These interactions play essential roles in many cellular processes, including signal transduction, enzyme regulation, cell proliferation, growth, differentiation, and apoptosis; so, the identification and characterization of some of them could reveal new therapeutic targets. The dysregulation of these interactions is therefore implicated in several human diseases, such as cancer, neurodegenerative disorders, autoimmune conditions, or infectious diseases (Skwarczynska & Ottmann, 2015; Bai et al., 2016; Macalino et al., 2018).

Initially, PPIs interfaces were perceived as a challenge because of their large (>1000 $Å^2$), shallow and hydrophobic surfaces. However, these interfaces were later elucidated through alanine scanning experiments, which revealed the importance of “hot spots” made up of tryptophan, isoleucine, arginine, and tyrosine residues. These elements, along with others like contact surface area, polarity, or flatness, are important in characterizing PPI interfaces (Macalino et al., 2018).

Improved understanding of druggability and molecular recognition in PPIs has enhanced efforts to find small molecule candidates for PPI-regulated pathways. The development of PPI modulators, however, is trailing behind that of conventional small molecule medications due to the complex structural optimization required to improve the pharmacokinetic properties and affinity of PPI ligands. The complexity of a PPI inhibitor is mostly determined by the interface's structure, which usually resembles that of its targets. Despite being hydrophobic, PPI ligands have a higher topological polar surface area than conventional medications. In addition, PPIs with grooves or small pockets usually work better than ones with scattered hot spot pockets over larger interfaces (Skwarczynska & Ottmann, 2015; Bai et al., 2016; Lu et al., 2023).

As such, PPI inhibitors require special assessment techniques because they are in a different chemical region from other types of small molecule inhibitors (Figure 9). Accordingly, several approaches are used for the discovery, design, and optimization of the PPI inhibitor. Some methods include the change of some peptides (peptidomimetic), the design of new proteins that can target the PPI surface with high affinity (high throughput screening, HTS/HTVS, or structure-based drug design, SBDD), or the use of fragment-based drug design (FBDD) to identify low molecular weight fragments that targets hot spot clusters. Additionally, because PPI binding site characteristics and ligand chemical space differ from those of typical protein targets, computational techniques have been used as a solution to fill in the blanks and enhance experimental approaches in the study of these challenging targets. Computer-based virtual screening is, therefore, a strong approach to find binding compounds using very large compound libraries at an acceptable cost-effectiveness. Structure-based virtual screening (SBVS) and

ligand-based virtual screening (LBVS) are the two categories in with virtual screenings could be divided. The main difference between both is the necessity of the 3D high-resolution, where SBVS molecule docking is ranked by the predicted affinity to the binding site; whereas the LBVS uses a native small molecule chemical scaffold or a functional ligand as a reference (Lawson et al., 2018; Macalino et al., 2018; Qiu et al., 2020).

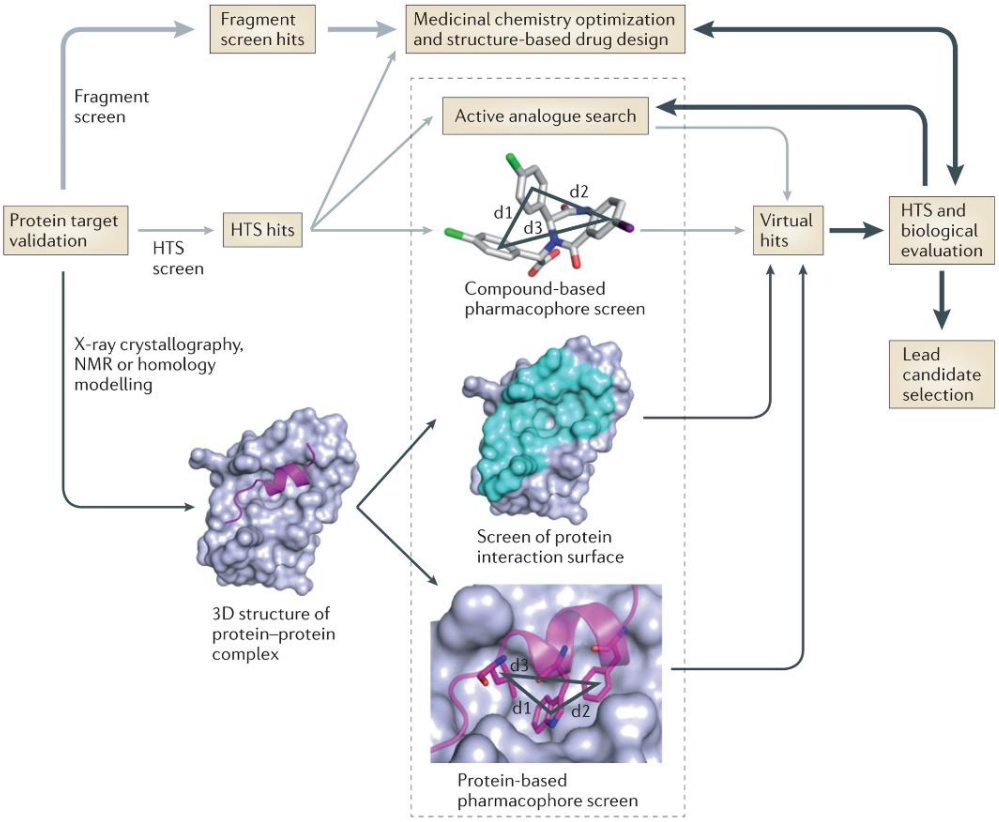


Figure 9. Drug discovery process and protein-protein interactions (PPIs). After the validation of the protein target, libraries of fragments or small-molecule compounds are screened to identify 'hits' that bind to the target protein and modulate the PPI. It is typical to employ a combination of fragment screening, high-throughput screening (HTS), and virtual screening (VS) in parallel, integrating the resulting data into the structure-based drug design and medicinal chemistry optimization process. Figure extracted from (Nero et al., 2014).

After the design, PPIs must be characterized and validated. There are several techniques that allow the identification, monitoring, and detailed characterization of PPIs. A variety of genetic, proteomic, biochemical, biophysical, and computational methods have been developed to enhance our understanding of protein interfaces. These methods can be broadly classified into three categories: *in vivo*, *in vitro*, and *in silico* techniques. The first ones are performed within the context of a living organism, including yeast two-hybrid (Y2H, Y3H) systems and SL approaches (Rao et al., 2014; Zhou et al., 2016; Titeca et al., 2019; Lu et al., 2020).

On the other hand, *in vitro* methods are conducted in a controlled environment outside a living organism, including tandem affinity purification, affinity chromatography, coimmunoprecipitation, protein arrays, protein fragment complementation, phage display, X-ray crystallography, and NMR (nuclear magnetic resonance) spectroscopy (Rao et al., 2014).

Biophysical techniques encompass also methods like fluorescence polarization, which detects changes in the rotation of a fluorophore-labeled protein upon binding; static and dynamic light scattering, which involves the interaction of light with a small particle or molecule; circular dichroism, with the measurement of dual polarization interferometry; isothermal titration calorimetry, which directly measures the heat change during protein binding; bio-layer

interferometry, which monitors biomolecular interactions by analyzing shifts in the wavelength of reflected light from a biosensor surface; and surface plasmon resonance (SPR), which measures refractive index changes upon analyte-ligand binding on a sensor chip surface (Rao et al., 2014; Zhou et al., 2016).

SPR is a label-free, real time, optical method based on the optimal measurement of changes in refractive index that occur when analyte molecules bind to bio-recognize sample that are immobilized on the SPR sensor. SPR biosensors have taken center stage as the primary instrument for studying biomolecular interactions in life science and drug discovery, and pharmaceutical research since the late 1990s (Piliarik et al., 2009; Olaru et al., 2015; Huo et al., 2023).

Proximity-based assays are also employed for PPI characterization. These include fluorescence resonance energy transfer (FRET), which detects non-radiative energy transfer between close-proximity fluorophores; homogeneous time-resolved fluorescence, combining FRET with time-resolved fluorescence measurement; bioluminescence resonance energy transfer, similar to FRET but based on a luciferase reaction; and amplified luminescent proximity homogeneous assay screen (AlphaScreen), a bead-based technology that detects energy transfer between beads bound to interacting proteins (Titeca et al., 2019; Lu et al., 2020; Sharp et al., 2020).

Finally, *in silico* methods are conducted using computer simulations and computational models. In silico methods for PPI detection encompass sequence-based approaches, structure-based approaches, chromosome proximity, gene fusion, in silico two-hybrid, mirror tree, phylogenetic tree, and gene expression-based approaches (Rao et al., 2014; Zhou et al., 2016; Titeca et al., 2019).

1.5.1. Small molecules as modulators in PPIs for cancer treatment

Nowadays, there are several examples of successful PPI modulators, such as the case of some MDM2-4/p53 interactors. The tumor suppressor gene *TP53* stands as the most prevalent mutational target in cancer, with mutations occurring in approximately 50% of human cancers, leading to the inactivation of the p53 protein. Acting as a transcription factor, p53 becomes active in response to various stressors like oncogenic triggers, oxidative stress, DNA damage, or metabolic imbalance, prompting the transcription of numerous genes aimed at suppressing tumor development (Zhang & Yan et al., 2022). Normally, p53 levels are kept low in unstressed cells by a negative feedback loop involving the MDM2 E3 ubiquitin-protein ligase, which marks p53 for degradation via the proteasome. Stressors like DNA damage or low oxygen levels disrupt the MDM2/p53 interaction, leading to p53 accumulation and activation. Taking that into account, restoring p53's tumor-suppressing role by inhibiting MDM2/p53 interaction presents a potential avenue for cancer treatment. Together with MDM2, MDM4 also cooperates in the negative regulation of p53, which explains the development of peptides and small molecules that interrupt this PPI. Some examples of that are nutlins, RG7112 (NCT00559533), idasanutlin (NCT02545283), or navtemadlin (NCT05797831) for MDM2/p53 interactions, and sulanemadlin (NCT02264613) for dual MDM2-4/p53 interactions (Shangary & Wang, 2009; Yu et al., 2009; Tisato et al., 2017; Kim et al., 2021; *clinicaltrials.gov*).

The inhibitors of BCL-2/BAX interactions are also studied in clinical assays. BCL family is involved in the regulation of the cell apoptosis: BCL-2 is an anti-apoptotic, meanwhile BAX is a pro-apoptotic protein. Accordingly, as the function of the pro-apoptotic proteins is blocked by the anti-apoptotic ones, a PPI modulator tip the scale to the pro-apopotic BAX, causing cell apoptosis. Navitoclax (NCT00887757, NCT00891605) and ruxoltinib (NCT04468984, NCT04472598) are examples of this type of modulators (Billard, 2012; Deng et al., 2022; *clinicaltrials.gov*). However, only venetoclax (Figure 10) is approved by the FDA and EMA (European Medicines Agency) for the treatment of chronic lymphocytic leukemia and small lymphocytic lymphoma (FDA and EMA websites).

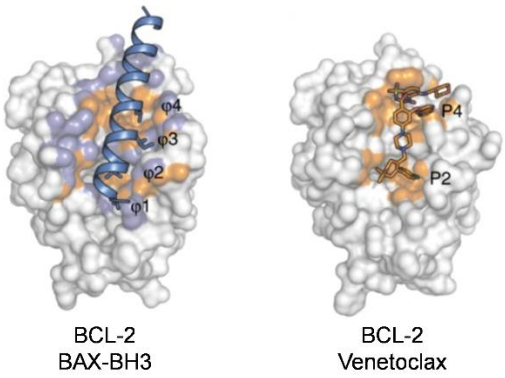


Figure 10. BCL-2 surface contacts with BAX-BH3 peptide and venetoclax, Structure of BCL-2 (PDB: 2XA0) with surface contacts colored according to interactions with BAX-BH3 peptide (slate) or venetoclax (orange). Key BCL-2 binding pockets (P2, P4) indicated for each compound and hydrophobic (ϕ) 1–4 residues from the BAX-BH3 peptide. Image adapted from Birkinshaw et al., (2019).

A significant class of endogenous negative regulators of apoptosis known as inhibitors of apoptosis proteins (IAPs) includes XIAP. One of the domains of XIAP binds to the proapoptotic protein caspase-9, inhibiting its activity and suppressing the apoptosis (Checinska et al., 2007). In the same way as happens with BCL-2/BAX, when a drug as Smac or tolinapart (NCT02503423, NCT05082259) interfere between XIAP and caspase-9, the inhibition of the apoptosis is suppressed, leading into the cell death (Sun et al., 2004; Kaminski, 2008; *clinicaltrials.gov*).

The heat shock protein 90 (HSP90) is a well-known eukaryotic chaperone that has many different substrates involved in various biological functions, such as cell survival and proliferation. HSP90 regulates its substrates protein their use of ATP, since many proteins depend on this activity, HSP90 inhibitors that block the binding site of the ATP could induce a heat-shock response, affecting cell survival. Keeping that in mind, inhibitors of HSP90/ATP interactions, such as tanespimycin (NCT00546780, NCT00514371) have been studied as PPI modulators. However, creating drugs that prevent HSP90 from interacting with its substrates or accessory proteins is thought to be a more difficult but possibly much more focused strategy. CDC37 is a HSP90 co-chaperone that is involved in cell cycle regulation and in protein folding and stability, thus the inhibition of the HSP90/CDC37 may inhibit the tumor growth and proliferation (Yoshimura et al., 2021; Tang et al., 2022; Dernovšek & Tomašič, 2023; Wang et al., 2024; *clinicaltrials.gov*).

MYC is a proto-oncogene that codifies for N-MYC, L-MYC and c-MYC, a highly conserved protein that is overexpressed in the majority of human malignancies (Singh et al., 2022). The activity of c-MYC is determined by the creation of the c-MYC/MAX dimer, which recognizes a DNA enhancer box and increases transcription of genes involved in cell division and proliferation. Consequently, the ratio of c-MYC/MAX expression controls whether a cell will divide and multiply (c-MYC/MAX). Lastly, it has been proposed that blocking the PPI between c-MYC and MAX, for example, may interfere with c-MYC dimerization and prevent the transcription or activation of oncogenes, which would have an anti-tumor effect. Numerous small compounds have been identified that have intriguing in vivo actions that obstruct c-MYC/MAX dimerization (Wang et al., 2015; Singh et al., 2021, 2022; Yao et al., 2022; Zhou et al., 2023; Atibalentja et al., 2024). In this sense, OmoMYC is one of such drugs targeting this dimerization pair, and it is currently being trialed (NCT04808362) (*clinicaltrials.gov*).

KRAS, NRAS and HRAS are RAS proteins, characterized by their on-off function as GTPases in the cell cycle. RAS proteins activate RAF1/MAPK/ERK and PI3K/PTEN/AKT/mTOR downstream signaling pathways, regulating cell growth, proliferation, differentiation, and survival processes. As these pathways are overactivated in carcinogenesis, the discovery of an effective RAS inhibitor would be interesting for cancer therapeutic. KRAS is one of the several RAS proteins that is frequently mutated in various malignancies, particularly in a significant percentage of pancreatic tumors (Luo et al., 2022). Accordingly, finding drugs that target KRAS signaling has grown importance in the fight against cancer, because KRAS can be inhibited primarily by targeting the downstream signaling pathway or preventing it from attaching to the plasma membrane

(Genovese et al., 2017; Luo et al., 2022; Fancelli et al., 2024). Taking into consideration that the guanine nucleotide exchange factors (GEFs) SOS1 and SOS2 convert KRAS from an inactive GDP-bound state to an active GTP-bound one, the inhibition of the KRAS/SOS1 interaction is a PPI modulator strategy that it is been studied during the last years. An example of an PPI inhibitor of this interaction is the small molecule BI-1701963, a SOS1 inhibitor that it is currently tasted in clinical trials (NCT04111458, NCT04627142, NCT04185883) (Hillig et al., 2019; Ikram et al., 2024; Stickler et al., 2024; *clinicaltrials.gov*).

The ubiquitin-proteasome system (UPS) is a fundamental mechanism in charge of protein degradation and recycling. For that reason, proteins are marked with ubiquitin molecules through ubiquitination, leading to their degradation by the proteasome. E1 (Ub-activating enzyme), E2 (Ub-conjugating protein), and E3 (Ub-protein ligase) are the three enzymatic components that carry out this procedure in a sequential cascade of enzymatic processes. As this pathway regulates key cellular functions and it is implicated in various diseases, targeting the UPS pathway holds therapeutic potential for modulating protein levels and cellular functions. SKP1 and SKP2 (S-phase kinase-associated protein 1-2) are two components of the SCF (Skp1-Cullin1-F-box protein) complex, which is an E3 ligase of the UPS pathway. SKP2/SKP1 interaction is necessary for SCF assembly, which affects a number of physiological functions including signaling pathways, apoptosis, and cell cycle progression. The blocking of this PPI prevents the formation of the complex and thus, inhibits the tumor growth. SZL-P1-41 compound was published as a small molecule inhibitor of SKP2 (Bornstein et al., 2006; Wu et al., 2020; Xie et al., 2023).

Immune responses against infections, allergens, and malignancies are coordinated by T-cells, which are activated by co-stimulatory signals, as well as antigenic stimulation. Co-stimulatory and co-inhibitory pathways are essential for deciding how T-cell signaling ends, and in this context, there is a crucial co-stimulatory pathway called the CD40/CD40L pathway. This interaction promotes the activation of T-cells and causes the production of genes that boost the inflammation; but it also contributes to the development of cancers, as evidenced by the increased expression of CD40 in a variety of tumor types (Strohm et al., 2024; Tian et al., 2024). Therefore, there is therapeutic promise for cancer, immunological rejection, diabetes, and atherosclerosis disorders by targeting the CD40/CD40L pathway. Antibodies as bleselumab, lucatumumab and dacetuxumab have been tested in clinical trials such as small molecules as suramin or some organic dyes (Kosaka et al., 2014; Kim et al., 2015; Bojadzic & Buchwald, 2018; Pandey et al., 2021; Ngo et al., 2024; Vermersch et al., 2024).

Another important PPI that could be inhibited as a potential tumor treatment is PD-1/PD-L1. PD-1 (programmed cell death protein 1) is a T-cell immunosuppressive receptor that promotes the maturation of the lymphocytes of the immune response. The L1 ligand is expressed in several cell types, including multiple cancer cells (Pandey et al., 2021). Therefore, when PD-L1 tumor cell attaches to PD-1 cells, it stops PD-1 T-cell from activating, triggering a suppression of the immune system's surveillance for the tumor escape (immune exhaustion). PD-1/PD-L1 inhibitors include monoclonal antibodies, peptides and small molecules. Although the antibody pembroluzimab is FDA and EMA approved for the treatment of various types of cancer, including melanoma, non-small cell lung cancer (NSCLC), head and neck squamous cell carcinoma (HNSCC), among others; the development of the small molecules is a complex and lengthy process. In 2015, Chupak and Zhen disclosed the patents WO2015034820A1 and WO2015034820A2, followed by Yeung et al. in 2017 with WO2017066227A1 and WO2018044963A1 in 2018 (Abdel-Magid, 2015). Finally, in 2021 it was published a small molecule that targets PD-L1 and VISTA (V-domain Ig suppressor of T cell activation) pathways, called CA-170, that is being tested in a clinical trial (NCT02812875) (Cai et al., 2021; Chen et al., 2024; Syamsu et al., 2024; Yin & Ren, 2024; *clinicaltrials.gov*).

1.6. Fanconi anemia /BRCA pathway

ICLs represent hazardous DNA lesions that hinder the separation of DNA strands within the double helix by forming covalent bonds between them. This impairs essential cellular processes like transcription and replication, potentially leading to significant chromosomal abnormalities such as deletion or amplification, as well as DNA breaks and rearrangements. During active

genome duplication, the DNA replication machinery acts as a sensor for ICLs, activating DNA damage checkpoints and initiating repair processes. In S-phase cells, HR and TLS pathways are predominantly employed for ICL repair, together with the FA pathway (Bhattacharjee & Nandi, 2017).

The FA pathway is a DNA repair pathway that identifies and removes DNA ICLs, incorporating steps of recognition and unhooking, TLS, HR and NER. As a result, there is a lot of overlap between the FA pathway's components and other DNA damage repair pathways. Until now, there are at least 23 FA proteins identified that have been recognized through genetic mutations resulting in loss of function of the pathway and hence susceptible to FA, a rare autosomal and X-linked genetic disease characterized by bone marrow failure (BMF), congenital defects, and increased cancer predisposition (Bogliolo & Surrallés, 2015; Schwab et al., 2015; Niraj et al., 2019; Taylor et al., 2020; Peake & Noguchi, 2022).

ICL repair is initiated when a replicating fork encounters a lesion on the DNA, triggering DNA repair mechanisms. In eukaryotes, the FA pathway coordinates the detection and removal of the ICL by the combined actions of structure-specific endonucleases, that create incisions flanking the ICL, followed by TLS and HR-mediated replication fork restart, which facilitate the rescue of stalled forks (Figure 11) (Bhattacharjee & Nandi, 2017; Niraj et al., 2019).

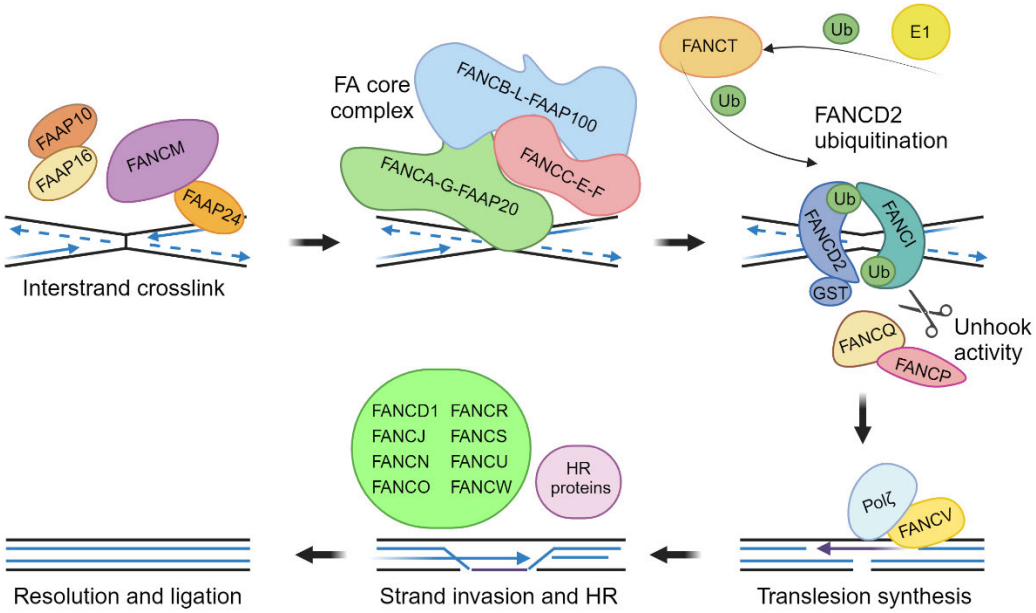


Figure 11. Schematic representation of the Fanconi anemia (FA) pathway. The FA pathway is initiated by the recognition of DNA ICLs and other types of DNA damage. This triggers the assembly of the FA core complex. Activation of the FA core complex leads to the monoubiquitination of FANCD2 and FANCI. Monoubiquitinated FANCD2-FANCI complexes serve as platforms for recruiting downstream repair proteins, facilitating the repair of DNA damage, particularly ICLs, through processes such as NER, TLS and HR pathways.

FA proteins, which are the main participants in the pathway, have been identified through genetic mutations that cause the pathway to stop functioning and increase a person's risk of developing FA. There are 23 genes discovered until now: *FANCA, FANCB, FANCC, FANCD1 (BRCA2), FANCD2, FANCE, FANCF, FANCG (XRCC9), FANCI, FANCJ (BRIP1* or *BACH1), FANCL, FANCM, FANCN (PALB2), FANCO (RAD51C), FANCP (SLX4), FANCQ (ERCC4), FANCR (RAD51), FANCS (BRCA1), FANCT (UBE2T), FANCU (XRCC2), FANCV (MAD2L2* or *REV7), FANCW (RFWD3),* and *FANCY* (FAAP100); and some FA-associated proteins (FAAP10, FAAP16, FAAP20, FAAP24) (see section 1.8.- Table 2) (Taylor et al., 2020).

FANCA and FANCG are essential for the localization of the FANC core complex; and it seems that FANCM also participates in this localization. After the initiation of the repair, the FA core complex, comprised by seven FANC proteins and two of the FA-associated proteins FAAP20 and FAAP100, binds the ICL site. FANCB-FANCL-FAAP100 (BL100) assemble in a complex that provides the catalytic ubiquitin ligase activity and forms a scaffold for other subcomplexes. The FANCC-FANCE-FANCF (CEF) complex tie down on the BL100 complex and transfers the FANCI-FANCD2 complex substrate to the FANCL ligase. FANCL is a monomeric RING E3 ligase with interacts with the E2, FANCT, to ubiquitinate FANCD2 (Figure 12) (Shakeel et al., 2019).

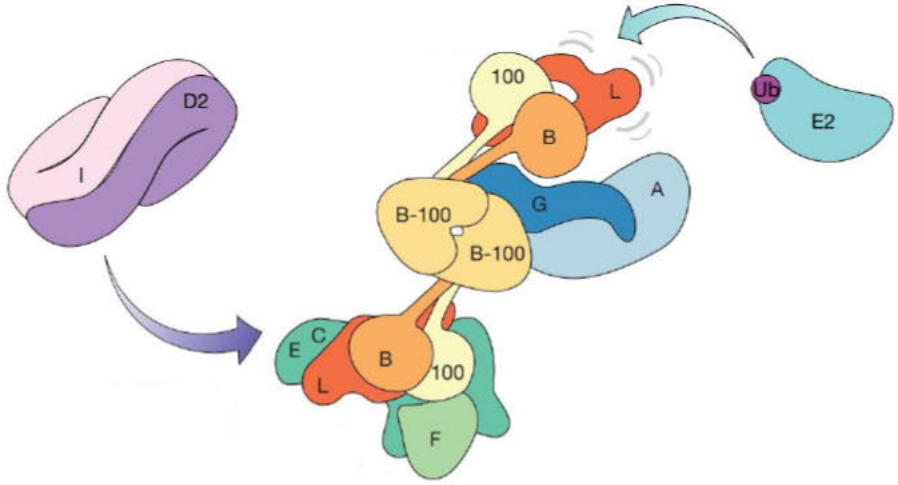


Figure 12. Schematic representation of the Fanconi anemia (FA) complex structure. The FA core complex consists of seven FANC proteins along with the FA-associated proteins FAAP20 and FAAP100 (also known as FANCY). The FANCB-FANCL-FAAP100 (BL100) subcomplex provides the catalytic ubiquitin ligase activity and forms a scaffold for the assembly of additional subcomplexes. The FANCC-FANCE-FANCF (CEF) complex binds to the BL100 complex and facilitates the transfer of the FANCI-FANCD2 complex to the FANCL ligase. FANCL, a monomeric RING-type E3 ligase, interacts with the E2 enzyme FANCT to ubiquitinate FANCD2. Figure extracted from Shakeel et al., 2019.

It is believed that monoubiquitinated FANCI and FANCD2 aid in the DNA cutting and repair process downstream (Alcón et al., 2020). As was explained by Bogliolo et al., ATR-mediated phosphorylation of H2AX is required for FANCD2 relocation to damaged sites. Thus, the stalled replication forks activate ATR, which phosphorylates H2AX and FANCD2; and phosphorylated FANCD2 is then monoubiquitinated by FANCL (Bogliolo et al., 2007). Once the FANCD2/FANCI complex is monoubiquitinated, it promotes the accumulation of the nucleases at the damage sites (Cole et al., 2010; Hodson et al., 2014). The FANCQ nuclease is the essential protein that make incisions around the lesion (unhooking activity), with the help of FANCP, a protein scaffold for MUS81 and SLX4 nucleases (Bogliolo et al., 2013). Once the lesion is unhooked, TLS proteins can use the DNA synthesized across it by Polζ, a specialized translesion polymerase that includes FANCV. Other proteins that participate in the HR during the ICL repair are FANCD1, FANCJ, FANCN, FANCO, FANCR, FANCS, FANCU, and FANCW (Bogliolo et al., 2018; Cole et al., 2010; Hodson et al., 2014; Chaugule et al., 2020; Jeong et al., 2020; Tan et al., 2020).

1.6.1. The role of FA pathway in replicative stress

FA pathway is increasingly recognized for its role in mitigating RS. The FA pathway responds to RS induced by agents like hydroxyurea (HU), exhibiting different functions under low and high levels of stress. Key FA proteins, FANCD2 and FANCI, protect stalled replication forks and promote new origin firing. Upon replication fork stalling, FANCD2-FANCI dimers (ID2) are recruited to chromatin, where they encircle DNA and undergo monoubiquitination. Although ID2 clamp closure is independent of FANCD2 monoubiquitination, this modification stabilizes the

clamped state. Under low stress, monubiquitinated FANCD2 recruits BLM helicase complex to restart stalled replication forks. While at high stress levels, FANCD2, FANCI, and other FA core complex proteins collectively stabilize forks and promote replication restart. FANCD2 also plays a role in protecting stalled replication forks from unwanted degradation by MRE11, particularly in BRCA1/2-deficient cells (Niraj et al., 2019; Brunner et al., 2023).

The involvement of monoubiquitinated ID2 in maintaining common fragile sites, is noteworthy. Common fragile sites are specific regions of the genome that are prone to forming gaps or breaks under conditions of RS, such as during DNA replication. These sites are termed "fragile" because they are more susceptible to DNA damage and chromosomal instability compared to other genomic regions. Accordingly, these regions are prone to chromosomal abnormalities like translocations and sister chromatid exchanges, often associated with malignancies. During mitosis, under-replicated common fragile sites can form ultrafine bridges between chromatids, which, if not resolved properly, can lead to chromosomal breakage and micronuclei formation, contributing to chromosomal instability. FANCI and FANCD2 play crucial roles in targeting the BLM complex to ultrafine bridges between chromatids, facilitating their processing, and preventing micronucleation (Figure 13) (Niraj et al., 2019).

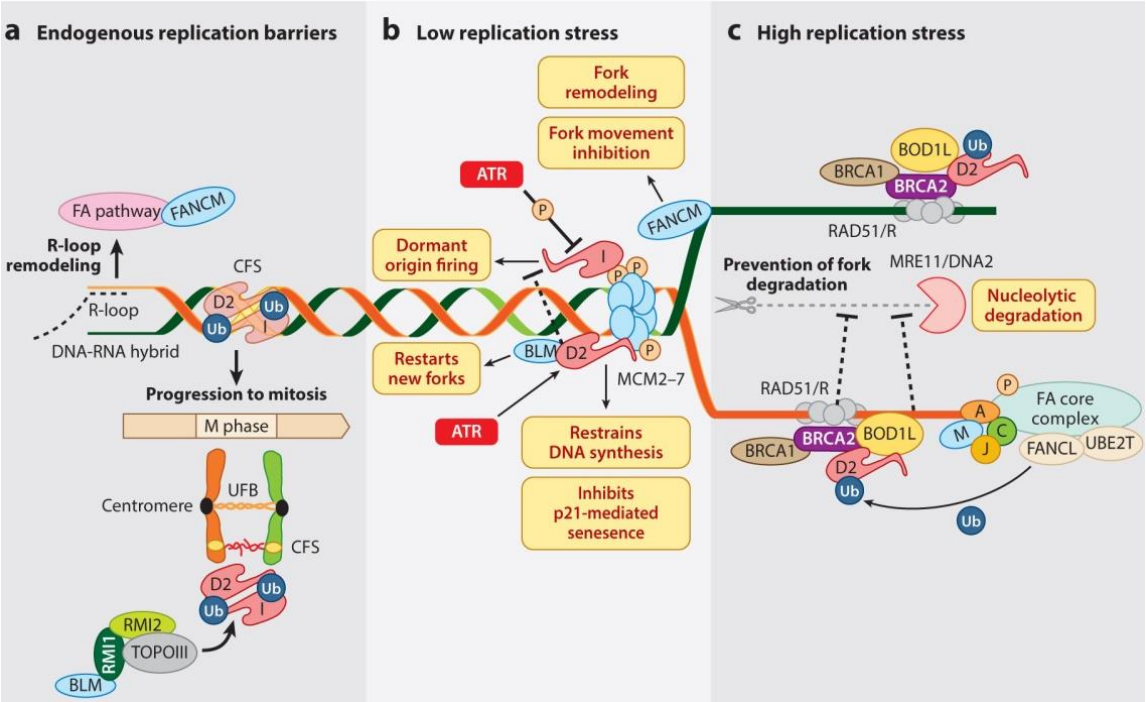


Figure 13. Roles of FA proteins in replication stress. A. The FANCI-FANCD2-Ub complex stabilizes extracentromeric chromosomal fragile sites and facilitates the loading of the BLM complex. This ensures their protection, repair, and uninterrupted mitosis. Additionally, components of the FA pathway remodel endogenously produced R-loops (RNA-DNA hybrids) at susceptible genetic loci. **B.** During low doses of RS, non-ubiquitinated FANCD2 binds to and inhibits the MCM2–7 helicase complex, restraining DNA synthesis. ATR kinase promotes the binding of FANCD2 to MCM 2–7, preventing p21-mediated cellular senescence by limiting the accumulation of ssDNA. FANCI also interacts with MCM2–7 to activate dormant origins, but this firing is inhibited by phosphorylation of FANCI by ATR kinase and the FANCD2-BLM complex. FANCM opposes fork movement, potentially by remodeling stalled replication forks. **C.** High doses of replication stress trigger the classical FA pathway. FANCA, FANCC, FANCJ, FANCM, along with BOD1L, bind to nascent DNA strands, safeguarding them from unwanted nucleolytic degradation mediated by MRE11 or DNA2. RAD51-ssDNA filaments on stalled replication forks are shielded by BRCA1, BRCA2, and FANCD2-Ub against nucleases. Figure extracted from Niraj et al., 2019.

The FA pathway modulates DNA damage signaling via interactions with the ATM, ATR, and CHK1 kinases. Upon DNA damage, FA proteins are phosphorylated, influencing cell cycle progression and checkpoint responses. Specifically, ID2 phosphorylation by ATM is crucial for establishing the intra-S checkpoint and proper cellular response to DSBs induced by ionizing radiation. Furthermore, the FA pathway intersects with ATR-mediated checkpoint signaling, as was explained before, evidenced by colocalization of FANCD2 and ATR in nuclear foci following exposure to DNA cross-linking agents. ATR-mediated phosphorylation of FANCD2 on threonine 691 and serine 717 is essential for ID2 monoubiquitination and the correction of sensitivity to certain DNA damaging agents in FANCD2-deficient cells. Notably, disruptions in proteins involved in the FA pathway, such as FANCM or FAAP24, adversely affect ATR-mediated checkpoint signaling, with clinical implications seen in conditions like Seckel's syndrome, which shares phenotypic similarities with FA. Additionally, CHK1, a substrate of both ATM and ATR, phosphorylates FANCE and FANCD2, contributing to cellular resistance against certain DNA damaging agents. Increased CHK1 activity is associated with early marrow failure, and its downregulation may promote leukemogenesis in certain contexts (Bogliolo et al, 2007; Longerich et al., 2014).

Removal of the monoubiquitinated ID2 complex from chromatin is facilitated by the deubiquitinating enzyme USP1-UAF1 (ubiquitin-specific protease 1 and its associated factor), although the mechanism of action remains unclear. Persistent presence of the ID2 complex, even in its di-monoubiquitinated (USP1-resistant) state, can exacerbate DNA damage during RS, potentially leading to genome instability (Nijman et al., 2005). In addition, Brunner et al., have emphasized in the importance of rapid removal of the ID2 complex to prevent replication obstacles. Depletion of FBXL12 and accumulation of FANCD2 on chromatin hinder replication fork progression and increase the proportion of stalled replication forks, contradicting previous reports of FANCD2 inhibiting dormant origin firing. This discrepancy may be attributed to elevated levels of FANCI resulting from stable FANCD2-FANCI heterodimer formation and the varying cell contexts influencing dormant origin firing (Brunner et al., 2023).

Furthermore, while both CHK1 and FANCD2 are involved in ATR signaling and DNA RS, they serve distinct functions. CHK1 facilitates polyubiquitination of FANCD2 by FBXL12, a protein that belongs to the F-box family of proteins, which are components of the SCF ubiquitin ligase complex. This polyubiquitination targets FANCD2 on chromatin for removal to enable replication recovery under favorable conditions. In fact, elevated levels of FBXL12 and FANCD2 are observed in aggressive malignancies susceptible to high RS, correlating with unfavorable patient outcomes. That opens the opportunity to study FBXL12 as a critical regulator of DNA RS and as a potential target for cancer therapy in contexts of high RS (Brunner et al., 2023).

1.7. [redacted]

1.7.1. [redacted]

[redacted]

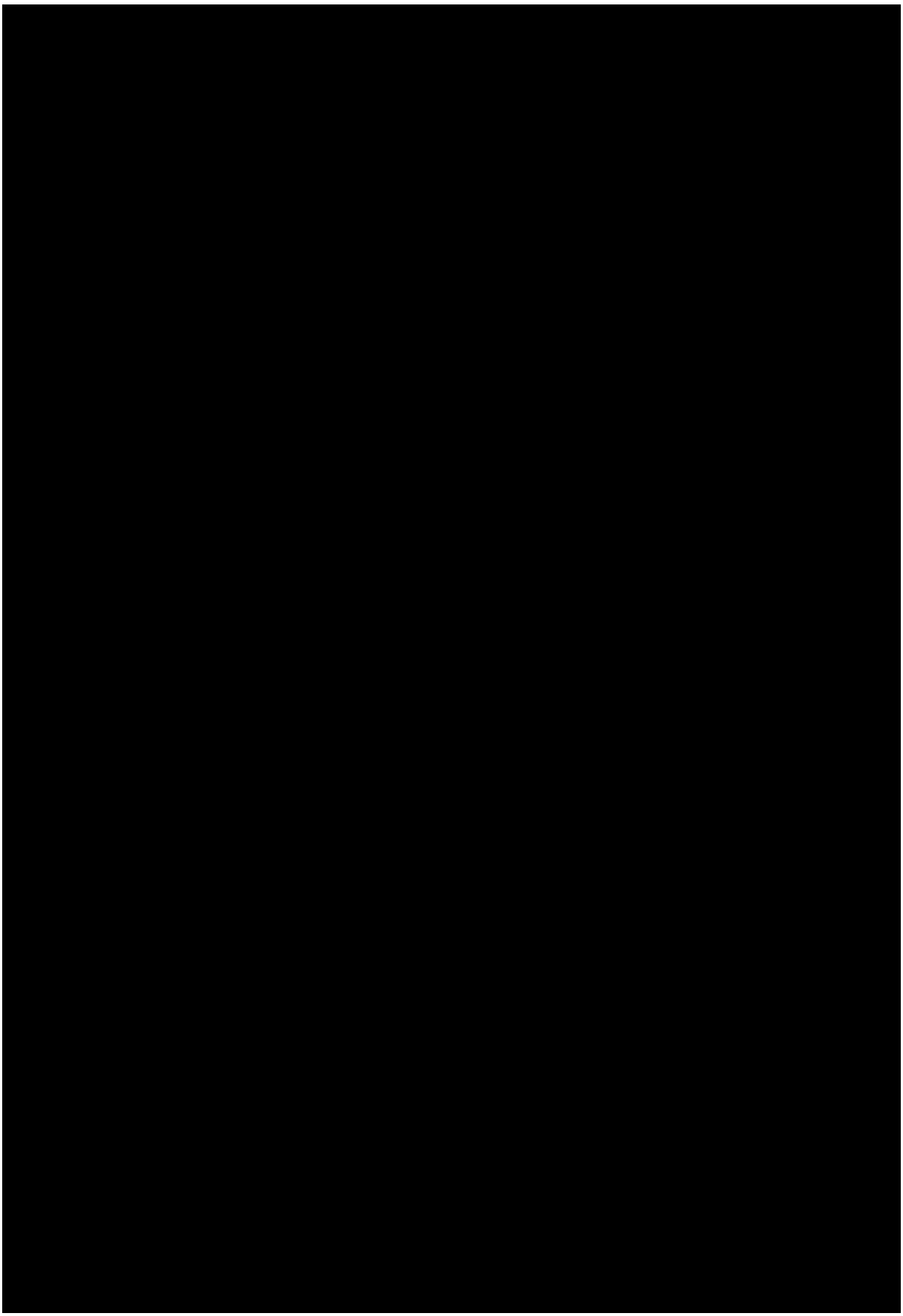
[redacted].

1.7.2. [redacted]

[redacted]

[redacted]

Table 1.[redacted]



[redacted]

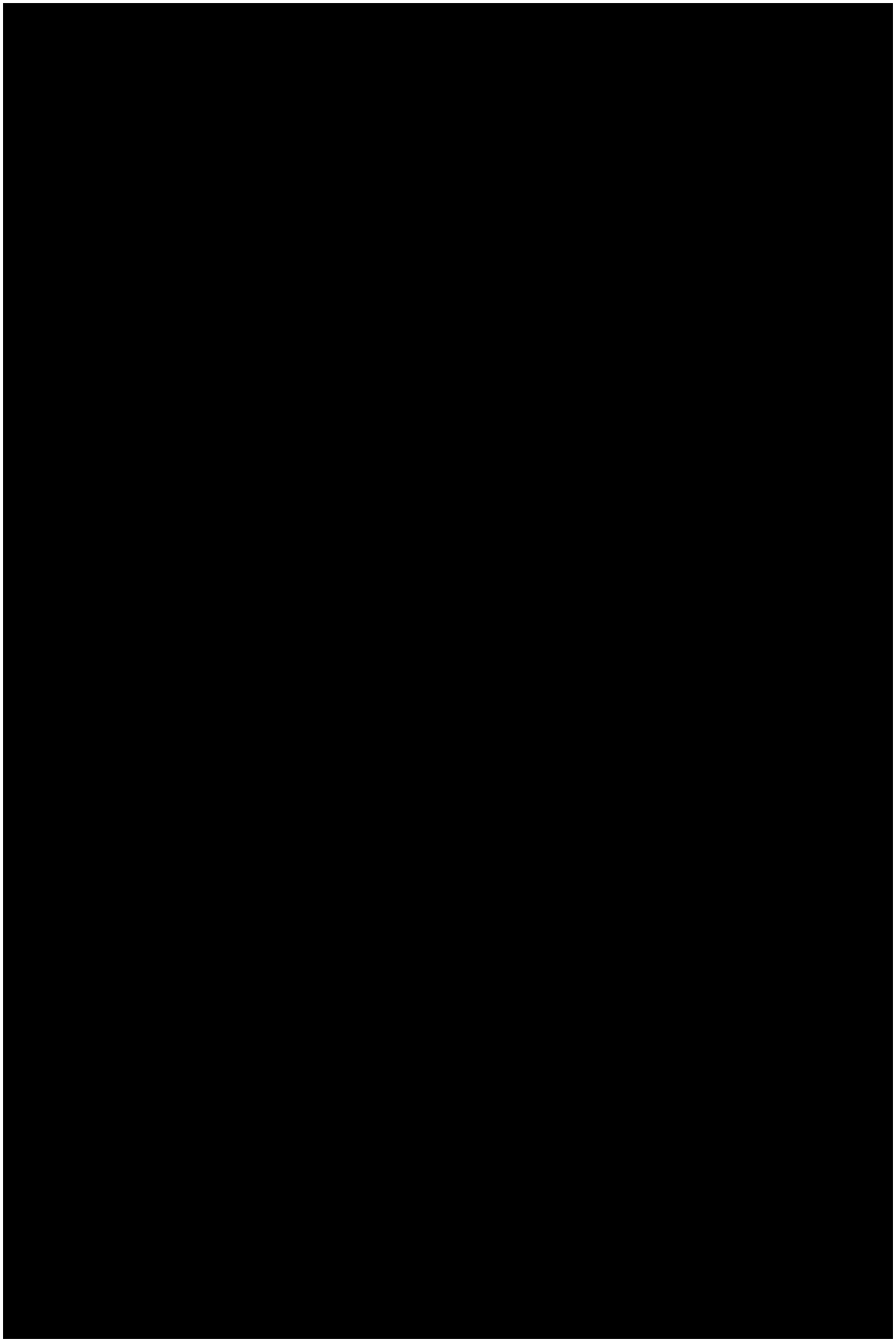


Figure 14. [redacted]

[redacted]

1.8. Fanconi anemia disease

FA is a rare genetic syndrome described in 1927 by the pediatrician Guido Fanconi, that nowadays affects 1 in 130,000-160,000 newborns worldwide (Minguillón & Surrallés, 2018; Lee et al., 2021;). This disease could be caused by X-linked (FANCB), monoallelic (FANCR), or biallelic mutations in one of the 23 genes discovered until now. However, the most mutated gene in cases of FA is FANCA (60–80% of cases), followed by FANCC (10–15%), and FANCG (10%) (Patel & Joenje, 2007; Green & Kupfer, 2009; Bogliolo et al., 2020; Lee et al., 2021).

Table below describe the 23 FA genes, their function, worldwide mutation frequency (Freq.) in patients and inheritance (Che et al., 2018; Niraj et al., 2019; Bogliolo et al., 2020; Taylor et al., 2020).

Table 2. FA genes classification.

	FA name	Other names	Function	Freq. (%)	Inheritance
FA proteins	FANCA		Functions in the AG20 subcomplex with FANCG to promote FA core complex localization and translocation	60-80	Autosomal recessive
	FANCB		Functions in the BL100 subcomplex with FANCL to improve efficiency of FANCD2/I ubiquitylation and provide structural scaffold	2	X-linked recessive

	FANCC		Component of the CEF subcomplex with FANCE, FANCF to stabilize interactions between FANCD2/I complex and FA core complex and improve ubiquitylation efficiency	10-15	Autosomal recessive
	FANCD1	BRCA2	Recruitment of RAD51 to ssDNA	2	Autosomal recessive
	FANCD2		Initiates unhooking by nucleases	4	Autosomal recessive
	FANCE		Component of the CEF subcomplex with FANCC, FANCF to stabilize interactions between FANCD2/I complex and FA core complex and improve ubiquitylation efficiency	1	Autosomal recessive
	FANCF		Component of the CEF subcomplex with FANCC, FANCE to stabilize interactions between FANCD2/I complex and FA core complex and improve ubiquitylation efficiency	2	Autosomal recessive
	FANCG	XRCC9	Functions in the AG20 subcomplex with FANCA to promote FA core complex localization and translocation	8	Autosomal recessive
	FANCI		Initiates unhooking by nucleases	1	Autosomal recessive
	FANCJ	BRIP1/ BACH1	Regulates pathway choice between TLS and HR repair	2	Autosomal recessive
	FANCL		Component of the BL100 subcomplex and E3 ubiquitin ligase controlling monoubiquitylation of FANCD2/I	0.4	Autosomal recessive
	FANCM		Binds FA core complex to chromatin at ICL sites	0.1	Autosomal recessive
	FANCN	PALB2	Mediates loading of BRCA1/2 complex on to single stranded DNA	0.4	Autosomal recessive
	FANCO	RAD51C	RAD51 nucleoprotein filament assembly	0.1	Autosomal recessive
	FANCP	SLX4	Recruits and regulates nuclease activity during unhooking	0.5	Autosomal recessive
	FANCQ	ERCC4/ XPF	Key endonuclease mediating incision of crosslink during unhooking	0.1	Autosomal recessive
	FANCR	RAD51	Forms nucleoprotein filaments which mediate template homology search and strand exchange	0.1	Autosomal dominant
	FANCS	BRCA1	CMG helicase eviction, HR pathway promotion and TLS inhibition in complex with FANCJ, complex formation with BRCA2 during HR	0.1	Autosomal recessive
	FANCT	UBE2T	E2 ubiquitin ligase controlling monoubiquitylation of FANCD2/I	0.1	Autosomal recessive
	FANCU	XRCC2	RAD51 nucleoprotein filament assembly	0.1	Autosomal recessive
	FANCV	MAD2L2/ REV7	Subunit of the TLS extension polymerase POLζ	<0,1	Autosomal recessive
	FANCW	RFWD3	Mediates RPA dynamics to promote HR	<0.1	Autosomal recessive
	FANCY	FAAP100	Functions within the BL100 subcomplex to provide structural scaffold	-	Autosomal recessive
FA-associated proteins	FAAP10	MHF2/ CENPX/ SRA13	Localization of FANCM to chromatin	-	
	FAAP16	MHF1/ CENPS/ APITD1	Localization of FANCM to chromatin	-	
	FAAP20		Promotes stability of the AG20 subcomplex	-	
	FAAP24		Associates with FANCM to mediate DNA binding of the FA core complex	-	

Mutation of one of FA genes may result in a rare inherited FA syndrome. However, the frequency depends on the country: the carrier frequency in the United States is estimated at 1:181, but is significantly higher in Israel at approximately 1:93, because of the Ashkenazi Jews; and 1:70 in the Spanish Gypsies (Callen et al., 2005; Bogliolo et al., 2020; Lee et al., 2021). Therefore, FA is more prevalent in certain populations, including Ashkenazi Jews, Spanish Gypsies, and Afrikaners. Many FA patients exhibit BMF, increased incidence of cancer, and characteristic congenital abnormalities, including short stature, skeletal malformations (particularly of the upper extremities), abnormal skin pigmentation, decreased fertility, and renal anomalies.

However, FA is highly heterogeneous, with different FANC mutations leading to a wide range of clinical syndromes. Taking that into consideration, some of the FA genes have been proposed to be FA-like genes, as patients with these mutations do not develop anemia (BMF). Among these proposed FA-like genes it can be found: FANCM, FANCR, FANCS, and FANCO (Figure 15) (Bogliolo & Surrallés, 2015).

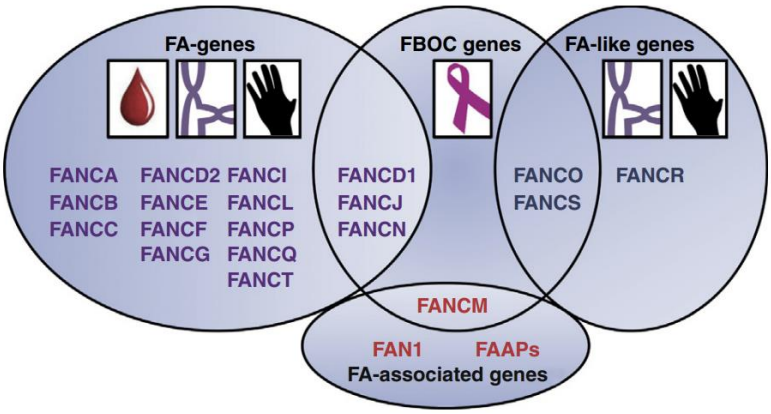


Figure 15. FA related genes. Biallelic mutations of 15 genes listed in purple (FA-genes: *FANCA, B, C, D1, D2, E, F, G, I, J, L, N, P, Q, T*) cause FA. Biallelic mutations in the three genes listed in blue (FA-like genes: *FANCO, R, S*) cause a similar condition (FA-like syndrome) without bone marrow issues. Several other genes (*FAAP20, 24, 100*, *250*) are linked to FA, but biallelic mutations do not seem to cause the typical FA disease. Notably, *FANCM* should belong to that group. Mutations in just one copy of six FA genes (FBOC genes: *FANCD1, J, M, N, O, S*) increase the risk of breast and ovarian cancer in families. Figure extracted from Bogliolo & Surrallés, 2015.

FA/BRCA DNA repair pathway includes a core complex, ID2 and effector proteins responsible for repairing DNA damage from ICL lesions, which lead to stalled DNA replication forks. As a result, cells from FA patients demonstrate a pronounced hypersensitivity to clastogenic agents such as MMC, diepoxybutane (DEB), HU, and cisplatin. This hypersensitivity is characterized by distinctive cellular markers unique to FA, including increased chromosomal breakage and the presence of multiradial figures.

Defective DNA repair results in impaired BM function, cytopenias, and ultimately BMF, which affects 80% of FA patients within the first decade of life. In fact, despite of the low incidence of the syndrome, FA is the most common genetic cause of bone marrow failure. FA is also marked by a predisposition to cancer: FA patients frequently develop hematologic malignancies, particularly myelodysplastic syndrome and acute myelogenous leukemia, with cumulative incidence of approximately 20% by age 20 and 30% by age 30 (Ramírez et al., 2020). The incidence of solid tumors similarly increases with age, reaching approximately 40% by age 40 (Green & Kupfer, 2009; Kee & D'Andrea, 2012; Bogliolo & Surrallés, 2015; Minguillón & Surrallés, 2018;). FA patients have a markedly higher incidence of head and neck, esophageal, and vulvar squamous cell carcinomas. The risk of developing head and neck squamous cell carcinomas (HNSCC) in FA patients is especially high, with an increase of 500–800 fold versus non-FA population (Errazquin et al., 2021; Lee et al., 2021).

While most FA diagnoses are made before the development of HNSCC, the phenotypic variability of FA mandates a heightened level of suspicion in teenagers or young adults who develop HNSCC unexpectedly. The presentation of FA-related cancer and DNA damage susceptibility without bone marrow failure might be due to differences in genetic alterations in the FA pathway, genetic modifiers, or mosaicism. In fact, somatic mosaicism in hematopoietic cells, also called "natural gene therapy", occurs in some FA patients due to a reversion or compensatory mutation in hematopoietic cells that restores the FA/BRCA pathway. In mosaic patients, there are typically distinct populations of hematopoietic cells that are either sensitive or resistant to ICL DNA-damaging agents. Patients with mosaicism have been reported to lead to spontaneous correction of BMF, sometimes resulting from reversion or compensatory mutations in hematopoietic stem and progenitor cells (HSPCs). In fact, some studies suggests that mosaicism may be associated with a lower incidence of BMF or hematologic malignancies, reduced need for allogeneic hematopoietic stem cell transplantation (HSCT), and relatively lower mortality during the first 2-4 decades of life, compared to non-mosaic FA patients (Ramírez et al., 2020, 2021; Persico et al., 2023).

Despite of the significant advancements in HSCT protocols, not all FA patients have access to transplantation or are suitable candidates, and compatible donors may be lacking. In cases where transplantation is not feasible, in vitro fertilization combined with preimplantation genetic diagnosis offers a potential solution to generate compatible human leukocyte antigen-identical offspring, providing a donor for affected siblings. Alternatively, androgen administration (oxymetholone, oxandrolone, danazol) may be used as a palliative measure to improve low blood counts. While 50-70% of patients exhibit a positive response to treatment, less than 20% tolerate it long-term, with many experiencing side effects such as virilization and liver toxicity. However, during the last 30 years, the advances in the field of the HSCT have been overcoming and more than 50 clinical studies have been conducted in FA population; and thanks to the improvement of the transplantation techniques, life expectancy of the FA patients has increased up in the last ages. The majority improved techniques have been focused from the transplantation of allogenic HSCs from healthy donors and the innovation of these protocols to the new gene modification therapies (Bueren et al., 2003; Río et al., 2019; Sevilla et al., 2021). Actually, the use of gene therapy to correct stem cells has a great potential to replace HSCT in FA patients, due to the side effects associated with the allosteric transplant or the difficult access to a compatible donor. Building on lessons from earlier studies, gene therapy approaches for FA have been refined, culminating in the first successful outcomes in 2019 with the FANCOLEN-1 (NCT03157804) trial for FANCA patients with BMF. This phase I/II clinical trial involved a short ex vivo transduction of a safe, integrative lentiviral vector for FANCA into CD34+ HSCs sourced from the patients' BM or mobilized peripheral blood, followed by reinfusion without conditioning. At 24 months post-reinfusion, significant increases in the percentage of corrected cells in both peripheral blood and bone marrow indicated stable engraftment across all subjects, with higher success rates in those receiving a greater number of HSPCs. The proliferative advantage of corrected cells over FA cells was linked to normalized cellular phenotypes, with no leukemogenesis events reported (Río et al., 2019; Sevilla et al., 2021). These findings correlated with halted BMF progression, despite modest increases in peripheral blood cell counts, suggesting a gradual, long-term hematological recovery similar to the phenotypic rescue observed in FA mosaic individuals. Additionally, ongoing monitoring of FANCOLEN-1 participants aims to evaluate the efficacy and safety of the ex vivo gene therapy approach over a 15-year period post-treatment.

Following the success of FANCOLEN-1, numerous other clinical trials have been initiated with the goal of increasing the number of corrected HSCs, employing non-genotoxic conditioning regimens, and improving the hematological response to chemotherapy in gene therapy-treated patients, particularly in the context of solid tumors. These advancements reflect significant progress in the development of gene therapy for FA, offering a promising therapeutic avenue while continuing to address existing challenges and limitations.

As people with FA are extremely vulnerable to radiation and chemotherapy, the treatment of solid tumors is still a challenge (Minguillón & Surrallés, 2018). Additionally, a significant concern is associated with HSCT and its indirect and direct impact on the development of solid tumors. Although modern HSCT protocols have enabled more FA individuals to overcome hematological anomalies and reach adulthood, this comes at the cost of increased age-related risk of solid tumors. The extended lifespan of transplanted patients also has shed light on the long-term effects of chemotherapy agents used in HSCT conditioning regimens and graft-versus-host disease (GVHD) risk. FA patients who undergo HSCT and develop GVHD have an elevated risk of developing HNSCCs, with a 4.4-fold higher incidence compared to non-transplanted individuals. Consequently, transplanted FA patients have a more than 500-fold increased likelihood of developing HNSCCs compared to healthy individuals. Furthermore, as FA oncology patients are ineligible for conventional anti-cancer therapies due to their heightened susceptibility to chemotherapy and radiation, surgical resection remains the only viable option for achieving favorable outcomes at early tumor stages. When malignancies are diagnosed late, palliative treatments such as surgery and low-dose chemotherapy/radiation have limited efficacy (Minguillón & Surrallés, 2018; Ramírez et al., 2020; Lee et al., 2021).

1.8.1. Head and neck squamous cell carcinomas

The most frequent solid tumors in these population are HNSCC, which incidence in FA population is between 500-800 fold higher than in non-FA, with an increased incidence after bone marrow transplantation. 35-75% of the cases develop when the patient is 30-45 years old, presuming an important matter that should be considered (Minguillón & Surrallés, 2018; Lee et al., 2021).

Although human papillomavirus (HPV) infection is a known factor in the development of HNSCC, the evidence in FA SCC (squamous cell carcinoma) is unclear. In fact, in Webster and coworkers publication, after the study of 55 FA SCC tumors, no HPV sequences were found in the patients to whom they belong, contrasting with 18 HPV-positive sporadic HNSCC cases. Additionally, *TP53* mutations were prevalent in 89% of FA SCCs, indicating an early transforming event (Webster et al., 2022). As it was explained in the PPI epigraph, *TP53* is a tumor suppressor gene that plays a critical role regulating cell growth and preventing cancer development. Mutations in *TP53* are commonly associated with many types of cancer, including HNSCC, and particularly in HPV-negative HNSCC cases (Seltzsam et al., 2019).

Compared to HPV-negative sporadic HNSCC, FA SCCs exhibit distinct mutational profiles characterized by reduced rate of single nucleotide variants (SNVs) and small insertion/deletion events (indels) in known SCC driver genes, chromosomal instability with elevated somatic copy-number alteration (CNA) frequencies, and alterations in oncogenes and tumor suppressor genes. Amplifications were common in *PIK3CA* (amplified in 78% of samples), *MYC* (71%), *TAZ* (65%), *CCND1* (62%), *PLEC* (53%), *YAP1*/*BIRC2*/*BIRC3* (38%), *CCND2* (36%), *KDM2A* (33%), and *EGFR* (31%). While deletions were prevalent in *PTPRD* (deleted in 62% of samples), *CSMD1* (60%), *CDKN2A* (55%), *MXD4* (49%), *KMT2C* (42%), *NSD1*/*FAT2* (36%), *FAT1* (35%), and *NOTCH1* (31%) (Figure 16) (Webster et al., 2022).

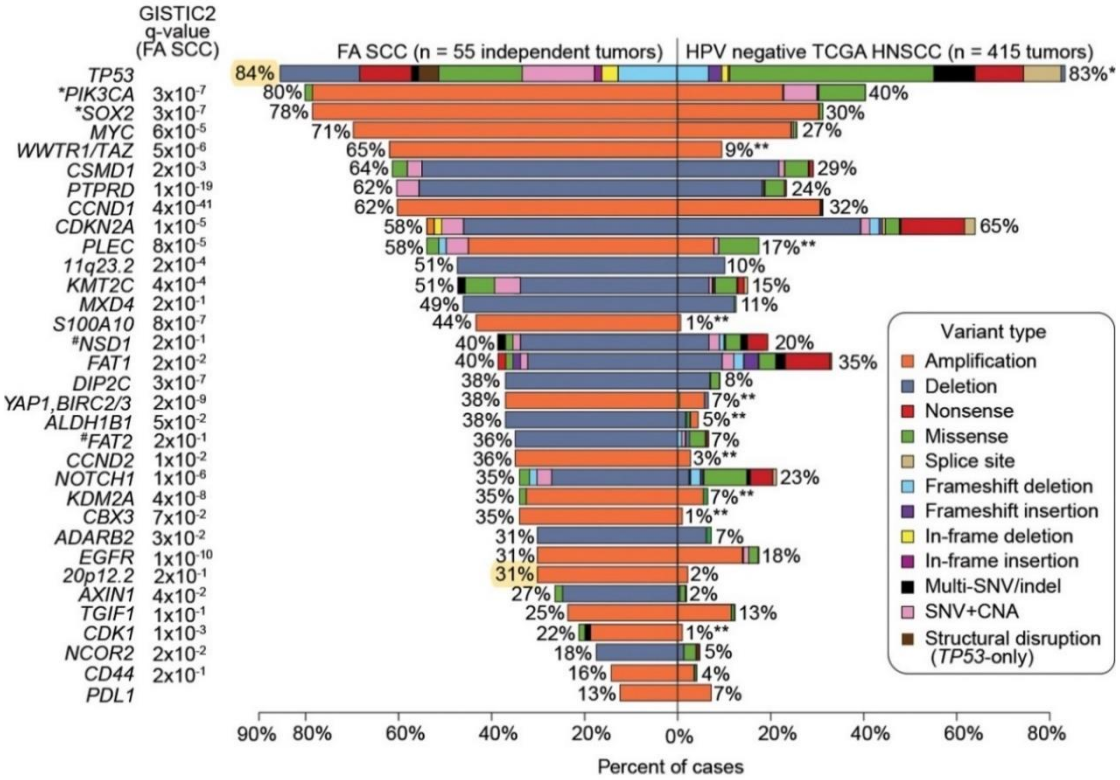


Figure 16. Gene alteration frequencies contrast between FA SCCs and HPV-negative sporadic HNSCCs. Comparation of the mutation genes frequencies between FA SCCs (n=55) and sporadic HNSCC (n=415). Figure extracted from Webster et al., 2022.

On the other hand, Webster's publication also refers to the role of alcohol consumption in the contribution to cellular accumulation of acetaldehyde, that can induce DNA adducts and ICLs, usually repaired by the FA pathway. That explains why individuals with acetaldehyde detoxification deficiency or dysfunctional FA pathway, have an increased risk of SCCs. Furthermore, the p53 DNA damage response is also increased in this context, in response to acetaldehyde levels (Peake et al., 2021, 2023; Wang et al., 2023). Recent research suggests that formaldehyde exposure can contribute to hematopoietic stem cell failure and cancer development, even in the presence of a functional FA pathway. Langevin et al., also showed that FANCD2 deficient cells were hypersensitive to acetaldehyde exposure; and the SL relation between ALDH2 and the FA pathway has been corroborated by Zhang and Fu (Langevin et al., 2011; Zhang & Fu, 2021). According to Webster et al.'s analysis, HNSCC with highest levels of CNAs were found to be enriched for signatures of exposure to endogenous and exogenous aldehydes, including acetaldehyde, formaldehyde, and acrolein (found in tobacco smoke). This could result in the significant genomic instability reported in these sporadic HNSCCs, marked by numerous amplifications and deletions, due to an overwhelmed FA pathway (Webster et al., 2022).

TP53 mutation's role in different types of cancer, including HNSCC has been demonstrated and published along the years. In 2022, Roohollahi et al., published a study in which, after the whole exome and whole genome mRNA sequencing, they identified the major genomic and transcriptomic events associated with FA HNSCC. Accordingly with the Webster's study mentioned before, *TP53* was the only gene mutated in most of the FA HNSCC cell lines studied; and *YAP1*, *BIRC2* and *BIRC3* were amplificated in FA HNSCC cell lines. Additionally, other genes as *TNFRSF11B*, *FAP* and *LPXN* were shown significatively upregulated in FA HNSCC in comparison to sporadic HNSCC (Roohollahi et al., 2022).

The same year, Jäwert et al., published a study in which utilizing a novel, custom-made tissue microarray comprising 28 high-risk oral leukoplakias and the corresponding oral squamous cell carcinomas (OSCC) in general population, from 14 cases that progressed to cancer, they investigated CNAs in OSCC driver genes. CNAs were identified in 14 out of 24 oral leukoplakias analyzable for one or more OSCC driver genes, where *EGFR* was the most frequently altered gene, with amplification in 43.5%, followed by *CCND1* (26.1%), and *MYC* (8.3%) (Figure 17). *CDKN2A* loss (26.1%), is also shown in this study, which accords with the data showed in Figure 16 (Jäwert et al., 2022, Webster et al., 2022).

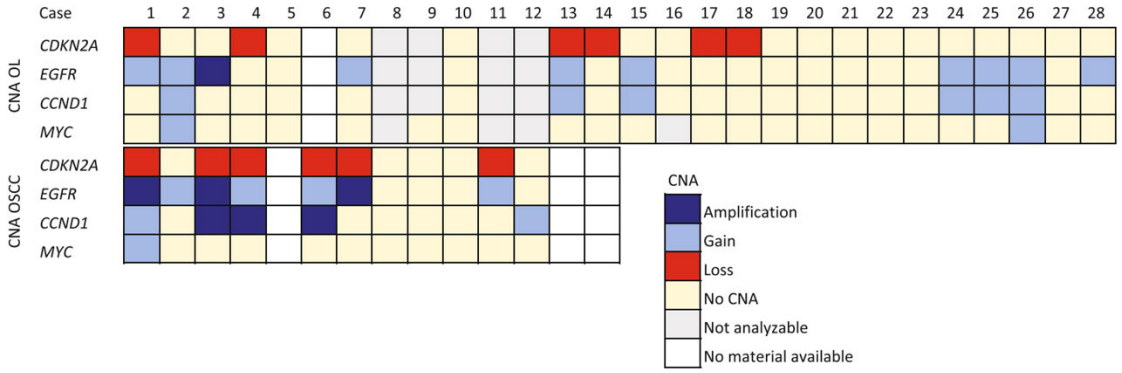


Figure 17. Analysis of copy number alterations (CNAs) in high-risk oral leukoplakias and corresponding oral squamous cell carcinomas (OSCCs). Analysis from 14 cases that progressed to cancer, using a custom-made tissue microarray. CNAs were identified in 14 out of 24 oral leukoplakias analyzable for OSCC driver genes. Figure adapted from Jäwert et al., 2022.

1.9. Target therapies in HNSCC

HNSCCs are characterized by an immunosuppressive environment that evades immune response though several resistance mechanisms. Immune checkpoint molecules, including PD-1, its ligand PD-L1, and cytotoxic T-lymphocyte-associated protein 4 (CTLA-4), play pivotal roles in maintaining self-tolerance and modulating immune responses within normal immunoregulatory pathways. Consequently, although cisplatin is the first line treatment for HNSCC patients, followed by cetuximab in combination with radiotherapy, immune checkpoint inhibitors (ICIs) has been proposed an alternative in this field. ICIs targeting PD-1, such as nivolumab or pembrolizumab, can effectively disrupt these inhibitory pathways, thereby enhancing immune surveillance against tumor cells (Burtness et al., 2019; Yamashita et al., 2023). PD-L1 inhibitors such as atezolizumab, avelumab, and durvalumab, and CTLA-4 inhibitors such as ipilimumab and tremelimumab are also used to treat HNSCC. Numerous clinical trials, both as monotherapy and in combination regimens, have been conducted with these antibodies, with a primary focus on patients diagnosed with recurrent or metastatic squamous cell carcinoma of the head and neck (Yokota et al., 2020).

1.9.1. ERBB receptor family inhibition

The effect of ERBB inhibitors against HNSCC have also been studied with cetuximab in the first line of treatment. The epidermal grow factor receptor (EGFR or ERBB1/HER1) is a tyrosine kinase inhibitor from the ERBB family of cell surface receptors, that is usually upregulated in epithelial malignancies, as colon carcinoma, bladder cancer, breast cancer or HNSCC (Grandis et al., 1997). Together with the other members of the family ERBB2/HER2, ERBB3/HER3 and ERBB4/HER4, participate in a downstream signaling cascade that regulates oncogenes as protein kinase B (PKB or AKT) and mammalian target of rapamycin (mTOR). These receptors, which share a similar structure, are single chain transmembrane glycoproteins. Among their structural domains, they have an outer section of the receptor that binds to signaling molecules (ectodomain), a transmembrane domain, a short segment near to the membrane, a tyrosine

kinase domain responsible for activating enzymes, and a C-terminal tail containing tyrosine molecules (Figure 18). When soluble signaling molecules attach to the ectodomain, it prompts the receptor to form a homo- or heterodimer between receptors. This pairing is crucial for activating the intracellular tyrosine kinase domain, leading the phosphorylation of the tyrosine-terminal tail. These phosphotyrosine residues activate downstream components of signaling pathways, including RAS/MAPK, PLCγ1/PKC, PI3K/AKT and STAT pathways. When these routes are activated, genes associated in adhesion, migration, proliferation, survival, and differentiation are transcriptionally triggered (Atalay et al., 2003; Wieduwilt & Moasser, 2008).

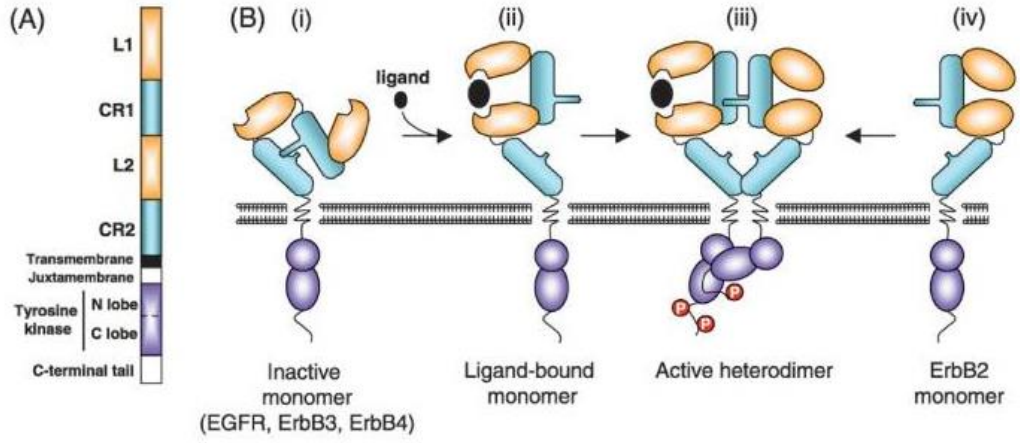


Figure 18. Structure and activation mechanism of ERBB receptors. A. Linear representation of ERBB receptor domains. The extracellular N-terminal domain comprises four subdomains: leucine-rich subdomains L1 and L2 involved in ligand interaction, cysteine-rich subdomain CR1 housing the dimerization loop, and the transmembrane domain linking to the tyrosine kinase domain and the C-terminal tail. **B.** Schematic overview of ERBB receptor dimerization and activation (**i**) Ligand-free state, where EGFR, ERBB3, and ERBB4 maintain a tethered conformation via CR1-CR2 interaction. (**ii**)Lligand binding induces an extended conformation, exposing the dimerization loop of CR1 and facilitating receptor homo- and heterodimerization. (**iii**) Dimerization aligns the N-lobe of one receptor's tyrosine kinase domain with the C-lobe of its partner, leading to C-terminal tyrosine phosphorylation and creation of phosphotyrosine binding sites. (**iv**) ERBB2 remains in an extended conformation, ready for interaction with other ERBB receptors. Figure extracted from Wieduwilt & Moasser, 2008.

The function of ERBB receptors relies on interactions involving their extracellular domains (ECDs), which bind activating ligands and interact with the ECDs of partner receptors to form dimers (Wieduwilt & Moasser, 2008). Thus, substances that disrupt them may significantly inhibit their functionality, negatively affecting to the growth and the spread of tumors (Zwick et al., 2001; Porta et al., 2014; Zibelman & Mehra, 2016). There are two types of inhibitors in this way: anti-EGFR monoclonal antibodies (mAbs), that inhibit the extracellular domain of the receptor or stimulate the host-innate antibody-dependent cellular cytotoxicity, and small-molecule tyrosine kinase inhibitors (TKIs), that bind to the intracellular domain of the receptor avoiding their autophosphorylation (Figure 19) (Zwick et al., 2001; Zibelman & Mehra, 2016).

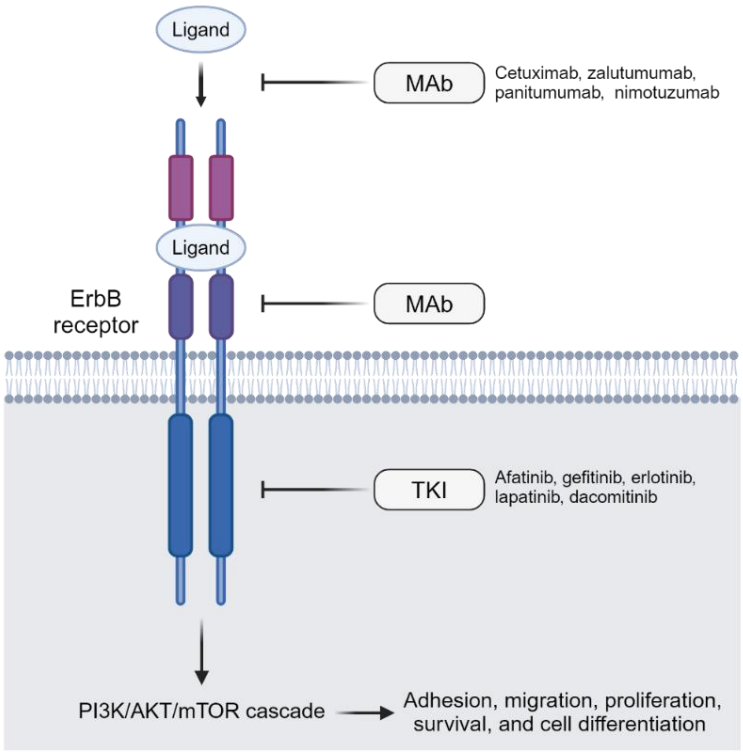


Figure 19. Diagram of an ERBB receptor and the two types of inhibitors that could target it in cancer therapy. Anti-ERBB monoclonal antibodies (mAbs) target the extracellular domain of the ERBB receptor, directly inhibiting the receptor activity or stimulating host-innate antibody-dependent cellular cytotoxicity mechanisms. Small-molecule tyrosine kinase inhibitors (TKIs) bind to the intracellular domain of the ERBB receptor, preventing its autophosphorylation and subsequent activation of downstream signaling pathways. Figure based on Zwick et al., 2001.

MAbs can access these ECDs and disrupt their function when appropriately targeted. Therefore, some humanized mAbs that target ERBB receptors have been approved for clinical use. The first of these, trastuzumab, targets ERBB2 and is used in ERBB2-amplified breast cancer, where it leads to tumor regression in a subset of patients with metastatic disease and improves disease-free survival when combined with chemotherapy in early-stage disease. Another ERBB2-targeting mAb, pertuzumab, has been developed to bind to the dimerization interface of ERBB2, potentially interfering with its dimerization and inhibiting oncogenic signaling. Cetuximab and panitumumab, target the ECD of EGFR and are approved for clinical use in colorectal cancer, which may exhibit overactivity of wild-type EGFR. These mAbs are also effective in HNSCC, which often overexpress EGFR (Wieduwilt & Moasser, 2008; Moradi-Kalbolandi et al., 2018).

Cetuximab is a chimeric human immunoglobulin G1 antibody, that targets domain III of the extracellular region of EGFR. Its anti-tumor effects are mediated through multiple mechanisms including induction of apoptosis, inhibition of proliferation, angiogenesis, and increased sensitivity to chemo- and radiotherapy. Furthermore, cetuximab prevents the attachment of other ligands to EGFR by directly binding to the receptor, inhibiting EGFR phosphorylation, and downstream signaling. It also induces antibody-dependent cellular cytotoxicity, leading to the removal of EGFR-coated cells. This interaction between cetuximab and EGFR may also result in receptor internalization and reduction of cetuximab on the cell surface. Although cetuximab was first approved by the FDA in 2004 for the treatment of EGFR-expressing metastatic colon cancer resistant to irinotecan-based chemotherapy, in 2006, FDA approval was granted for cetuximab in combination with radiotherapy for the treatment of locally advanced HNSCC (Kozakiewicz & Grzybowska-Szatkowska, 2018).

Other mAbs against ERBB family are detailed in Table 3, in which are detailed their specific targets and their current clinical status. In blue the mAbs that have ongoing clinical trials in HNSCC patients or have HNSCC use approved, with (*) the ones that have also ongoing HNSCC clinical

trials despite their approval for other cancer types (Wieduwilt & Moasser, 2008; Moradi-Kalbolandi et al., 2018; Cai et al., 2020; clinicaltrials.org).

Table 3. ERBB monoclonal antibodies (mAbs).

ERBB mAb	Target receptor	Status
Cetuximab	EGFR	FDA and EMA approved
Depatuxizumab	EGFR	Phase I (NCT01800695), I/II (NCT02590263), II (NCT02343406), III (NCT02573324, NCT03419403)
Duligotuzumab	EGFR, HER3	Phase I (NCT01911598)
Elgemtumab	HER3	No data
Ertumaxomab	EGFR, HER2	Phase I/II (NCT01569412), II (NCT00522457, NCT00351858, NCT00452140)
Futuximab	EGFR	Phase I (INCT05162755), II (NCT03549338, NCT02083653), III (NCT05223673, NCT03717038
Imgatuzumab	EGFR	Phase II (NCT04985825)
Laprituxumab	EGFR	No data
Lumretuzumab	HER3	Phase I (NCT01918254, NCT01482377) I/II (NCT02204345)
Margetuximab	HER2	FDA approved (*)
Matuzumab	EGFR	Phase I (NCT00113581, NCT05360368), II (NCT00111839, NCT00215644, NCT00073541, NCT05238363, NCT05354700, NCT05215925, NCT05290220, NCT05239650, NCT05221658, NCT0524698)
MM-111	HER2, HER3	Phase I (NCT01097460, NCT01304784, NCT00911898), II (NCT01774851)
MM-141	HER3	Phase I (NCT01733004, NCT02538627), II (NCT02399137)
Modotuximab	EGFR	Phase I (INCT05162755), II (NCT03549338, NCT02083653), III (NCT05223673, NCT03717038)
Necitumumab	EGFR	FDA approved (*)
Nimotuzumab	EGFR	EMA approved
Panitumumab	EGFR	FDA and EMA approved (*)
Patritumab	HER3	Pending of EMA approval (*)
Pertuzumab	HER2	FDA and EMA approved
SCT200	EGFR	Phase I (NCT03692520, NCT03808701, NCT04229537, NCT05552807, NCT02211443), I/II (NCT03817567), II (NCT03744208, NCT03713372, NCT03692689, NCT03874741, NCT03405272, NCT03744208)
Seribantumab	HER2, HER3	Phase I (NCT00734305, NCT01451632, NCT01209195, NCT01436565, NCT02538627, NCT01447225), I/II (NCT00994123), II (NCT04383210, NCT04790695, NCT03241810, NCT01421472, NCT01447706, NCT02387216, NCT01151046)
Trastuzumab	HER2	FDA and EMA approved (*)
Zalutumumab	EGFR	Phase I/II (NCT01054625, NCT00677924, NCT00093041, NCT00707655, NCT00401401), II (NCT01449357, NCT00542308, NCT00460551), III (NCT00382031, NCT00496652)

In addition to mAbs, TKIs provide another class of targeted therapies by inhibiting the enzymatic function of ERBB receptors. Gefitinib, afatinib, dacomitinib, erlotinib and lapatinib are TKIs approved for clinical use. They competitively bind within the ATP-binding region of the kinase domain of ERBB receptors, blocking downstream signaling. Gefitinib and erlotinib primarily target EGFR, while lapatinib is equally active against EGFR and HER2, dacomitinib targets ERBB1, ERBB2 and ERBB4, and afatinib is a panERBB (Zibelman & Mehra, 2016; Lee et al., 2021).

Afatinib is an irreversible TKI, that blocks signal transmission from ERBB family receptor dimers. Tathineni et al., last publication evaluates afatinib as first-line treatment in EGFR-mutated NSCLC, where it seems to show significant improvements in progression-free survival (PFS) and overall survival. In HNSCC patients, afatinib improved PFS compared to methotrexate in the second-line recurrent and/or metastatic setting (Marret et al., 2023; Tathineni et al., 2023). Furthermore, dacomitinib, another EGFR inhibitor, has shown promising clinical activity in the first-line treatment of recurrent or metastatic HNSCC, as demonstrated in phase II trials. These findings underscore the potential of EGFR inhibitors like afatinib and dacomitinib in the management of HNSCC and other EGFR-driven cancers (Kozakiewicz & Grzybowska-Szatkowska, 2018).

Since the identification of the EGFR gene and the development of gefitinib in 2004, researchers have developed three generations of EGFR inhibitors, which have changed therapeutic strategies and have provided substantial survival benefits to patients. Among EGFR mutations, EGFR exon 20 insertion (ex20ins) mutations are the third most common subtype, affecting around 4% of EGFR-mutant NSCLC patients (Gou et al., 2024). Research indicates that changes in the drug-binding pocket of exon 20 result in decreased effectiveness of EGFR inhibitors, leading to drug resistance. Consequently, alternative treatments such as osimertinib, poziotinib, and mobocertinib have been developed to target EGFR ex20ins mutations (Meador et al., 2021; Hou et al., 2022; Gou et al., 2024).

Although EGFR-TKI have shown promise in treating tumors, resistance often develops. Understanding the mechanisms underlying this resistance is crucial for developing effective therapies. Resistance to ERBB-directed therapies can occur through activation of parallel or downstream pathways, enabling tumor growth independent of ERBB receptor signaling. For example, mutations in EGFR or HER2 activate the Ras/MAPK pathway, but mutations in KRAS render tumors resistant to ERBB receptor targeting TKIs. Additionally, mutations on the TKI-binding site are other mechanisms of resistance. On the other hand, monoclonal antibody-based cancer therapy has gained prominence as a therapeutic strategy, but resistance to these antibodies has emerged as a significant challenge. Resistance can be primary, inherent to solid tumors, or acquired over time. While targeting HER1, HER2, or HER3 individually has shown success in clinical settings, interference with receptor-associated signaling pathways encounters resistance due to crosstalk with other EGFR family members. Resistance also occurs with other monoclonal antibodies like cetuximab and panitumumab in NSCLC and colorectal cancer, due to mutations in EGFR extracellular domain. Trastuzumab, targeting HER2, encounters resistance due to PI3K pathway activation and structural changes in HER2 interactions (Wieduwilt & Moasser, 2008; Moradi-Kalbolandi et al., 2018).

Strategies like pan-ERBB targeting, a mixture of antibodies targeting several ERBB family members simultaneously, inhibits the tumor growth and reduces resistance. Multispecific mAbs against different epitopes of EGFR or HER2 enhance receptor internalization and degradation, leading to improved antitumor activity. These strategies offer potential avenues for addressing resistance and improving therapeutic outcomes in EGFR family receptor-positive cancers (Moradi-Kalbolandi et al., 2018).

Other strategies for ERBB-directed therapy have been proposed, including inhibition of molecular chaperones like HSP90, metalloproteinases such as ADAM17, cyclooxygenase-2, histone deacetylase, siRNAs, ribozymes, and antisense technologies. However, these approaches have yet to be widely adopted in clinical practice due to challenges such as lack of specificity or unclear clinical utility (Wieduwilt & Moasser, 2008).

An overview of TKIs against ERBB family are detailed in Table 4, in which are shown their specific targets and their current clinical status. In blue the TKIs that have ongoing clinical trials in HNSCC patients or have HNSCC use approved (Montanuy, Camps-Fajol, et al., 2020; Montanuy, Martínez-Barriocanal, et al., 2020; Gou et al., 2024; Grant & Nagasaka, 2024; *clinicaltrials.gov*).

Table 4. ERBB tyrosine kinase inhibitors (TKIs).

ERBB TKI	Target receptor	Status
Afatinib	panERBB	FDA and EMA approved
Dacomitinib	EGFR, HER2, HER4	FDA and EMA approved
Erlotinib	EGFR	FDA and EMA approved
Furmonertinib	EGFR ex20ins	Phase I (NCT05364073), II (NCT05987826, NCT06394674, NCT05334277, NCT06339242, NCT04970693, NCT05379803, NCT05445310…)
Gefitinib	EGFR	FDA and EMA approved
Lapatinib	EGFR, HER2	FDA and EMA approved
Mobocertinib	EGFR ex20ins, HER2	FDA approved
Neratinib	HER2	FDA and EMA approved
Osimertinib	EGFR ex20ins	FDA and EMA approved
Poziotinib	EGFR ex20ins, HER2	Phase I (NCT01455571), II (NCT03744715, NCT04044170, NCT02659514, NCT03066206, NCT02979821, NCT03318939, NCT02544997, NCT01819428, NCT02216916, NCT03292250...), III (NCT05378763)
Pyrotinib	HER2	Phase I (NCT01937689, NCT02378389, NCT02500199), I/II (NCT05575804), II (NCT05834764, NCT05880927, NCT04126525, NCT02535507, NCT05751018...), III (NCT04254263, NCT05910398)
Rociletinib	EGFR	Phase I/II (NCT01526928, NCT02547675, NCT02580708), II (NCT02147990, NCT02705339), II/III (NCT02186301), III (NCT02322281)
Tarloxotinib	HER2	Phase I/II (NCT05313009), II (NCT02449681, NCT02454842, NCT03805841, NCT02449681)
Tuxobertinib	EGFR ex20ins	No data
Sunvozertinib	EGFR ex20ins	Phase I/II (NCT06195189), II (NCT06182761, NCT06348927, NCT06355609)
Vandetanib	EGFR (and other RTK)	FDA and EMA approved
Zipalertinib	EGFR ex20ins	Phase I/II (NCT04036682), II (NCT05967689), III (NCT05973773)

1.9.2. Alternative therapies

1.9.2.1. CAR-T cell therapy against ERBB

In the same line of the ERBB inhibitors, new genetic therapies have been developed during the last years. The field of cancer therapy has undergone a revolution with the advent of the new techniques of immunotherapy. That is the case of cellular therapy with chimeric antigen receptor–modified T cells (CAR-T cells), that has been widely used in the field of cancer immunotherapy. T cells can be modified to express an ectopic T-cell receptor (TCR) or a chimeric antigen receptor (CAR), which confers an antibody-like recognition capacity. This way, targets for CAR-T cells include both antigens overexpressed in malignant cells compared to normal tissue, or specific mutations of the cancer type (Ma et al., 2019; Sterner & Sterner, 2021; Zhang et al., 2022; Wang et al., 2023; Hu et al., 2023). A variable light chain (VL) and a variable heavy chain (VH) make up the antigen-binding single-chain variable fragment (scFv) that makes up the extracellular domain of CARs. This scFV is derived from antibody proteins that can specifically recognize tumor-associated antigens. In addition, it is connected to a transmembrane structure that is linked to an intracellular domain, constituted by a CD3ζ signal chain and co-stimulation domains, that can mediate T-cell activation in a T-cell receptor-independent manner (Figure 20) (Wang et al., 2023).

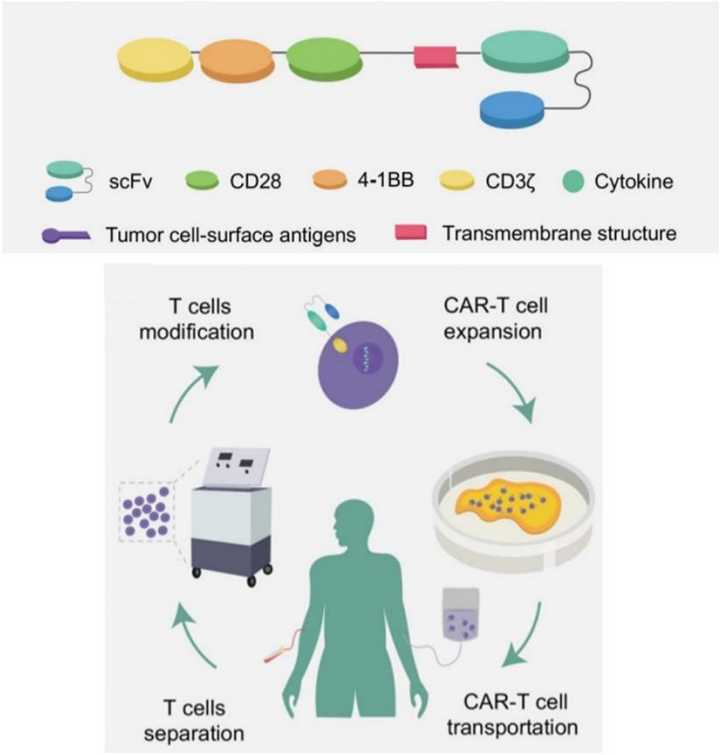


Figure 20. Chimeric antigen receptor (CAR) structure, and schematic CAR-T cell synthesis. Illustration of the structure and production process of chimeric antigen receptor (CAR). The antigen-binding domain of CARs consists of a single-chain variable fragment (scFv), comprising a variable light chain (VL) and a variable heavy chain (VH), derived from antibody proteins that recognize tumor-associated antigens. This scFv is connected to a transmembrane structure linked to an intracellular domain containing a CD3ζ signal chain and co-stimulation domains. The CAR-T cell synthesis involves three main steps: leukapheresis to collect the patient's autologous T cells, activation and transduction of these cells using viral vectors encoding specific CAR genes, and in vitro expansion of the CAR-T cells before reintroduction into the patient to target tumor cells. Figure adapted from Wang et al., 2023.

Overexpressed proteins in tumor cells are protein targets for CAR-T cells. Despite the expression of the ERBB family in many tissues, EGFR and HER2 overexpression is associated with parthenogenesis in several carcinomas, such HNSCC, making them potential targets for CAR-T cell therapy. In fact, several studies with CAR-T cells against EGFR and HER2 have been

developed as clinical trials, as NCT01818323 and NCT03740256, for patients with HNSCC or other tumors as breast cancer (Whilding & Maher, 2015; Papa et al., 2015, 2023). A published study by Papa and coworkers showed the results of the intratumoral pan-ERBB administration against HNSCC. After a human-dose escalation study and a clinical trial with 17 subjects, they concluded with the safety of their protocol, despite the issues with off-tumor toxicity of the ERBB family, and the intramural approach to the solid tumor (Papa et al., 2023).

However, a significant challenge in the field remains in replicating CAR-T against blood tumors success in solid tumors. A primary obstacle encountered in CAR-T therapy for solid tumors are the physical barriers that could block the CAR-T cell infiltration, including compact tumor structures, angiogenesis, and tumor stromal cells. Physiochemical barriers are also an obstacle in solid tumors CAR-T therapy, due to the downregulation of the cytokines, hypoxia, and the lack of nutrients within the tumor environment. The immunosuppressive tumor microenvironment, which predominantly recruits regulatory T cells, tumor-associated macrophages (TAM), and myeloid-derived suppressor cells (MDSC), also impedes CAR-T cell function. Furthermore, tumor immune evasion due to antigen loss poses a significant challenge, especially in solid tumors characterized by heterogeneous antigen expression (Wing et al., 2018; Wang et al., 2023).

1.9.2.2. Targeted therapies beyond ERBB

Identifying novel targets for HNSCC is crucial for enhancing the specificity and minimizing the adverse effects of CAR-T cell therapy, thus facilitating its clinical translation. Selection criteria for CAR-T cell targets in HNSCC typically involve two considerations: firstly, proteins previously implicated in solid tumor therapy; and secondly, proteins exhibiting high expression on HNSCC cell surfaces while being minimally expressed in normal tissues (Wang et al., 2023).

Taking the previous considerations into account, and beyond targeting ERBB family, the tumor necrosis factor ligand CD70 is significantly upregulated in solid tumors, including HNSCC. Its overexpression correlates with a decrease in CD8+ T cells, contributing to an immunosuppressive tumor microenvironment. Park et al. identified CD70 as a potential target for CAR-T cell therapy in HNSCC, demonstrating effective elimination of HNSCC cells by anti-CD70 CAR-T cells (Park et al., 2018). Targeting MUC1 has emerged as a promising strategy for HNSCC treatment, because of its overexpression in these types of tumors linked to advanced tumor stage (Huang et al., 2020). As B7-H3, an immune checkpoint protein, contributes to T cell dysfunction and tumor progression in HNSCC, Scribner et al. conducted a preclinical study that highlights the potential of B7-H3 as a therapeutic target in HNSCC treatment (Scribner et al., 2020; Wang et al., 2023). CD98hc, a protein strongly associated with T-cell activation that has been observed to be highly expressed on the surface of HNSCC, has also been suggested as target in this type of tumors (Hu et al., 2023).

Regarding the involvement of the immune system, NK (natural killer) cells have also been considered for CAR-T therapy strategies. NK cells are lymphocytes of the innate immune system, which function is to eliminate cancer and infected cells. NKG2D is an activating member of the NKG2 family receptors that allows immune cells to recognize and interact with cell-surface ligands of damaged cells. Although NKG2D receptor is present on NK cells, NKG2D ligands (NKG2D-Ls) are generally not expressed on healthy cells. However, high expression of NKG2D-Ls has been documented in damaged cells or during cancer processes (González et al., 2008; Nausch & Cerwenka, 2008; Casado et al., 2022). Accordingly, NKG2D-based CAR-T cells have received increased attention during the last years due to their capacity to recognize the NKG2D-Ls MICA, MICB, ULBP1-6. The development of preclinical studies with these NKG2D CAR-T cells has been explored by different groups, and nowadays there are currently multiple ongoing clinical trials that use this immunotherapy to treat different types of cancer (Tay et al., 2021; *clinicaltrials.gov*). The overexpression of NKG2D-Ls in HNSCC therefore suggests a promising CAR-T therapy against HNSCC.

Additionally, a variant of CD44 (CD44v6) is overexpressed in HNSCC, serving as a potential target for CAR-T cell therapy. CD44v6-targeting CAR-T cells have shown efficacy in several clinical trials (*clinicaltrials.gov*). Haist et al. demonstrated that this CAR-T cells can also kill CD44v6-positive HNSCC cell lines, leading to nearly complete eradication of tumor cells is preclinical models (Haist et al., 2021). Interestingly, CAR-NK cells also offer a safe and allogenic alternative to CAR-T cells cancer therapy in this field. That is the case of the study published by Ciulean, which shows how anti-CD44v6 CAR-NK cells could be generated and used against solid tumors (Ciulean et al., 2023). They conclude that their study demonstrates the specific anti-tumor efficacy of anti-CD44v6 CAR-NK cell therapy against HNSCC cell lines. However, further optimization and future investigations are necessary to enhance its effectiveness in clinical settings. Additionally, in vivo preclinical studies are crucial for assessing the durability of CAR-NK cell therapy, its ability to migrate to diverse locations, and the risk of off-tumor effects. These efforts will contribute to advancing the clinical translation of CAR-NK cell therapy for the treatment of HNSCC.

1.9.3. HNSCC treatment in FA patients

Excluding the surgical resection of the tumor, which is usually combined with intensity-modulated radiotherapy, there are no alternatives for the treatment of the HNSCC in FA patients (Lee et al., 2021). However, some case reports have studied the effect of ICIs, monoclonal antibodies that target PD-1 to stimulate lymphocyte-mediated anti-tumor activity. The US FDA approved two of them, pembrolizumab and nivolumab, for sporadic HNSCC treatment; and in 2019, pembrolizumab was FDA-approved as a first line monotherapy for unresectable sporadic HNSCC in patients with PDL-1 expressing tumors. In the case of FA HNSCC, there are only three case reports with different outcomes, so there is not a conclusion about their effectiveness in these cases (Yearley et al., 2017; Lewis et al., 2020; Yokota et al., 2020; Lee et al., 2021; Zhang et al., 2023).

As was explained before, cetuximab is an anti-EGFR mAb that acts by blocking the union between the ligand and the receptor, and inducing the receptor internalization (Zwick et al., 2001). It was FDA approved in 2006 for the treatment of primary HNSCC in combination with radiotherapy (Lee et al., 2021). In 2022, S. Zhang et al., compared 802 patients in a meta-analysis in which 684 of them were treated with PD-1 inhibitor, meanwhile 118 of them were treated with PD-1 inhibitor in combination with cetuximab. After this study, they determined that the addition of cetuximab to PD-1 inhibitor improved the response rate in HNSCC patients HPV-negative, suggesting the design of clinical trials to verify that information (Zhang, Zheng, et al., 2022). Although there are others anti-EGFR mAb (Table 3), only cetuximab has been tested in FA HNSCC in combination of low doses of radiotherapy, without encouraging results (Zibelman & Mehra, 2016; Lee et al., 2021).

On the TKIs therapies, EMA approved the use of gefitinib or afatinib for FA HNSCC in 2018, but only gefitinib has been tested in a FA HNSCC patient once in 2005 (Sun Jung et al., 2005; Lee et al., 2021). After a high content drug screening for FA therapeutics developed by our team (Montanuy, Camps-Fajol, et al., 2020), it was published a study showing the effect of gefitinib and afatinib in FA HNSCC cell lines (Figure 21). This work showed the effectiveness of these drugs in the three FA HNSCC cell lines studied and on *in vivo* xenografts experiments carried out with immunodeficient mice. In addition, this study highlighted the cancer-specific lethality in FA HNSCC of afatinib and gefitinib, without toxicity targeting DNA, hematotoxicity, activation of the FA/BRCA pathway in non-tumor cells, and without induction of chromosome instability (Montanuy, Martínez-Barriocanal, et al., 2020). The afatinib study shapes the preclinical research necessary for the subsequent clinical trial, in which the pan-ERBB inhibitor should demonstrate its effectiveness in FA HNSCC patients.

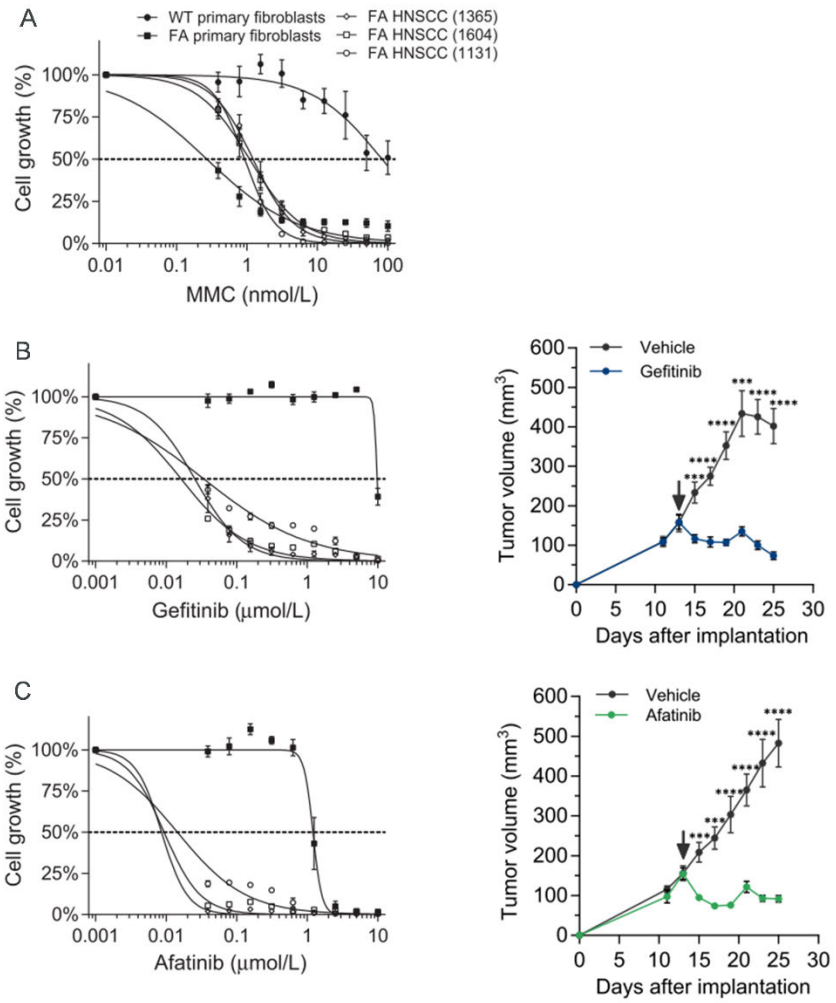


Figure 21. Gefitinib and afatinib effect in FA HNSCC. A. Cytotoxicity analysis in presence of mitomycin C (MMC), in primary fibroblasts and three different Fanconi anemia HNSCC cell lines. **B**. Cytotoxicity analysis in presence of gefitinib. Comparison of the xenograft tumor growth by vehicle (black lines) and gefitinib (blue lines) treatment, where the arrow indicates the start of the treatment. **C**. Cytotoxicity analysis in presence of afatinib. Comparison of the xenograft tumor growth by vehicle (black lines) and afatinib (green lines) treatment, where the arrow indicates the start of the treatment. Figures adapted from Montanuy, Martínez-Barriocanal, et al., 2020.

Objectives

2. Objectives

This thesis is focused on [redacted] research therapeutic approach in two different manners. Accordingly, one of the topics of this thesis is a drug discovery project started in 2017 with the target identification [redacted] Over the following years, the project was developed through a virtual screening [redacted] and a hit validation round, followed by a hit optimization round. The target identification, initial screening and first hit optimization round are described in Camps-Fajol' thesis (2022). As the current thesis is the continuation of the mentioned one, the objectives in this area are:

- Characterization and validation of specific [redacted] inhibitors, with the specific aims of:
    - Validation of the [redacted] candidates that were identified in the first optimization round.
    - Further optimization and validation of [redacted] inhibitor with more affinity to the target (low micromolar range), lower toxicity levels, and effectiveness in different cell lines.

Based on the knowledge of the group about FA disease, and while our group is committed to demonstrate efficacy and safety of afatinib in FA patients with HNSCC in a repurposing clinical trial, we sought to go one step further and find new therapeutic targets in afatinib-resistant FA HNSCCs, as potential second-line of therapies. The objectives of this project were:

- Identification of a potential second line of therapy for FA patients with HNSCC, that could be treated and become resistant to afatinib or another EGFR inhibitor. The specific aims of this topic are:
    - Obtaining and characterization of stable afatinib-resistant HNSCC cell lines.
    - Identification of potential second lines of therapy for the afatinib-resistant FA

Materials and methods

3. Materials and methods

Due to the differences between the projects, the methods are divided in two different parts: "[redacted] developing inhibitors of DNA damage repair for cancer therapy" and "Obtaining and characterization of afatinib-resistant HNSCC cell lines".

3.1. [redacted] developing inhibitors of DNA damage repair for cancer therapy

3.1.1. Cell lines

All cell lines were grown as attached monolayers in 75 cm^2 flasks and were all cultured in DMEM high glucose (ref. L0104, Biowest) medium supplemented with 10 % of heat inactivated fetal bovine serum (FBS, ref. S181S, Biowest) and Plasmocin (PlasmocinTM prophylactic, InvivoGen) at a concentration of 0.25 µg/ml. All cell lines were incubated at 37 °C and 5 % of CO2. The trypsin used was 10X (ref. X0930, Biowest) and was diluted in Phosphate-Buffered Saline (PBS, ref. 18912-014, Gibco).

The main experiments were done with U2OS and immortalized human fibroblasts (hFIB). U2OS cell line was established in 1964 and was cultivated from a moderately differentiated osteosarcoma of the tibia of a fifteen-year-old human female (ATCC accession number: HTB-96TM). Wild type (WT) fibroblasts (PN, from prepuce cells from a 5-year-old boy) came from "Banc de Cèl.lules Eucariotes CellTec" from the Cell Biology Department from Barcelona University, and were immortalized with h-TERT in our laboratory.

[redacted]

3.1.2. Virtual screening of First-In-Class specific inhibitors [redacted]

3.1.2.1. Target identification for a [redacted] and virtual screening

As this thesis is a continuation of a previous one, the target identification [redacted], analysis of [redacted] and selection of the preferred binding area for this potential inhibitor, virtual screening by molecular docking (FX candidates), and second virtual screening by fragment-based drug discovery (F2.X candidates) were detailed described in Camps-Fajol's thesis (2022). Therefore, previous screenings data shown in this thesis has been selected to provide context the steps of the project.

The [redacted] drug discovery project was initiated in 2017, targeted [redacted] By the study of this crystal structure, a preliminary analysis of the interacting residues at the interface between both domains was performed working with the *in silico* drug discovery CRO Intelligent Pharma (company later acquired by MindTheByte). The Schrödinger site map tool (*https://www.schrodinger.com/platform/products/sitemap/*) was used to select the most adequate zone to search for binding molecules. [redacted]

[redacted]

The subsequent virtual screening by molecular docking was also carried out in collaboration with Intelligent Pharma. It was done by selecting the compounds that could potentially interact with [redacted], using the 3D ZINC15 database library (136 million of molecules) and the Schrödinger site map tool to analyze the docking poses of the compounds. Using a multi-step docking process that included HTVS, standard and extra precision, the resulting compounds were docked [redacted]. After the final compounds were sorted according to the criteria used by chemists, 39 molecules out of the 57 potential inhibitors were selected and bought. Sequential numbers ranging from F1 to F39 were assigned to these hits.

A second virtual screening by FBDD was done in collaboration with the *in silico* drug discovery CRO MindTheByte. The 3 best molecules of the first round (F27, F32, F1, respectively) were fragmented and multiple substitutions were added employing the hit optimization software mXpander, to grow them up. Compounds were sorted based on their activity, druggability (Lipinski's rule of 5) (Volak et al., 2023), toxicity properties (low or moderate mutagenic, tumorigenic, and irritant profiles), and binding energy (less than -5 Kcal/mol). After a final visual evaluation, 4 commercial inhibitors were purchased, and 20 more candidates were synthesized in collaboration with Galchimia chemical synthesis company (*https://www.galchimia.com/es/*). These new hits were given sequential numbers, ranging from F2.1 to F2.24 (Camps-Fajol's thesis, 2022).

3.1.2.2. First virtual structural optimization (F3.x candidates)

After the selection of the compounds with better activity in the previous virtual screening rounds (F27 and F2.14 candidates), a virtual optimization of the molecules by structure activity relationships (SAR) and medicinal chemistry was performed in collaboration with the *in silico* drug discovery CRO Nostrum Biodiscovery (NBD) (*https://www.nostrumbiodiscovery.com/*).

Firstly, the interaction between the best candidates and [redacted] was studied using GLIDE, a docking program based in rigid-body and induced-fit methods, and PELE's induced-fit simulation. The main optimization ideas were [redacted]

Secondly, the growth of the best candidates withing the binding site was studied with FragPELE software, described by (Perez et al., 2020) and developed by NBD.

Finally, the candidates which interaction with the target and with better binding energy were selected, according with the chemists' criteria. All these molecules were non-commercial and were synthetized by TCG Lifesciencies Contract Research and Manufacturing Services company (https://www.tcgls.com/). These 13 new hits were given number names, starting from F3.4.

3.1.2.3. Second virtual structural optimization (F4.x candidates)

The second virtual structural optimization was carried out with the collaboration of NBD. For that, the structure of the best candidates until that moment was combined to reach a new potential hit with better affinity for [redacted]. Five new compounds were synthetized in collaboration with Galchimia, by combination of the residues with better activity in F1, F27, F2.14 and F3.10. These new hits were given sequential numbers, from F4.1 to F4.5.

3.1.2.4. Third virtual structural optimization (F5.x candidates)

The strategy of this optimization was based on exploring a new replacement point maintaining the central scaffold [redacted] and boosting the interactions of the new groups [redacted]

As in the first virtual screening, virtual molecular docking was performed using the GLIDE docking program. Candidates were then evaluated according to the binding energy and the chemists' criteria.

Despite of many of the proposal compounds could not be synthetized, 11 of them were successfully obtained in collaboration with Medicinal Chemistry & Synthesis (MCS) CSIC company (https://www.iqac.csic.es/mcs/). The sequential numbers assigned to these new hits ranged from F5.1 to F5.11.

3.1.2.5. Fourth virtual structural optimization (F6.x candidates)

This hit optimization was done in collaboration with NBD in order to define the best [redacted] As before, the GLIDE docking program was used for virtual structural optimization and binding energy was taken in consideration for candidates' selection. Potential candidates were also ranked by solubility.

In collaboration with MCS, 7 out of 9 candidates designed, and 3 additional candidates were synthetized, named by F6.1 to F6.10.

3.1.2.6. Alternative virtual screening approach

Using the ZINC22 database library (13 M small molecules), filtered by [redacted], *de novo* design was carried out in collaboration with NBD. GLIDE docking program was used for the docking process, what included HTVS and standard precision. Docking score filtering and visual inspection were taken in consideration for the final selection of the best potential compounds. Compounds that where finally selected were evaluated by their overall interactions, chemical diversity, shape complementary and potential toxicity and reactivity; and 26 commercial molecules were bought, named between 2F1 to 2F26.

All the compounds were diluted in dimethyl sulfoxide (DMSO, 23500.260, VWR) to prepare 100 mM stock solutions.

3.1.3. Surface Plasmon Resonance (SPR) assay

The interaction [redacted] and the ability of the compounds to inhibit [redacted] was analyzed by the SPR method, using Biacore T200 and a dextran-based sensor chip (Series S Sensor Chip CM5, BR100530, Cytiva).

SPR phenomenon occurs when a photon of incident light hits a metal surface (typically a gold surface) at a certain angle, leading to excitation of electrons in the metal layer, creating plasmons that propagate parallel to the surface. In SPR biosensors, incident light is used in a configuration employing a high-refractive index glass prism, enabling detection of changes in the reflective index near the metal surface, typically induced by biomolecule attachment. Detection is achieved

by measuring changes in reflected light intensity or resonance angle shifts. SPR biosensors enable detection of target molecules bound to probe molecules immobilized on the sensor surface, with detection limits typically around 10 pg/mL. Resonance or response units (RU), where 1 RU is equal to a critical angle shift of 10^{-4} degrees, are employed in SPR investigations to characterize the signal change. Since there haven't been any probe-target interactions at the beginning of the experiment, the first RU value corresponds to the starting critical angle. When incident light is coupled into a propagating surface plasmon on a gold surface, it can detect changes in the refractive index in real time (Figure 22). As a result, SPR evaluation of binding kinetics can be used to determine the rate of association (K_{ON}) during the association phase, the rate of disassociation (K_{OFF}) when target molecules are removed from the continuous flow by buffer washing, and the association rate constant (K_A) and dissociation rate constant (K_D). The limit of detection in SPR experiments depends on various factors including molecular weight, optical properties, binding affinity, and surface coverage of the probe molecule (O'Shannessy et al., 1993; Nguyen et al., 2015; Song et al., 2015).

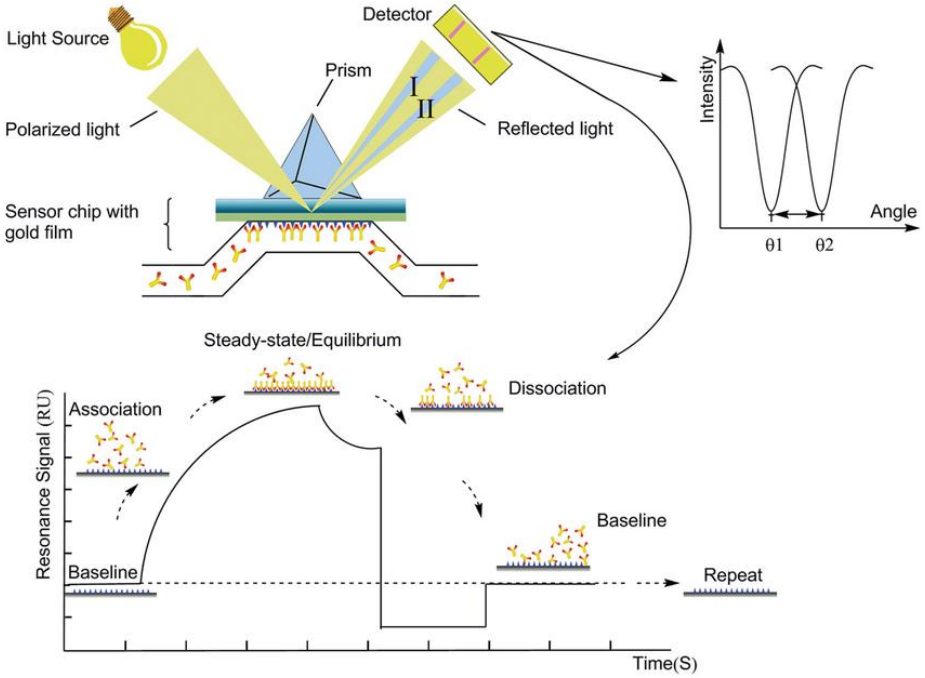


Figure 22. Diagram of SPR System. The SPR system works by detecting alterations in the refractive index near the surface layer of a sensor chip. During measurement, the chip is exposed to a broad-angle beam of light from below, typically within the range of total internal reflection. As biomolecules bind to the surface, the SPR angle shifts (from I to II in the diagram) due to changes in the refractive index. The detector identifies the angle where the intensity decreases because of binding events. This shift in resonant angle can be continuously monitored in real-time as a plot of resonance signal (related to mass change) against time. Figure extracted from Song et al., 2015.

The interference between the immobilized ligand and the sensor surface is one of the most important components of an SPR biosensor. Biacore technology utilizes a patented carboxymethyl-dextran-chip, that reduces non-specific biomolecule binding to the surface and boosts the surface's binding capacity. In addition, the high stability of the dextran allows several hundred binding cycles over an immobilized ligand (Jason-Moller et al., 2006). The most commonly used is the Sensor Chip CM5, which have a carboxymethyl dextran matrix covalently bound to the gold surface, allowing interaction analysis with various biomolecules. This chip has 4 different flow cells (Fc1-Fc4), what allows single or multichannel analysis. In SPR experiments, ligands are immobilized onto the sensor surface, and analyte solutions flowing over the surface induce changes in the refractive index, detected as shifts in resonance angle. However, SPR measurements are sensitive to temperature changes, requiring careful control during experiments. The Biacore software displays data as sensorgrams, representing changes in RU over time, which can be analyzed to determine binding kinetics. The response in a Biacore system

correlates with changes in surface mass concentration, making it suitable for analyzing interactions between biomolecules of different sizes (Biacore Assay Handboock, 2012).

Taking that into consideration, firstly, the chip was docked in Biacore, and primed 3 times with running buffer. For the pre-conditioning, several injections of 100 mM HCl, 50 mM NaOH, 0.1% SDS and miliQ water were done at a flow rate of 100 µL/min during 10 s. After that, the activation of the carboxyl groups of the dextran matrix was done with EDC (1-Ethyl-3-[3-dimethylaminopropyl]carbodiimide hydrochloride) and NHS (N-hydroxysuccinimide) 50:50 at 10 µL/min during 420 s, followed by [redacted]protein immobilization in the chip [redacted] To determine the optimal preconcentration conditions the ligand immobilization was tested at different pH: [redacted]Considering a total analyte response (R_{max}) of 20, the amount of ligand or R_L (in response units), [redacted] RU were immobilized. That was done by successive injections of 400 s at 5 µL/mL of [redacted] in one of the chip channels (in channel 2, because channel 1 is the reference one). Once the desired RUs were obtained, ethanolamine was used as a deactivation solution for 120 s at a flow rate of 10 µL/min, to wash away most of the electrostatically bound ligand. Finally, several washings were done in order to equilibrate the surface after using several chemicals.

As all the compounds were diluted in DMSO, the working temperature of the Biacore was higher than 15 ºC (usually at 25 ºC), the running buffer also contained DMSO (1X PBS, 0.125 mg/mL dextran and 1% DMSO), and a solvent correction was prepared.

Table 5. DMSO solvent correction.

Solvent correction	1	2	3	4	5	6	7	8
0.5% DMSO solution	-	100 µL	200 µL	300 µL	400 µL	500 µL	600 µL	700 µL
3% DMSO solution	700 µL	600 µL	500 µL	400 µL	300 µL	200 µL	100 µL	-

The stock used to prepare the samples is at 100 mM (in DMSO), so the dilutions for the assay were done in 1X PBS with 0.125 mg/mL dextran in order to decrease the DMSO percentage to 1%. The hit concentrations of the samples were 200, 100, 50, 25, 12.5, 6.25, 3.125 and 1.5625 µM, and they were plated in a 96-well plate, with a total volume of 100 µ/L per well.

Biacore enables high-resolution real-time monitoring of analyte-ligand interactions (association and dissociation rate constants). Affinity constants, which describe the intensity of the binding but not the rate, can be determined either from the kinetic constants or from the level of binding at steady state (Biacore Assay Handbook, 2012). The process of kinetic analysis involves tracking the interaction over time at various analyte concentrations, then fitting the data to a mathematical model. Most of the time, a 1:1 binding between the analyte and the ligand is taken into consideration, despite the fact that there are other binding models to analyze the interaction.

When the candidates (A) and [redacted] (B) meet as a result of diffusion with sufficient energy and in the right direction, binding occurs (association), forming a complex (AB) for an arbitrary period of time (Goldstein et al., 1999; Jason-Moller et al., 2006). The complex follows first-order kinetics and the binding occurs independently at each binding site. When the connection breaks (dissociation) and the analyte is washed away, it is visible at a sensorgram as single decay kinetics. The rate of formation of the complex (association) is represented with the association constant K_A and the rate of separation of the complex (dissociation) is represented by the dissociation constant K_D. Both constants are independent of time and concentration of the

reactants, although they may be affected by other parameters such as temperature and viscosity (Goldstein et al., 1999; Biacore Assay Handbook, 2012).

The closeness of fit between the fitted and experimental curves and the statistical significance of the parameters are the two main instruments for evaluating the importance of the reported constants. First one can be inspected by visually analyzing the residual plot or the fitted curves overlaid on the experimental data. Ideally, the residuals should form a random scatter with the magnitude of the signal noise level, which corresponds to the short-term noise in the detection system. It is quantified in terms of the Chi^2 (X2) value, which describes the average of the squared differences between the measured data point and the fitted curves. On the other hand, the standard error or T-value indicates the relevance of the parameters obtained with the fitting technique. High values suggest that substantial changes to the parameter value can be made without substantially compromising the fit's quality. Finally, as an additional indicator of the parameter relevance for the 1:1 binding model, the U-value indicates the particularity of the computed rate constants and R_{max}, and it is determined by assessing the dependence of fitting on correlated fluctuations between chosen variables. That means that lower values indicate greater confidence in the results.

3.1.3.1. [redacted] production and purification

For the SPR assay, we started using a commercial [redacted] but later, we produced and purified [redacted] where our hits should join. The amplification of [redacted] performed previously in the laboratory with specifically designed primers for PCR, using [redacted] plasmid as a DNA template; and cloned in [redacted]

The [redacted] plasmid was used for the transformation of the BL21 (DE3) (ref. EC0114, Thermo Scientific) competent cells. For this step, 0.5 µL of DNA sample were mixed with the E. coli cells, ice- incubated for 30 minutes (min), heat-shocked at 42ºC for 30 seconds, and ice-incubated again for 2 min. Then, 500 µL of S.O.C medium were added to de mix, and the tube was placed in a shaking incubator (Inforce HT, Ecotrol) at 37ºC 225 rpm. 1 hour later, the tube was centrifugate at 3000 rpm for 5 min in order to concentrate the transformed cells in 50 µL, volume that was plated in LB with kanamycin (1:1000, ref.11815024, Thermo Scientific) plates ON at 37ºC.

After several trials, 10 colonies were added to an erlenmeyer with 100 mL of broth and 100 µL of kanamycin, and it was placed ON in a shaking incubator at 37ºC 2200 rpm. The following day, the culture was split in two different erlenmeyers, with 1.5 L of LB, 1.5 mL of kanamycin and 15 mL of $ZnCl_2$, and shacked in an incubator at 37ºC 2200 rpm. When the OD of the culture was 0.55-0.56, IPTG 25 µM was added to induce the protein expression, allowing the growing of the cells ON at the same conditions (37ºC, 2200 rpm). The culture growth was stopped 20h later, and centrifugated at 4ºC 5000 rpm 8 min in a (Avanti J-30I, Beckman Coulter, JA-14 rotor). After throwing the supernatant, cells were frozen at -80ºC. In collaboration with the Protein Production Platform -Nanbiosis from the Autonomous University of Barcelona (UAB), the cell lysis and the protein extraction and purification were done. The lysis buffer used [redacted] The final protein concentration was 0.19 mg/mL in 4.5 mL, 0.86 mg with 88,2% purity.

3.1.4. Western blot (WB)

3.1.4.1. Cell lysates preparation

To evaluate the effect of the candidates [redacted], U2OS and hFIB cells were seeded on 6-well plates at $5 \cdot 10^5$ cells in each well. After 24 hours (h), cells were treated with different concentrations of the candidates (Fx) [redacted]. A

positive control was stablished [redacted], meanwhile a negative control did not received any treatment. Two different times of treatment were stablished: 6h and 18h (overnight, ON); and after this time, whole cell extracts were lysed using 250 µL of 1x RIPA buffer (RIPA lysis buffer, ref. 20-188 EMD Milipore), containing protease and phosphatase inhibitors (cOmplete ULTRA tablets EDTA-free, ref. 0589295300, Roche; and PhosStop EASYpack, ref. 04906837001, Roche) and benzonase nuclease (ref. 70746-3. EMD Milipore). Samples were then sonicated for 15 seconds and 25% amplitude, centrifuged at maximum speed for 5 min and quantified with Pierce BCA Protein Assay Kit (ref. 23225, ThermoFisher Scientific) according to manufacturer's instructions. Absorbance was measured at 562 nm with the Thermo Scientific Multiskan Sky microplate reader (Thermo Scientific). The concentration of the protein lysates was calculated to load 15-30 µg of protein, based on the quantification results and the creation of a linear standard curve.

3.1.4.2. Immunoblotting

Protein extracts were mixed with Laemmli buffer containing Tris-HCL 0.31 M at pH 6.8, 25% of glycerol, 10% of SDS, 0.125% of bromophenol blue, 2-mercaptoethanol 1.5 M and miliQ water (ref. M6250, Merck). Then, samples were heated at 95ºC for 5 min, and loaded on a [redacted] polyacrylamide SDS-PAGE gel (ref. A1672, PanReac Applichem), in 125 mM Tris-HCL buffer at pH 6.8 (stacking gel 0.5M, ref. 1610799, BioRad), 375 mM Tris-HCL buffer at pH 8.8 (resolving gel 1.5M, ref. 1610798, BioRad), 0.1% of SDS, 0.05% APS and 3.34 mM TEMED (N,N,N,N-Tetrametiletilendiamina, ref. T9281, Merck). The voltage for gel electrophoresis was started at 70 V and increased to 120 V when the dye front passed over the stacking gel and continued until the electrophoretic front reached the gel's end. [redacted]

Proteins were then transferred to a nitrocellulose membrane (Mini or Midi Nitrocellulose Transfer Packs, Bio- Rad) by using Trans-Blot TurboTM Transfer System (Bio-Rad) with a specific program for high molecular weights. Nitrocellulose membranes were blocked with TBST (1X Tris-Buffered Saline, 0.1% Tween 20 (ref. 93773, Fluka) containing 5% non-fat dried milk for 1h at RT. After that, membranes were incubated [redacted] primary antibodies properly diluted in blocking solution ON at 4ºC (Table 6), and with anti-rabbit secondary antibody for 1h at room temperature (RT) the following day. Membranes were washed before and after the antibody exposition with TBST to eliminate the non-specific unions. Immunodetection was operated with Immobilon Crescendo Western HRP Substrate (ref. WBLUR0500, EMD Millipore) and Immobilion Forte Western HRP Substrate (ref. WBLUF0500, EMD Millipore) to detect [redacted] Membranes were revealed using the iBright 1500 (ThermoFisher) and quantified with the Image J software (https://imagej.nih.gov/ij/). Graphs and statistical analysis were performed using GraphPad Prism software (8.4.0 version, Dotmatics).

Table 6. Antibody list

Antibody	Reference		Used dilution	Secondary
[redacted]	[redacted]	[redacted]	[redacted]	[redacted]
[redacted]	[redacted]	[redacted]	[redacted]	[redacted]
[redacted]	[redacted]	[redacted]	[redacted]	[redacted]
[redacted]	[redacted]	[redacted]	[redacted]	[redacted]
[redacted]	[redacted]	[redacted]	[redacted]	[redacted]
Anti-rabbit	A120-101p		1:5000	-
Anti-mouse	A90-116p		1:5000	-
Dylight 800-conjugated streptavidin	S000-32	Rockland	1:5000	-

3.1.5. [redacted]

[redacted] biochemical screening that uses [redacted] added to the 384-well alpha plate as was stablished in the protocol. The addition of the different compounds of the Fx-F4.x rounds were done at the same time as the [redacted] mastermix, by triplicate, at a final concentration of 100, 50, and 20 µM. [redacted]

These experiments and the WB described below were done during a 4-months research stay in the [redacted], in the SVI (St Vincent's Institute) in Melbourne. They, their team, and [redacted] team kindly provided all the necessary [redacted] resources, as well as their knowledge, in order to adapt their procedures to our hits.

3.1.6. [redacted] WB

As an alternative to [redacted] and due to solubility issues of most of the compounds in little volumes, alternative protocol was developed. The mix [redacted] was done in tubes, improving the mixture. [redacted], reaction was stopped by adding 7 µL of loading buffer (2x Laemmli buffer), heating at 80ºC for 5 min, and freezing at -20ºC.

Samples were loaded on an 4-12% precast polyacrylamide gel (ref. NP0321BOX, Invitrogen) and blotted on a nitrocellulose as a conventional western blot. After transfer, the membrane was stained with Revert 700 Total Protein Stain (ref. 926-11011, Li-cor) by adding 4 ml of stain and leaving it shake for 5 min. The membrane was then washed and exposed on Odyssey scanner (Li-cor) at 700 nm for a normalization image. After that, the membrane was rinsed again with PBS and blocked with 0.5% non-fat dried milk for 30 min, to be incubated with Streptavidin DyLight 800-conjugated antibody (Table 6) for 45 min at RT. The membrane was then washed with PBS and visualized on Odyssey using 800 nm channel. ImageStudio software (Image Studio Lite Ver 5.2) was used for image analyses.

3.1.7. Immunofluorescence analysis [redacted]

[redacted] the effect of F4.3 –our best candidate so far- [redacted] For that, $4 \cdot 10^5$ U2OS [redacted] YFP-[redacted] cells/well were plated over a glass coverslip in a 6-well plate. The following day, cells were treated with the F4.3 at 5 and 10 µM firstly, [redacted] leaving a positive control treated [redacted] and a negative control without any treatment. After 6h of the treatment, cells were washed twice with PBS and subsequently fixed by addition of 1X PBS with 4% paraformaldehyde (ref. sc-281692, Santa Cruz Biotechnology) for 15 min at RT. The fixation was stopped washing twice with PBS, and cell permeabilization was done with PBS with 0.5% Triton X-100 (ref. T8787, Merck) for 10 min at RT. Afterwards, the coverslips were washed twice with PBS, once with distilled H2O, and they were left to dry. Coverslips were finally mounted in mounting medium containing 4'-6'-diamino-2-phenylindole (DAPI) 2 µg/mL (DAPI, ref. D1306, Invitrogen) as a DNA counter stain, and analyzed using a Zeiss microscope (Axiovert 200M).

3.1.8. Clonogenic assay

The cytotoxicity of the hits and their capacity to induce chemosensitivity to DNA damaging agents, [redacted], was determined using the clonogenic assay. For this assay, U2OS and hFIB cells were seeded on 12-wells plates at 1-5·10^2 cells in each well, respectively. The second day, one of the plates was treated with F4.3 10, other one with 15 µM, and 30 min later, [redacted] was added in both at 25, 50, 100, 150 and 200 µM duplicate-doses, leaving a duplicate of wells only with the hit treatment. A third plate was only treated with the different doses of cisplatin, but without preincubation with F4.3, to compare the effect of the chemosensitivity between both drugs. The medium was changed 1h after the addition of [redacted], and the plates with the new medium were incubated for 7 days. To stop the experiment, cells were fixed by adding 250 µL/well of trichloracetic acid solution (TCA) 10% (ref. A0590, PanReac Applichem), and the fixation was allowed for 1h at room temperature (RT) or overnight (ON) at 4ºC. After that, the medium with TCA was discarded and plates were rinsed 3 times with distilled water, and dried at RT until no moisture was visible. The staining of the cells was done by adding 500 µL/well of Sulforhodamine B (SRB) solution (0.4% SRB (Sulforhodamine B sodium salt, ref. S1402) in acetic solution 1%) (acetic acid glacial, ref. 20104.298, VWR) and keeping it for 30 min at RT with mild shaking. After that, plates were rinsed 3-5 times with 1% acetic acid solution to remove the unbound dye. When plates were dry, 500 µL/well of tris solution (10 mM, pH 10 in distilled water) (tris(hydroxymethyl)aminomethane, ref. 0497, VWR) were added, and the measure of the OD at 510 nm was done in a Thermo Scientific Multiskan Sky (Thermo Scientific) microplate reader. GraphPad Prism software (8.4.0 version, Dotmatics) was used for the statistical analysis of the results of at least four independent experiments. Data were expressed as mean ± SEM and their parametrical distribution.

3.1.9. [redacted]

[redacted] assay was performed with U2OS [redacted]. For that experiment, 2·10^4 cells/well were plated in a 96-well plate. 24h later, cells were treated with the best hits at 5, 10, 50 µM, [redacted]. After 6-18h (depending on the compound), culture medium was changed to avoid the toxicity effects of the compounds, and cells were kept in culture another 24 hours (48h after treatment).

As cells grow attached to the wells, the lysis procedure could be done in the same plate. [redacted] After 30 min incubation in dark conditions at RT, cells were resuspended in each well to read the plate in a flow cytometer (MACSQuant 10, Miltenyi Biotec).

[redacted] The obtained data were analyzed with FlowJo X (Tree Star, Inc.), and statistical analysis was done with GraphPad Prism software with the results of at least four independent experiments. Data were expressed as fold induction.

3.2. Obtaining and characterization of afatinib-resistant HNSCC cell lines

3.2.1. Cell lines

All cell lines were grown as attached monolayers in 75 cm^2 flasks and were all cultured in DMEM high glucose (Biowest) medium supplemented with 10 % of heat inactivated fetal bovine serum (FBS, Biowest) and Plasmocin (PlasmocinTM prophylactic, InvivoGen) at a concentration of 0.25 µg/ml. All cell lines were incubated at 37 °C and 5 % of CO2.

The sporadic HNSCC cell lines CAL 27 and CAL 33 were provided by Dr. Silvio Gutkind (UC San Diego, CA, USA). From these cell lines, clones 34 and 47 from CAL 27 (CAL 27-34 and CAL 27-47) and clones 5 and 11 from CAL 33 (CAL 33-A5 and CAL 33-A11) were obtained and provided by Dr. Ricardo Errazquin using CRISPR/Cas9 editing to “fanconize” the cell lines (Errazquin et al., 2021).

VU-SCC-1131 (FANCC mutant), VU-SCC-1365 (FANCA mutant), and VU-SCC-1604 (FANCL mutant) HNSCC cell lines from FA patients, were provided by Dr. Josephine Dorsman (Amsterdam UMC, Netherlands) (van Zeeburg et al., 2005). The first two cell lines were provided by Dr. Jose Antonio Casado after their correction using the retroviral vectors provided by Lombardy and coworkers (Lombardi et al., 2015). Whereas the third one was corrected with a FANCL lentiviral vector during this project. OHSU-SCC-974 (FANCA mutant) and the correct cell line were provided by FARF foundation (https://apps.ohsu.edu/research/fanconi-anemia/cell_line/).

All afatinib-resistant cell lines (AR) were created during this project by the addition of increasing doses of afatinib (ref. HY-10261, Santa Cruz), starting from 5 nM and increasing the doses when cell lines growth was stable, during a total of 90-100 days. After the consolidation as AR cell lines, the appropriate dose of afatinib was always added to the cell culture medium.

3.2.2. Cell line correction

3.2.2.1. Lentivirus production and concentration

The human embryonic kidney (HEK) 293 cell line used for the lentiviral correction, was originally isolated and cultured from normal fetal human embryonic kidney cells in the early 1970s by transformation with sheared adenovirus 5 DNA (ATCC accession number CRL-11268).

To generate the infectious lentiviral particles, $4 \cdot 10^6$ cells of HEK293T packaging cells were seeded in 10 cm diameter dishes (3 plates per each infection). After 24h of incubation with fresh medium supplemented with 100 mM chloroquine (ref. C6628, Merck), solution A of Calphos-kit infection (ref. 631312, Takara Bio) was prepared employing 10 µM transfer plasmid (FANCL_OHu26403C_pGenlenti, 10 µg), 6.5 µL psAX2 packaging plasmid (6.5 µg), 3.5 µL ENV lenti VSV G envelope plasmid (3.5 µg), 87 µL calcium solution (Calphos), and dH2O up to 700 µL per a single reaction. One volume of solution B was next added dropwise, and the solution was incubated for 15’ at RT, vortexed and released dropwise onto the cells. Cell culture medium was changed after 24h, and lentivirus-containing supernatant was collected at 48h and 72h. The whole supernatant was centrifuged in Amicon Ultra-15 centrifugal filter units (ref. UFC910024, Milipore) at 4000 rpm during 30’ at 6 ºC. Lentiviral particles were stored at -80 ºC until further use.

3.2.2.2. Cell transduction

$5 \cdot 10^5$ cells of VU1604 were seeded in a well of a 6-well plate and incubated ON. Culture medium was then changed and supplemented with 1:1000 polybrene (ref. TR-1003-G, Sigma-Aldrich) and, after 15’, 1:50 lentiviral particles were added. Infected cells were incubated for 24h to allow proper transduction, and medium was subsequently replaced to avoid the potential cytotoxic

effects. The cells were expanded in culture and selected with the resistance of the plasmid (puromycin dihydrochloride, ref. P8833, Sigma Aldrich).

3.2.3. DEB survival assay

Survival assays were performed following an adaptation of the protocol established by Vichai and Kirtikara (Vichai & Kirtikara, 2006).

FA HNSCC and corrected cell lines were exposed to increasing concentrations of DEB (0, 25, 50, 100, 200 nM) in culture medium in order to verify the restorage of the FA/BRCA pathway after the complementation.

Following the SRB assay protocol used commonly in the laboratory, 500-1000 cells/well (depending on the cell line growth) were seeded in 100 µL of medium/well, in 6 replicates for every point assessed, in a 96-well plate. An extra plate (t=24h) was seeded with the same number of cells to determine black values. The following day, 100 µL of medium with different concentrations of DEB was added to the plate. The 24h plate growth was stopped at this day.

After 7 days, cells were fixed by adding 50 µL/well of trichloracetic acid solution (TCA) 10%, and the fixation was allowed for 1h at RT or ON at 4ºC. After that, the medium with TCA was discarded and the plates were rinsed 3 times with distilled water, and dried at RT until no moisture was visible. The staining of the cells was done by adding 50 µL/well of SRB solution (0.4% SRB in acetic solution 1%) and keeping it for 30 min at RT with mild shaking. After that, plates were rinsed 3-5 times with 1% acetic acid solution to remove the unbound dye. When plates were dry, 200 µL/well of tris solution (10 mM, pH 10 in distilled water) were added, and the measure of the OD at 510 nm was done in a microplate reader. GraphPad Prism was used for the statistical analysis of the results of at least four independent experiments. Data were expressed as mean ± SEM and their parametrical distribution.

3.2.4. Afatinib survival assay

Sporadic HNSCC, FA-edited HNSCC, FA HNSCC, FA-corrected HNSCC and afatinib resistant cell lines were exposed to increasing concentrations of afatinib (0, 3.90625, 7.8125, 15.625, 31.25, 62.5, 125, 250, 500, 1000 nM) in culture medium in order to verify the acquisition of resistance to afatinib after 100 days of treatment, in comparison with the original cell lines.

The SRB assay protocol explained above was used.

3.2.5. Gefitinib survival assay

Sporadic HNSCC, FA HNSCC and afatinib resistant cell lines were exposed to increasing concentrations of gefitinib (ref. HY-50895, MedChemExpress) (0, 3.90625, 7.8125, 15.625, 31.25, 62.5, 125, 250, 500, 1000 nM) in culture medium in order to compare if the acquisition of resistance to afatinib is also compatible with the acquisition of resistance to gefitinib.

The SRB assay protocol explained above was used.

3.2.6. Cetuximab survival assay

Sporadic HNSCC, FA HNSCC and afatinib resistant cell lines were exposed to increasing concentrations of cetuximab (from clinical use in Sant Pau Hospital) (1, 10, 20, 50 µg/mL) in

culture medium to compare if the acquisition of resistance to afatinib is also compatible with the acquisition of resistance to cetuximab.

The SRB assay protocol explained above was used.

3.2.7. Human Phospho-RTK array dot blot

The Human Phospho-Receptor Tyrosine Kinase (Phospho-RTK) Array Kit (ref. ARY001B, R&D Systems, Biotechne) is a proteome profiler array which can detect changes in phosphorylation between samples. It allows the detection of 49 different phosphorylated human RTKs: EGFR, ERBB2, ERBB3, ERBB4, FGFR1, FGFR2α, FGFR3, FGFR4, Insulin-R, IGF-IR, AXL, DTK, MER, HGFR, MSPR, PDGFRα, PDGFRβ, SCFR, FLT-3, M-CSFR, c-Ret, ROR1, ROR2, TIE-1, TIE-2, TRKA, TRKB, TRKC, VEGFR1, VEGFR2, VEGFR3, MUSK, EPHA1, EPHA2, EPHA3, EPHA4, EPHA5, EPHA6, EPHA7, EPHA10, EPHB1, EPHB2, EPHB3, EPHB4, EPHB6, ALK, DDR1, DDR2, and RYK.

Following the protocol of the kit a pool of lysates of HNSCC (CAL 27 and CAL 33), FA HNSCC (VU 1131 and VU 1365), AR HNSCC (CAL 27 AR and CAL 33 AR), and AR FA HNSCC (VU 1131 AR and VU 1365 AR) were prepared to compare the phospho-RTK profile of each pool. Firstly, cells were cultured, and 2-3·10^6 cells were lysed with RIPA buffer (with protease and phosphatase inhibitors), in triplicates. After quantifying the protein, 1000 µg of total protein were incubated ON at 4ºC with the dot blot membranes following manufacturer's instructions. Next day, membranes were washed and incubated with an anti-phospho antibody for 2h at RT, before the revelation step in iBright 1500 (ThermoFisher), using Immobilon Crescendo Western HRP Substrate.

To verify the obtained results in each cell line separately, the experiment was repeated with all the FA HNSCC cell lines, sensible and AR ones: VU 1131, VU 1131 AR, VU 1365, VU 1365 AR, OHSU 974 and OHSU 974 AR, following the same protocol.

The analysis of both experiments was done by the specific program Quick Spots (Ideal Eye Systems), and the graphs and statistical analysis were performed using GraphPad Prism software.

3.2.8. Cell membrane marker's expression

As some of the marker's expression could be interesting for designing new potential targeted therapies, the differential expression of them were measured by flow cytometry in sensitive and AR cell lines. These experiments were done during a 4-months research stay in the Dr. Juan Bueren's laboratory, under the supervision of Dr. Jose Antonio Casado, in CIEMAT (Centro de Investigaciones Energéticas, Medioambientales y Tecnológicas), Madrid.

For this experiment, 5·10^6 cells were used, in order to have around 3-4·10^5 cells for each marker and controls. After washing the cells with 3 mL of PBS with 0.05% Azide (PB-Azide), 650 µL were added to the cells and spilt in 50 µL/tube for measure the ERBBs (ERBB1, ERBB2, ERBB3 and ERBB4), the NKG2D-ligands (MIC-A, MIC-B, ULBP-1, ULBP-2,5,6, ULBP-3, ULBP-4 and all the ligands together), and CD44v6. As some of the antibodies (Table 7) are conjugated with APC, some are conjugated with PE, and some need a secondary antibody conjugated with APC, there was needed a non-marker antibody control and an only marked with APC-secondary antibody control. After an incubation of 20 min, cells were washed with 3 mL of PB-Azide and incubated with the secondary antibody for another 20 min if the first one was not conjugated with APC or PE. For running the samples, cells were resuspended in 250 µL/tube of PB-Azide with DAPI. The cytometer used was a Fortessa (BD LSR Fortessa), and obtained data were analyzed with FlowJo X. Subsequent statistical analysis and graphs were performed using GraphPad Prism software.

Table 7. Antibody list

Antibody	Reference		Channel
Anti-hERBB1 (EGFR)	352906	Biolegend	APC (660nm)
Anti-hERBB2 (HER2)	BMS120BT	Invitrogen	-
Anti-hERBB3	MA5-12864	Invitrogen	-
Anti-hERBB4	MA5-13013	Invitrogen	-
Anti-hMICA	FAB1300P	R&D systems	PE (574nm)
Anti-hMICB	FAB1599P	R&D systems	PE (574nm)
Anti-hULBP1	FAB1380P	R&D systems	PE (574nm)
Anti-hULBP2/5/6	FAB1298P	R&D systems	PE (574nm)
Anti-hULBP3	FAB1517P	R&D systems	PE (574nm)
Anti-hULBP4	FAB6285P	R&D systems	PE (574nm)
Anti-hCD44v6	130-111-425	Miltenyi	APC (660nm)
APC-Streptavidin	405207	BioLegend	APC (660nm)

3.2.9. Multiplex Ligation-dependent Probe Amplification (MLPA) assay

The SALSA MLPA Probemix P483 HER gene family (P483-025R, MRC Holland) is an assay for the detection of deletions or duplications in the ERBB family of receptor tyrosine kinases: EGFR (ERBB1/HER1), ERBB2 (HER2), ERBB3 (HER3), and ERBB4 (HER4).

DNA extraction of cell pellets (1-2·10^6 cells) from HNSCC, FA HNSCC, and AR cell lines was done using the DNeasy Blood & Tissue Kit (69504, Quiagen). Quantification of DNA concentration was done using a nanodrop spectrophotometer (ThermoFisher). Following the manufacturer's protocol of the MLPA assay, 50 µg/µL of DNA was denaturalized at 98ºC for 5 min. After that, 1.5 µL of MLPA buffer and 1.5 µL of probemix were added to each tube for the hybridization step, 1 min at 95ºC and 16-20h at 60ºC. The following day, ligation reaction was done adding to each reaction 32 µL/tube of the ligase master mix (25 µL of ultrapure water, 3 µL of ligase buffer A, 3 µL of ligase buffer B and 1 µL of Ligase-65 enzyme). Thermocycler was programmed 15 min at 54ºC, 5 min at 98ºC and then 20ºC. Finally, PCR reaction was done adding 10 µL/tube of the polymerase mix (7.5 µL of ultrapure water, 2 µL of PCR primer mix, and 0.5 µL of polymerase). Tubes were immediately placed in the thermocycler for 35 cycles of 95ºC for 30 seconds, 60ºC for 30 seconds and 72ºC for 60 seconds, followed of keeping the 72ºC during 20 min, and final decreased the temperature to 15ºC. All thermocycler steps were done in a VerityPro 96-Well Thermal Cycler (Applied biosystems, ThermoFisher Scientific).

3.2.10. RNA sequencing

3.2.10.1. RNA extraction and mRNA library preparation and sequencing

For RNA-sequencing (RNA-seq), three biological replicates were analyzed per each cell line: two HNSCC (CAL27 and CAL33), four FA HNSCC (VU1131, VU1365, VU1604, and OHSU), and the corresponding AR cell lines, being a total 33 samples, as FA HNSCC 1604 doesn't show afatinib resistance.

RNA extraction of cell pellets (2-3·10^6 cells) was done using the RNeasy Mini Kit (74104, Quiagen) and the QIAshredder kit (79654, Quiagen), according to the manufacturer's instructions. RNA was

digested with DNase TURBO DNA-free (AM1907, Invitrogen) and total content was assessed using a nanodrop spectrophotometer. Concentrations were adjusted to 200 ng/µL in RNase-free water and 2 µg of total RNA was sent to the Centre Nacional d'Anàlisi Genòmica (CNAG, Barcelona, Spain) for RNA-seq.

The quality control of the total RNA was conducted using the Qubit RNA BR Assay kit (ThermoFisher Scientific) and the Fragment Analyzer RNA Analysis Kit (Agilent). All the samples used in this study had RNA integrity numbers (RIN) above 9. For RNA-seq, libraries were prepared using the TruSeq Stranded mRNA LT Sample Prep Kit (Illumina Inc.) following manufacturer's protocols. The libraries were sequenced on a NovaSeq 6000 S4 (Illumina) in paired-end mode with a read length of 2 × 150 bp. Image analysis, base calling, and quality scoring of the run were processed using the manufacturer's software Real Time Analysis (RTA 3.4.4) followed by the generation of FASTQ sequence files.

3.2.10.2. RNA-seq data processing and analysis

RNA-seq reads were mapped against the human reference genome (GRCh37/hg19 assembly) using STAR software version v2.7.8a with ENCODE parameters. Annotated genes were quantified using human GENCODE annotation file version 34 with RSEM v1.3.0 (Li & Dewey, 2011) and default parameters. Normalization and differential expression (DE) analyses were done using the limma package with default settings (Ritchie et al., 2015). This analysis was performed in the R Statistical Computing environment (https://www.r-project.org/). A Principal Component Analysis (PCA) plot was generated with the rlog transformed counts using the top 500 most variable genes and the ggplot2 R library (Wickham, 2009). The differential expression analysis was performed globally (sporadic HNSCC against FA HNSCC, and AR cell lines against non-resistant cell lines) and individually (each cell line against its corresponding AR cell line) with the objective of obtaining the genes that were differently expressed between these conditions. Genes were considered differentially expressed with an adjusted p-value of < 0.05 and an absolute fold change of $|FC| > 1.5$. R studio and GraphPad Prism were used for the statistical analysis of the results of three independent samples for each cell line. Data were expressed as mean ± SEM and their parametrical distribution.

Results

4. Results

Due to the differences between the projects, the results are divided in two different parts: "[redacted] developing inhibitors of DNA damage repair for cancer therapy" and "Obtaining and characterization of AR HNSCC cell lines".

4.1. [redacted] developing inhibitors of DNA damage repair for cancer therapy

4.1.1. Virtual screening of First-In-Class specific inhibitors of [redacted] target identification for a [redacted] and virtual screening (Fx and F2.x candidates)

[redacted] When this project began, in 2017, it was searched for [redacted] specific approach.

Al the beginning of the project (Camps-Fajol thesis, 2022), interacting residues [redacted] were analyzed [redacted] Therefore, a preliminary study was done with Intelligent Pharma (*in silico* drug discovery CRO), focused on the evaluation of [redacted], the available bibliography [redacted] and the site map tool of Schrödinger software.

[redacted]

Together with this knowledge, the Schrödinger site map tool was used to find the areas of the binding site that can be occupied by hydrophobic groups or ligand hydrogen-bond donors, acceptors, or metal-binding positions. The method was adapted taking into consideration the most important interacting residues [redacted] listed in Figure 23.

[redacted]

Figure 23. [redacted]

As it was explained in Camps-Fajol's thesis, the first virtual screening (Figure 24) was done in collaboration with Intelligent Pharma (Camps-Fajol's thesis, 2022), starting from a 3D ZINC15 database. Therefore, 136 million molecules were analyzed by molecular docking and using the Schrödinger software, in order to select the compounds that could interact with [redacted]

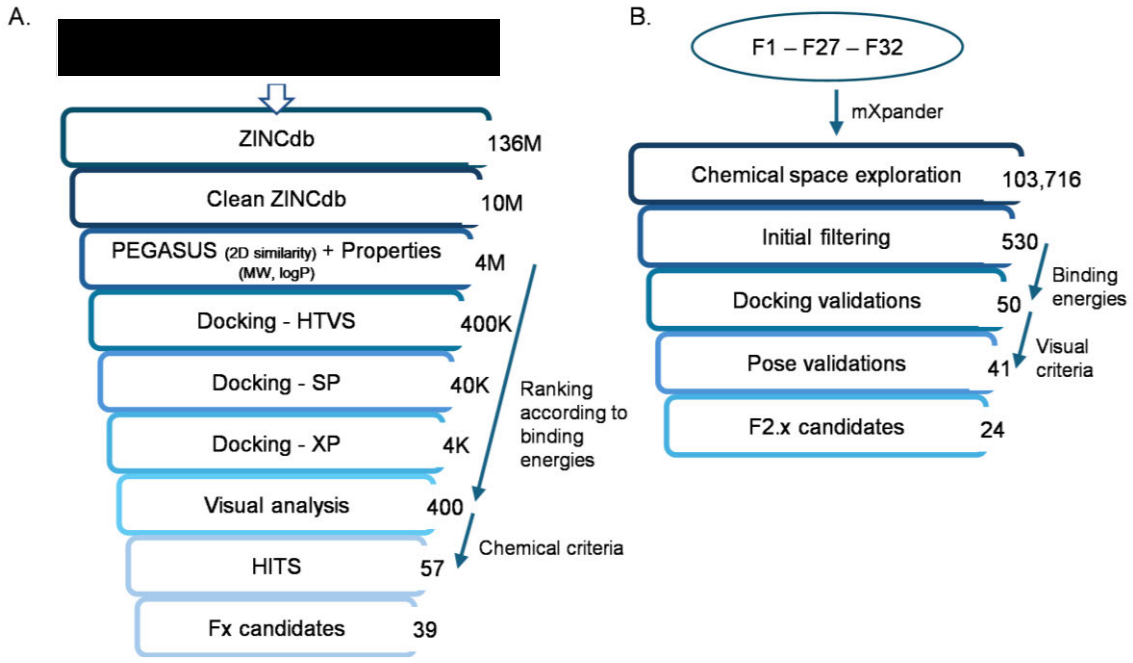


Figure 24. Virtual screening and fragment-based drug design workflow. A. Fx approach. **B.** F2.x approach. Figures edited from Camps-Fajol's thesis, 2022.

The first filter of this analysis was performed taking in consideration four different aspects: (1) reactivity, to eliminate the pan assay interference compounds (PAINs) (Baell & Nissink, 2018; Kirsch et al., 2019); (2) availability to purchase (in stock); (3) neutral pH; and (4) charges. A technology owned by Intelligent Pharma (named Pegasus), that used the 2D structural information of compounds to estimate the molecular similarity, was performed to study the initially filtered structures (7.8 million molecules). According to that, 1 million molecules similar to [redacted] were selected for the docking procedure. Using MOLPRINT2D fingerprints and based on the properties selected, 4 million molecules were ready to dock [redacted]

By the use of HTVS, standard and extra precision (SP and XP in Figure 24) in the Schrödinger docking process, the results were energetically ranked, and the best 10 % were kept for the following step (400 K compounds after HTVS, 40 K after SP and 4K after XP). The first 400 compounds after the docking were ranked using chemists' standards based on the previously discussed ligand-protein interactions. Consequently, 57 potential inhibitors [redacted] with good docking scores were chosen.

Finally, 39 molecules out of these 57 were purchased according to the budget availability (Fx candidates). The validation of these molecules was done by their effect on the inhibition [redacted] (Figures 25, 26).



Figure 25. **Workflow of [redacted] western blot assay.** U2OS or hFIB cells were cultured in 6-well plates and treated with increasing concentrations of [redacted] candidates [redacted] for 6 hours or overnight (18 hours). Cell extracts were prepared using RIPA buffer with inhibitors, and after their protein content quantification, samples were loaded onto an acrylamide gel and electrophoresed (see methods). Gel was transferred to a nitrocellulose membrane, where the incubation with [redacted] antibodies was done. Membranes were imaged and analyzed using ImageJ software.

Compounds were tested at concentrations between 10 to 100 µM during 18h (ON), but given the cytotoxic effects of some of them, the treatment time was reduced to 6h. Figure 26 shows the result of the best candidates of this validation: F27, F32 and F1 (Camps-Fajol's thesis, 2022).

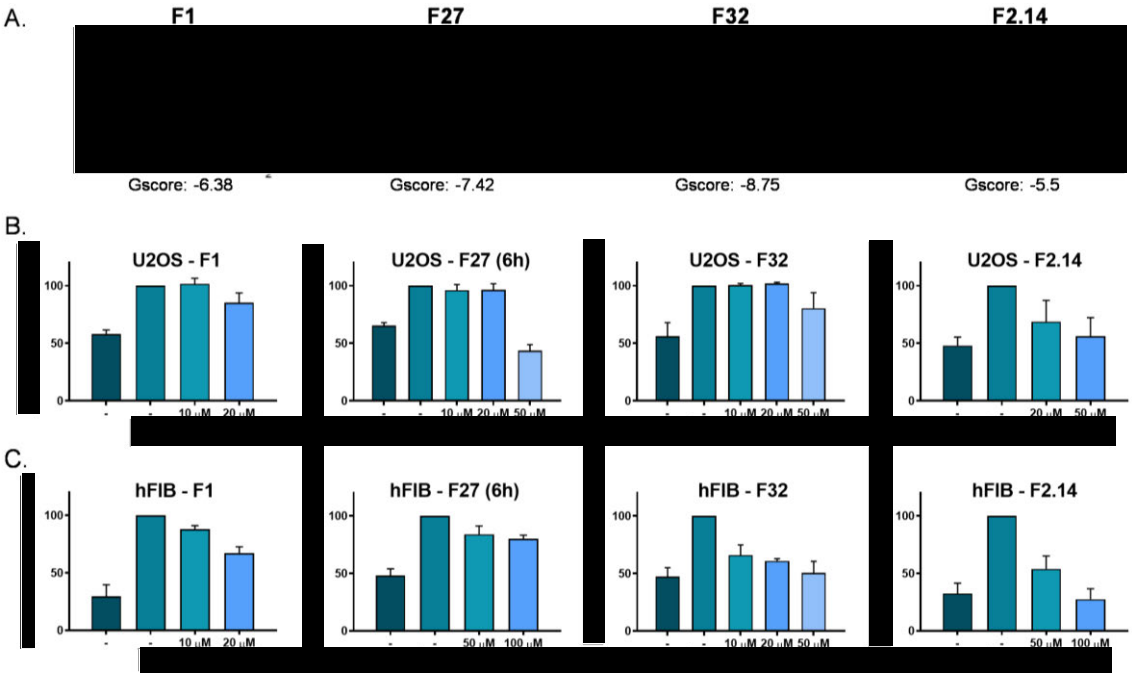


Figure 26. [redacted] **inhibition by best candidates for the virtual screening and the fragment-based drug design**: chemical formulation with the glide score (Gscore, kcal/mol) obtained by docking (**A**.) and in vitro validation in U2OS (**B**.) and hFIB cell lines (**C**.). Experiments were performed by treating the cells with potential [redacted] inhibitors at concentrations between 10-100 μM, [redacted] (see methods). The treatment with F27 was for 6h, meanwhile the treatment with F1, F32 and F2.14 was overnight. [redacted] was analyzed by WB and quantified using ImageJ software and data normalized. Graphs represent mean ± SEM of at least three independent experiments. Part of these data shown in this figure (U2OS graphs) are edited from Camps-Fajol's thesis (Camps-Fajol's thesis, 2022). A representative WB of each candidate is showed in Appendix 1.

The second virtual screening (Figure 24) was done in collaboration of MindTheByte (*in silico* drug discovery CRO) started from the three best candidates from the first screening: F27, F32 and F1, in decreasing order of activity. This virtual screening was done using *mXpander* software and a FBDD approach, which consist of the fragmentation of the molecules into synthetic feasible compounds, and the subsequent addition of multiple substitutions to the main fragment. That allowed the growth of the molecules to virtually explore until 103,716 new molecules. After that, the molecules were filtered and selected by their potential interest according to their activity, druggability and toxicity properties (530 molecules). To finalize, the molecules were docked to [redacted] to check the binding energy, and 50 molecules were selected. After a visual criteria validation, 41 molecules were finally selected: 4 molecules were commercially available, and 21 molecules were synthesized in collaboration with Galchimia chemical synthesis company (F2.x candidates) (Camps-Fajol's thesis, 2022).

4.1.2. Fx and F2.x candidates' validation

The candidates of the second virtual screening were also validated measuring their effect over the inhibition of [redacted]. WBs were done after treating U2OS cells with doses between 10 to 100 μM during 18h. Figure 26 shows the result of the best candidate of this validation: F2.14 (Camps-Fajol's thesis, 2022).

Later, as shown in Figure 26, the best candidates of the first and second virtual screening were tested in hFIB, in order to evaluate if the effect is the same than in U2OS. As seen in this figure, the doses of F1, F27 and F2.14 in hFIB were higher than in U2OS, because the cytotoxic effect and the [redacted] inhibition were lower.

In addition, [redacted] the ability of the compounds to interact with the target was analyzed using Biacore T200 (SPR) and a dextran-based sensor chip (Chip CM5) (Figure 27). Table 8 summarized the results of the best candidates F27 and F2.14, extracted from the Cristina Camps-Fajol's thesis.

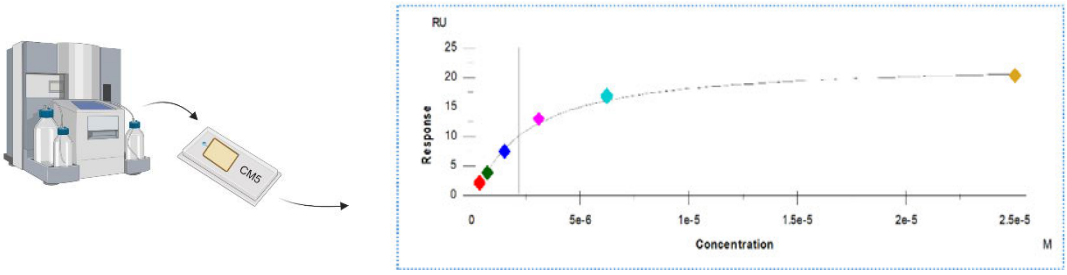


Figure 27. Biochemical validation with SPR: candidate and target interaction. Biacore was used to monitoring of analyte-ligand interactions, offering insights into association and dissociation rate constants.

KD (µM)	DMSO 1%. 15°C, HD						DMSO 5%. 25°C, HD			
	1st exp		2nd exp		Average 2-1 corr		1st exp		Average 2-1 corr	
	2-1 corr	Chi2	2-1 corr	Chi2	Mean	SD	2-1 corr	Chi2	Mean	SD
F27	16.30	0.44	51.30	0.27	**33.8**	24.7	35.10	7.11	**35.10**	-
F2.14	8.23	0.08	-	-	**8.23**	-	-	-	**-**	-

Table 8. Results of SPR experiments performed with the best candidates of the first and second virtual screening (Fx and F2.x) at 1% and 5% DMSO and 15-25ºC. Columns "2-1 corr" represent values of flow channel 2 subtracting the signal from the channel 1 (reference channel) of the same chip. The percentage of DMSO was changed to solve the solubility issues of these compounds. Table extracted from Camps-Fajol's thesis, 2022.

4.1.3. Virtual structural optimization of the candidates by Structure Activity Relationships (SAR) and medicinal chemistry (F3.x candidates)

The first virtual optimization was done from the best candidates of the previous virtual screenings (F27 and F2.14), following 2 approaches: SAR by medicine chemistry expertise, and a later optimization step using rigid body and induced-fit docking.

SAR analysis was focused in a scaffold analysis and risk assessment of F27 and F2.14. Dr. Andy Baxter, from ProPharma Partners Ltd, considered both candidates with a sub-optimal physicochemical properties because of their relatively high lipophilicity, high predicted metabolic turnover, low predicted solubility, and high risk of toxicity due to [redacted]. Despite of these facts, both candidates presented low molecular weight (<300 g/mol), what allows to incorporate functionality at adjusting physicochemical characteristics. Finally, F27 was considered the one with more favorable properties for a "hit to lead" exploration. Accordingly, the new strategy was focused on [redacted] in order to reduce the toxicity (Camps-Fajol's thesis, 2022).

After the medicine chemistry analysis, the interaction between the hits and [redacted] was studied using FragPele software from NBD (*in silico* drug discovery CRO). The first visual analysis and validation of the interaction was performed with the docking program "GLIDE", using rigid-body and induced-fit methods. PELE's induced-fit simulation was applied later. FragPELE software involves a fragment library preparation, fragment linkage, fragment reduction, fragment growing, and sampling and scoring (Perez et al., 2020). After both strategies, the final proposes for F27 analogues were (Figure 28): [redacted]

[redacted] From all those hits, the ones with better binding energies were selected for synthesis, and finally, 13 out of 18 molecules selected were synthetized by TCG Lifesciences Contract Research and Manufacturing Service Company (F3.x), as shown in Figure 29.

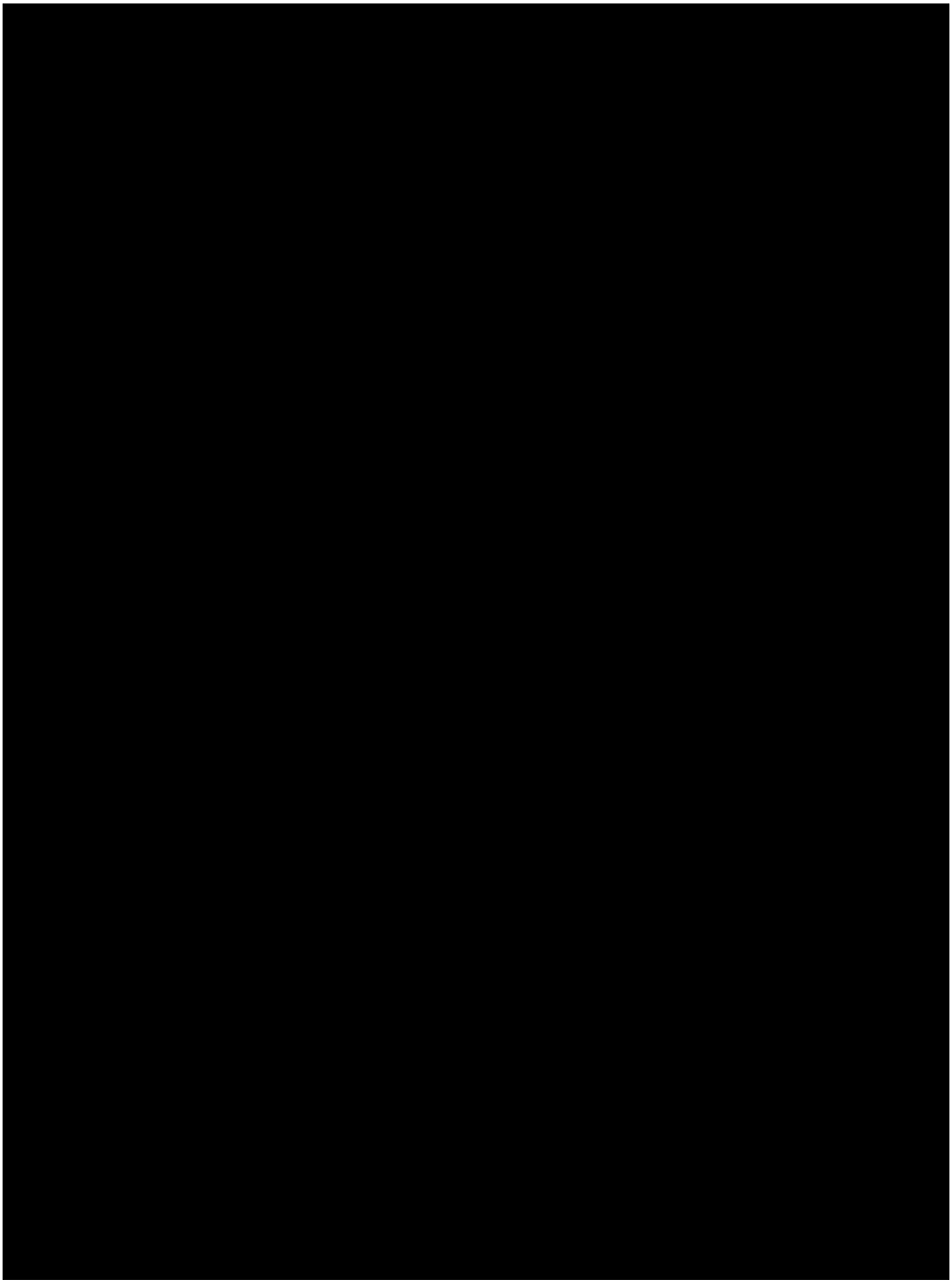


Figure 28. **First optimization round**: F3.x design strategy.

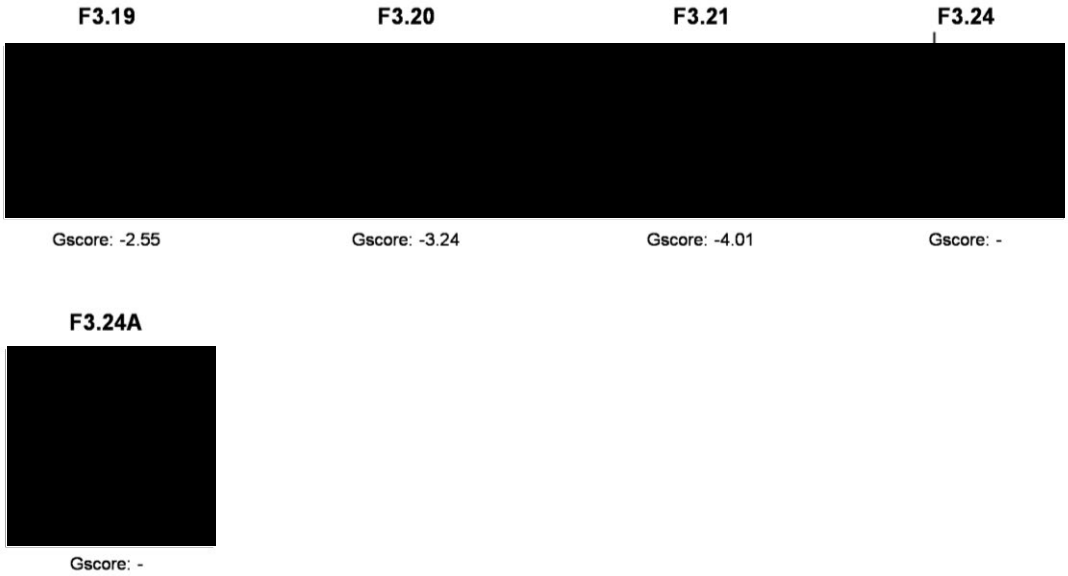


Figure 29. **F3.x candidates for synthesis**. Candidates in green were synthetized while candidates in red could not be synthetized.

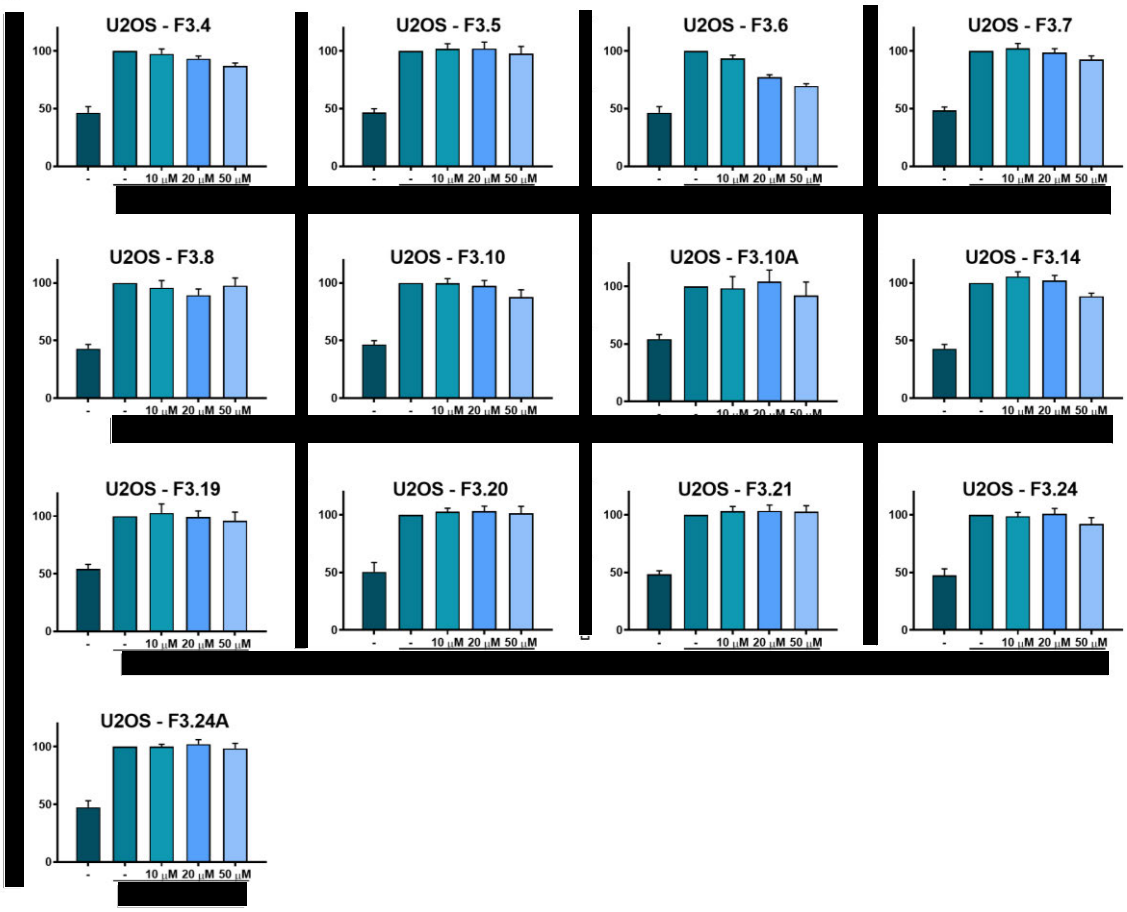
4.1.4. F3.x candidates' validation

The validation of the ability of the candidates of the first virtual optimization to inhibit [redacted] was studied in U2OS and hFIB cells in parallel. Cells were treated [redacted] at 10, 20 and 50 µM for 18h (Figure 30).




F3.19
F3.20
F3.21
F3.24
Gscore: -2.55
Gscore: -3.24
Gscore: -4.01
Gscore: -
F3.24A
Gscore: -

B.


U2OS - F3.4
U2OS - F3.5
U2OS - F3.6
U2OS - F3.7
U2OS - F3.8
U2OS - F3.10
U2OS - F3.10A
U2OS - F3.14
U2OS - F3.19
U2OS - F3.20
U2OS - F3.21
U2OS - F3.24
U2OS - F3.24A
100
50
0
- - 10 μM 20 μM 50 μM

C.

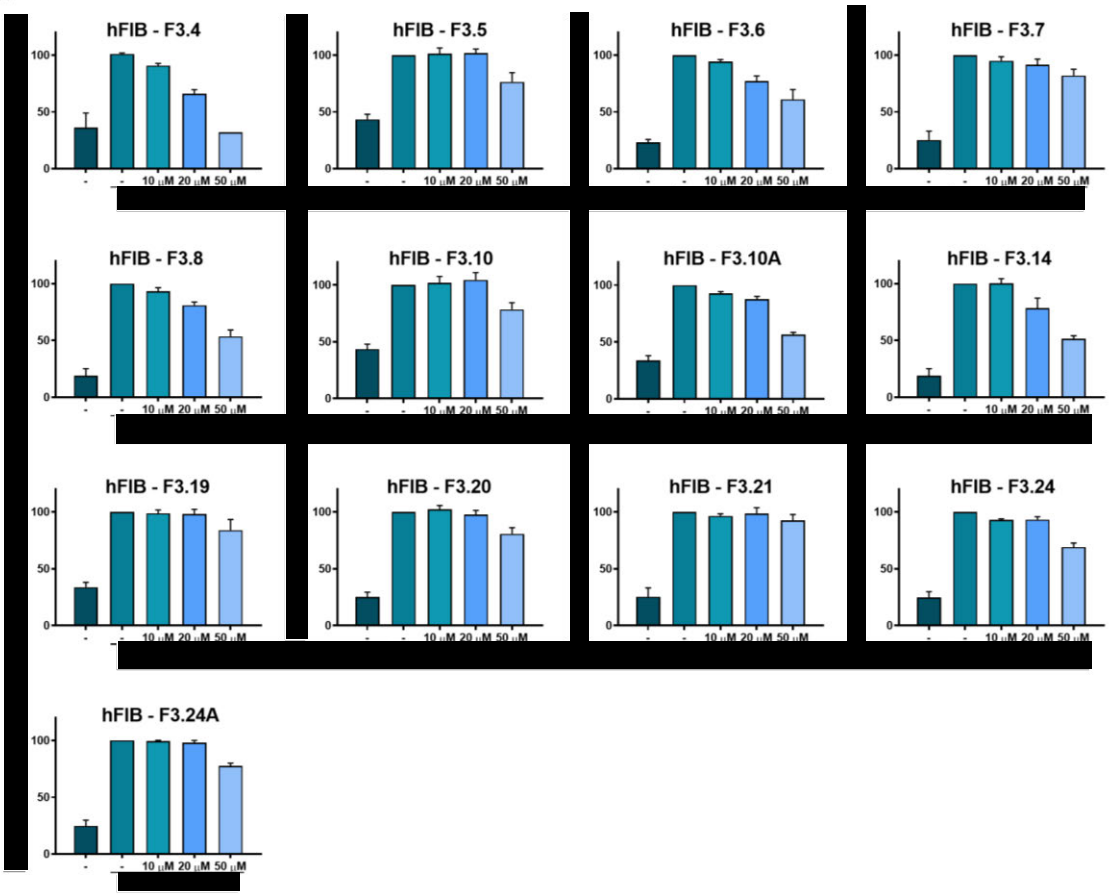


Figure 30. [redacted] **inhibition by F3.x candidates for the first optimization round**: chemical formulation with the glide score (Gscore, kcal/mol) obtained by docking (**A**.) and in vitro validation in U2OS (**B**.) and hFIB cell lines (**C**.). Experiments were performed by treating the cells with potential [redacted] inhibitors at concentrations between 10-50 μM, [redacted] (see methods). Culture was incubated overnight. [redacted] was analyzed by WB and quantified using ImageJ software and data normalized. Graphs represent mean ± SEM of at least three independent experiments. A representative WB of each candidate is showed in Appendix 1.

Almost all candidates inhibited [redacted] better in hFIB that in U2OS cells; highlighting F3.6, with good inhibition effect in both cell lines, and F3.8, F3.10A and F3.14 in hFIB.

After the WB validation of these candidates, an in vitro study of the interaction between [redacted] and F3.x hits were performed using SPR. At the beginning of the project, [redacted] concentrations between 0.3125 and 10 μM were tested at different temperatures between 10 to 25 ºC, obtaining the best results at 10ºC, with K_D of 3.96 μM (Chi^2= 113). The K_D at 25ºC was higher, 15.43 μM (Chi^2= 2.39), but due to the solubility of the compounds -which were diluted in DMSO-, was the measure stablished for the following experiments (Camps-Fajol's thesis, 2022). The results of SPR with F3.x candidates and some of the best candidates of the Fx, were collected in Table 9.

KD (μM)	DMSO 1%. 25°C, HD																											
	1st exp		2nd exp		3rd exp				4th exp				5th exp				6th exp				Average 2-1 corr			Average 4-3 corr			TOTAL	
	2-1 corr	Chi^2	2-1 corr	Chi^2	2-1 corr	Chi^2	4-3 corr	Chi^2	2-1 corr	Chi^2	4-3 corr	Chi^2	2-1 corr	Chi^2	4-3 corr	Chi^2	2-1 corr	Chi^2	4-3 corr	Chi^2	Mean	SD	SEM	Mean	SD	SEM	Mean	SD
F1	-	-	-	-	-	-	-	-	-	-	-	-	-	-	-	-	28.85	657	31.88	347	**28.9**	-	-	**31.9**	-	-	**30.4**	2.1
F27	13.96	0.62	0.6	7.93	29.39	117	25.76	12.2	23.68	129	21.67	13.8	20.75	5.63	15.82	6.69	12.43	46.6	12.27	32.4	**16.8**	10.1	5.1	**18.9**	6.0	3.0	**17.8**	1.5
F32	-	-	-	-	-	-	-	-	-	-	-	-	-	-	-	-	23.94	1630	24.74	632	**23.9**	-	-	**24.7**	-	-	**24.3**	0.6
F3.4	×	×	×	×	-	-	-	-	-	-	-	-	-	-	-	-	-	-	-	-	×	×	×	×	×	×	×	×
F3.5	17.9	0.24	76.04	77.6	-	-	-	-	-	-	-	-	-	-	-	-	-	-	-	-	**47.0**	41.1	20.6	**-**	-	-	**47.0**	-
F3.6	×	×	×	×	-	-	-	-	-	-	-	-	-	-	-	-	-	-	-	-	×	×	×	×	×	×	×	×
F3.7	17.8	5.15	73.83	119	-	-	-	-	-	-	-	-	-	-	-	-	-	-	-	-	**45.8**	39.6	19.8	**-**	-	-	**45.8**	-
F3.8	12.96	0.19	21.14	0.0654	-	-	-	-	-	-	-	-	5.14	1.15	3.09	0.797	13.63	1.59	11.24	0.392	**13.2**	6.5	3.3	**7.2**	5.8	2.9	**10.2**	4.3
F3.10	1.87	0.05	6.65	0.143	-	-	-	-	-	-	-	-	-	-	-	-	-	-	-	-	**4.3**	3.4	1.7	-	-	-	**4.3**	3.4
F3.10A	36.54	2.21	27.9	230	-	-	-	-	19.11	2.040	36.83	12.3	-	-	-	-	-	-	-	-	**27.9**	8.7	4.4	**36.8**	-	-	**32.3**	6.3
F3.14	98.57	9.79	197.9	↑	-	-	-	-	-	-	-	-	-	-	-	-	-	-	-	-	**148.2**	-	-	**-**	-	-	**148.2**	-
F3.19	18.52	50.2	23.26	15.3	-	-	-	-	26.96	2.710	31.24	39.2	38.15	50.9	34.96	43.9	-	-	-	-	**26.7**	8.4	4.2	**33.1**	2.6	-	**29.9**	4.5
F3.20	-	-	-	-	76.4	7.85	27.61	7.94	4.01	161	1.917	10.2	7.24	18.3	8.18	2.69	-	-	-	-	**29.2**	40.9	20.4	**12.6**	13.4	6.7	**20.9**	11.8
F3.21	153	20.9	122.4	179	-	-	-	-	-	-	-	-	-	-	-	-	-	-	-	-	**137.7**	21.6	10.8	**-**	-	-	**137.7**	-
F3.24	-	-	-	-	58.08	2.75	198	0.0929	42.9	5.64	167.3	0.0748	-	-	-	-	-	-	-	-	**50.5**	10.7	5.4	**182.7**	0.01	0.01	**116.6**	93.5
F3.24A	-	-	-	-	37.89	11.6	98.07	2.12	31.02	10.4	123	0.204	-	-	-	-	-	-	-	-	**34.5**	4.9	2.4	**110.5**	1.4	0.7	**72.5**	53.8

Table 9. Results of SPR experiments performed with the best candidates from the first virtual screening and the candidates of the first virtual optimization (F3.x) at 1% DMSO and 25ºC. Columns "2-1 corr" or "4-3 corr" represent values of flow channel 2 or 4 subtracting the signal from the channel 1 or 3 (reference channels) of the same chip. Cells highlighted in green represent results of the candidates with good interaction between the ligand and sensorogram shapes; crosses represent the cases with no detected interaction and upward arrows describe Chi^2 values extremely higher. Table edited from Camps-Fajol's thesis, 2022.

4.1.5. Second virtual structural optimization of the candidates by medicinal chemistry (F4.x candidates)

Considering the best candidates of the first and second screening, and the first optimization round, the second virtual structural optimization was done with the collaboration of the CRO NBD. This optimization round was based in the visual analyses of the functional structures of the best candidates until the moment, as it is shown in Figure 31.



Figure 31. **Second optimization round:** F4.x design strategy.

The binding energy of these compounds was not measured because the optimization was focused on the medicinal chemistry advise. A total of 5 compounds were designed following these strategies: (Figure 32).

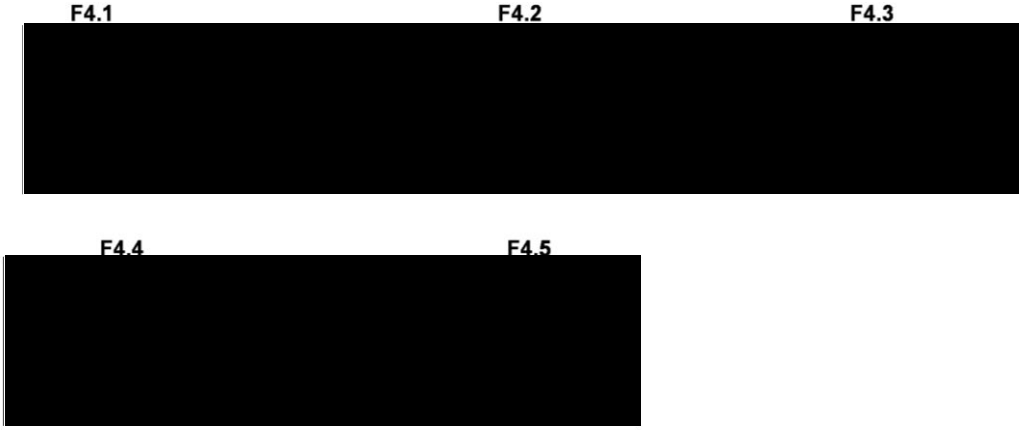


Figure 32. **F4.x candidates for synthesis**. Five compounds were designed: F4.1 combining F27 and F3.10 structures, [redacted] F4.2, F4.3 and F4.4, mixing F1 and F27 structures, [redacted]; and F4.5 [redacted]

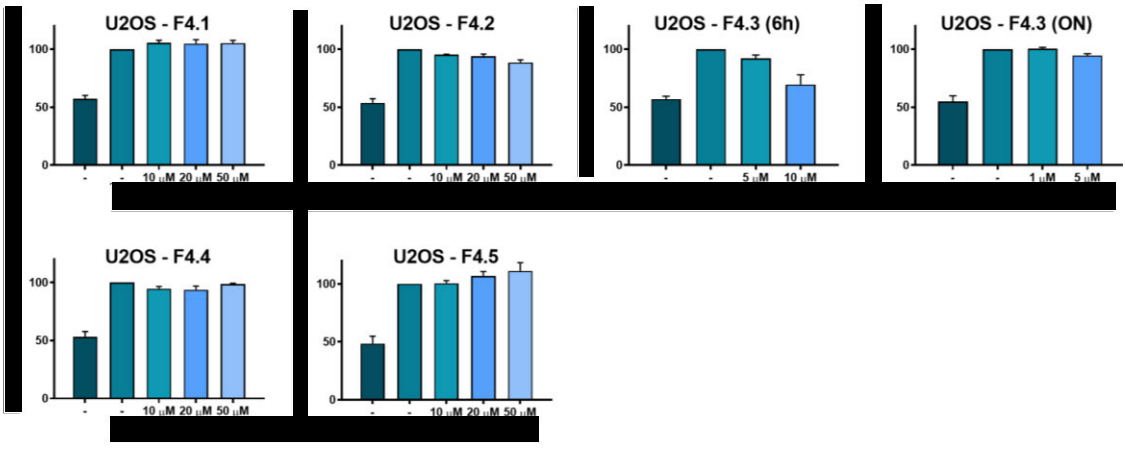
4.1.6. F4.x candidates' validation

The validation of the ability of the candidates of the second virtual optimization to inhibit the [redacted] was studied in U2OS and hFIB cells. Cells were treated [redacted] at 10, 20 and 50 µM over 18h, firstly. The F4.3 candidate presented toxicity at the stablished doses at 18h, and therefore, additional conditions were tested in order to find the doses that were effective in inhibiting [redacted], but non-toxic to the cells. As shown in Figure 33, the higher dose of this compound was 10 µM for ON treatment in hFIB and 20 µM for 6h treatment in the same cell lines, with lower doses in U2OS. In both cases, [redacted] reduced in cells upon F4.3 treatment.

A.



B.



C.

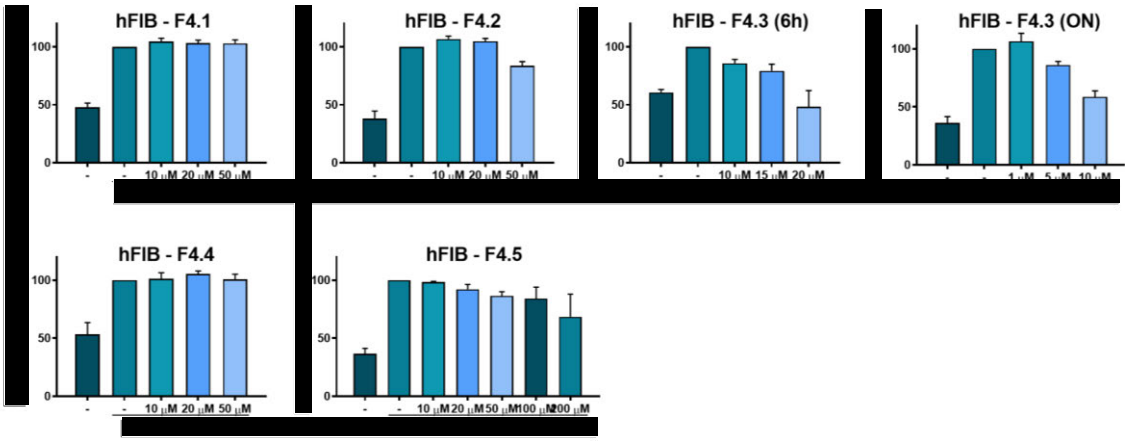


Figure 33. [redacted] **inhibition by F4.x candidates for the second optimization round**: chemical formulation (**A**.) and in vitro validation in U2OS (**B**.) and human hFIB cell lines (**C**.). Experiments were performed by treating the cells with potential [redacted] inhibitors at concentrations between 1-50 µM, [redacted] (see methods). Culture was incubated overnight except with the F4.3, in inhibitory effect was observed at 6h and with lower doses (1-20 µM). [redacted] was analyzed by WB and quantified using ImageJ software and data normalized. Graphs represent mean ± SEM of at least three independent experiments. A representative WB of each candidate is showed in Appendix 1.

After the WB validation of these candidates, an in vitro study of the interaction between [redacted] and F4.x hits was performed using SPR, as in previous rounds. The conditions of the first experiments with the F4.x hits were DMSO 1% and 25ºC, at high density program. But in an attempt to correct the solubility issues of some of the molecules, the percentage of DMSO was increased to 5% (Table 10). Even that, the measures of F4.4 and F4.5 were not confinable, whereas F4.1 was shown the best soluble compound in K_D terms. As shown in Table 10, F1, F27 and F32 were also measured in this round.

KD (µM)	DMSO 1%. 25°C, HD									DMSO 5%. 25°C, HD						
	1st exp		2nd exp		3rd exp		Average 2-1 corr			1st exp		2nd exp		Average 2-1 corr		
	2-1 corr	Chi2	2-1 corr	Chi2	2-1 corr	Chi2	Mean	SD	SEM	2-1 corr	Chi2	2-1 corr	Chi2	Mean	SD	SEM
F1	-	-	-	-	87.6	7.01	**87.6**	-	-	-	-	↑	0.02	↑	-	-
F27	11.98	1.07	39.56	2.5	33.84	0.88	**28.5**	14.6	7.3	0.26	37.5	1681	0.06	**840.6**	1188.5	594.2
F32	-	-	-	-	2245	0.12	**2245.0**	-	-	-	-	507.2	0.007	**507.2**	-	-
F4.1	0.16	0.04	0.87	0.01	7.72	0.007	**2.9**	4.2	2.1	0.05	0.23	1.46	0.13	**0.8**	1.0	0.5
F4.2	1199	0.004	1498	0.02	-	-	**1348.5**	211.4	105.7	248	1.01	128.2	0.15	**188.1**	84.7	42.4
F4.3	4.73	0.07	1.67	0.02	3.56	4.56	**3.3**	1.5	0.8	8.02	0.05	26.54	0.06	**17.3**	13.1	6.5
F4.4	×	×	×	×	-	-	×	×	×	×	×	-	-	×	×	×
F4.5	×	×	332	0.04	-	-	**332.0**	234.8	117.4	×	×	-	-	×	×	×

Table 10. Results of SPR experiments performed with candidates of the second virtual optimization (F4.x) at 1% and 5% DMSO and 25ºC. Columns "2-1 corr" represent values of flow channel 2 subtracting the signal from the channel 1 (reference channel) of the same chip. The percentage of DMSO was changed to solve the solubility issues of these compounds. Cells highlighted in green represent results of the candidates with good interaction between the ligand and sensorgram shapes; crosses represent the cases with no detected interaction and upward arrows describe Chi^2 values extremely higher.

One of the main limitations of [redacted] candidates is that the effect is usually associated with cell toxicity, impeding common experiments as traditional cell survival assays. However, another approach that was used at the beginning of the project to test whether the best candidates chemosensitized cells in presence of [redacted] was the clonogenic assay. That assay was done previously with F27 using U2OS cells (Camps-Fajol's thesis, 2022), treated 30 min with the test compound, and an additional 90 min with [redacted] (Figure 34). Figure 35A shows the chemosensitivity [redacted] by F27 in hFIB cells, in order to be compared the hFIB and U2OS results. Figure 35B shows the effect [redacted] of the best candidates of the F3.x, F3.14, in hFIB. Figure 35C shows the chemosensitivity effect of F4.3 in U2OS and in hFIB.

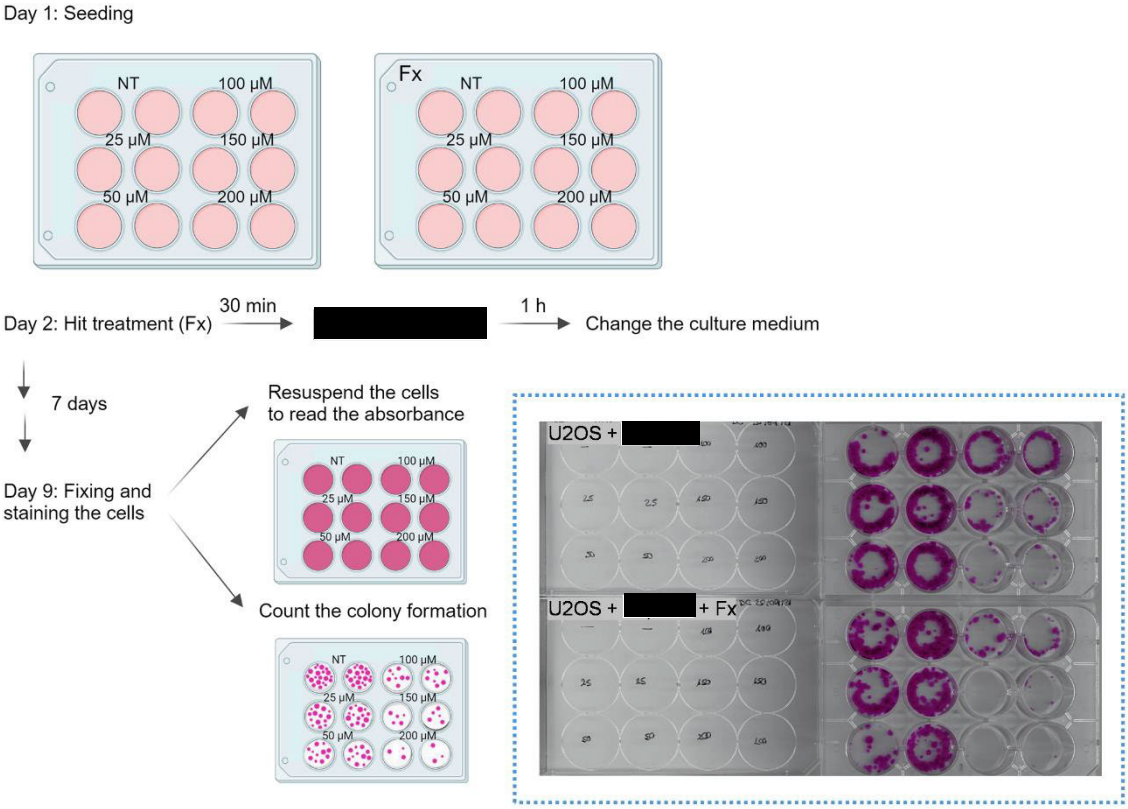


Figure 34. **Workflow of cytotoxicity clonogenic assay.** U2OS and hFIB cells were seeded onto 12-well plates at densities of 1-5×10^2 cells per well. The following day, one plate received treatment with a stablished dose of the compound, followed by addition of [redacted] at doses ranging from 25 to 200 µM, 30 min later. Duplicate doses were used for each concentration, with a duplicate set of wells treated solely with the hit compound. Another plate was treated with [redacted] alone at the same doses, without pre-incubation with the [redacted] candidate, to compare the chemosensitivity effects between the two drugs. One hour after adding [redacted] the medium was changed, and the plates were incubated for 7 days. The experiment was terminated by fixing and staining the cells. Optical density measurements at 510 nm were obtained using a microplate reader. Statistical analysis was performed using GraphPad Prism software, expressing data as mean ± SEM from at least four independent experiments with parametrical distribution.

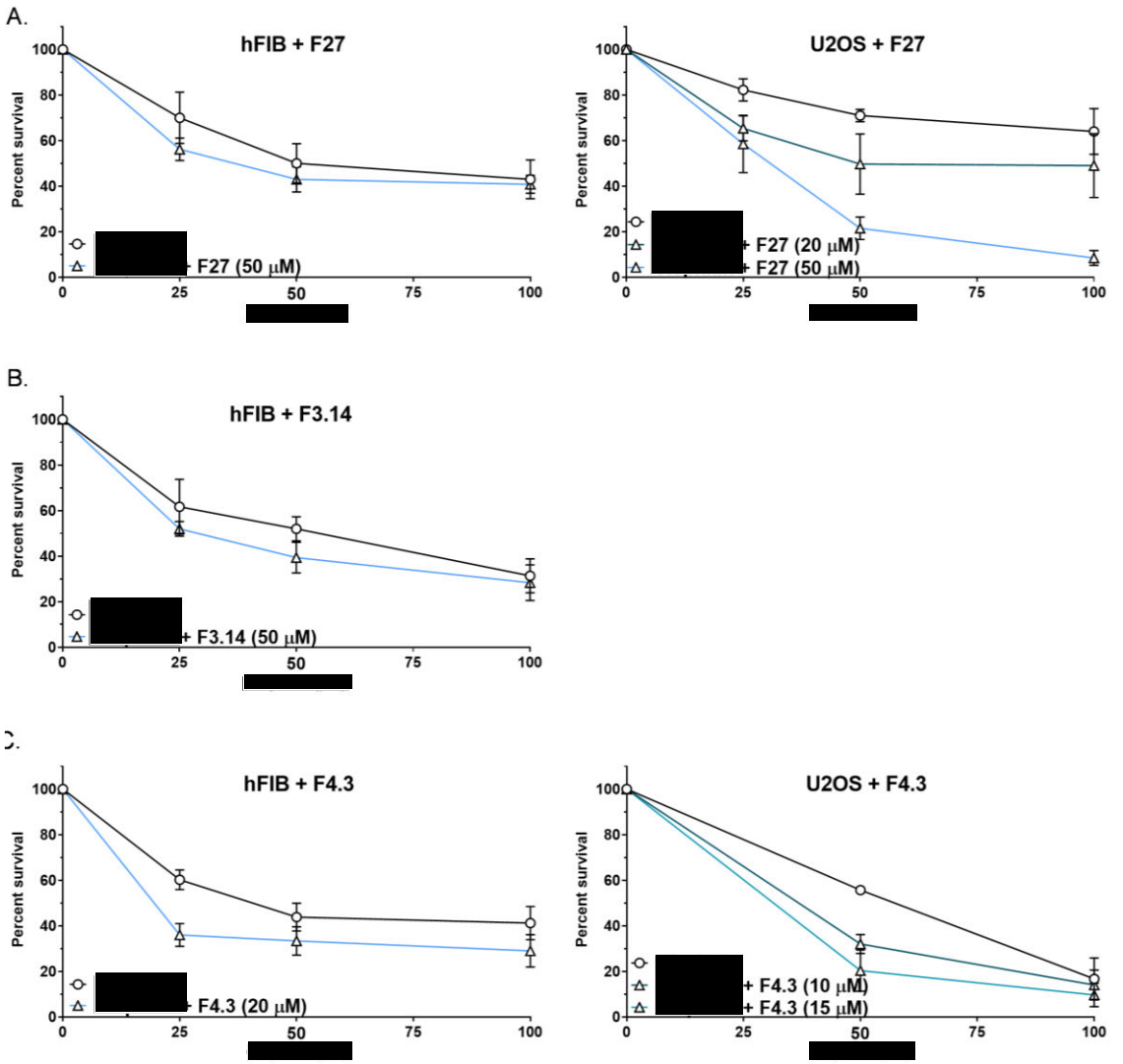


Figure 35. Clonogenic assay in hFIB and U2OS. Graphs represent the percentage of cell survival after 30 minutes of a [redacted] hit pre-incubation followed by 1h of this compound + [redacted] in different dosses (0-25-50-100 µM). After changed the culture medium, growth was allowed for 7 days. **A**. Graph represents the percentage of cell survival in hFIB (left) treated with 50 µM of F27 in comparison with 20 and 50 µM of F27 in U2OS (right). U2OS graph was extracted from the Camps-Fajol's thesis (2022) for the comparison. **B**. Graph represents the percentage of cell survival in hFIB treated with 50 µM of F3.14. **C**. Graph represents the percentage of cell survival in hFIB (left) treated with 20 µM of F4.3 in comparison with 10 and 15 µM of F4.3 in U2OS (right). Mean ± SEM of at least three independent experiments with similar results is shown in these graphs.

[redacted] To test F4.3, U2OS YFP-[redacted] cells were seeded on glass coverslips in a 6-well plate. The treatment with F4.3 was done 24h later [redacted] Cells were washed, fixed, permeabilized, and dried 6h after the treatment. Coverslips were then mounted with DAPI-containing mounting medium.

[redacted] shown in Figure 36. As no other candidate from the F2.x and F3.x rounds was better than F27, this experiment was not considered necessary to be repeated until the F4.3. In Figure 37, U2OS cells with yellow [redacted] protein are shown [redacted]



Figure 36. Workflow of immunofluorescence assay. [redacted] Immunofluorescence assay done with 4×10^5 U2OS YFP-[redacted] cells, that were seeded on glass coverslips in a 6-well plate, to be treated with the [redacted] compound [redacted] Coverslips were mounted with DAPI-containing mounting medium for DNA counterstaining. [redacted]



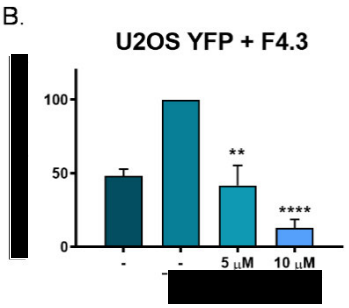


Figure 37. inhibition by F4.3. A. immunofluorescence in U2OS YFP cells. **B**. Quantification of three independent experiments. Graph represent mean ± SEM. ANOVA test was done to compare the results, with adjusted Pvalue <0.05% (5 µM) and Pvalue <0.0001 (10 µM).

.

Figure 38.

The main experiments that were used for the candidates' validation were done in cells, except for SPR, in which the low solubility of the hits acted a bottleneck. During the international stay at , an adapted protocol using the knowledge of the group about the was conducted to test the best hits , but in a cell-independent manner.

Despite the initial objective was to test the candidates in their assay , the protocol was finally adapted. Due to the DMSO in which the hits were dissolved, and the small volumes needed for , buffer and compounds were not mixture properly. Therefore, instead of using , samples were mixture with Laemmli 2x in order to load an acrylamide gel and transfer it to a nitrocellulose membrane. After the incubation with a streptavidin antibody, membrane was exposed to measure (Figure 39).

[redacted]

Figure 39. **Workflow of biochemical western blot** [redacted].

Figure 40 shows the [redacted] results from the experiments that were carried out after following mentioned protocol, [redacted]

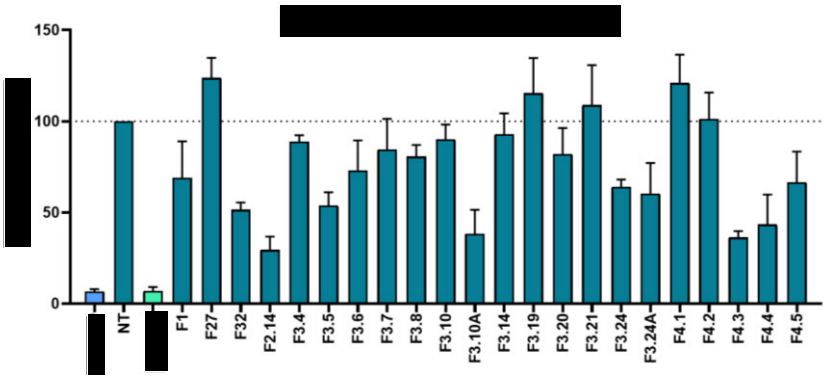


Figure 40. [redacted] **activity** [redacted] Graphs represent mean ± SEM of at least three independent experiments.

Despite the increase [redacted] in presence of F27, other compounds previously considered as interesting hits showed [redacted] decrease, as F2.14, F3.6, F3.10A or F4.3. F3.5, F3.24, F3.24A, F4.4 and F4.5 also showed a decrease [redacted] in that experiment.

4.1.7. Third virtual structural optimization of the candidates by molecular docking and medicinal chemistry (F5.x candidates)

The third virtual screening was also done in collaboration with NBD. As was mentioned previously, the strategy of this optimization was based on maintaining the central scaffold [redacted] and exploring a new replacement point [redacted] to boost the interactions of the new groups [redacted]. After the design, a virtual molecular docking screening was done using GLIDE docking program, as in the first virtual screening. Candidates to synthetize were evaluated according to binding energy and chemists' criteria (Figure 41).



Figure 41. **Third optimization round:** F5.x design strategy.

The main limitation of this optimization round was the synthesis of the compounds: initially, 18 compounds were proposed to synthetize, but only 5 of that 18 were finally synthetized (Figure 42). As additional 6 synthetic intermediaries were synthetized, the final assessment was of 11 new compounds (Figure 43A).



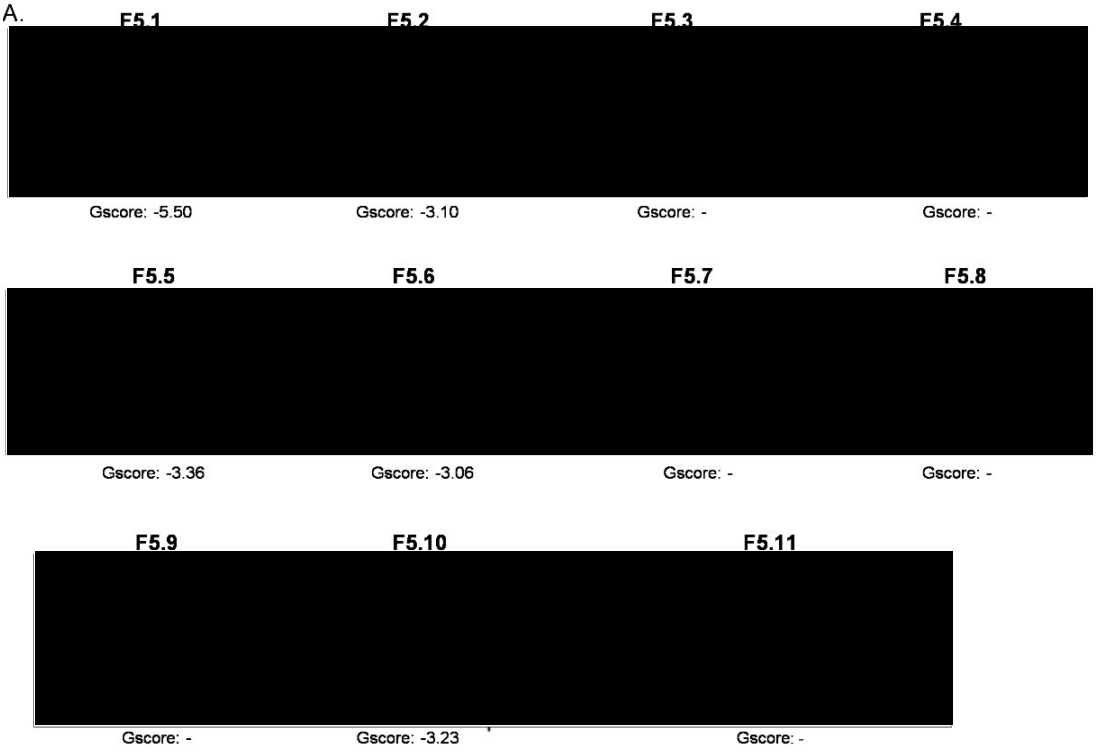


Figure 42. F5.x candidates for synthesis. Proposed candidates for synthesis: in green candidates that could be synthetized, in red candidates that could not be synthetized. Chemical formulation with the glide score (Gscore, kcal/mol) obtained by docking.

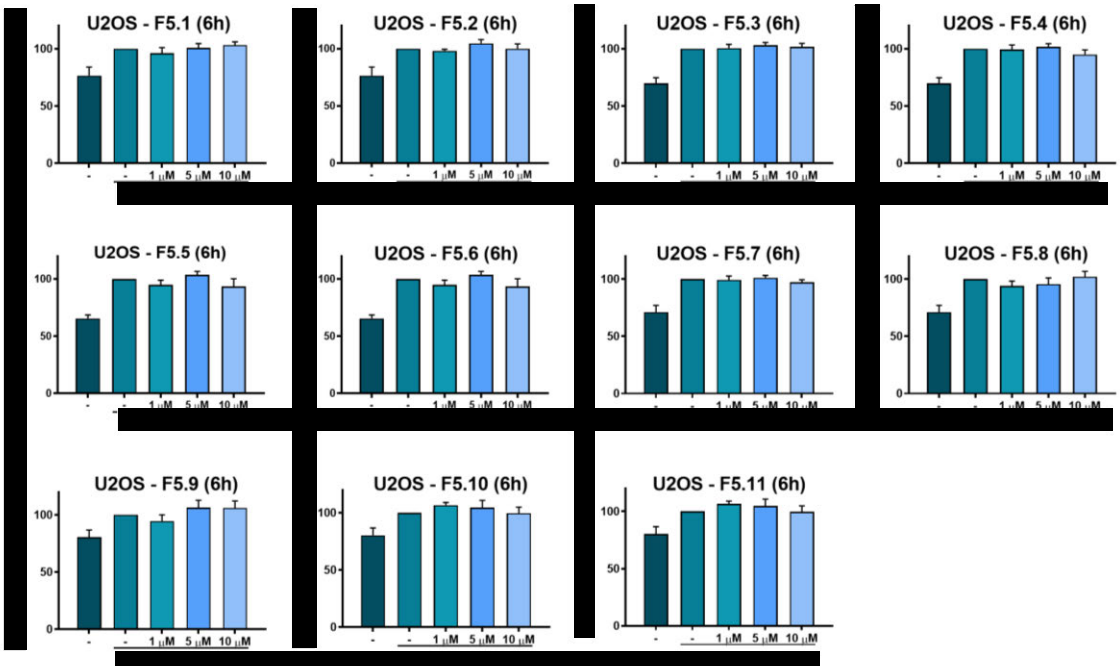
4.1.8. F5.x candidates' validation

The validation of the third virtual optimization candidates by their ability to inhibit [redacted] was studied in U2OS and hFIB cells. Cells were treated [redacted] at 1, 5 and 10 µM at 6h and ON, to evaluate the effect of the candidates in short and long time (Figure 43). After 6h of treatment, the candidates' effect was not as visible as with ON treatment, in which 10 µM of F5.6 could reduce [redacted] almost 60% in U2OS and in hFIB.

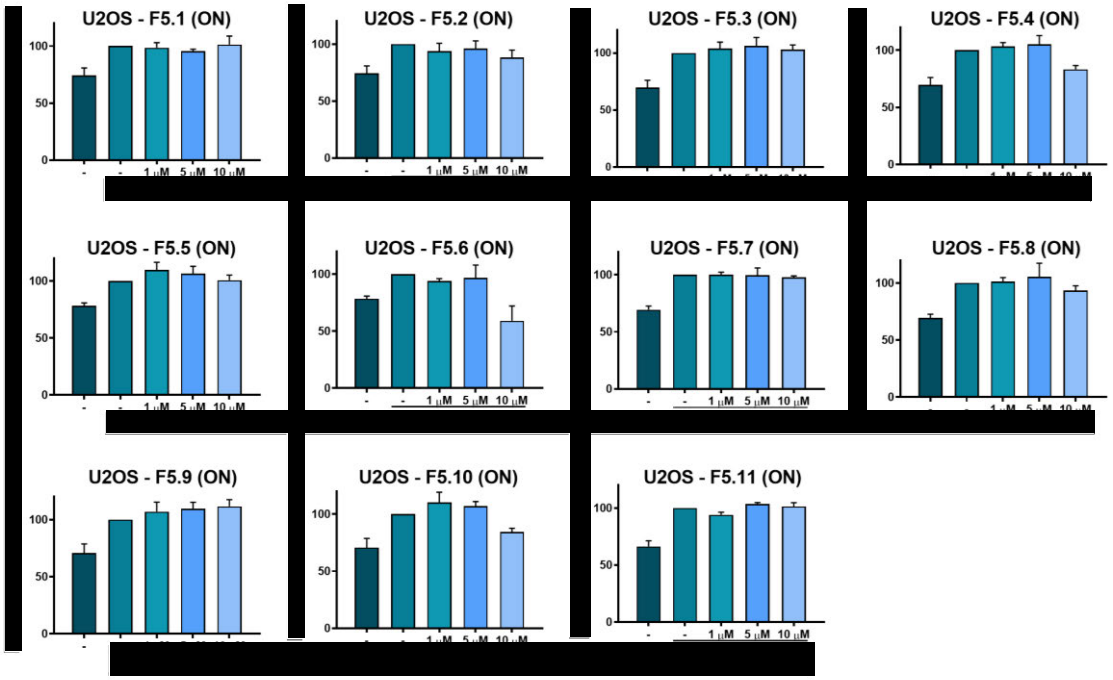
A.


F5.1
F5.2
F5.3
F5.4
Gscore: -5.50
Gscore: -3.10
Gscore: -
Gscore: -
F5.5
F5.6
F5.7
F5.8
Gscore: -3.36
Gscore: -3.06
Gscore: -
Gscore: -
F5.9
F5.10
F5.11
Gscore: -
Gscore: -3.23
Gscore: -

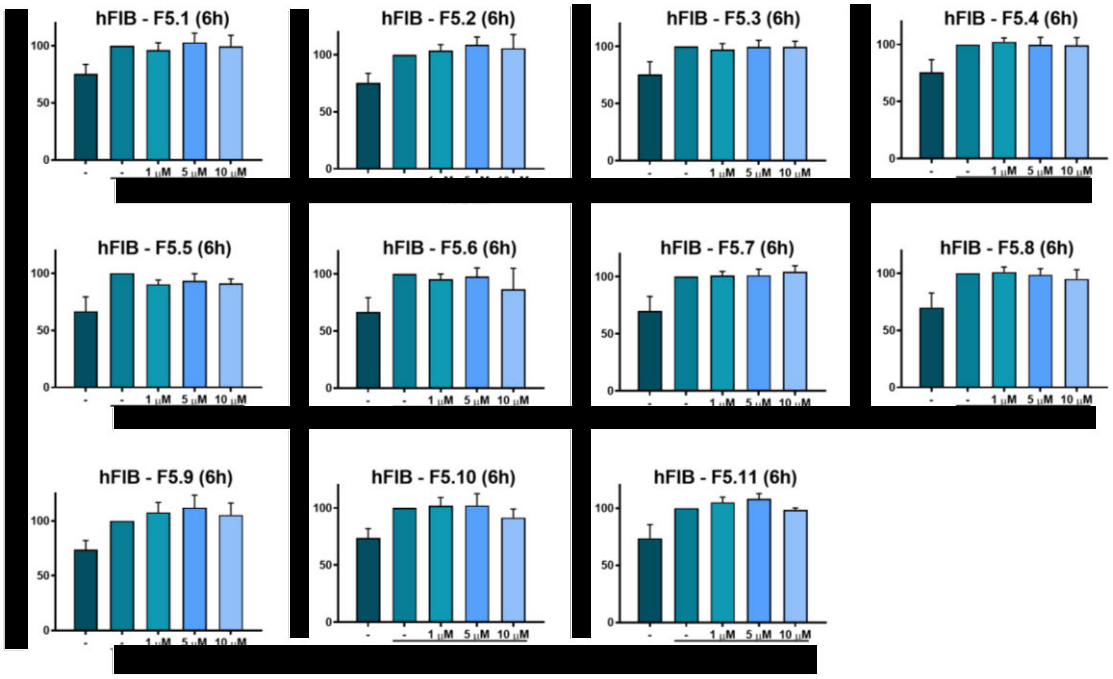
B.


U2OS - F5.1 (6h)
U2OS - F5.2 (6h)
U2OS - F5.3 (6h)
U2OS - F5.4 (6h)
U2OS - F5.5 (6h)
U2OS - F5.6 (6h)
U2OS - F5.7 (6h)
U2OS - F5.8 (6h)
U2OS - F5.9 (6h)
U2OS - F5.10 (6h)
U2OS - F5.11 (6h)

C.


U2OS - F5.1 (ON)
U2OS - F5.2 (ON)
U2OS - F5.3 (ON)
U2OS - F5.4 (ON)
U2OS - F5.5 (ON)
U2OS - F5.6 (ON)
U2OS - F5.7 (ON)
U2OS - F5.8 (ON)
U2OS - F5.9 (ON)
U2OS - F5.10 (ON)
U2OS - F5.11 (ON)
100
50
0
- - 1 μM 5 μM 10 μM

D.


hFIB - F5.1 (6h)
hFIB - F5.2 (6h)
hFIB - F5.3 (6h)
hFIB - F5.4 (6h)
hFIB - F5.5 (6h)
hFIB - F5.6 (6h)
hFIB - F5.7 (6h)
hFIB - F5.8 (6h)
hFIB - F5.9 (6h)
hFIB - F5.10 (6h)
hFIB - F5.11 (6h)
100
50
0
- - 1 μM 5 μM 10 μM

E.

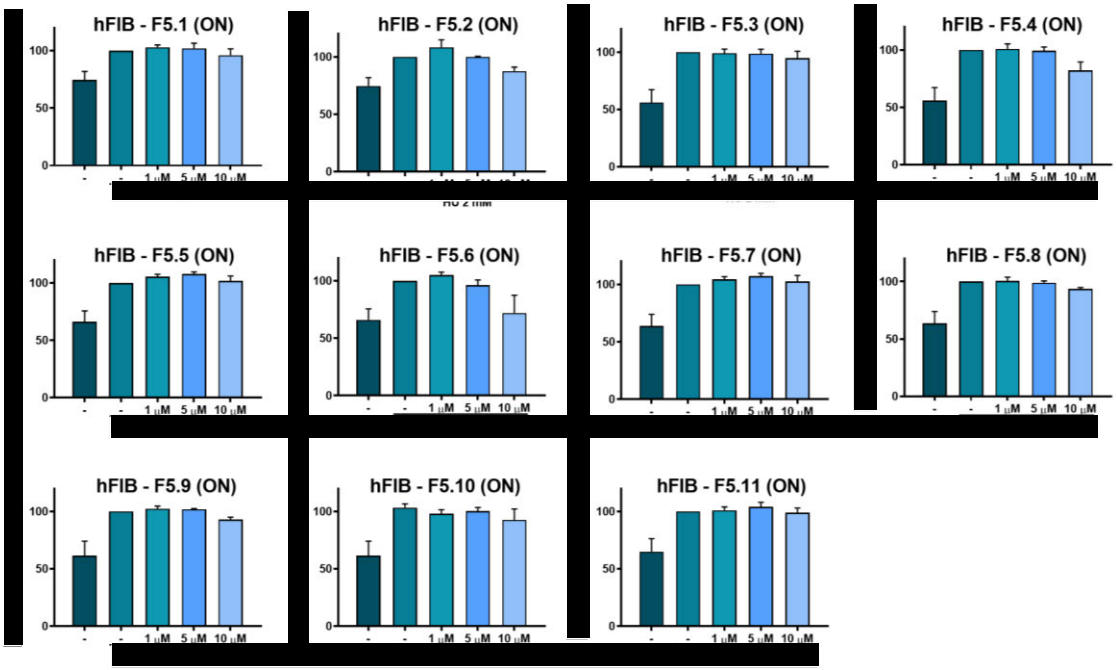


Figure 43. [redacted] **inhibition by F5.x candidates for the third optimization round**: chemical formulation with the glide score (Gscore, kcal/mol) obtained by docking (**A**.) and in vitro validation in U2OS (**B.,C**.) and in hFIB cell lines (**D.,E**.). Experiments were performed by treating the cells with potential [redacted] inhibitors at concentrations between 1-10 μM, [redacted] (see methods). Culture was done for 6 hours (**B**., **D**.) and overnight (ON) (**C**., **E**.). [redacted] was analyzed by WB and quantified using Image J software and data normalized. Graphs represent mean ± SEM of at least three independent experiments. A representative WB of each candidate is showed in Appendix 1.

After this validation, an in vitro study in Biacore was done with the candidates, as in previous rounds. Commercial [redacted] and own-synthetized [redacted] were tested in different channels in order to compare the results (2-1 and 4-3, respectively). K_D was measured in DMSO 1% and 25ºC at high density program, and only two of the compounds showed poor solubility in those conditions (Table 11).

As shown in Table 11, results obtained with commercial [redacted] and synthesized and purified [redacted] were comparable in the most of the cases. However, mean value obtained in F5.4 using commercial [redacted] was 10 times lower than when it was verified its interaction with [redacted] In F5.5, mean value obtained with commercial [redacted] was also lower than with [redacted] Contrarily, in mean value obtained in F5.11 interaction with commercial [redacted] was higher than with [redacted] Mean between both conditions was done in order to compare the final results, and F5.2 and F5.6 showed affinity with the target similar than the obtained with F27 or F4.3.

KD (μM)	DMSO 1%. 25°C, HD																			
	1st exp				2nd exp				3rd exp				Average 2-1 corr			Average 4-3 corr			TOTAL	
	2-1 corr	Chi^2	4-3 corr	Chi^2	2-1 corr	Chi^2	4-3 corr	Chi^2	2-1 corr	Chi^2	4-3 corr	Chi^2	Mean	SD	SEM	Mean	SD	SEM	Mean	SD
F27	24.50	41.1	48.30	3.35	23.5	4.11	30.9	4.87	8.9	8.59	12	2.28	**19.0**	8.7	2.9	**30.4**	18.2	6.1	**24.7**	8.1
F4.3	1.6	2.62	1.2	3.00	0.8	4	1.9	0.498	2.1	0.433	2.4	0.09	**1.5**	0.7	0.2	**1.8**	0.6	0.2	**1.7**	0.2
F5.1	↑	0.68	9.3	4.75	-	-	-	-	6.14	0.28	↑	14	**-**	-	-	-	-	-	-	-
F5.2	3.78	466	4.46	133	1.16	3.86	2.25	1.44	0.12	0.48	3.11	0.36	**1.7**	1.9	0.6	**3.3**	1.1	0.4	**2.5**	**1.1**
F5.3	8.47	2.54	12.62	1.9	47.09	4.35	56.01	0.45	209.7	2.13	226.3	1.04	**88.4**	106.8	35.6	**98.3**	112.9	37.6	**93.4**	7.0
F5.4	2.99	0.24	162	0.29	10.09	0.08	28.79	0.05	4.79	0.07	13.31	0.15	**6.0**	3.7	1.2	**68.0**	81.7	27.2	**37.0**	43.9
F5.5	18.4	1.15	44.78	0.28	34.47	1.64	68.37	0.37	34.94	1.25	63.28	0.25	**29.3**	9.4	3.1	**58.8**	12.4	4.1	**44.0**	20.9
F5.6	5.2	18.9	24.87	0.37	0.11	0.1	9.61	0.09	0.43	0.328	2.73	0.13	**1.9**	2.9	1.0	**12.4**	11.3	3.8	**7.2**	7.4
F5.7	414	5.62	↑	3.97	646.5	9.89	562.2	1.6	-	-	-	-	↑	164.4	54.8	↑			↑	
F5.8	1.22	1.32	0.18	2.27	28.44	1.16	88.84	0.29	38.61	1.9	47.27	1.23	**22.8**	19.3	6.4	**45.4**	44.4	14.8	**34.1**	16.0
F5.9	62.4	170	43.6	110.00	59.7	158.00	59.6	34.30	59.8	226	64.4	54.6	**60.6**	1.5	0.5	**55.9**	10.9	3.6	**58.3**	3.4
F5.10	27.3	61.9	36	9.14	11.1	56.50	42.6	0.343	28.7	17	32.7	4.42	**22.4**	9.8	3.3	**37.1**	5.0	1.7	**29.7**	10.4
F5.11	68.2	193	66.5	51.4	119.9	5.14	31	1.63	102	42.2	104	12.1	**96.7**	26.3	8.8	**67.2**	36.5	12.2	**81.9**	20.9

Table 11. Results of SPR experiments performed with candidates of the third virtual optimization (F5.x) at 1% DMSO and 25ºC. Columns "2-1 corr" or "4-3 corr" represent values of flow channel 2 or 4 (with commercial [redacted] or synthetized and purified [redacted] respectively) subtracting the signal from the channel 1 or 3 (reference channels) of the same chip. Cells highlighted in green represent results of the candidates with good interaction between the ligand and sensorogram shapes; crosses represent the cases with no detected interaction and upward arrows describe Chi^2 values extremely higher.

4.1.9. Forth virtual structural optimization of the candidates by virtual molecular docking and medicinal chemistry (F6.x candidates)

As the scaffold of F27, F4.3 and F5.6 -the best candidates until the moment- is similar, the fourth optimization round was focused in improve the characteristics of these compounds. Therefore, the first step in this optimization was based on stablish the importance [redacted] as a functional group in the hits, taking into consideration that the scaffold of all of them is composed by [redacted]. As the main hypothesis was that this quinoline confers cytotoxicity to the candidates, the design [redacted] dispensing with it was considered as favorable to this project. This optimization step was accomplished in collaboration with NBD. Virtual screening was done using GLIDE docking program, as well as considering the [redacted] structure [redacted] (Figure 44).



Figure 44. **Fourth optimization round:** F6.x design strategy.

The binding energy of structures [redacted] were compared to define the best [redacted] scaffold. [redacted] The final suggested candidates were ranked by binding energy (firstly), and by solubility (secondly). After that, candidate's evaluation was done taking in consideration if they were suitable for being synthetized, and 9 candidates were proposed for the synthesis (Figure 45). In collaboration with MCS, 7 out of 9 candidates and 3 intermediates were synthetized, named by F6.1 to F6.10 (Figure 46A).

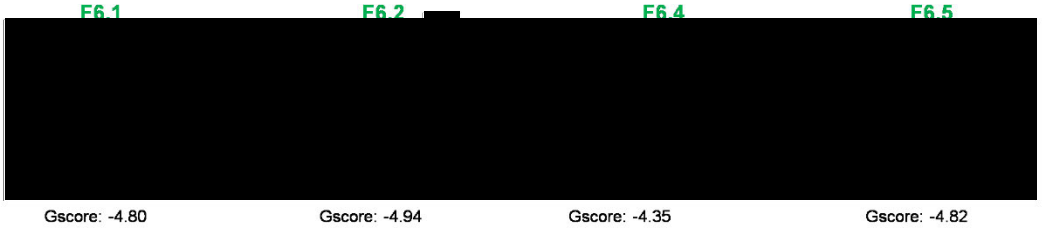
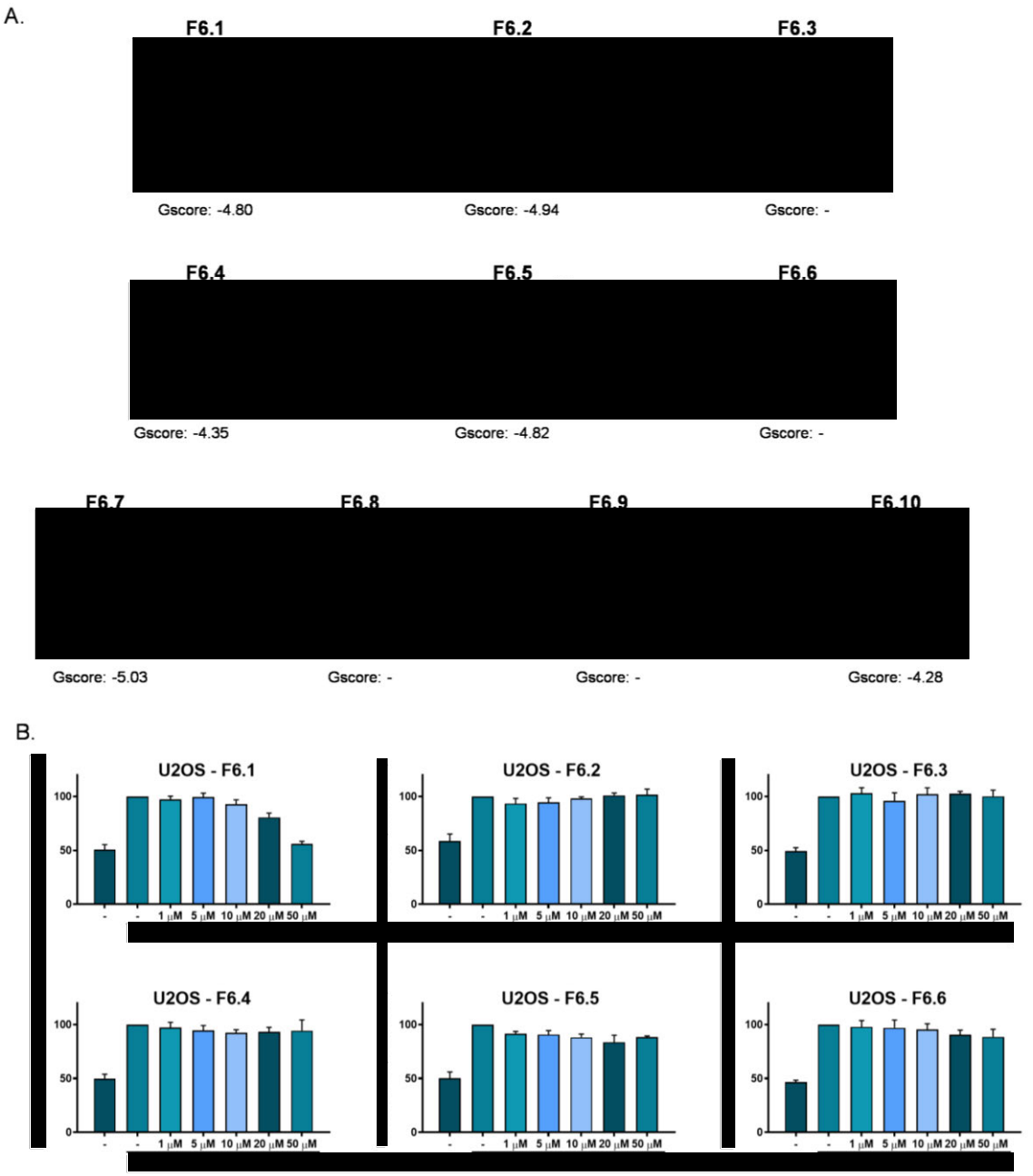




Figure 45. F6.x candidates for synthesis. Proposed candidates for synthesis: in green candidates that could be synthetized, in red candidates that could not be synthetized. Chemical formulation with the glide score (Gscore, kcal/mol) obtained by docking.

4.1.10. F6.x candidates' validation

The validation of the fourth set of virtual optimization candidates was conducted by assessing their ability to inhibit [redacted] in both U2OS and hFIB cells in parallel. [redacted] candidates at concentrations of 1, 5, and 10 µM for durations of 6 hours and ON, allowing examination of the candidates' effects over short and long durations, respectively. Due to the light effect observed at 6h (results not shown) and lower doses, experiments were also done ON with higher concentrations of the compounds (50-100 µM) (Figure 46). After ON treatment, F6.1, F6.4 and F6.5 show some [redacted] inhibition in hFIB, whereas only F6.1 shows it in U2OS.



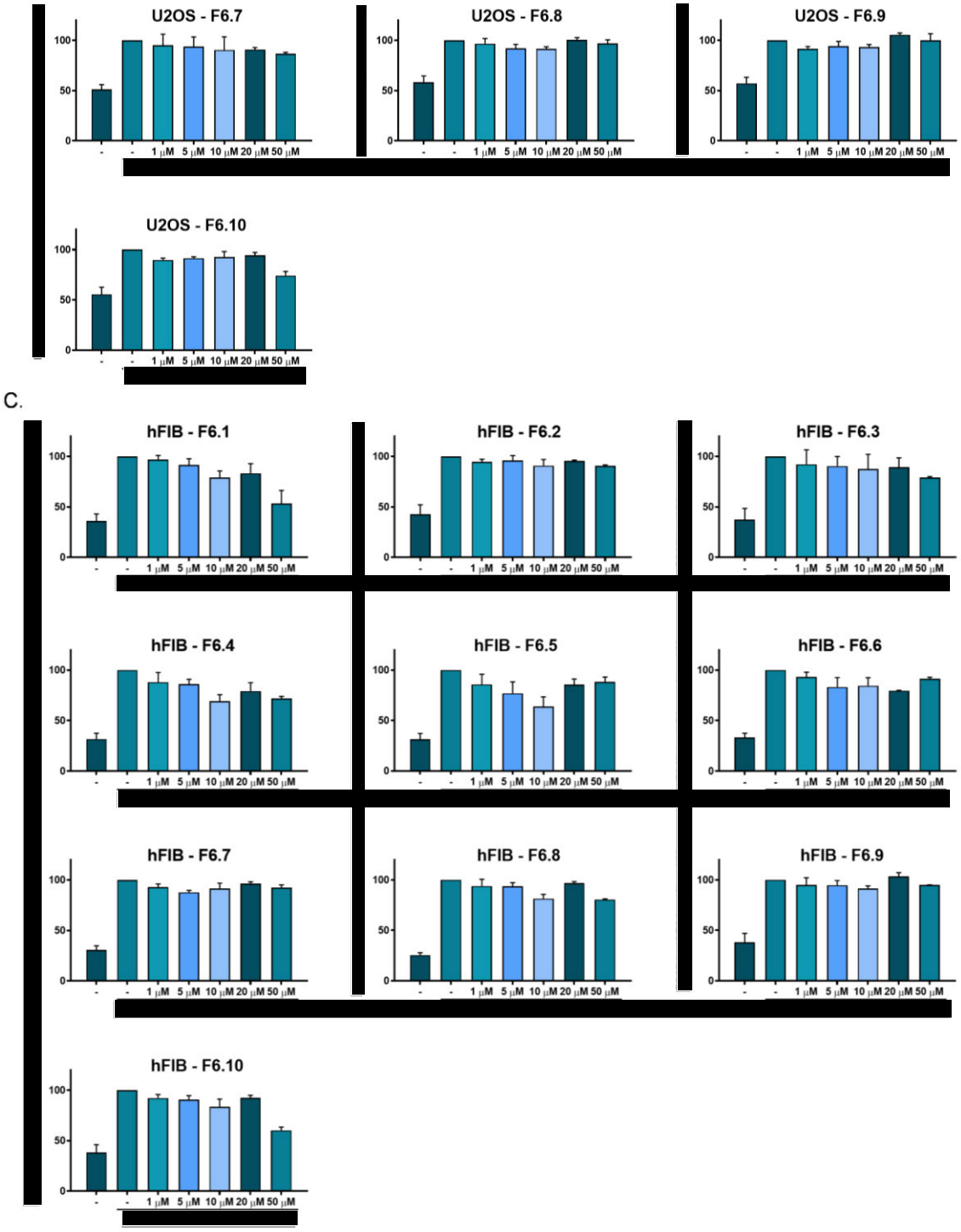


Figure 46. [redacted] **inhibition by F6.x candidates for the fourth optimization round**: chemical formulation (**A**.) and in vitro validation in U2OS (**B**.) and in hFIB cell lines (**C**.). Experiments were performed by treating the cells with potential [redacted] inhibitors at concentrations between 1-50 μM, [redacted] (see methods). Culture with the candidates was done overnight. [redacted] was analyzed by WB and quantified using ImageJ software and data normalized. Graphs represent mean ± SEM of at least three independent experiments. A representative WB of each candidate is showed in Appendix 1.

After this validation, an in vitro study in Biacore was done with the candidates, as in previous rounds (Table 12). Commercial [redacted] and own-synthetized [redacted] were tested in different channels: 3-1 and 4-1, respectively. K_D was measured in DMSO 1% and 25ºC at high density program. RUs obtained in most of the cases were not enough to verify the obtained results.

KD (μM)	DMSO 1%. 25°C, HD																							
	1st exp				2nd exp				3rd exp				4th exp				Average 3-1 corr			Average 4-1 corr			TOTAL	
	3-1 corr	Chi^2	4-1 corr	Chi^2	3-1 corr	Chi^2	4-1 corr	Chi^2	3-1 corr	Chi^2	4-1 corr	Chi^2	3-1 corr	Chi^2	4-1 corr	Chi^2	Mean	SD	SEM	Mean	SD	SEM	Mean	SD
F27	X	0.19	120.4	0.03	5.41	19.6	7.42	5.24	31.26	0.197	40.14	0.43	4.5	0.898	7.18	1.36	**18.3**	15.2	5.1	**43.8**	2.4	0.8	**31.1**	18.0
F6.1	253	0.108	↑	0.249	-	-	-	-	19.23	1280	312.6	30.3	↑	516	211.9	250	**136.1**	165.3	55.1	**262.3**	136.3	45.4	**199.2**	89.2
F6.2	-	-	-	-	↑	8.16	↑	0.11	-	-	-	-	-	-	-	-	↑			↑			↑	
F6.3	-	-	-	-	X	X	X	X	-	-	-	-	↑	0.009	↑	0.454	↑			↑			↑	
F6.4	-	-	-	-	X	X	↑	2.48	-	-	-	-	-	-	-	-				↑			↑	
F6.5	-	-	-	-	X	X	X	X	-	-	-	-	-	-	-	-	**-**	-	-	**-**	-	-	**X**	X
F6.6	-	-	-	-	160	0.008	X	X	↑	0.086	↑	0.004	224.5	0.032	2.961	0.769	**160.0**	45.6	15.2	**3.0**	0.5	0.2	**81.5**	111.0
F6.7	-	-	-	-	144.7	0.023	32.17	0.003	-	-	-	-	-	-	-	-	**144.7**			**32.2**			**88.4**	79.6
F6.8	-	-	-	-	-	-	-	-	↑	25.1	↑	14.5	X	X	30.13	5.23	↑			**30.1**	6.6	2.2	**30.1**	
F6.9	-	-	-	-	-	-	-	-	↑	0.421	↑	1.56	↑	3.13	↑	0.245	↑			↑	0.9	0.3	↑	
F6.10	-	-	-	-	-	-	-	-	616.8	0.194	186.6	0.431	9.69	165	9.52	35.8	**616.8**	429.3	143.1	**98.1**	25.0	8.3	**357.4**	366.8

Table 12. Results of SPR (Surface Plasmon Resonance) experiments performed with candidates of the fourth virtual optimization (F6.x) at 1% DMSO and 25ºC. Columns "3-1 corr" or "4-1 corr" represent values of flow channel 3 or 4 (with commercial [redacted] or synthetized and purified [redacted] respectively) subtracting the signal from the channel 1 (reference channel) of the same chip. Crosses represent the cases with no detected interaction and upward arrows describe Chi2 values extremely higher.

4.1.11. De novo [redacted] inhibitors design and virtual screening by molecular docking and medicinal chemistry (2Fx candidates)

While the fourth virtual screening was being done, a new design strategy was suggested in collaboration with NBD. ZINC22 database library (13 M small molecules) was used to start this strategy. Taking as reference the [redacted] used before, the core for the docking was stablished on [redacted]. As it was done in the first screening, HTVS and standard precision were carried out as multi-step docking process, reducing the number of available molecules to 100 K. After that, the molecules were filtered by their docking score, stablishing the limit in -6 kcal/mol. The 600-1K molecules that rested after this step were evaluated by visual inspection, taking in consideration their overall interactions, chemical diversity, shape complementarity, and potential toxicity and reactivity (Figure 47). Finally, from the 39 candidates proposed, 26 were bought (Table 13).

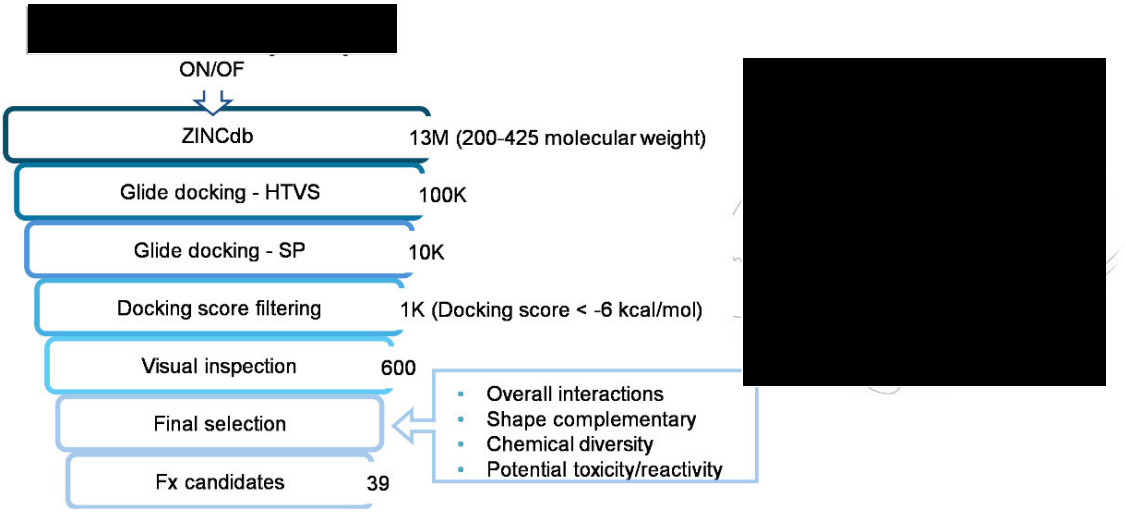


Figure 47. New virtual screening design workflow.

[redacted] In order to address this new target, [redacted] (Figure 48).

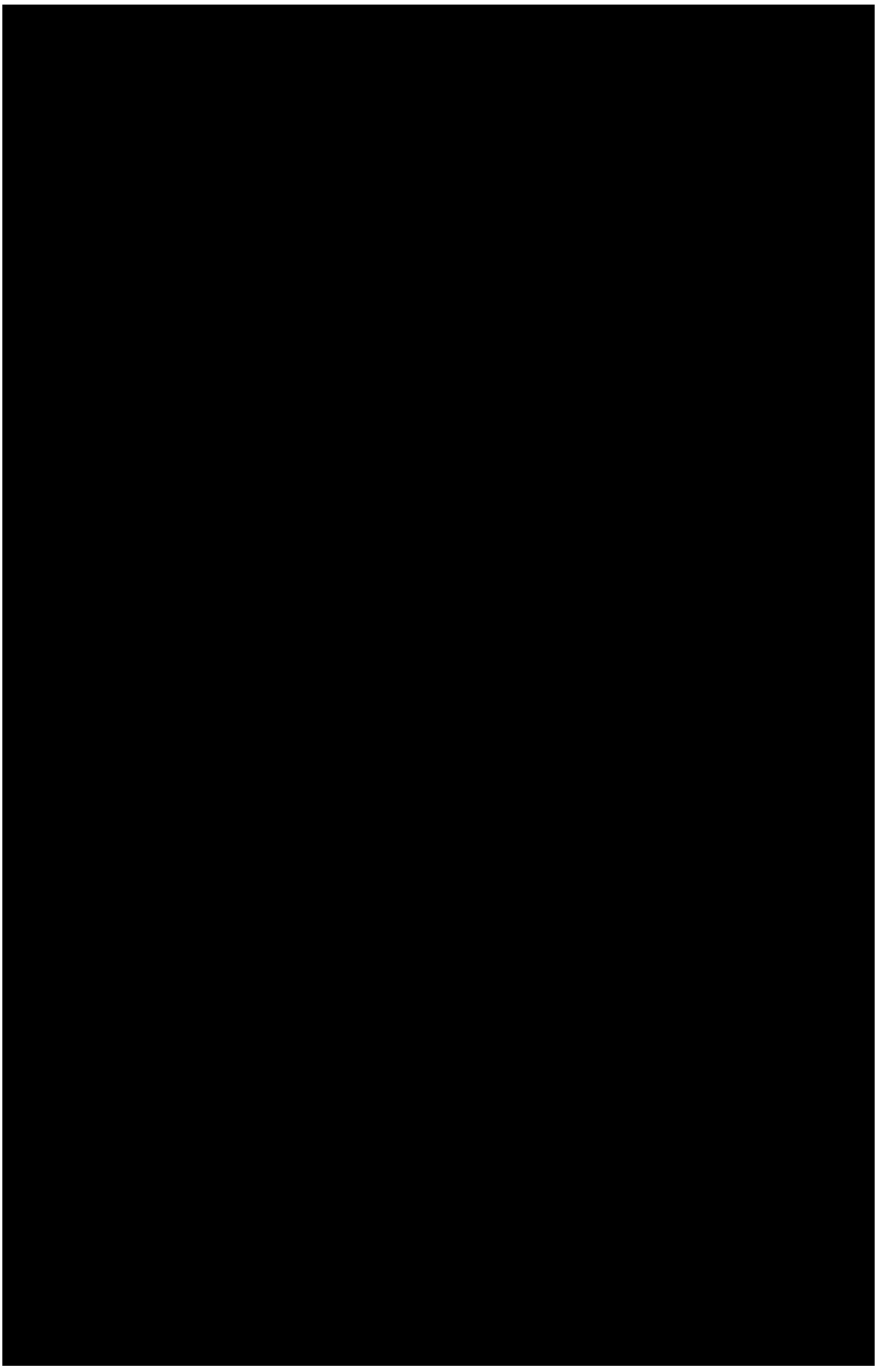


Figure 48. ***De novo* design approach**. ZINC database library underwent filtration based on two criteria:



The table below show the 26 commercial molecules that were bought (Table13).

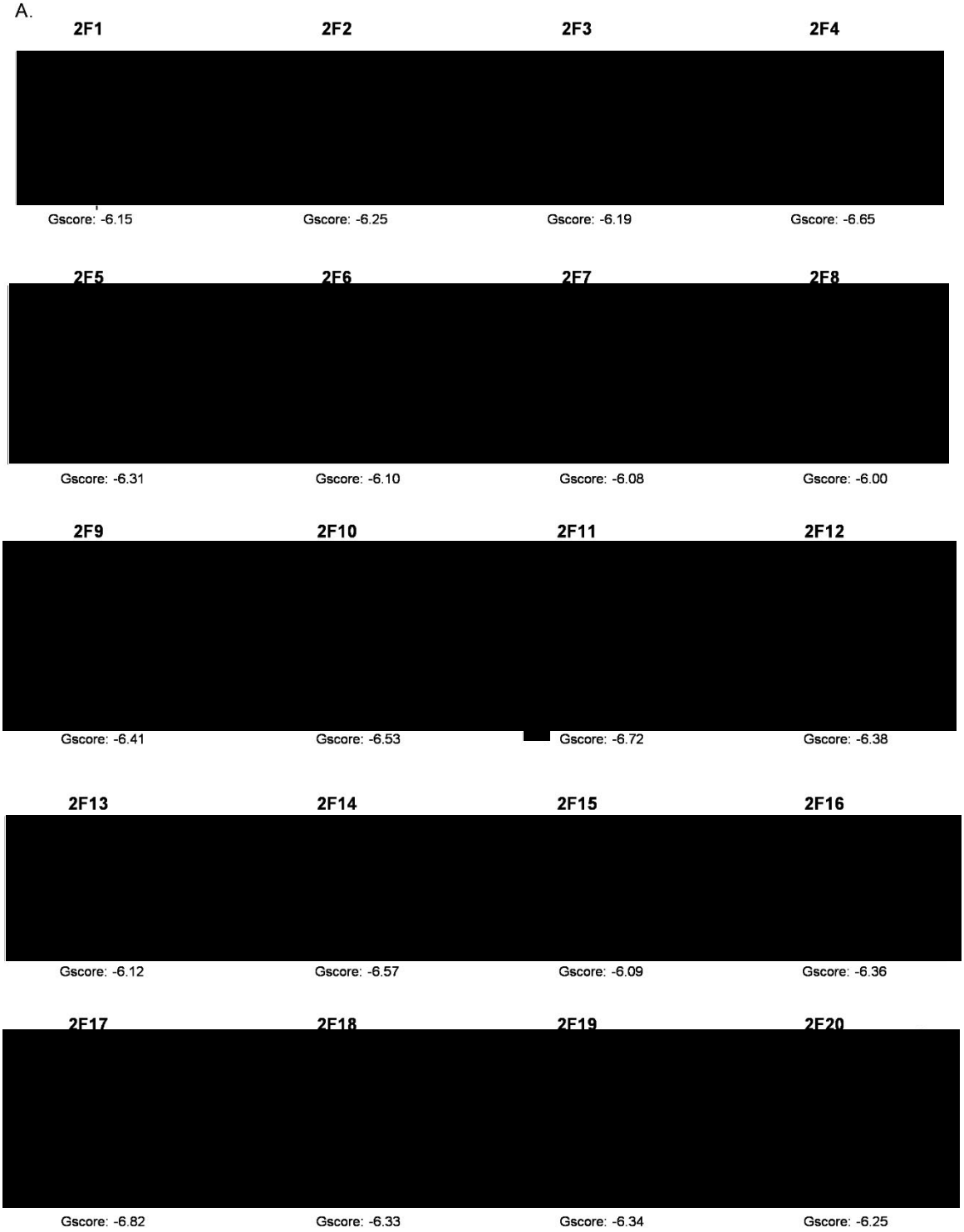
Table 13. Commercial molecules bought for the *de novo* virtual screening.

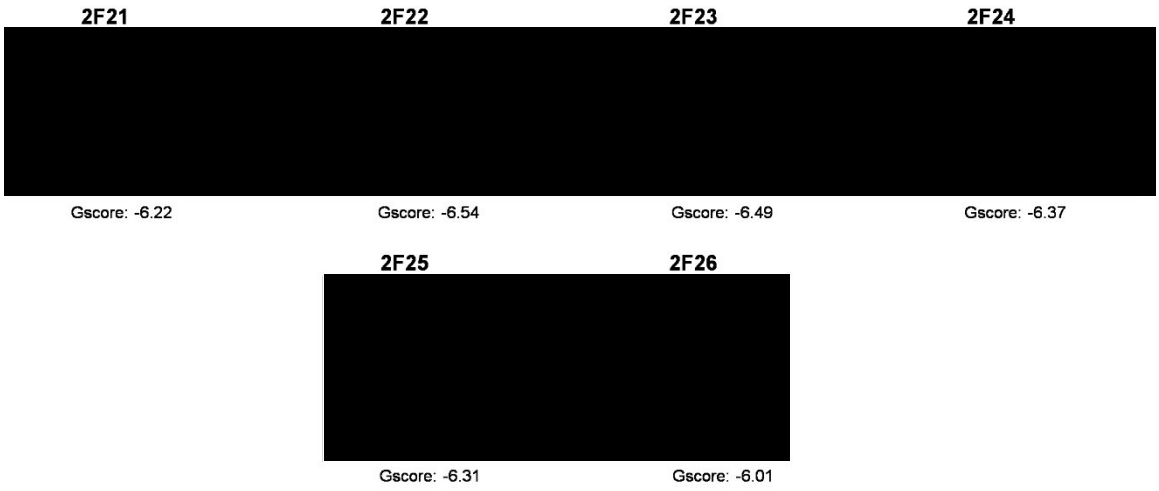
Candidate identification code	ZINCdb identification code	Supplier	Supplier identification code	Molecular weight
2F1				
2F2				
2F3				
2F4				
2F5				
2F6				
2F7				
2F8				
2F9				
2F10				
2F11				
2F12				
2F13				
2F14				
2F15				
2F16				
2F17				
2F18				
2F19				
2F20				
2F21				
2F22				
2F23				
2F24				
2F25				
2F26				

4.1.12. 2Fx candidates' validation

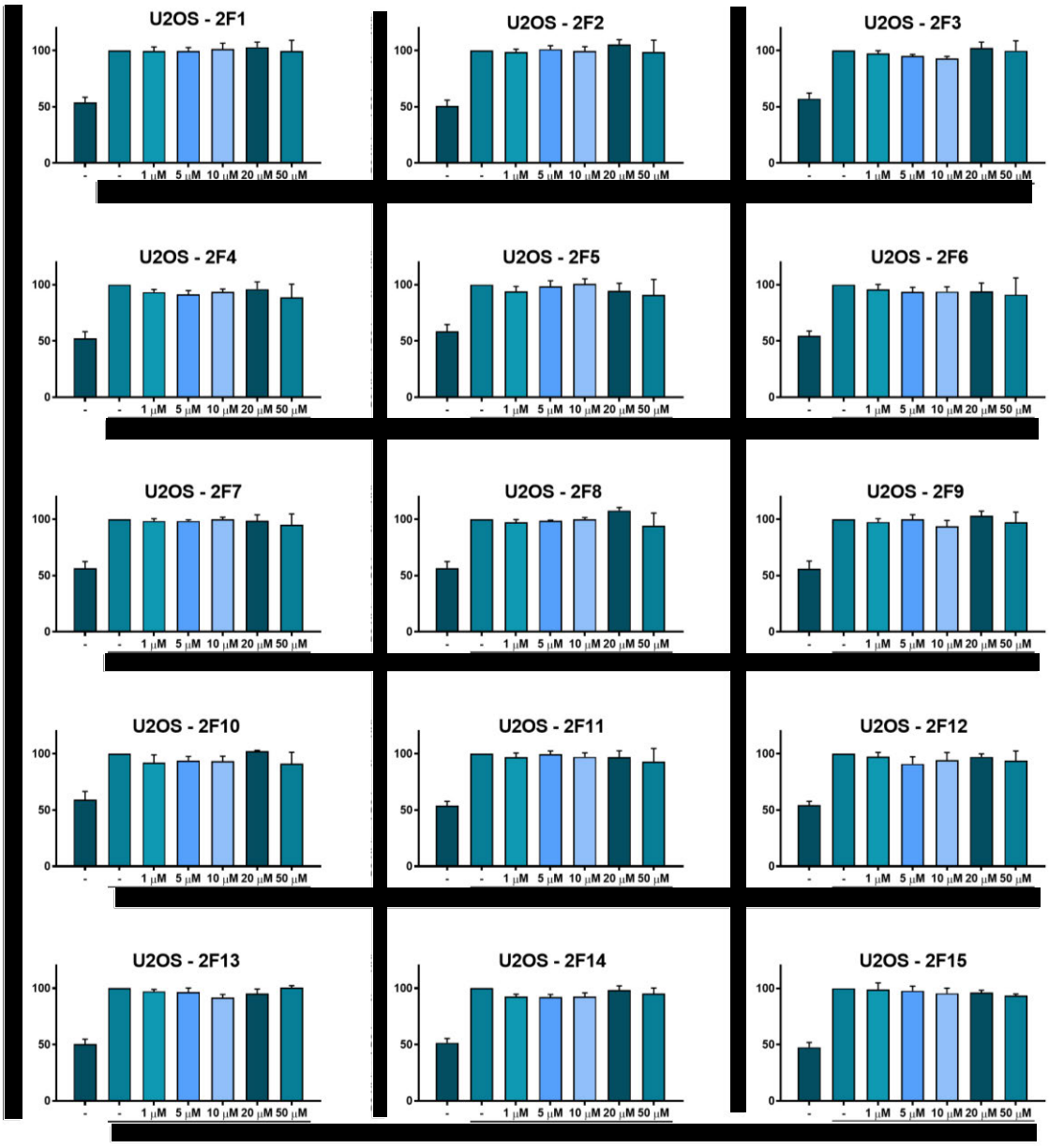
The candidates of this new design strategy were bought and validated at the same time that the compounds of the fourth virtual optimization. For this reason, all candidates were tested by their capacity to inhibit [redacted]. U2OS and hFIB cells were treated with 1, 5, and 10 µM of each candidate for 6 hours and ON. As explained above, after testing the compounds at low doses at 6h (data not shown), they were tested in higher doses and ON (Figure 49). As shown in Figure 49B and C, 2F3 demonstrated inhibitory effect in hFIB, whereas 2F17 and 2F26 in both hFIB and U2OS. In addition, the effect with the higher doses and during more hours allows to test the long-term toxicity of the candidates.

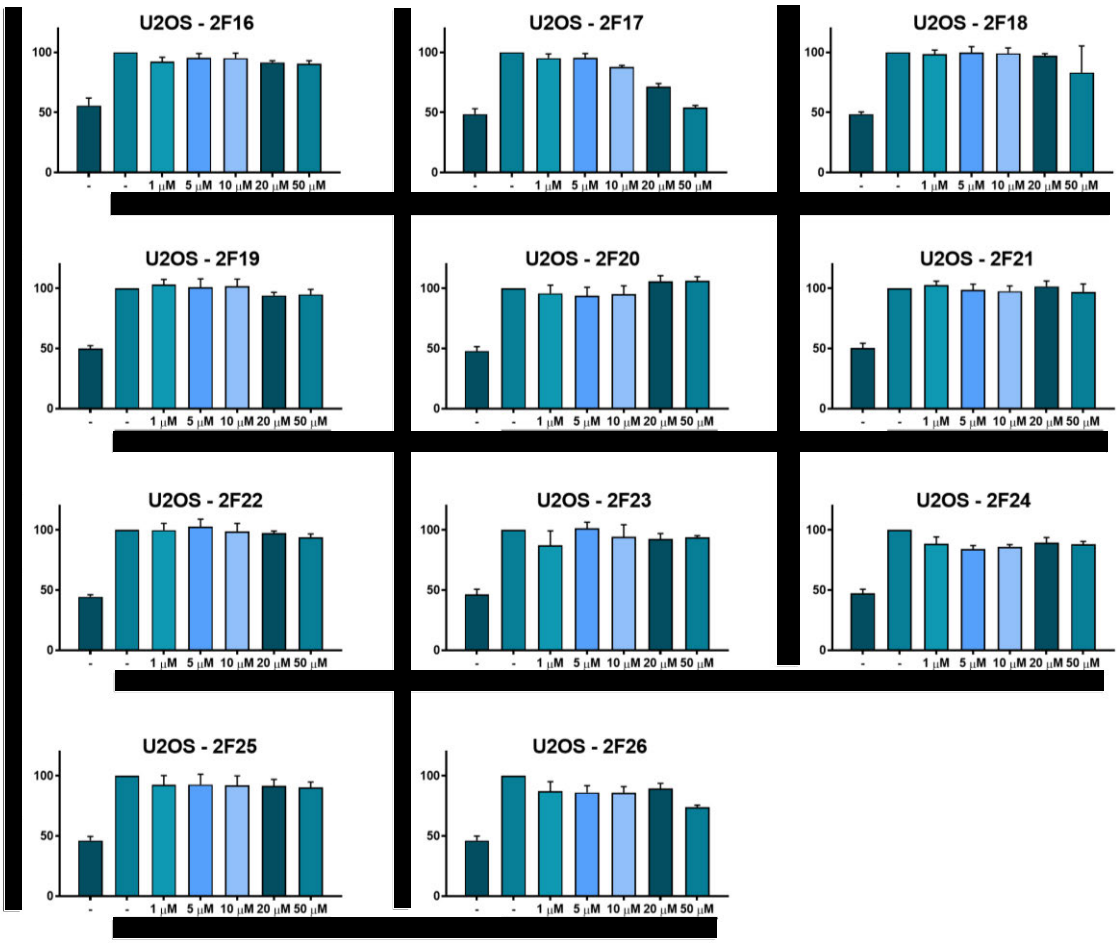
A.



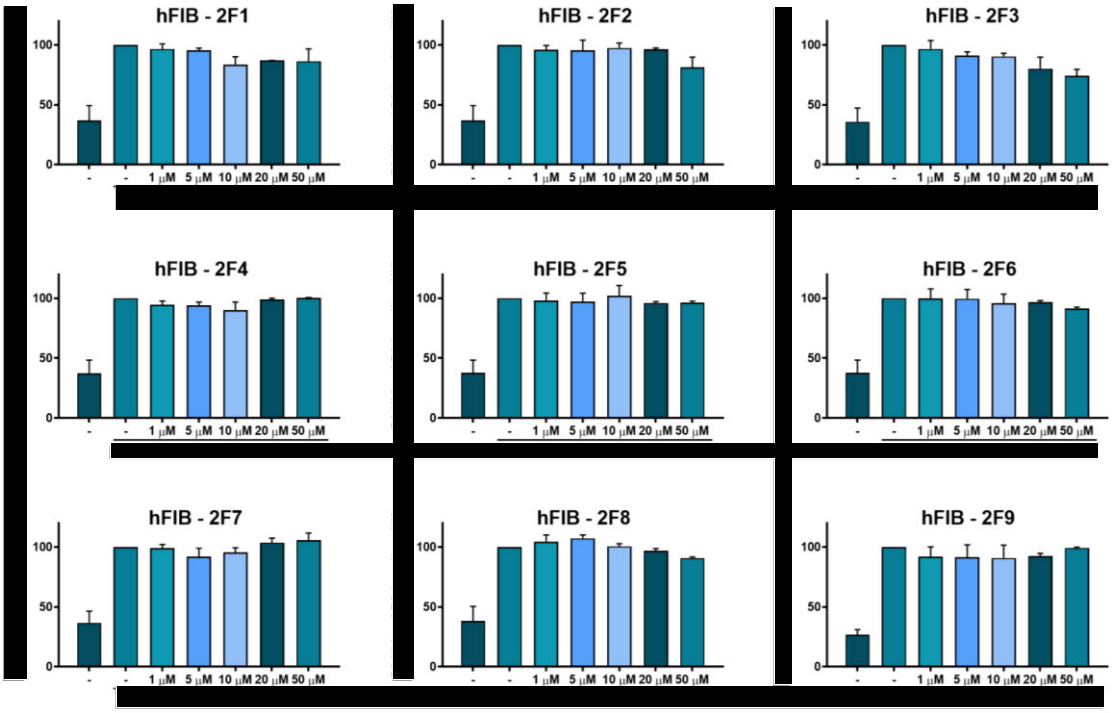

2F21
2F22
2F23
2F24
Gscore: -6.22
Gscore: -6.54
Gscore: -6.49
Gscore: -6.37
2F25
2F26
Gscore: -6.31
Gscore: -6.01

B.


U2OS - 2F1
U2OS - 2F2
U2OS - 2F3
U2OS - 2F4
U2OS - 2F5
U2OS - 2F6
U2OS - 2F7
U2OS - 2F8
U2OS - 2F9
U2OS - 2F10
U2OS - 2F11
U2OS - 2F12
U2OS - 2F13
U2OS - 2F14
U2OS - 2F15
100
50
0
- - 1 μM 5 μM 10 μM 20 μM 50 μM


U2OS - 2F16
U2OS - 2F17
U2OS - 2F18
U2OS - 2F19
U2OS - 2F20
U2OS - 2F21
U2OS - 2F22
U2OS - 2F23
U2OS - 2F24
U2OS - 2F25
U2OS - 2F26
100
50
0
- - 1 μM 5 μM 10 μM 20 μM 50 μM

C.


hFIB - 2F1
hFIB - 2F2
hFIB - 2F3
hFIB - 2F4
hFIB - 2F5
hFIB - 2F6
hFIB - 2F7
hFIB - 2F8
hFIB - 2F9
100
50
0
- - 1 μM 5 μM 10 μM 20 μM 50 μM

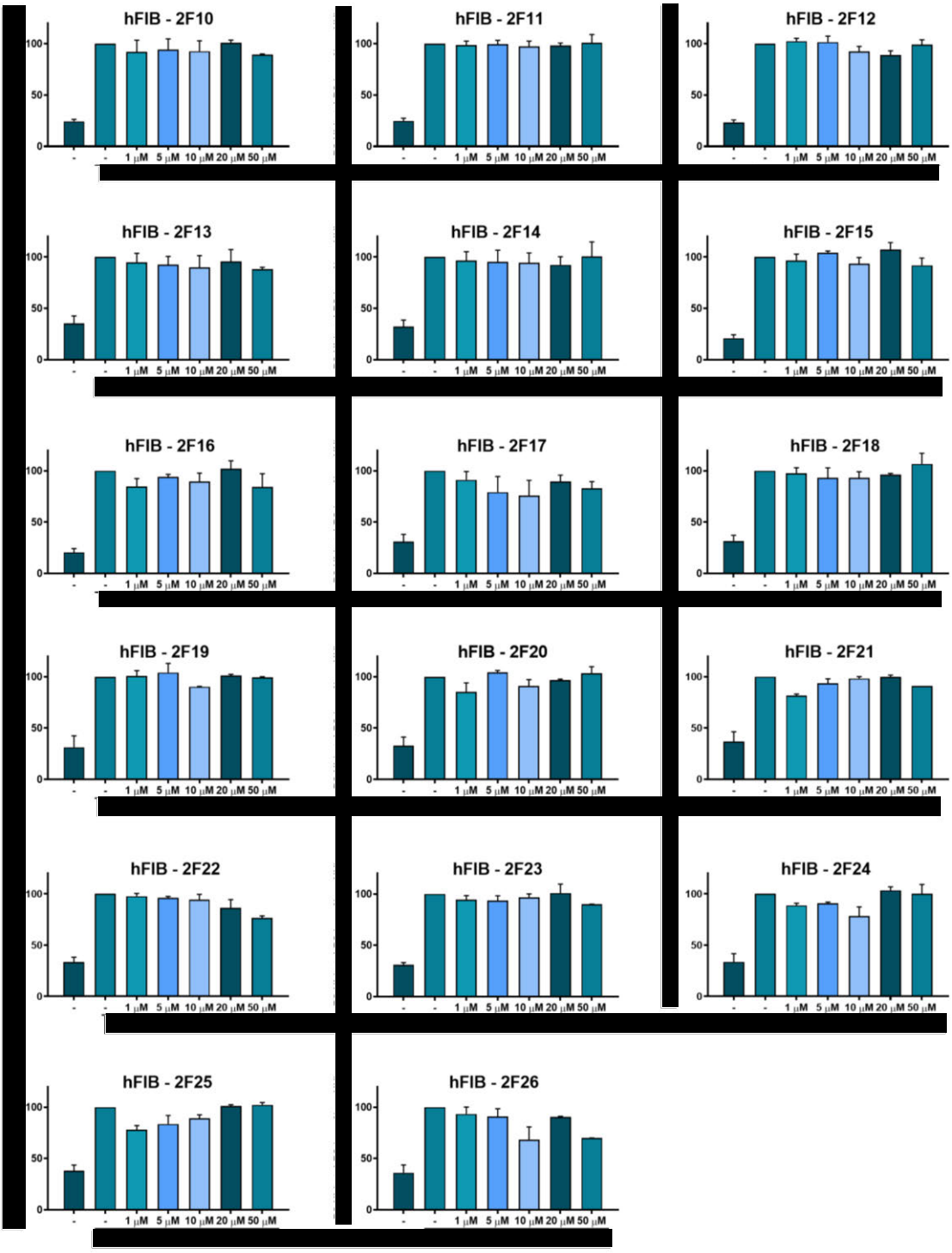


Figure 49. [redacted] **inhibition by 2Fx candidates for the *de novo* round**: chemical formulation (**A**.) and in vitro validation in U2OS (**B**.) and in hFIB cell lines (**C**.). Experiments were performed by treating the cells with potential [redacted] inhibitors at concentrations between 1-50 μM, [redacted] (see methods). Culture with the candidates was done overnight. [redacted]b was analyzed by WB and quantified using ImageJ software and data normalized. Graphs represent mean ± SEM of at least three independent experiments. A representative WB of each candidate is showed in Appendix 1.

After this validation, an in vitro study in Biacore was done with the 2Fx candidates (Table 14), together with the F6.x candidates.

KD (µM)	DMSO 1%. 25°C, HD																							
	1st exp				2nd exp				3rd exp				4th exp				Average 3-1 corr			Average 4-1 corr			TOTAL	
	3-1 corr	Chi^2	4-1 corr	Chi^2	3-1 corr	Chi^2	4-1 corr	Chi^2	3-1 corr	Chi^2	4-1 corr	Chi^2	3-1 corr	Chi^2	4-1 corr	Chi^2	Mean	SD	SEM	Mean	SD	SEM	Mean	SD
F27	X	0.19	120.4	0.03	5.41	19.6	7.42	5.24	31.26	0.197	40.14	0.43	4.5	0.898	7.18	1.36	**18.3**	15.2	5.1	**43.8**	2.4	0.8	**31.1**	18.0
2F1	X	X	X	X	-	-	-	-	-	-	-	-	-	-	-	-	**-**	-	-	**-**	-	-	**X**	X
2F2	X	X	X	X	-	-	-	-	-	-	-	-	-	-	-	-	**-**	-	-	**-**	-	-	**X**	X
2F3	X	X	X	X	-	-	-	-	-	-	-	-	-	-	-	-	**-**	-	-	**-**	-	-	**X**	X
2F4	X	X	X	X	-	-	-	-	-	-	-	-	-	-	-	-	**-**	-	-	**-**	-	-	**X**	X
2F5	↑	0.01	↑	0.07	-	-	-	-	-	-	-	-	-	-	-	-	↑			↑			↑	
2F6	X	X	X	X	-	-	-	-	-	-	-	-	-	-	-	-	**-**	-	-	**-**	-	-	**X**	X
2F7	X	X	X	X	-	-	-	-	-	-	-	-	-	-	-	-	**-**	-	-	**-**	-	-	**X**	X
2F8	X	X	X	X	-	-	-	-	-	-	-	-	-	-	-	-	**-**	-	-	**-**	-	-	**X**	X
2F9	↑	0.39	50.33	0.07	-	-	-	-	-	-	-	-	-	-	-	-	↑			**50.3**			↑	
2F10	X	X	X	X	-	-	-	-	-	-	-	-	-	-	-	-	**-**	-	-	**-**	-	-	**X**	X
2F11	↑	0.16	109.8	0.011	-	-	-	-	-	-	-	-	↑	2020	345.6	7.82	↑			**227.7**	5.5	1.8	**227.7**	5.5
2F12	X	X	X	X	-	-	-	-	-	-	-	-	-	-	-	-	**-**	-	-	**-**	-	-	**X**	X
2F13	X	X	X	X	-	-	-	-	-	-	-	-	-	-	-	-	**-**	-	-	**-**	-	-	**X**	X
2F14	18.1	0.0002	X	X	-	-	-	-	-	-	-	-	-	-	-	-	**18.1**						**X**	
2F15	-	-	-	-	53.84	0.05	5.58	0.04	X	X	X	X	-	-	-	-	**53.8**			**5.6**			**29.7**	34.1
2F16	-	-	-	-	8.899	2.33	11.1	0.87	-	-	-	-	-	-	-	-	**8.9**			**11.1**			**10.0**	1.6
2F17	-	-	-	-	183.7	0.04	7.3	0.04	239.9	0.092	74.21	0.017	X	X	X	X	**211.8**	39.7	13.2	**40.8**	0.0	0.0	**126.3**	120.9
2F18	-	-	-	-	X	X	X	X	-	-	-	-	-	-	-	-	**-**	-	-	**-**	-	-	**X**	X
2F19	-	-	-	-	↑	7.48	↑	3.55	71.0	1.5	72.6	2.27	X	X	162.1	0.694	**71.0**			**117.4**	1.4	0.5	**94.2**	32.8
2F20	-	-	-	-	99.45	26.40	↑	0.649	403	21.1	313	294	103.7	35.7	148.4	82.9	**251.2**	174.0	58.0	**230.7**	151.3	50.4	**241.0**	14.5
2F21	-	-	-	-	370	35.3	271	5.81	X	X	161	61.8	X	X	2.61	24.2	**370.0**			**144.9**	28.5	9.5	**257.4**	159.2
2F22	-	-	-	-	X	X	X	X	-	-	-	-	-	-	-	-	**-**	-	-	**-**	-	-	**X**	X
2F23	-	-	-	-	67.1	0.005	↑	0.08	-	-	-	-	-	-	-	-	**67.1**			↑			**X**	
2F24	-	-	-	-	-	-	-	-	X	X	X	X	-	-	-	-	**-**	-	-	**-**	-	-	**X**	X
2F25	-	-	-	-	-	-	-	-	X	X	X	X	-	-	-	-	**-**	-	-	**-**	-	-	**X**	X
2F26	-	-	-	-	-	-	-	-	3.28	1.9	X	X	-	-	-	-	**3.3**						**X**	

Table 14. Results of SPR experiments performed with candidates of the "*de novo*" virtual screening (2Fx) at 1% DMSO and 25ºC. Columns "3-1 corr" or "4-1 corr" represent values of flow channel 3 or 4 (with commercial [redacted] or synthetized and purified [redacted] respectively) subtracting the signal from the channel 1 (reference channel) of the same chip. Crosses represent the cases with no detected interaction and upward arrows describe Chi^2 values extremely higher.

As explained in Table 12, commercial [redacted] and own-synthetized [redacted] were tested in different channels: 3-1 and 4-1, respectively (Table 14). K_D was measured in DMSO 1% and 25ºC at high density program. The RUs obtained in most of the cases were not enough to verify the obtained results.

To summarize, after one first virtual screening, a following fragment-based screening, fourth optimization rounds, and a new virtual screening, a total of 128 candidates (Figure 50) were tested and validated in different ways, mainly by their cellular activity and by their interaction with the target [redacted].

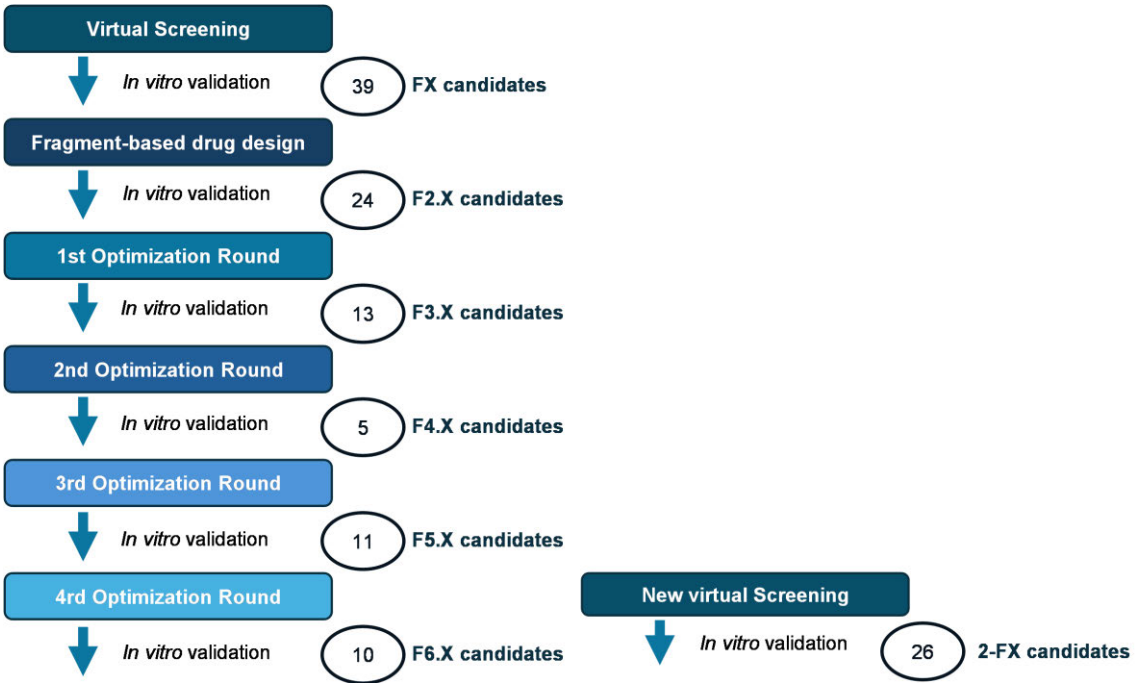


Figure 50. Workflow of the virtual screening and optimization rounds of First-In-Class specific inhibitors for the [redacted].

The best results of these candidates are summarized in Figures 51 and 52.

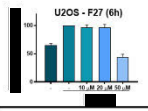
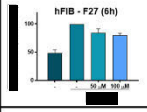
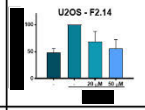
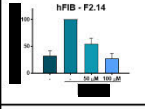
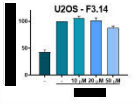
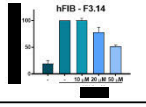
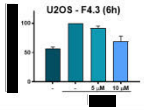
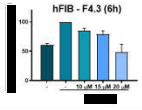
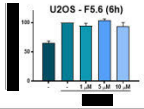
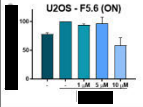
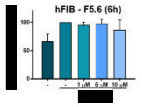
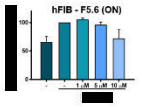
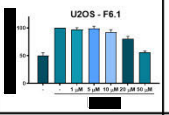
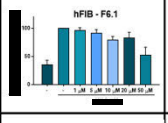
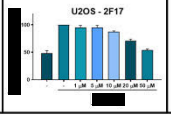
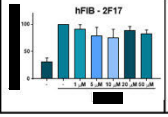
		In vitro inhibition (µM)				K_D (SPR, µM)		Docking	FQ Prop.	Others	Toxicity (µM)
		U2OS (6h)	U2OS (24h)	hFIB (6h)	hFib (24h)	Mean	SD	Gscore	LogS		
[redacted]	**F27**		-		-	17.8	1.5	-7.42	-5.35	[redacted] Clonogenic assay	>50(6h)/ >20(24h)
[redacted]	**F2.14**	-		-		8.23	-	-5.50	-4.62	-	>100(24h)
[redacted]	**F3.14**	-		-		148.2	-	-3.24	-	Clonogenic assay	No
[redacted]	**F4.3**		-		-	3	2	-	-	[redacted] Clonogenic assay	>10(6h)/ >5(24h)
[redacted]	**F5.6**					7.2 (↓solub)	7.4	-3.06	-5.7	-	>10(6h)/ >10(24h)
[redacted]	**F6.1**	-		-		199.2	89.2	-4.80	-	-	No
[redacted]	**2F17**	-		-		126.3	120.9	-6.82	-	-	No

Figure 51. Best candidates of optimization rounds. *In vitro* inhibition, biochemical validation (SPR), bocking, fit quality properties (FQ Prop.), other validation [redacted] clonogenic assay) and toxicity for the best candidate in each round.

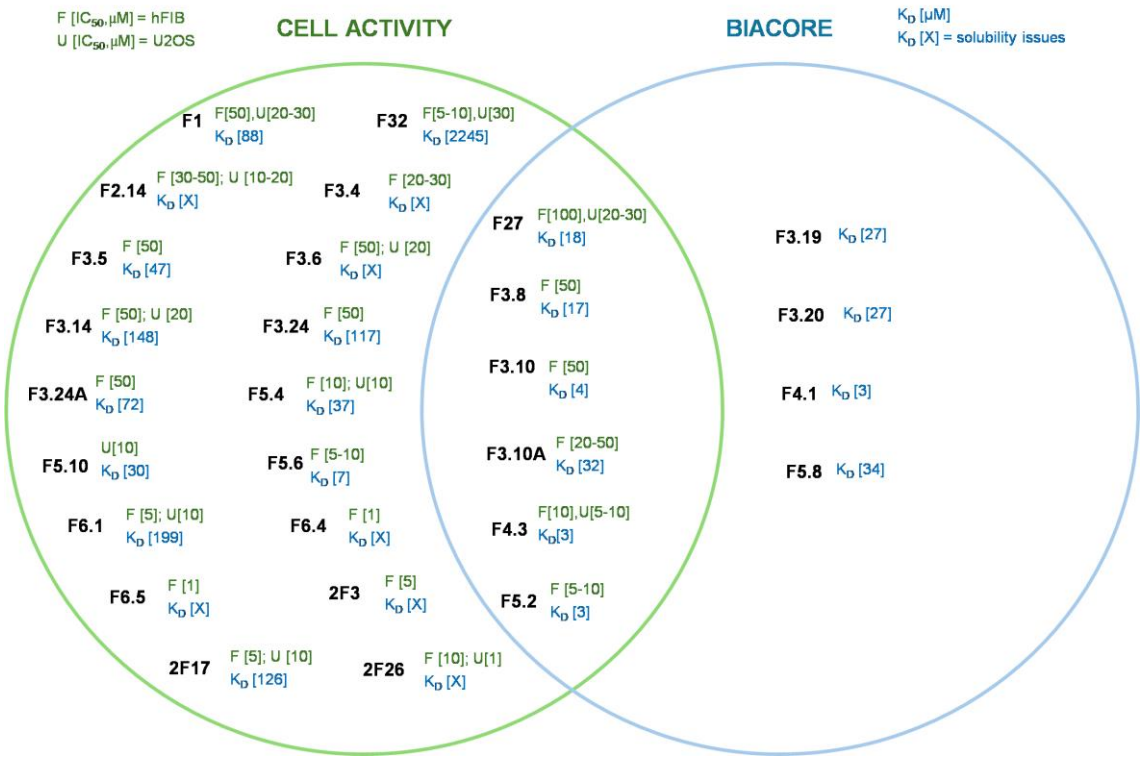


Figure 52. **Best candidates of optimization rounds**: cell activity of the compounds in U2OS (U) and hFIB (F) cells; and SPR dissociation constant (K_D).

4.2. Obtaining and characterization of AR HNSCC cell lines

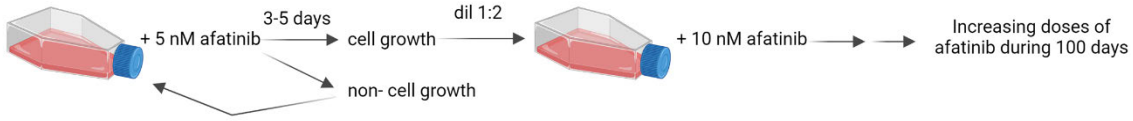
4.2.1. Generation of AR HNSCC cell lines

FA patients are more prone to develop HNSCC at early ages, and due to DNA repair deficiency, currently approved treats with, chemo or radiotherapy are not an option due to excess toxicity. In the search of alternative therapies for FA HNSCC, our group identified a panERBB inhibitor called afatinib as a potential treatment in preclinical models of FA HNSCC (Montanuy, Martínez-Barriocanal, et al., 2020) and obtained Orphan Drug Designation by the EMA. A clinical trial on afatinib to treat advanced FA HNSCC is already submitted to the Clinical Trials Information System of the European Medicines. With the aim to obtain additional information to guide the repurposing of afatinib to treat FA HNSCCs we investigated to what extent FA HNSCC cells become resistant to afatinib and the mechanisms behind. This information is expected to of value to design novel therapeutic avenues in afatinib resistant FA HNSCC

Starting from the HNSCC cell lines that were available in the laboratory, the first objective in this field was to study their potential to acquire resistance to afatinib. In order to compare FA and non-FA HNSCC, CAL 27 and CAL 33 FANCA mutant clones (Errazquin et al., 2021) were used in comparison with the parental CAL 27 and CAL 33 cell lines. In addition, FA HNSCC cell lines VU 1131, VU 1365, VU 1604 and OHSU 974 were used in comparison with their genetically corrected counterparts, using virus-mediated FA gene complementation (see methods). Additional material of characterization of FA and corrected cell lines shown in Appendix 2.

To create that AR cell lines, the above FA and non-FA HNSCC cell lines were treated with increasing doses of afatinib, starting from 5 nM. When cell growth was stable, afatinib doses were increased 5-10 nM per week, reaching their higher dose after several weeks of treatment. To stablish the afatinib-resistant (AR) cell line, cells were grown for 100 days under increasing doses of afatinib-treatment up to maintaining growth with the higher afatinib-dose (Figure 53A, 54, Table 15). Therefore, if the dose of afatinib at the end of the fixed period will be increased, cells could not further survive. To verify the acquisition of resistance, survival assays were done to compare resistant and not-resistant cell lines, subjected at the same doses of afatinib (Figure 53B, 55).

A.



B.

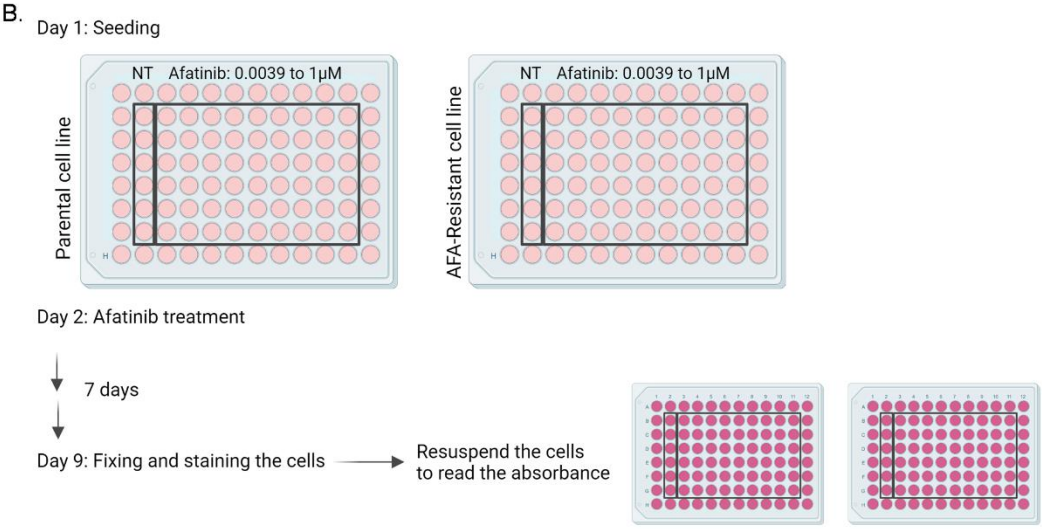


Figure 53. **AR cell lines design workflow**. **A**. Generation of afatinib resistant cell lines by the addition of increasing doses of afatinib, for 90-100 days. **B**. Design of survival assay with different doses of afatinib to confirm the resistance of the AR cell lines in comparison with the non-resistant (parental cell line). Sporadic HNSCC, FA-edited HNSCC, FA HNSCC, FA-corrected HNSCC and afatinib resistant cell lines were exposed to increasing concentrations of afatinib (0, 3.90625, 7.8125, 15.625, 31.25, 62.5, 125, 250, 500, 1000 nM) in culture medium. After 7 days of incubation, cells were fixed and stained. Stain was resuspended and optical density was measured at 510 nm. Statistical analysis was conducted using GraphPad Prism software on data from at least four independent experiments.

Table below shows the characteristics of each cell line and their resistance. VU-SCC-1604 was kept resistant to 5 nM of afatinib (*), but due to its unstable growth, cells died after 10 passages.

Table 15. HNSCC: characteristics and afatinib-resistance.

Cell line	Characteristics	Afatinib-resistance (nm)
CAL 27	Sporadic HNSCC	600
CAL 33	Sporadic HNSCC	900
CAL 27 CLONE 34	FA-edited sporadic HNSCC	250
CAL 27 CLONE 47	FA-edited sporadic HNSCC	250
CAL 33 CLONE A5	FA-edited sporadic HNSCC	120
CAL 33 CLONE A11	FA-edited sporadic HNSCC	150
VU-SCC-1131	FA HNSCC	45
VU-SCC-1365	FA HNSCC	20
VU-SCC-1604	FA HNSCC	Non-resistant*
OHSU-SCC-974	FA HNSCC	80
VU-SCC-1131 + FANCC	Corrected FA HNSCC	1000
VU-SCC-1365 + FANCA	Corrected FA HNSCC	25
VU-SCC-1604 + FANCL	Corrected FA HNSCC	1500
OHSU-SCC-974 + FANCA	Corrected FA HNSCC	80

Comparing the results of the capacity of the different cell lines of acquiring resistance to afatinib, worth highlighting that sporadic HNSCC cell lines acquired resistance at 800-1000 nM range, FA-edited sporadic HNSCC at 100-200 nM and FA HNSCC at 5-80 nM, 20-200 times lower than sporadic cell lines (Figure 54).

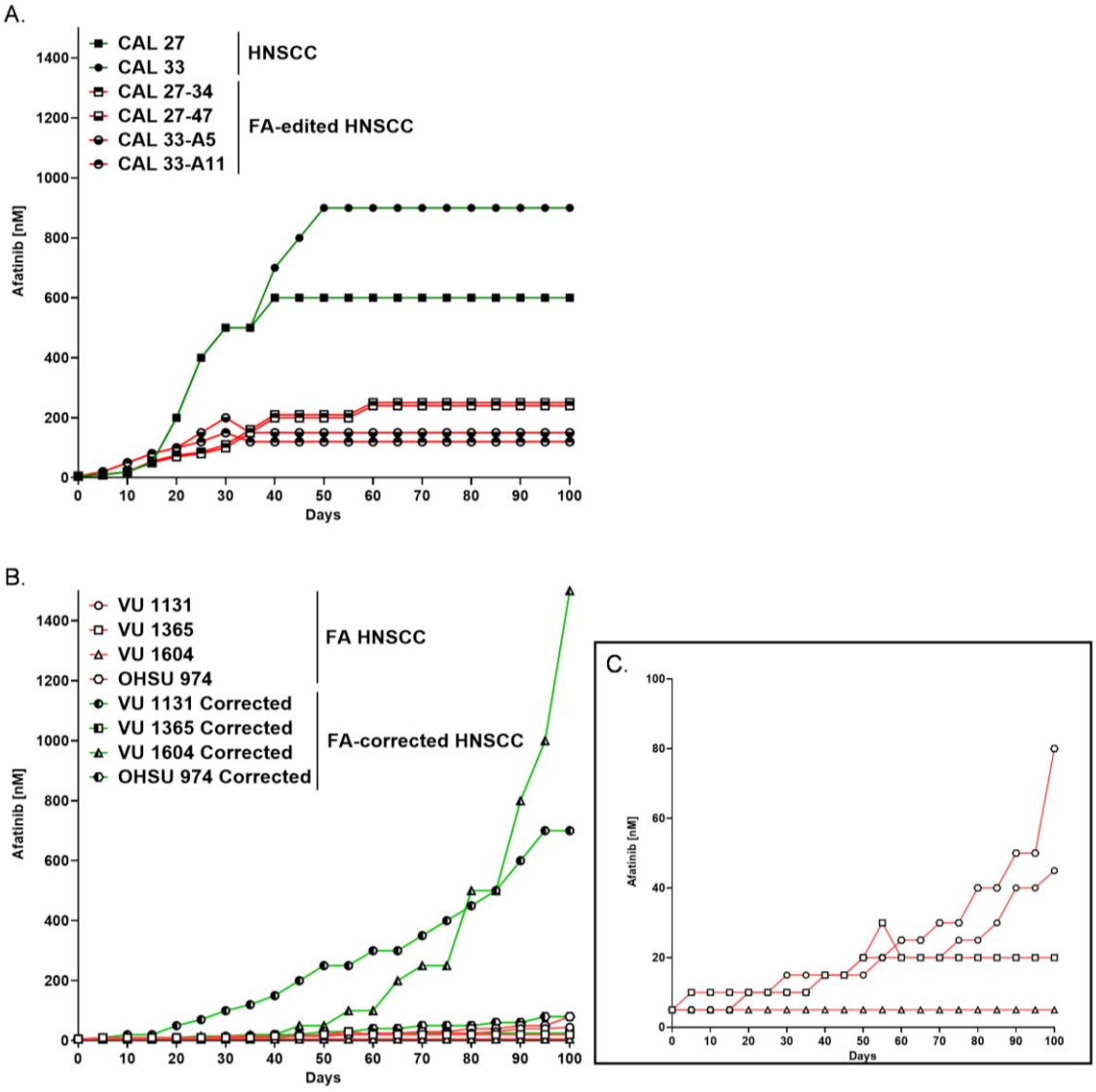
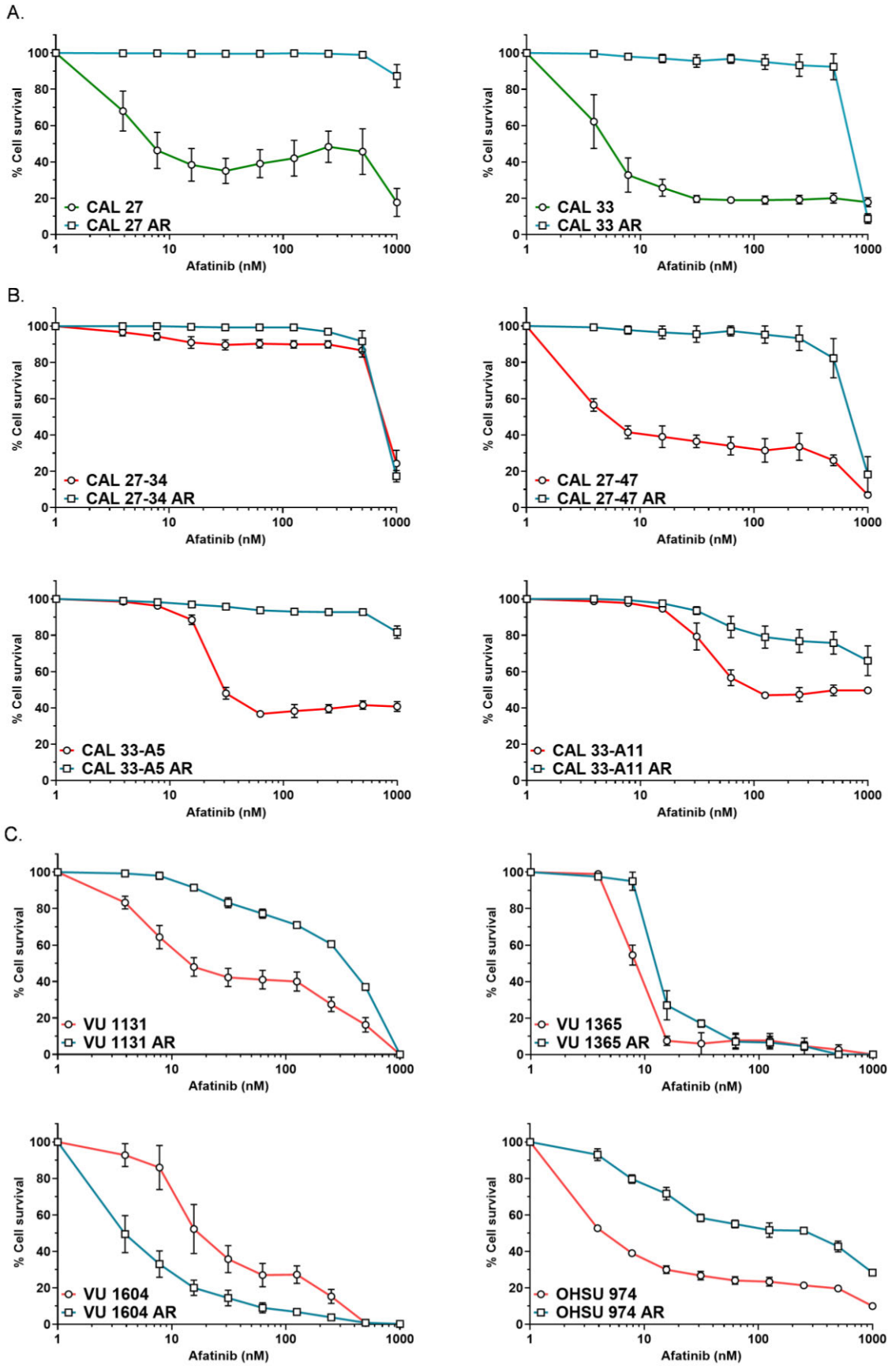


Figure 54. **Acquisition of resistance to afatinib:** (**A**.) in sporadic HNSCC cell lines (dark green) in contrast with FA-edited HNSCC cell lines (dark red) (**B.**) in FA HNSCC cell lines (light red) in contrast with FA-corrected cell lines (light green). **C.** Detail of the afatinib resistance accumulation in FA HNSCC cell lines. Y-axe shows the afatinib concentration the cells are resistant to, and X-axe shows the days after the treatment with increased doses of afatinib.

Figure 55 shows the SRB survival assay between AR and non-resistant cell lines after stablishing AR cell lines, in order to verify that new cell lines are consistently resistant to afatinib. Figure 55C shows VU1604 cell line, whose AR cell line was less resistant than the parental one. As was mentioned before, this cell line has a non-regular growth, and the cells finished dying when we tried to increase the afatinib doses. For this reason, these cell lines were discarded in the experiments that were carried out later.


A.
% Cell survival
Afatinib (nM)
CAL 27
CAL 27 AR
CAL 33
CAL 33 AR
B.
CAL 27-34
CAL 27-34 AR
CAL 27-47
CAL 27-47 AR
CAL 33-A5
CAL 33-A5 AR
CAL 33-A11
CAL 33-A11 AR
C.
VU 1131
VU 1131 AR
VU 1365
VU 1365 AR
VU 1604
VU 1604 AR
OHSU 974
OHSU 974 AR

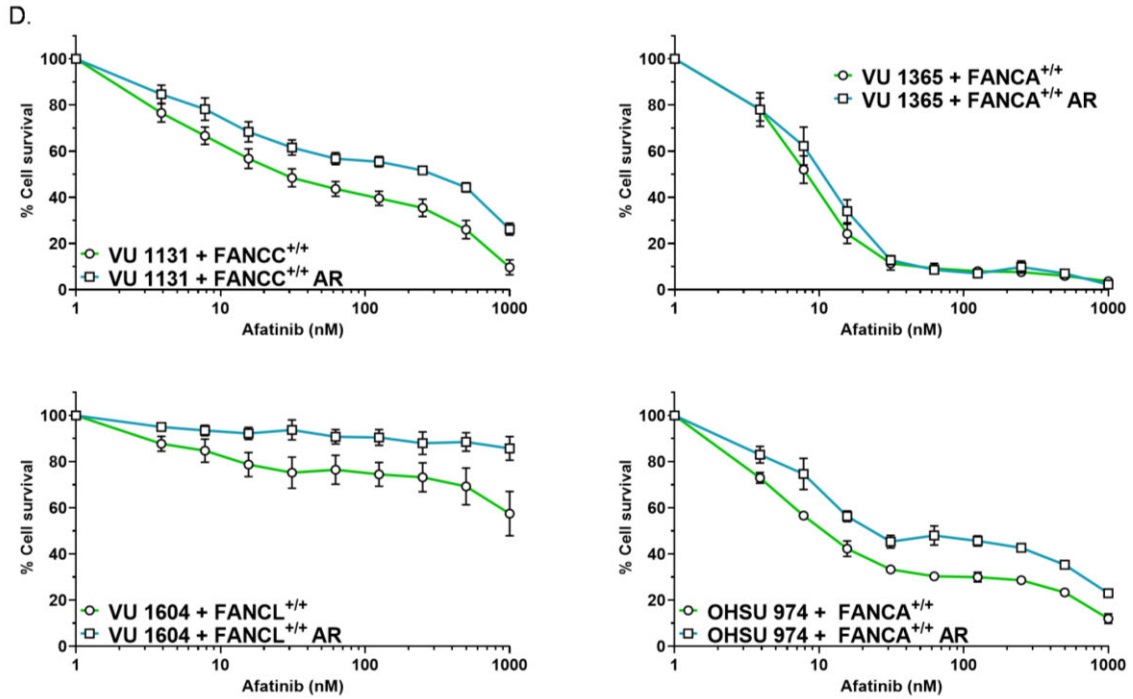
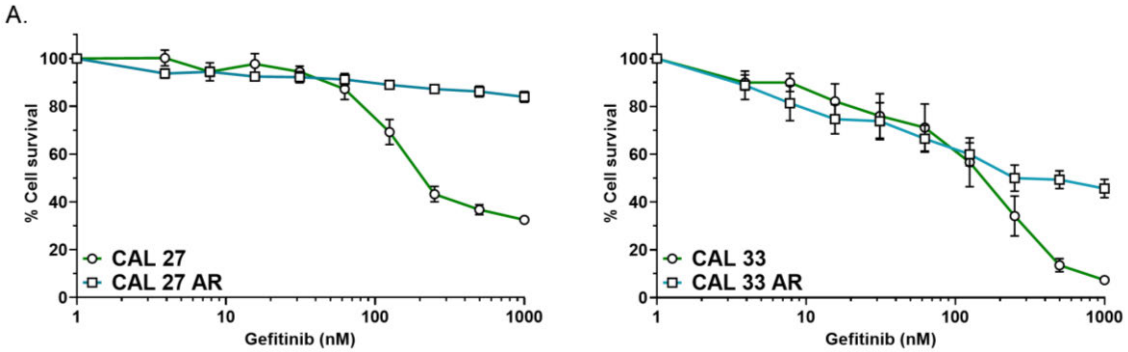


Figure 55. Survival assays for the validation of the afatinib resistance in HNSCC cell lines: (**A**) in sporadic HNSCC CAL 27 and CAL 33, (**B**) in FA-edited CAL 27-34, CAL 27-47, CAL 33-A5, CAL 33-A11 cell lines, (**C**) in FA HNSCC VU 1131, VU 1365, VU 1604 and OHSU 974, and (**D**) in FA-corrected HNSCC cell lines. Cell lines treated with increased doses of afatinib to compare the acquisition of resistance between parental and AR cell lines. Graphs show mean +/- SEM of 3-5 experiments with similar results.

4.2.2. Gefitinib cytotoxicity in AR HNSCC cell lines

Gefitinib is an ERBB1 inhibitor commonly used for lung cancer treatment in general population (Zibelman & Mehra, 2016). Taking into consideration that afatinib is also an ERBB1 inhibitor (panERBB inhibitor), and having established the AR cell lines, we evaluated the AR cell lines' capacity to resist to gefitinib. Survival assay experiments were carried out, in which cells were treated with increasing doses of gefitinib. Figure 56 shows that AR cell were also resistant to gefitinib, but in a lesser extent.



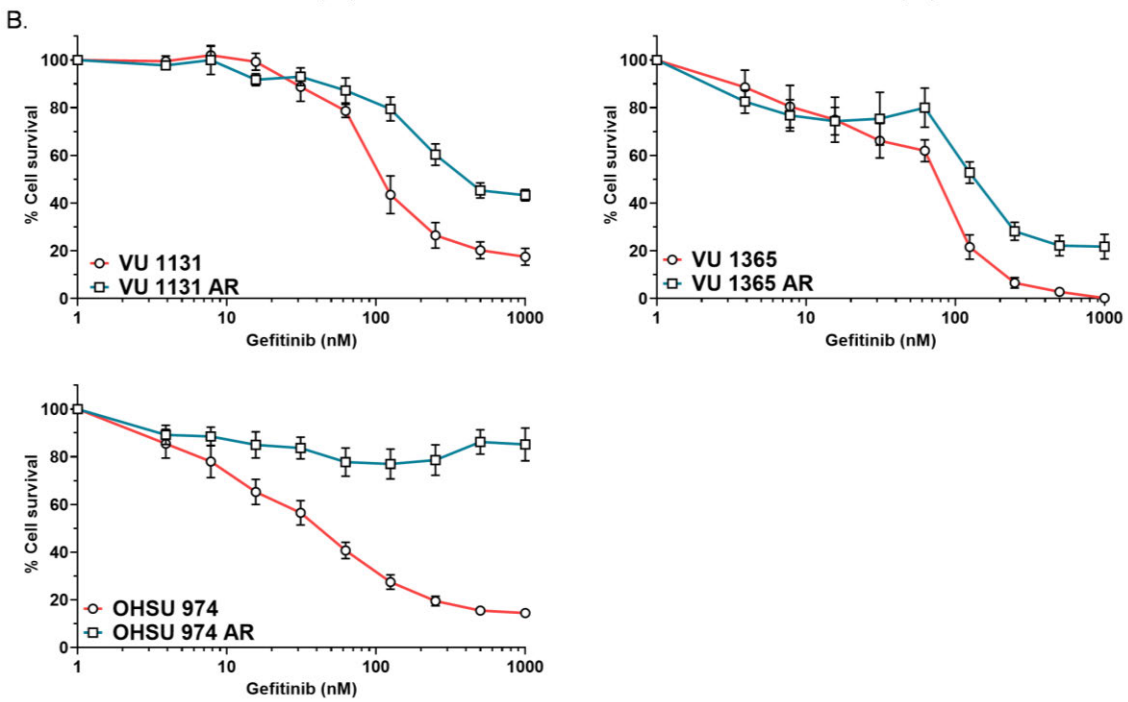
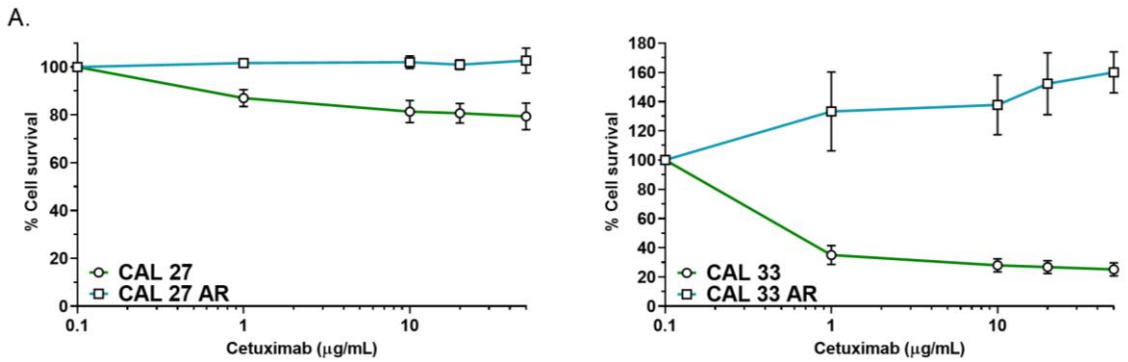


Figure 56. Survival assays of the effect of gefitinib on AR HNSCC cell lines: (**A**.) in sporadic HNSCC CAL 27 and CAL 33, (**B**.) in FA HNSCC VU 1131, VU 1365 and OHSU 974. SRB assay done with cell lines treated with increased doses of gefitinib. Graphs show mean +/- SEM of 3-5 experiments with similar results.

4.2.3. Cetuximab cytotoxicity in AR HNSCC cell lines

Cetuximab is a monoclonal antibody that blocks ERBB1, and it is used to treat HNSCC in general population (Burtness, 2005). Cytotoxicity to cetuximab in AR and non-resistant cell lines was tested by a SRB survival assay, as in the previous case. Figure 57 shows higher cytotoxicity to cetuximab in non-resistant cell than in AR cell lines, in which cell growth was maintained at 100% during all the experiment. However, highlighting the differences between CAL 33 and CAL 33 AR cell lines, non-resistant cell line was almost 4 times less resistant to cetuximab that the AR cell line (Figure 57A).



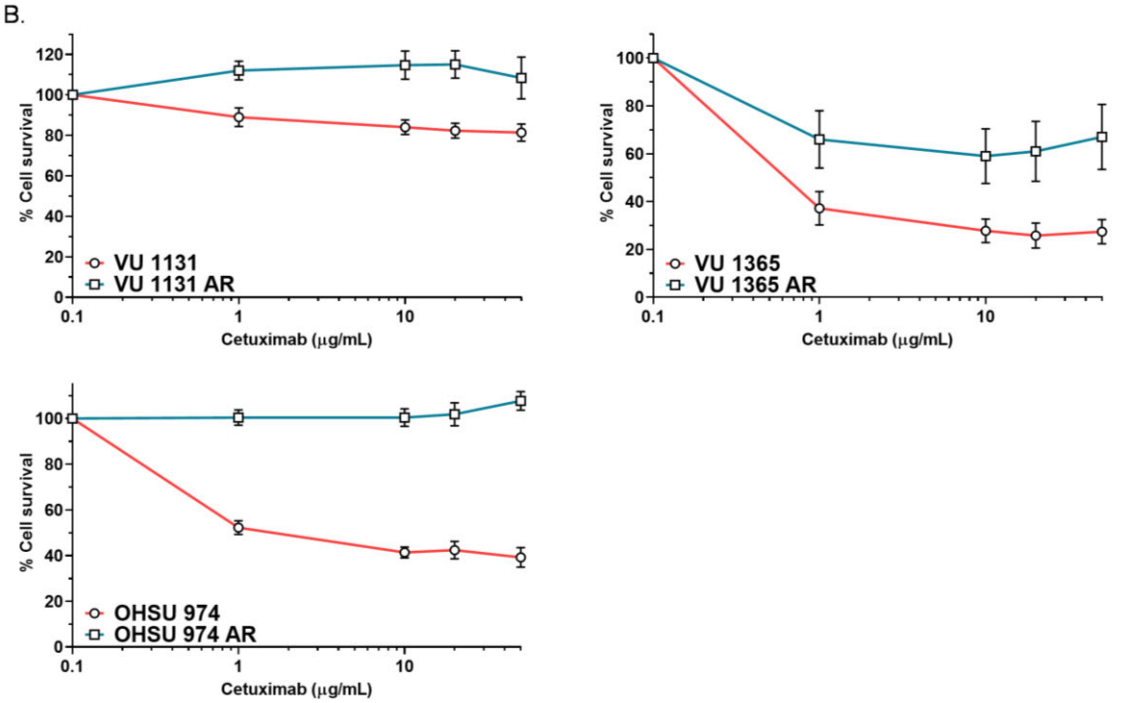
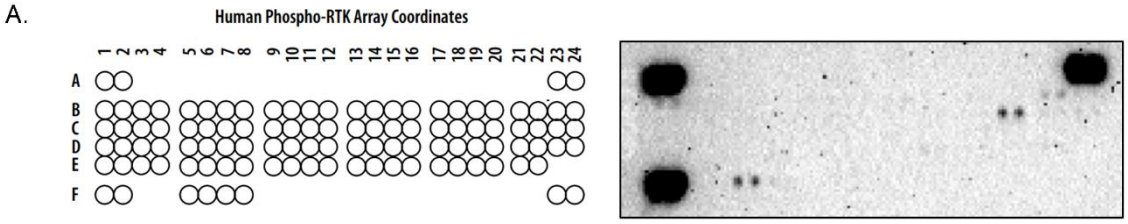


Figure 57. Survival assays of the effect of cetuximab on AR HNSCC cell lines: (**A**) in sporadic HNSCC CAL 27 and CAL 33, (**B**) in FA HNSCC VU 1131, VU 1365 and OHSU 974. SRB assay done with cell lines treated with increased doses of cetuximab. Graphs show mean +/- SEM of 3-5 experiments with similar results.

4.2.4. Tyrosine kinase receptors (RTKs) expression in AR HNSCC cell lines

As the sporadic HNSCC were more prone to acquire resistance to afatinib than FA HNSCC cell lines, and afatinibinhibits ERBB1-ERBB4, a 49-RTK dot blot array (Figure 58) was performed in order to verify if cell lines had active another RTK pathway to compensate for the loss of the ERBB family activity.



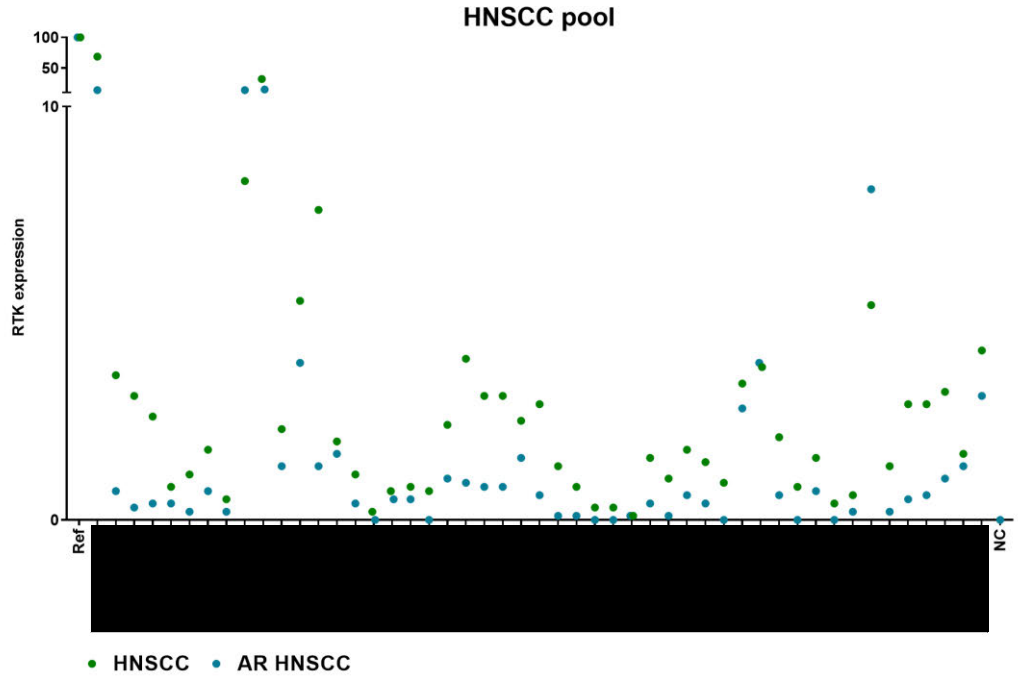
B.

Coordinate	Receptor Family	RTK/Control	Coodinate	Receptor Family	RTK/Control
A1, A2	Reference Spots	——	D1, D2	Tie	Tie-2
A23, A24	Reference Spots	——	D3, D4	NGF R	TrkA
B1, B2	EGF R	EGF R	D5, D6	NGF R	TrkB
B3, B4	EGF R	ErbB2	D7, D8	NGF R	TrkC
B5, B6	EGF R	ErbB3	D9, D10	VEGF R	VEGF R1
B7, B8	EGF R	ErbB4	D11, D12	VEGF R	VEGF R2
B9, B10	FGF R	FGF R1	D13, D14	VEGF R	VEGF R3
B11, B12	FGF R	FGF R2α	D15, D16	MuSK	MuSK
B13, B14	FGF R	FGF R3	D17, D18	Eph R	EphA1
B15, B16	FGF R	FGF R4	D19, D20	Eph R	EphA2
B17, B18	Insulin R	Insulin R	D21, D22	Eph R	EphA3
B19, B20	Insulin R	IGF-I R	D23, D24	Eph R	EphA4
B21, B22	Axl	Axl	E1, E2	Eph R	EphA6
B23, B24	Axl	Dtk	E3, E4	Eph R	EphA7
C1, C2	Axl	Mer	E5, E6	Eph R	EphB1
C3, C4	HGF R	HGF R	E7, E8	Eph R	EphB2
C5, C6	HGF R	MSP R	E9, E10	Eph R	EphB4
C7, C8	PDGF R	PDGF Rα	E11, E12	Eph R	EphB6
C9, C10	PDGF R	PDGF Rβ	E13, E14	Insulin R	ALK
C11, C12	PDGF R	SCF R	E15, E16	——	DDR1
C13, C14	PDGF R	Flt-3	E17, E18	——	DDR2
C15, C16	PDGF R	M-CSF R	E19, E20	Eph R	EphA5
C17, C18	RET	c-Ret	E21, E22	Eph R	EphA10
C19, C20	ROR	ROR1	F1, F2	Reference Spots	——
C21, C22	ROR	ROR2	F5, F6	Eph R	EphB3
C23, C24	Tie	Tie-1	F7, F8	——	RYK
			F23, F24	Control (-)	PBS

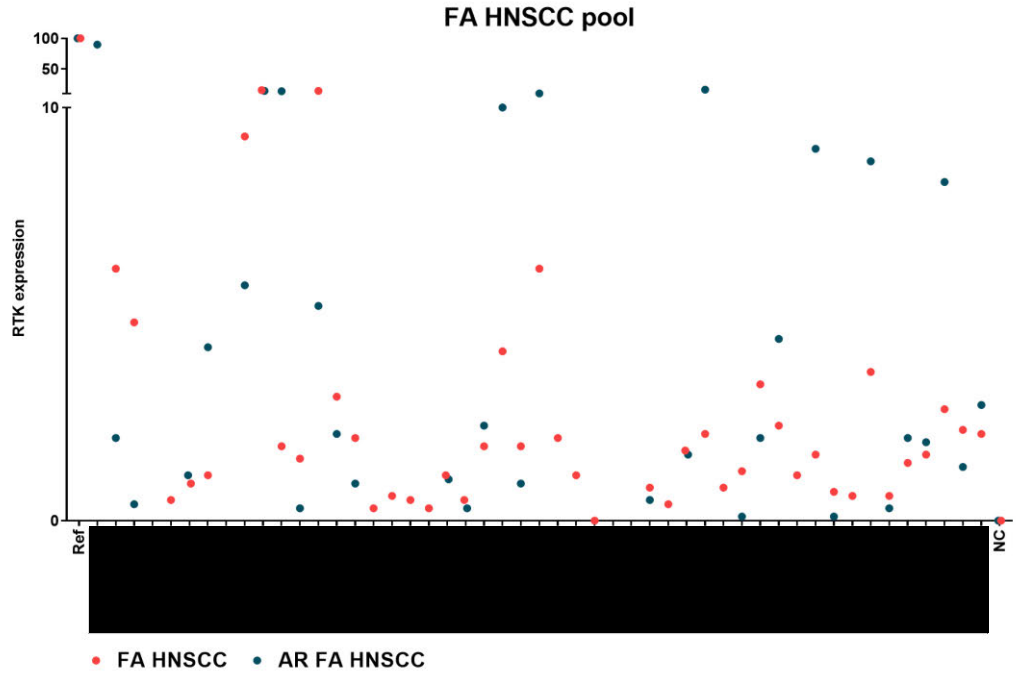
Figure 58. **Human phospho-RTK dot blot array design**: 49 phospho- tyrosine kinase receptors were analyzed. **A**. Dot blot membrane design. **B**. RTK table, extracted from the dot blot array kit.

The first approach was to study the RTKs differential expression in a CAL 27 and CAL 33 pool (sporadic HNSCC cell lines pool) and in VU 1131 and VU 1365 pool (FA HNSCC cell lines pool), in comparison with their matching AR cell lines. Figure 59 shows the results obtained once the AR cell lines where stablished.

A.


HNSCC pool
100
50
10
0
RTK expression
Ref
NC
HNSCC
AR HNSCC

B.


FA HNSCC pool
100
50
10
0
RTK expression
Ref
NC
FA HNSCC
AR FA HNSCC

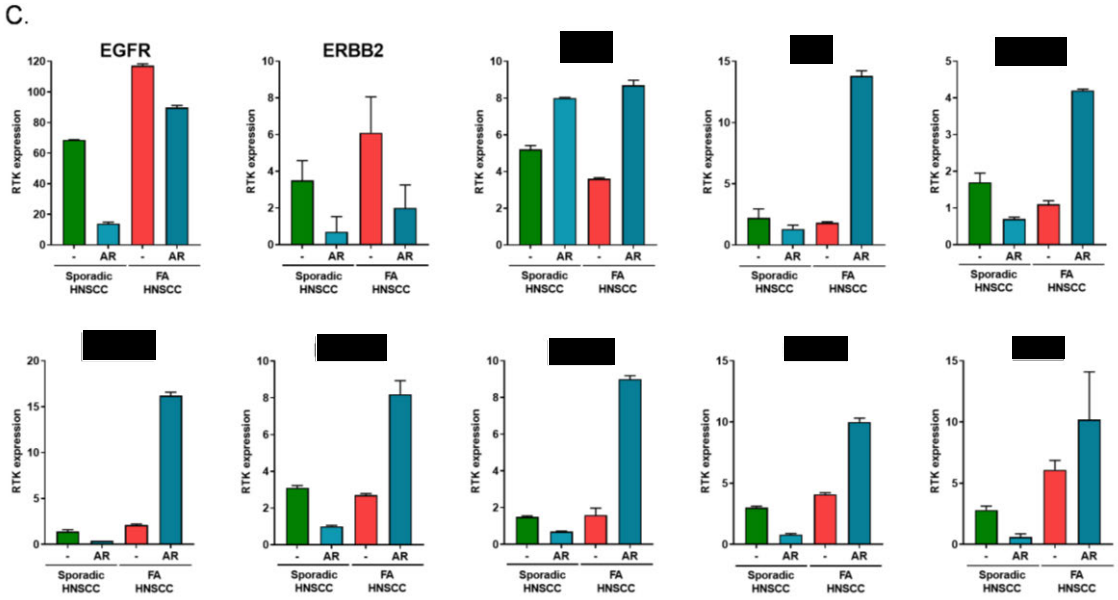
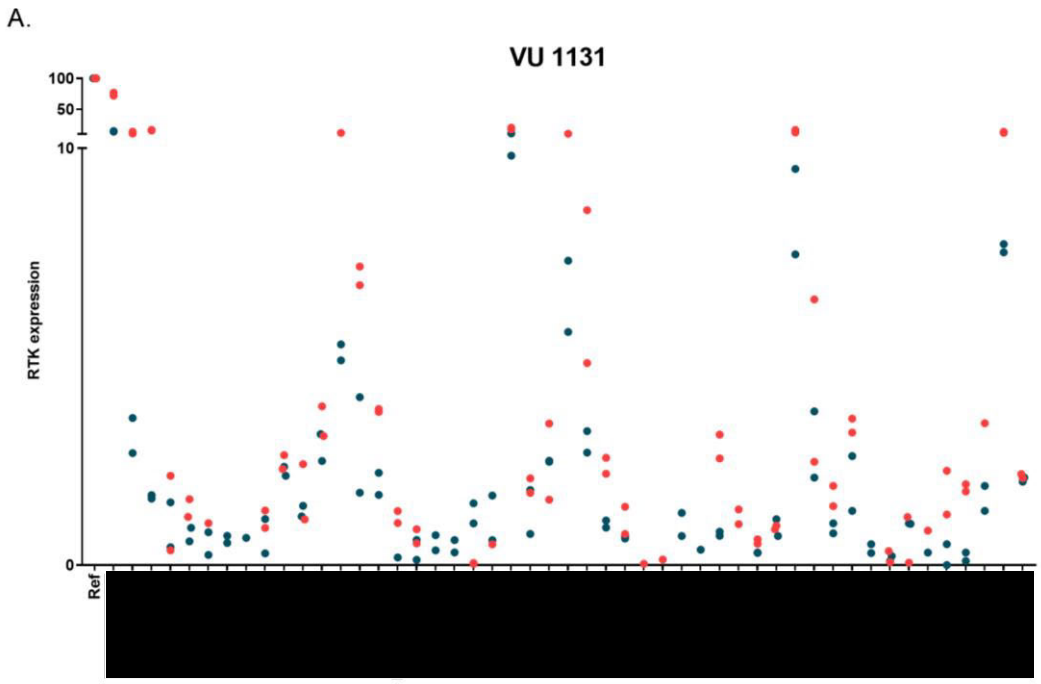


Figure 59. **Dot blot assays of the most relevant tyrosine-kinase receptors (RTKs):** (**A**) in sporadic HNSCC pool, CAL 27 and CAL 33 (green), and afatinib resistant cell lines pool (AR HNSCC, blue); (**B**) in FA HNSCC pool, VU 1131 and VU 1365 (red), and afatinib resistant cell lines pool (AR FA HNSCC, blue). **C**. Main results of the RTKs that were overexpressed in AR FA HNSCC cell lines. Graphs show mean +/- SD of duplicate spots.

The first two graphs in Figure 59C represent two members of the ERBB family (EGFR or ERBB1 and ERBB2). As afatinib is a panERBB inhibitor, the decrease in ERBBs expression in AR cell lines -treated with afatinib at the same time as the experiment was done- was expected. Contrarily, expression of some RTKs as [redacted] was higher in AR FA HNSCC in comparison with non-resistant or sporadic cell lines.

To validate the results obtained, the previous experiment was repeated with all FA HNSCC cell lines, including both sensitive and AR counterparts: VU 1131, VU 1131 AR, VU 1365, VU 1365 AR, OHSU 974, and OHSU 974 AR, in an independent manner (no cell line pool). Figure 60 shows the results obtained in each cell line.



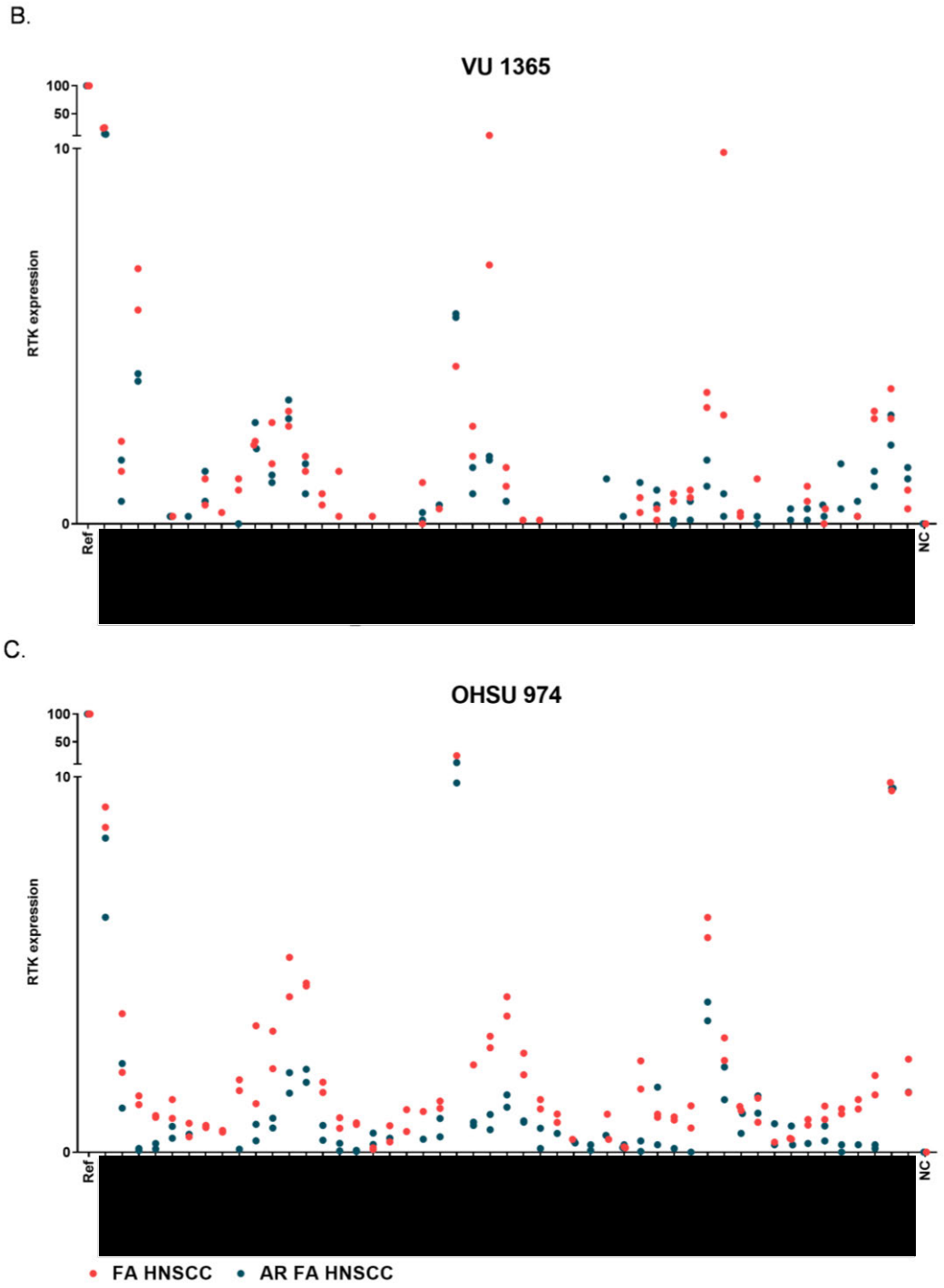


Figure 60. **Dot blot assays of the most relevant tyrosine-kinase receptors (RTKs):** (**A**) in VU 1131 and VU 1131 afatinib resistant cell line (AR FA HNSCC), (**B**) in VU 1365 and VU 1365 AR, (**C**) in OHSU 974 and OHSU 974 AR. Graphs show mean +/- SD of duplicate spots.

However, comparing these results with the previous ones, there were not any RTK overexpressed in AR FA HNSCC cell lines in comparison with non-resistant cell lines.

4.2.5. ERBB family expression in AR FA HNSCC cell lines

The expression of ERBB receptors was also studied in the FA HNSCC cells by flow cytometry. Therefore, differential expression of ERBB1-4 was compared between AR and non-resistant cell lines VU 1131, VU 1365 and OHSU 974 (Figure 61). Although the expression of ERBB2-4 was barely appreciable, there were some changes between ERBB1 expression depending on the cell line. ERBB1 expression in VU 1131 AR was higher than in the non-resistant cell line. VU 1365 AR ERBB1 expression was almost the double than VU 1365 (non-resistant). However, in OHSU 974 AR cell line the expression of ERBB1 was significantly lower. That study was done in CIEMAT laboratory, in collaboration with Dr. Bueren and Dr. Casado.

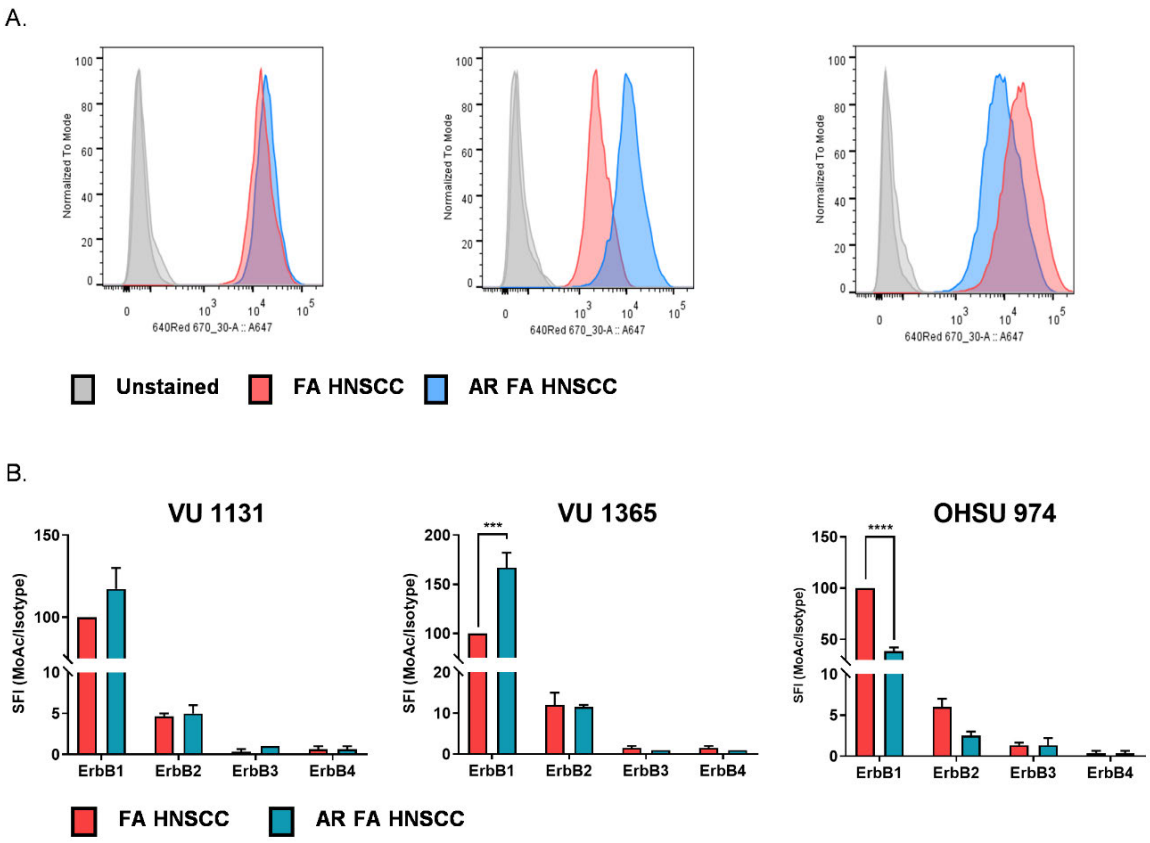


Figure 61. **ERBB family receptors expression in FA HNSCC**. **A**. Flow cytometry differences between FA HNSCC and AR cell lines comparing the level of expression of ERBB1. **B**. Quantification of the level of the specific fluorescence intensity (SFI) of each of the ERBB family receptors: ERBB1 (EGFR), ERBB2 (HER2), ERBB3 (HER3), ERBB4 (HER4). Graphs show mean +/- SEM of 3 experiments. Statistical parameters were analyzed by 2-way ANOVA, adjusted Pvalue <0.001 (VU 1365) and Pvalue <0.0001 (OHSU 974).

4.2.6. CD44v6 expression in AR FA HNSCC cell lines

CD44v6 is an isoform of the CD44 protein that it is associated with the metastatic dissemination in tumors and commonly present in SCC (Haist et al., 2021; Ciulean et al., 2023). Taking that into consideration, the expression of this transmembrane protein in FA HNSCC and AR FA HNSCC cell lines was studied in CIEMAT laboratory (Figure 62). In this case, CD44v6 expression in VU 1131 and VU 1365 was the double than in AR cell lines, meanwhile in OHSU 974 the results were the opposite.

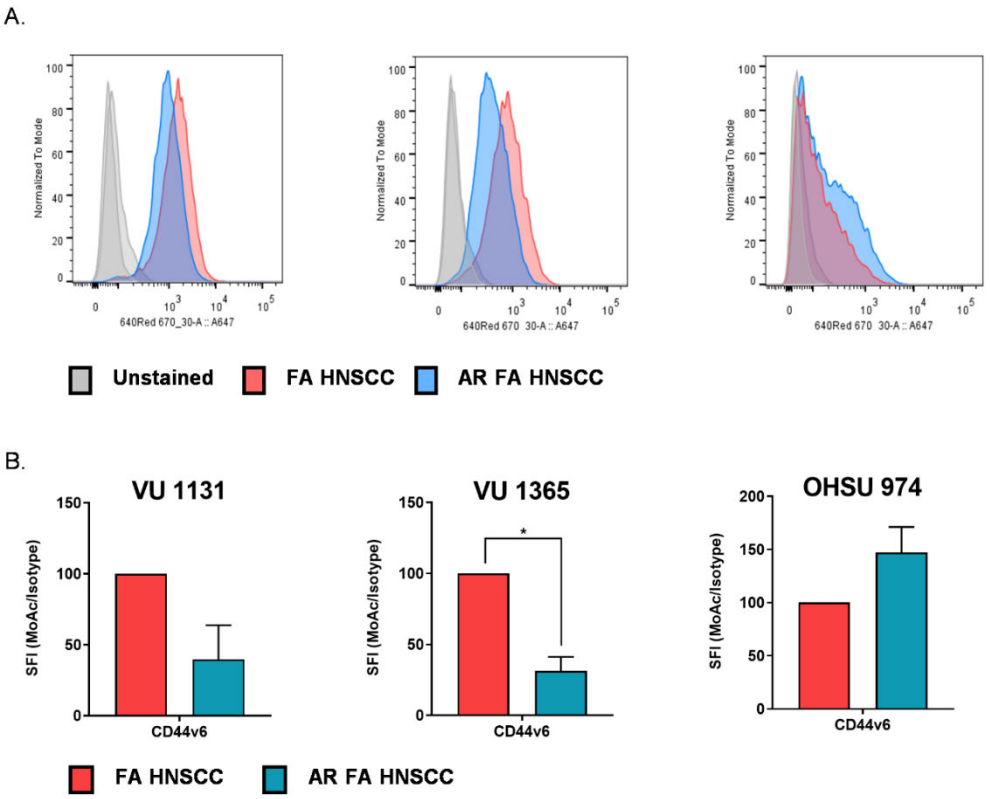


Figure 62. CD44v6 expression in FA HNSCC. A. Flow cytometry differences between FA HNSCC and AR cell lines comparing the level of expression of the CD44v6 receptor. **B**. Quantification of the level of the specific fluorescence intensity (SFI). Graphs show mean +/- SEM of 3 experiments. Statistical parameters were analyzed by paired T-test, Pvalue <0.05 (VU 1365).

4.2.7. NKG2D ligands expression in AR FA HNSCC cell lines

The NKG2D ligands pathway has been considered as a promising target in immunotherapy because of their important role in immune response and antitumor effects (González et al., 2008; Nausch & Cerwenka, 2008; Casado et al., 2022). Therefore, the expression of these ligands in FA HNSCC and AR FA HNSCC cell lines was also measured (Figure 63) in collaboration with CIEMAT laboratory. Comparing the total expression of the ligands, the level in AR cell lines was higher than in the non-resistant cell lines (Figure 63B and C). But the level of expression of each ligand changed in each cell lines, as shown in Figure 63A. Expression of ULBP 2-5-6 in VU 1131 AR cells were considerably higher than in non-resistant cells, whereas in VU 1365 and in OHSU 974 the difference was not as significant. On the other hand, the expression of MICB and ULBP 3-4 in OHSU 974 AR was higher than in OHSU 974; and these differences were not observed in VU 1131 or in VU 1365.

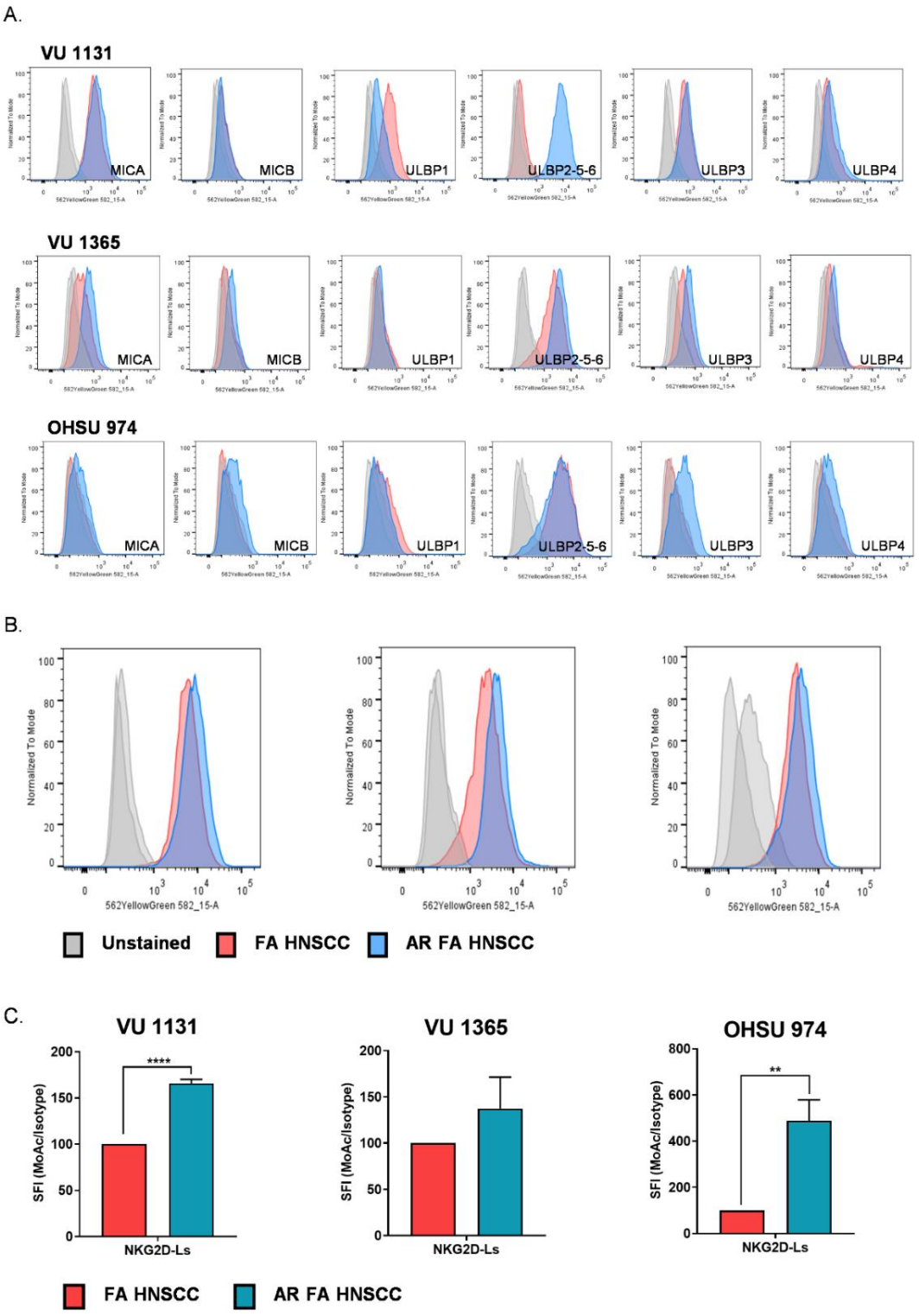


Figure 63. NKG2D-ligands expression in FA HNSCC. A. Flow cytometry differences between FA HNSCC and AR cell lines comparing the level of expression of the NKG2D ligands: MIC-A, MIC-B, ULPB-1, ULPB-2-5-6, ULPB-3, ULPB-4. **B**. Flow cytometry differences between FA HNSCC and AR FA HNSCC comparing the level of the total expression of the NKG2D ligands**. C**. Quantification of the level of the specific fluorescence intensity (SFI). Graphs show mean +/- SEM of 3 experiments. Statistical parameters were analyzed by 2-way ANOVA, adjusted Pvalue <0.0001 (VU 1131) and Pvalue <0.01 (OHSU 974).

4.2.8. Number of copies of ERBB receptors in AR HNSCC cell lines

Due to the afatinib resistance differential acquisition between sporadic HNSCC and FA HNSCC, the number of copies of the *ERBB* receptors genes was studied in AR and non-resistant cell lines. That verification was done using a MLPA assay kit targeting the fourth *ERBB* receptors in DNA extracted from the cells.

Figure 64 shows the results obtained, in which CAL 27, CAL 33, VU 1131, VU 1365, and their respective AR-cell lines presented one or two copies more of *ERBB1* than the control cell lines (PN, FA55, FA139, FA551). In contrast with these data, OHSU 974 and OHSU 974 AR cell lines presented the same number of copies of *ERBB1* than the control cell lines, but a reduction in one copy of the *ERBB4* gene. In that case, VU 1604 was also studied, and it presented the same number of copies as the other FA HNSCC VU 1131 and VU 1365.

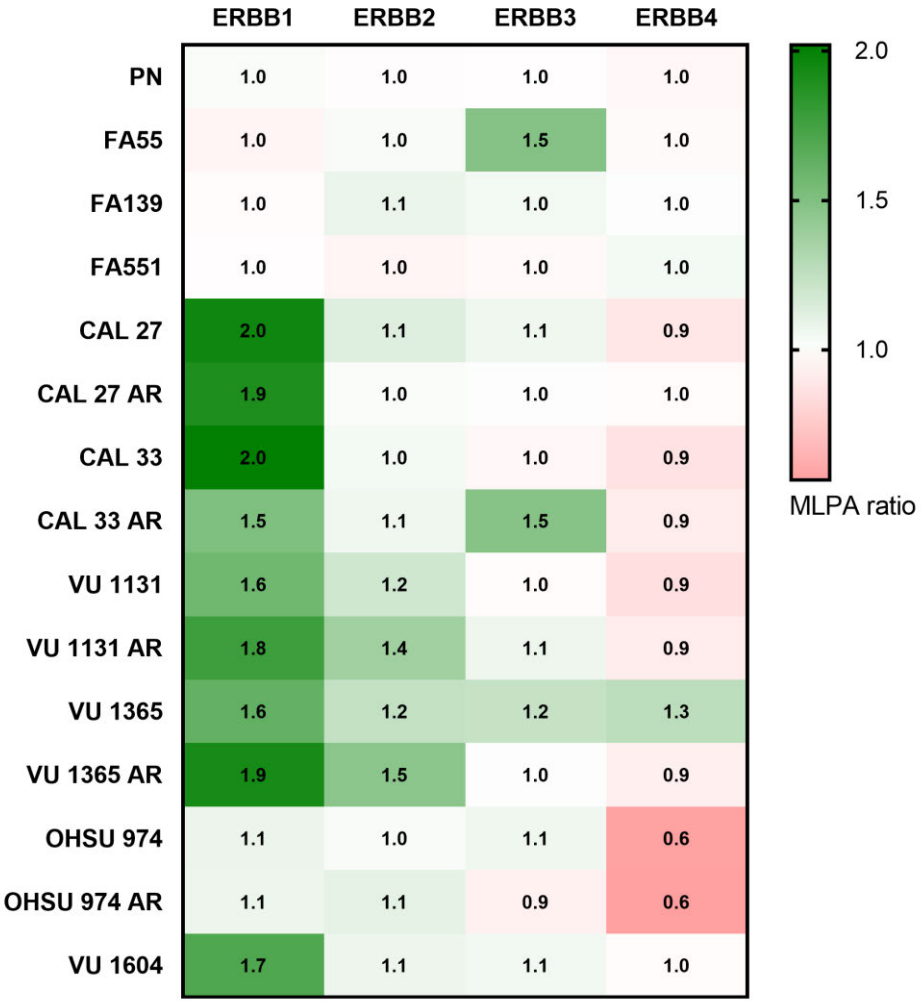


Figure 64. Heat map correlation between the number of copies of ERBB genes with HNSCC cell lines. The detection was done by MLPA of the ERBB genes in sporadic HNSCC (CAL 27 and CAL 33), FA HNSCC (VU 1131, VU 1365, VU 1604 and OHSU 974) and AR cell lines. PN is a human fibroblast control. FA55, FA139, FA551 are FA cell lines controls. 1.0 means that there are 2 copies of the gene (normal diploid status, n=2), meanwhile, 1.5 means that there are 3 copies of it, and 2.0 means that there are 4 copies. 0.5 means that one of the alleles have a depletion of this gene, so there is only 1 copy.

4.2.9. RNA expression in AR HNSCC cell lines

After the study of the ERBB receptors, and due to the unconclusive results obtained after the study of the human phospho-RTKs, we decided to perform RNA sequencing of the AR and non-resistant cell lines, including sporadic and FA HNSCC cell lines. The aim with this analysis was to evaluate and quantify gene expression differences between sporadic and FA HNSCC cell lines. Additionally, up and downregulated pathways were identified in AR in comparison to the non-resistant cell lines.

Figure 65 shows the upregulated genes observed in each cell line, as well as and the common genes that were upregulated in both sporadic HNSCC cell lines (Figure 65A), in FA HNSCC cell lines (Figure 65B), and between all the cell lines studied (Figure 65C).

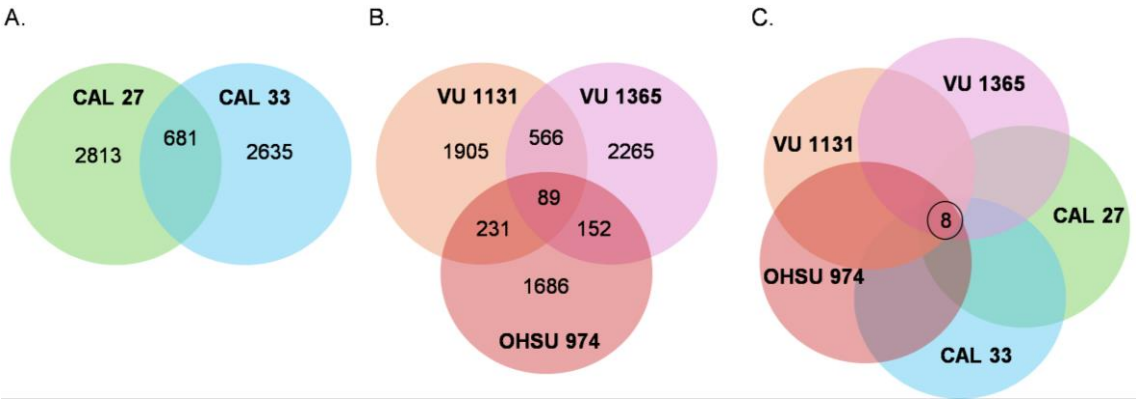


Figure 65. Common upregulated genes in HNSCC cell lines. The detection of the differential expression between cell lines was done by RNAseq in triplicate samples for each cell line, comparing each line with its AR counterparts, all the sporadic with the FA HNSCC, and all the AR with the non-resistant cell lines (see methods). Each cell line in the Venn diagram appears with the number of genes that were upregulated, and the common genes that were upregulated in both sporadic HNSCC cell lines (**A**.), in FA HNSCC cell lines (**B**.), and between all the cell lines studied (**C**.).

From the comparison between sporadic HNSCC cell lines, 681 genes were detected with a base 2 logarithm fold change equal or higher than 0.58 and an adjusted p-value equal or lower than 0.05 (see methods) in AR cell lines, compared with sensible cell lines (data shown in Appendix 2). Whereas in AR sporadic HNSCC cell lines 681 genes were detected as upregulated, in AR FA HNSCC 89 genes were significant differentially expressed and upregulated (Figure 65B, 67, Appendix 2). The protein-protein interaction networks between these proteins shown in Figure 66. Figure 66B shows AR FA HNSCC protein-protein interaction network, in which a main node with [redacted] located in the center.

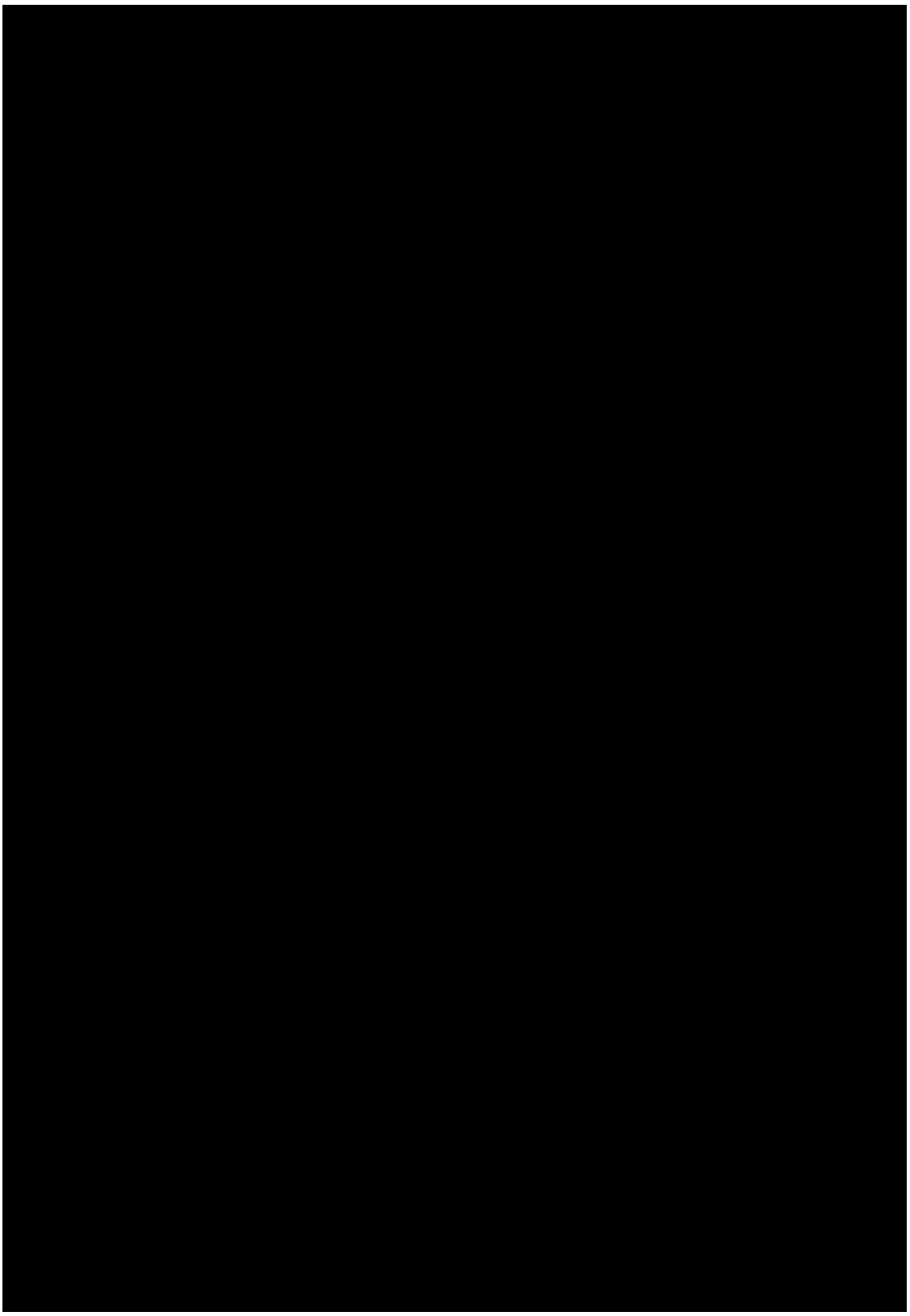


Figure 66. Protein-protein interaction networks for the significantly upregulated genes in HNSCC. Protein-protein interaction network between the significant differentially expressed, upregulated and common proteins in both sporadic HNSCC (**A**.) and in the three FA HNSCC cell lines studied (**B**.). The models were done with STRING 12.0 database (https://string-db.org/), confidence level 0.4. Each protein is represented by an individual node, connected with others by colored lines, which represent different evidence types for protein interaction.

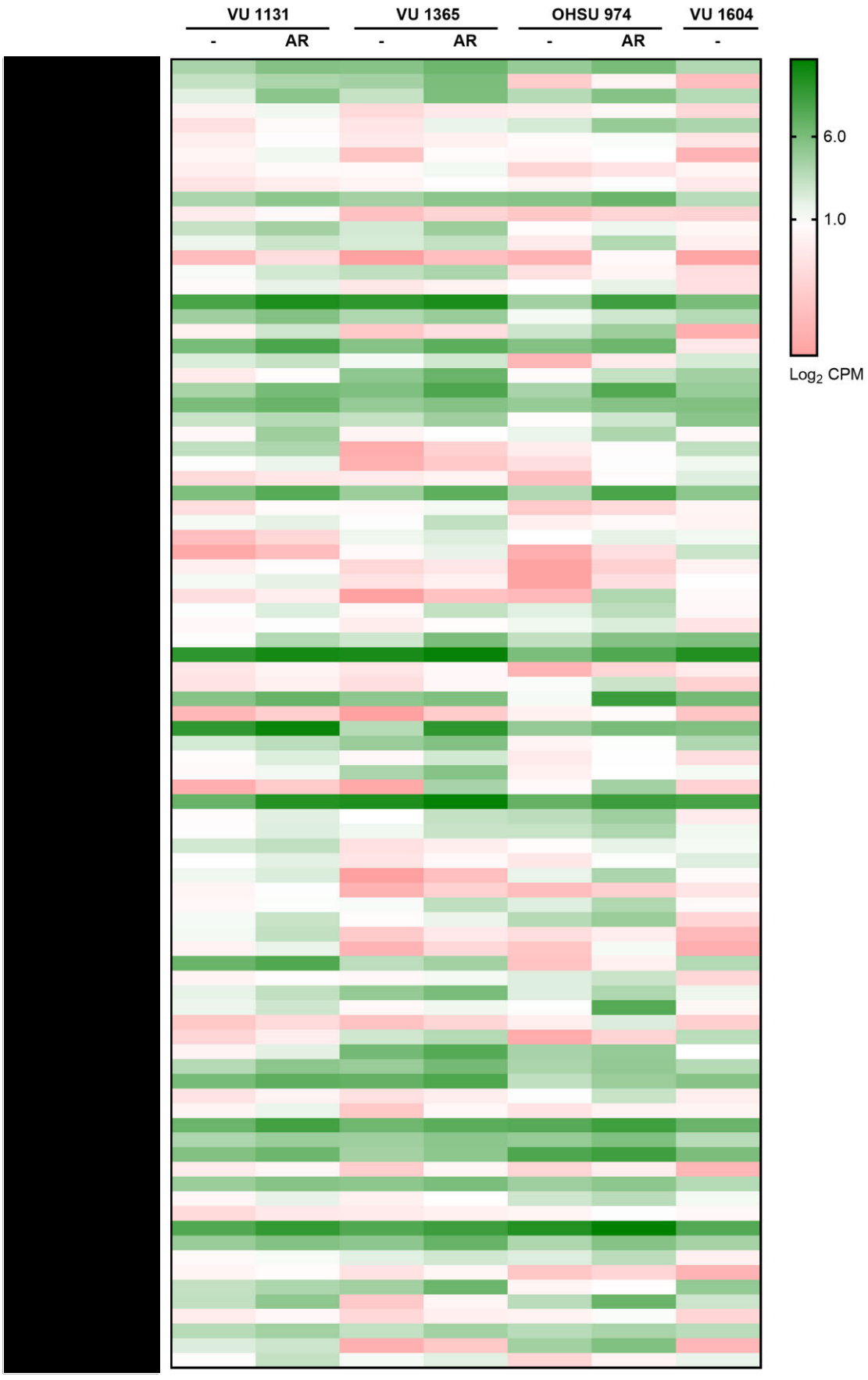

VU 1131
-
AR
VU 1365
-
AR
OHSU 974
-
AR
VU 1604
-
6.0
1.0
Log2 CPM

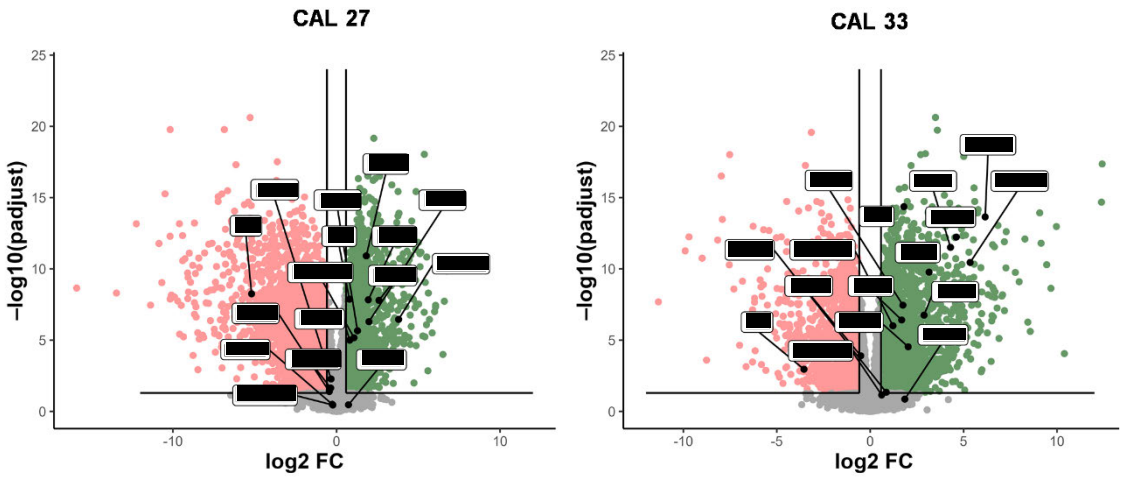
Figure 67. Correlation between the significantly upregulated genes in FA HNSCC cell lines. Heatmap with the 89 genes that were detected upregulated in AR FA HNSCC. The detection of the differential expression between cell lines was done by RNAseq in triplicate samples for each cell line (see methods). Each FA HNSCC is followed by its resistant cell line except VU 1604, which resistant cell lines was not stablished.

The comparison of VU 1131 AR, VU 1365 AR and OHSU 974 AR against the non-resistant cell lines revealed 89 genes significantly upregulated in AR cell lines. VU 1604 cell line was also studied in this case, in order to compare its expression pathway with the other FA HNSCCs. Some of the genes listed are also upregulated in the AR sporadic HNSCC, as it is shown in the next figures.

Figure 68 shows differentially expressed genes that were down- or up-regulated in AR cell lines in comparison with the non-resistant HNSCC cell lines, taking into consideration that genes with an adjusted p-value of < 0.05 and an absolute fold change of |FC|> 1.5 (log2 FC > or < 0.58) were considered differentially expressed. Some interesting genes are indicated inside the plot, like [redacted].

As shown in Figure 65C, the comparison between the genes with higher expression in AR cell lines gave us 8 genes: [redacted], also pointed in graphs below (Figure 68).

A.



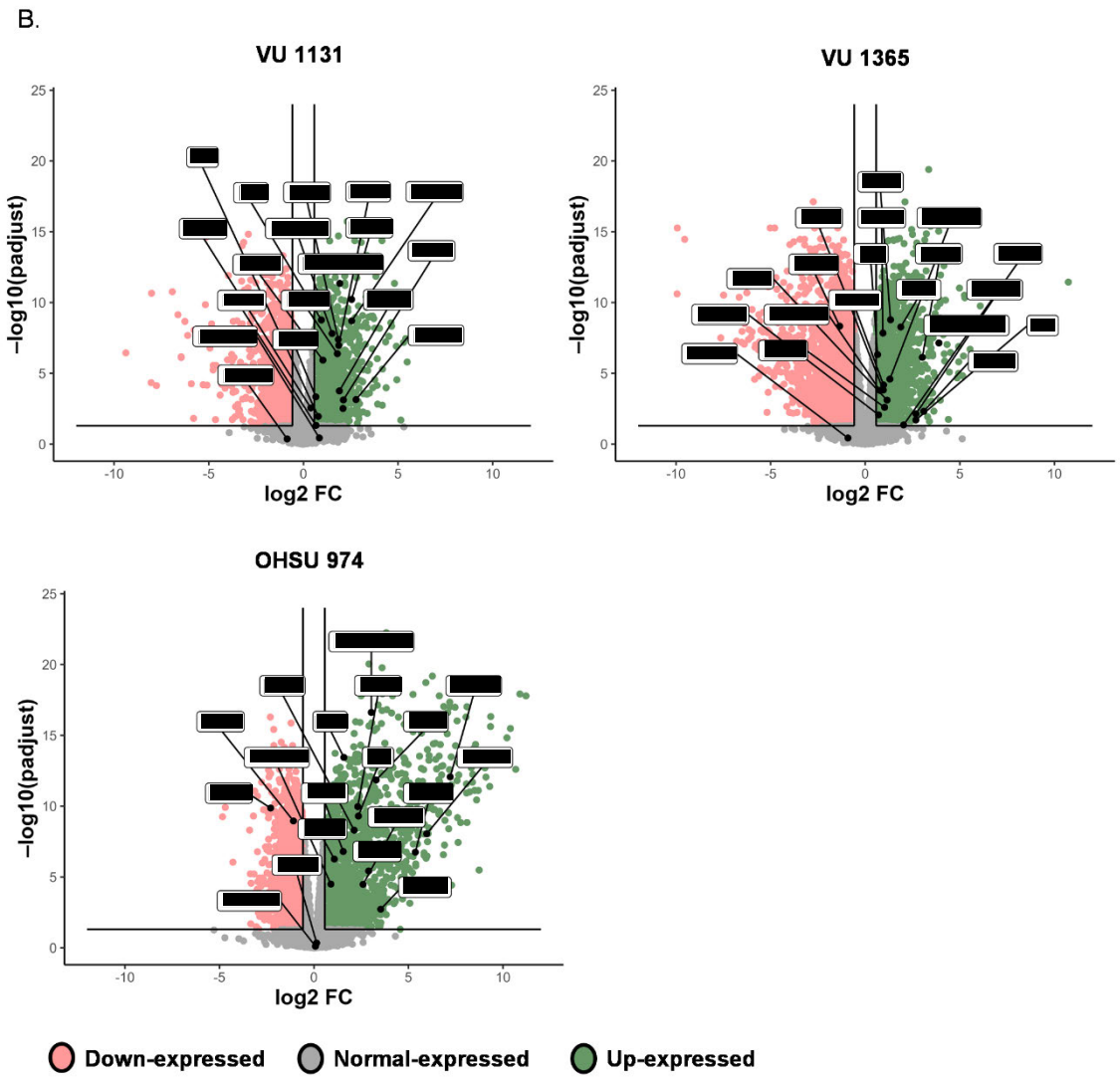
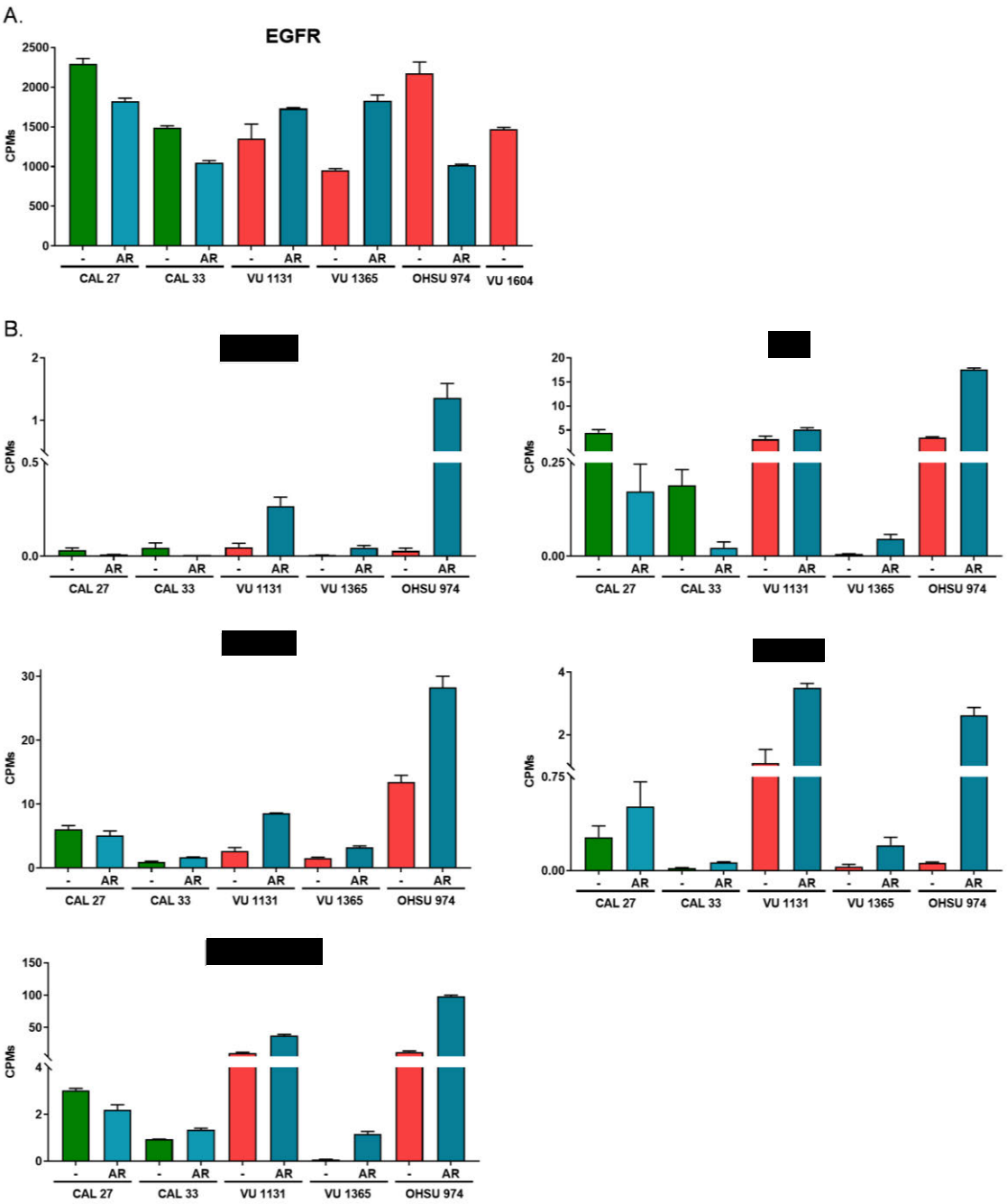


Figure 68. Volcano plots of differential gene expression between HNSCC cell lines. Detection of the differential expression between cell lines was done by RNAseq in triplicate samples for each cell line (see methods). Each line was compared against its correspondent AR cell line. Dots showed the genes down-expressed (pink), normal-expressed (grey) or up-expressed (green) in each AR cell line in comparison with the non-resistant cell line. Genes were considered differentially expressed with an adjusted p-value of < 0.05 and an absolute fold change of |FC|> 1.5 (log2 FC > or < 0.58).

Finally, graphs below show the expression of some of the genes mentioned before, depending on the cell line. EGFR expression was constant in all cell lines, including VU 1604, and its changes between AR and non-resistant cell lines were minimal (Figure 69A). As shown in Figure 69B the expression of [redacted] was higher in AR FA HNSCC than in non-resistant FA HNSCC and sporadic HNSCC cell lines. Figure 69C shows the differential expression between cell lines of the 8 genes that were overexpressed in AR cell lines. Therefore, as shown, [redacted] were more expressed in AR than in not-resistant cell lines.


A.
EGFR
CPMs
2500
2000
1500
1000
500
0
- AR - AR - AR - AR - AR -
CAL 27
CAL 33
VU 1131
VU 1365
OHSU 974
VU 1604
B.
[redacted]
CPMs
2
1
0.5
0.0
- AR - AR - AR - AR - AR
CAL 27
CAL 33
VU 1131
VU 1365
OHSU 974
[redacted]
CPMs
20
15
10
5
0.25
0.00
- AR - AR - AR - AR - AR
CAL 27
CAL 33
VU 1131
VU 1365
OHSU 974
[redacted]
CPMs
30
20
10
0
- AR - AR - AR - AR - AR
CAL 27
CAL 33
VU 1131
VU 1365
OHSU 974
[redacted]
CPMs
4
2
0.75
0.00
- AR - AR - AR - AR - AR
CAL 27
CAL 33
VU 1131
VU 1365
OHSU 974
[redacted]
CPMs
150
100
50
4
2
0
- AR - AR - AR - AR - AR
CAL 27
CAL 33
VU 1131
VU 1365
OHSU 974

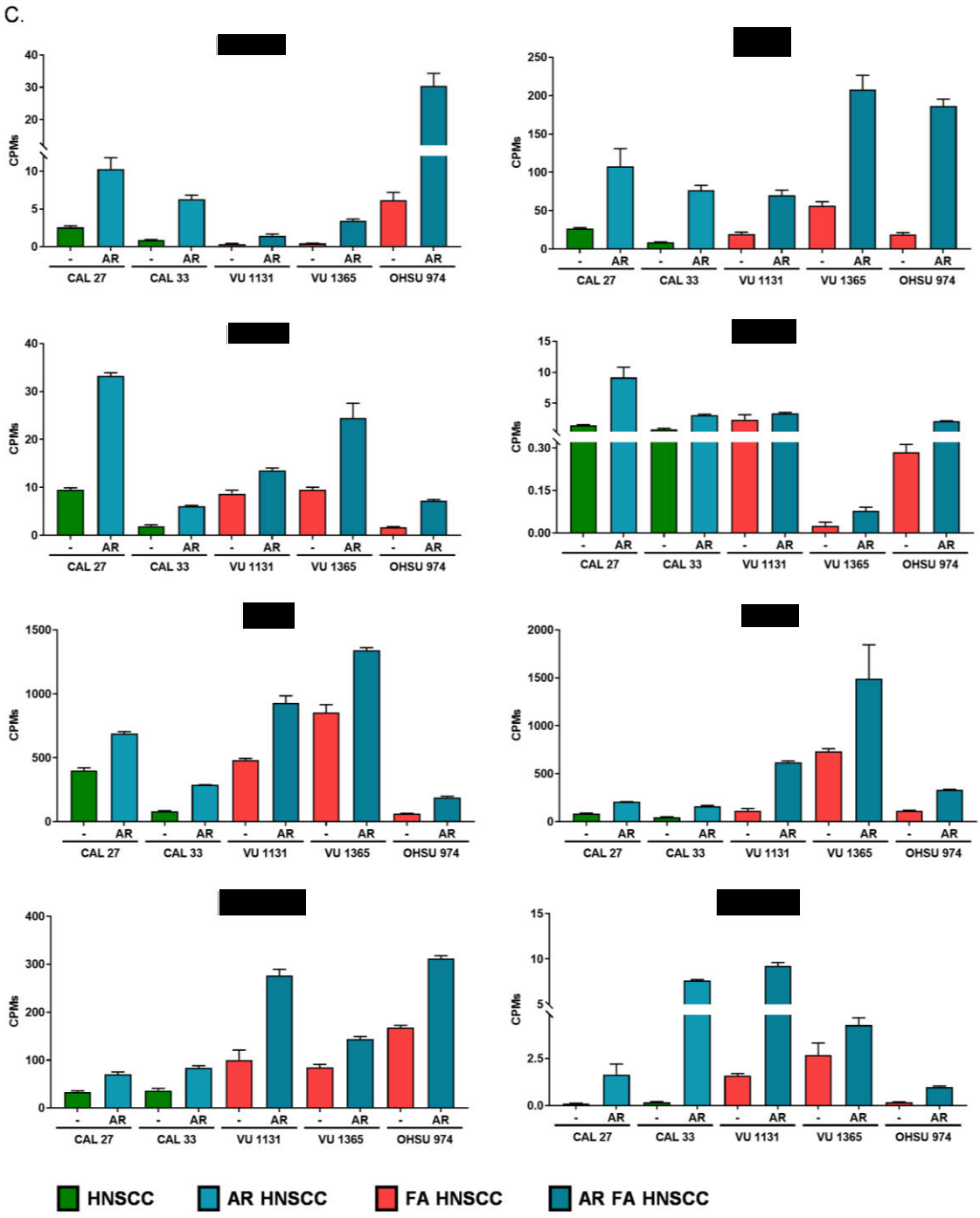


Figure 69. Differential gene expression between HNSCC cell lines. Detection of the differential expression between cell lines was done by RNAseq in triplicate samples for each cell line (see methods). Data of the graphs correspond to the normalized counts per million (CPMs) obtained for each cell lines (mean of 3 samples for each cell line). **A**. *EGFR* expression in HNSCC cell lines. **B**. Different cell lines expression of 5 out of the 89 genes that were overexpressed in AR FA HNSCC. **C**. Expression of the 8 genes that were detected overexpressed in AR sporadic and FA HNSCC cell lines, compared with non-resistant cell lines.

Discussion

5. Discussion

5.1. [redacted] developing inhibitors of DNA damage repair for cancer therapy

[redacted]

[redacted]

Thanks to the availability of atomic-resolution structures [redacted], the comprehension of the molecular interfaces has undergone an exponential growth, allowing virtual drug screenings with computational methods. The pros and cons of designing [redacted] inhibitor have been studied in detail, such as the importance [redacted] Although the results reported by other groups until now have not been successful [redacted], our target on intercepting specific [redacted] has been developed over the last 7 years. Initially, the project focused on identifying potential nodes for intervention within the pathway and the associated protein entities, [redacted] Therefore, a virtual screening was done to identify small molecules that could inhibit [redacted]. In collaboration with the *in silico* drug discovery CRO Intelligent Pharma, the interacting residues [redacted] were analyzed (Camps-Fajol's thesis, 2022). [redacted]

[redacted] At the beginning of the project, this genetic validation was useful to select the preferred interaction area within [redacted] for small molecule interactions and provided a basis for analyzing the poses of molecules obtained through virtual screenings and optimization. Nowadays, one of our next steps will be the design of [redacted] mutants in order to test our candidates in them, to evaluate the specificity between hits and target interaction.

As it was also explained in Camps-Fajol' thesis, after the initial virtual screening, 57 candidate compounds with favorable binding constants for [redacted] were identified. Filtering by their commercial availability and selected by the budget of the project, 32 out of the 57 candidates were acquired (Fx). However, later on, the 57-compounds list was reviewed, and 7 additional compounds were purchased. In the second virtual screening (F2.x), only 4 out of 41 candidates were commercially available, requiring the custom synthesis of 20 compounds by Galchimia, a Spanish chemical synthesis company. The first optimization round concluded with the validation of 13 new compounds, that needed to be synthetized by TCGLS, an Indian chemical synthesis company. These subsequent syntheses significantly increased costs and delayed the time of the research processes.

If we compared our drug discovery process in an academic laboratory with those which are executed on a big scale in pharmaceutical companies (big pharma), there are many differences in several key aspects, including resources, scale, expertise and infrastructure. Therefore, large pharmaceutical companies have substantial financial resources, which enable them to fund extensive and prolonged research and development projects, with advanced computational tools, large compound libraries, and new equipment and technologies. Whereas academic laboratories typically rely on grants from government agencies, what makes the funding limited and competitive, impeding, sometimes, the use of large research facilities and equipment. In our case, the economic budget has led an additional bottleneck, limiting the medicinal chemistry assessment, the number of molecules that can be synthetized (10-30 compounds per round), or the synthesis company selected.

Non-fluent interactions with the Indian synthesis company and international customs requirements, difficulted the arrival of the candidates to the laboratory, which in turn further delayed the hit validation. These difficulties made us to think about synthesize next optimized candidates by Spanish companies, despite of the increase of costs that it would imply. Therefore, second optimization-round candidates were synthetized again by Galchimia, and third and fourth optimization-rounds candidates were synthetized by the CSIC company MCS.

Compounds were experimentally validated by their ability to inhibit [redacted] using *in vitro* assays, such as a cell-based WB [redacted]. Although this method required multiple replicates (typically 4-6) and was time-consuming, results were reliable. The first top candidate, F27, was initially validated in different cell lines, [redacted]. From this point, all the candidates were tested in the same conditions (10-50 μM, ON), mainly in U2OS, but usually also in hFIB cells. Alternative cell-based strategies, such as [redacted], were initially considered but deemed less specific and prone to generating off-target effects. Finally, some of these strategies were used for further characterization of the best candidate inhibitors.

To detect [redacted] interaction and validate the [redacted] inhibition, different methods like pull-downs and immunoprecipitations were initially tested (Camps-Fajol's thesis, 2022). Due to the false positives obtained with these technics, SPR was finally validated as the best method to evaluate the interaction between the target and the compounds. This technique together with others like microscale thermophoresis, differential scanning fluorimetry, isothermal titration calorimetry or FRET are highly used for pharmaceutical companies to detect compounds binding to target proteins. [redacted]

[redacted] As shown in Table 8, different DMSO concentrations were tested during the first and second screening, in order to afford the solubility issues of the compounds.

After these virtual screenings, Dr. Andy Baxter, medicinal chemistry consultant company from ProPharma Partners Ltd, was hired to perform a medicinal chemistry assessment of the best compounds of these rounds (F27 and F2.14). The analysis done was exhaustive and it was detailed described in Camps-Fajol's thesis. In it, the physicochemical properties of the candidates were analyzed in order to evaluate a risk assessment with specific recommendations about the metabolism of the compounds and the next optimization strategy. Therefore, filters related to bioavailability, druggability and toxicity were applied for the following virtual screening. Both candidates showed toxicity with exposures longer than 6 hours, difficulty functional validation studies as cellular survival assays. Despite of that, clonogenic assays were adapted to the favorable time to evaluate inhibitory effect of the candidates, but without toxic off-targets, as shown in Figure 35.

The 13 candidates of the first optimization round (F3.x) were synthetized "*de novo",* and validated in U2OS and hFIB at 10, 20 and 50 µM, and though SPR. Focused on cell validation, most of the candidates showed better [redacted] inhibition in hFIB than in U2OS. Therefore, F3.6 and F3.24 showed [redacted] inhibition activity in U2OS cells, meanwhile F3.4, F3.5, F3.6, F3.8, F3.10, F3.10A, F3.14, F3.24 and F3.24A inhibited [redacted] in hFIB (Figure 30). However, only F3.8, F3.10, F3.19 and F3.20 showed good activity evaluated as K_D constant in SPR (Table 9). None of these candidates, thus, demonstrated better activity than F27.

Second optimization round was focused on the medicinal chemistry advise, and not on the evaluation with the FragPele software, used by NBD in the round before. Considering the structures od F27, F1, F2.14 and F3.10, five new candidates were synthetized and validated (F4.x). F4.3 candidate was the one with the best [redacted] inhibition in cells, whose effect was seen even at 6h (Figure 33). However, F4.3 inhibition effect was joined with a high toxicity off-target effect, which difficulty longer experiments. Results obtained in SPR were also favorable to this compound, reaching the F27 best results. In addition, F4.1 SPR results were also remarkable (Table 10) despite of its inactivity in [redacted] inhibition. That could suggest a high affinity for the target, even if F4.1 compound cannot enter into the cell.

Despite of the limited optimization round, F4.3 demonstrated good affinity for the target and good [redacted] inhibition. Although [redacted] WB and SPR were the main experiments done during the rounds before, functional assays are also important to verify if the compounds could inhibit [redacted]. Therefore, F4.3 was also tested in other functional analyses such as clonogenic assay (Figure 35), in which results were comparable with the ones obtained with F27 before (done in Camps-Fajol's thesis). The inhibition of [redacted] was also measured with F4.3 in U2OS cells, as shown in Figure 37, [redacted]. F4.3 toxicity was also revealed in this experiment, where many cells died because of the treatment with the hit. Lastly, this candidate was also tested by [redacted] As Figure 38A shown, [redacted] However, we did not observe mentioned effect. As this hit was toxic at higher doses and for more than 6 hours, time duration of this experiment was adapted for those requirements. [redacted]. In light of the findings, the off-target toxicity removal was emphasized by its relevance in future candidate optimization rounds.

During the research-stay in [redacted] laboratory, the best candidates from initial screenings (F1, F27, F32 and F2.14) and all the compounds of the two optimization rounds at that moment were tested. Following the [redacted] compounds were added to the [redacted] master mix (see methods). However, results obtained were inconclusive (data not shown). Due to the solubility issues of the tested compounds -diluted in DMSO-, the small amounts of [redacted] and buffer did not allow a properly mixture of the reactive. That was corrected using the same FANC master mix in higher volumes, mixed in a tube instead of in a 384-well plate. Finally, [redacted]

[redacted], Laemmli buffer was added to prepare the samples for a WB run. [redacted]. Although F27 results were not as the previous inhibition evidence, most of the candidates showed the expected activity (Figure 40). In fact, F32, F2.14, F3.5, F3.10A, F4.3 and F4.4 showed a [redacted] activity reduced by the 50%, according to [redacted] levels. The importance of these results lies on the evidence that some of the compounds such as F4.3 o F2.14 showed satisfactory outcomes in all the assays applied, whereas some other candidates seemed to have more affinity for the target when they do not need to enter into the cell. The relevance of the hit solubility in order to improve the optimization rounds was evidenced by mentioned limitations.

Third and fourth optimization screenings were done with the collaboration of NBD for virtual screening and medicinal chemistry assessment. Although 18 new compounds were proposed for synthesis, only 5 could be synthetized due to the technical difficulties and the unexplored synthesis pathways. However, an additional 6 synthetic intermediates were incorporated to the round. Finally, 11 candidates (F5.x) were tested by WB in U2OS and hFIB cells at 1, 5 and 10 µM, in order to evaluate the improvements over previous optimization rounds. Although [redacted] inhibition was tested at 6h and ON, the inhibition effect of the candidates at 6h was mostly unappreciable. However, the inhibition effect of F5.4, F5.6, F5.10 in U2OS, and F5.2, F5.4 and F5.6 in hFIB, incubated ON was notable (Figure 43). F5.6 was the candidate with the best [redacted] inhibition effect in both cell types. In addition, this hit also showed better K_D than F27 (Table 11), measured with its interaction with commercial [redacted] as well as with synthetized and purified [redacted] (see methods). Taking that into consideration, the main advances in this round were the decrease of the off-target toxicity in some of the candidates and the improve of the candidate's solubility, maintaining their effect [redacted] inhibition, as shown in Figure 52.

For the last optimization round until now (F6.x), 7 out of the 9 candidates proposed were synthetized, but 3 additional synthetic intermediate candidates were added to the final list. Accordingly, 10 compounds were validated. Simultaneously, a new "*de novo*" design and virtual screening (2Fx) was proposed by NBD as an alternative of the optimization round. As happened with the start of the project, first screening was done beginning from a ZINC database library. After a multi-step docking process, molecules were filtered and finally selected considering their interactions, shape, chemical diversity and potential reactivity. Proposed candidates were analyzed by their potential interest and availability, and 26 compounds were bought. This new screening provided new interesting structures to be validated in its interaction with the target.

As the 10 synthetized compounds (F6.x) of the fourth optimization round and the 26 bought compounds (2Fx) of the new design round were acquired at the same time, the validation of these 36 hits was done in parallel. In fact, candidates' inhibition was firstly tested at 6h and ON incubation. However, due to the workload and the lack of inhibitor effect of many of the candidates at 6h (data not shown), ON incubation was prioritized. Thus, results show [redacted] inhibition ON (Figures 46, 49). As shown in Figure 46, F6.1 inhibited [redacted] in U2OS and hFIB and F6.4 and F6.5 inhibited [redacted] in hFIB. The same happened with 2F1, 2F2 and 2F3 in hFIB, and 2F17 and 2F26 in hFIB and U2OS (Figure 49). Although F6.x and 2Fx candidates' molarity was higher than in previous rounds, the inhibition effect in [redacted] was validated without side toxic effects. As mentioned before, [redacted] inhibition was associated with unlikely toxic effects in previous optimization rounds, leading in premature cell death. That limitation hindered hit validations, because some of the experiments needed 24h (or more) cells' treatment. F27, F4.3 and F5.6 were toxic at >6h. Therefore, the synthesis and validation of non-toxic candidates supposed a huge step for the project.

For SPR analysis, a determined number of RUs (4400 RU, approximately) of [redacted] must be immobilized in the chip. However, during the last SPR experiment, the immobilization of [redacted] was not as successful as in previous rounds. Probably, that was the cause of the results obtained during F6.x and 2Fx rounds, whose results, shown in Tables 12 and 14, were not completely reliable. As shown in these tables, the interaction between the target and most of the hits could not be evaluated. And in those in which the interaction was evaluated, the differences between the commercial [redacted] channel and the [redacted] channel were higher than in the previous round.

Despite of this fact, the measured interaction between the target and some of these compounds, such as F6.8, 2F15, and 2F16 was comparable with the data obtained with F27 (control).

Comparing the best candidates' structures, the same [redacted] scaffold of F27 was constant in all the optimized hits (F3.14, F4.3, F5.6, F6.1), meanwhile the 2Fx round added additional functional structures (2F17) that could be considered for next optimization rounds. 2Fx screening provided additional information of the functional structures of the candidates, that has not been evaluated until now. The double strategy used, by the optimization of the F5.x round and the development of a new virtual screening in parallel, allowed us to take a sensible step in a good direction. However, this drug discovery project must grow up, and future optimization of these new hits should be done in order to improve the results. As mentioned before, the [redacted] scaffold of the best optimized candidates and the new structures evaluated in the 2Fx round must be taken in consideration for further optimizations. Additionally, the addition of other functional studies such as SRB survival assays (see methods), [redacted], will constitute the next steps of this project. Additionally, hits should be tested in other cell lines, as well as in [redacted] SL cell lines, to corroborate the therapeutic potential of this compounds as DNA repair pathway inhibitors. The design and synthesis of mutant [redacted] proteins in order to verify the specific binding of our best candidates with the target, is a further step that is being considered. And finally, the synthesis of the [redacted] crystal with the best hits until now would also help us to validate our *in silico* model, adding value to our research.

The evolution of artificial intelligent (IA) technologies has overcome an important step in most of the fields in our live, including the research field. Although virtual screenings and optimizations done in our project have been built by NBD using FragPELE and the knowledge on medicinal chemistry, the development of tools like the AlphaFold platform (*https://deepmind.google/technologies/alphafold/*), are currently being a powerful help in research progress. In fact, AlphaFold is described as a tool for "accelerating research in nearly every field of biology", and the potential of this tool in the virtual validation of PPI in drug discovery research should be taken in consideration. However, further validation steps must be lastly tested in living entities.

Our group has been able to study a total of 128 [redacted] inhibitor candidates, including 59 newly synthesized small molecules. The validation has allowed to find many of them with the expected inhibition effect, and, finally, few of them without cell toxicity side effect.

5.2. Obtaining and characterization of AR HNSCC cell lines

As mentioned in the introduction, FA is a DNA repair syndrome characterized by high cancer predisposition. The risk of HNSCC in FA patients is 500-800 folds higher than in the general population and this is becoming their main treat in recent years as, thanks to improved care of the blood disease, many patients reach adulthood. Given their deficiency in DNA repair, FA patients do not tolerate conventional chemo/radiotherapy and the only curative therapy is surgery when the tumor is still resectable (Minguillón & Surrallés, 2018).

In general population, HNSCCs are distinguished by an immunosuppressive microenvironment that evades the immune system through various resistance mechanisms. Immune checkpoint molecules, such as PD-1, its ligand PD-L1, and CTLA-4, are crucial for maintaining self-tolerance and modulating immune responses within normal immunoregulatory pathways. As a result, ICIs targeting PD-1, can effectively block these inhibitory pathways, thereby enhancing immune surveillance against tumor cells (Yamashita et al., 2023). Additionally, PD-L1 inhibitors, as well as CTLA-4 inhibitors, could be used in the treatment of sporadic HNSCC. Numerous clinical trials, both as monotherapy and in combination regimens, have been conducted with these antibodies, focusing primarily on patients with recurrent or metastatic HNSCC (Yokota et al., 2020a). Additionally, efficacy of ERBB inhibitors against HNSCC has also been investigated, with the EGFR inhibitor cetuximab as first-line treatment in combination with chemo/radiotherapy (Kozakiewicz & Grzybowska-Szatkowska, 2018). Although cetuximab was the first antibody approved by the FDA in 2006, for the treatment of locally advanced HNSCC, in combination with radiotherapy (Kozakiewicz & Grzybowska Szatkowska, 2018), other ERBB inhibitors are currently approved by the FDA and EMA for sporadic HNSCC, such as pertuzumab, an HER2 inhibitor. Other ERBB inhibitors such as margetuximab, necitumumab, panitumumab, patritumumab and trastuzumab, that are approved against other cancer types, are involved in ongoing clinical trials with sporadic HNSCC patients.

Besides mAbs, ERBB-TKI are being also used for sporadic HNSCC treatment. Gefitinib, afatinib, dacomitinib, erlotinib and lapatinib are TKIs approved for clinical use. Gefitinib and erlotinib primarily target EGFR, while lapatinib is active against both EGFR and HER2. Dacomitinib targets ERBB1, ERBB2, and ERBB4, and afatinib is a pan-ERBB inhibitor (Zibelman & Mehra, 2016; Lee et al., 2021). In HNSCC patients, afatinib improved progression-free survival compared to methotrexate in second-line treatment for recurrent and/or metastatic disease; and dacomitinib has shown promising clinical activity in the first-line treatment of recurrent or metastatic HNSCC, as demonstrated in phase II trials. Since the identification of the EGFR gene and the development of gefitinib in 2004, three generations of EGFR inhibitors have been developed, significantly altering therapeutic strategies, and providing substantial survival benefits to patients. These findings underscore the potential of EGFR inhibitors in managing HNSCC and other EGFR-driven cancers (Kozakiewicz & Grzybowska Szatkowska, 2018).

In 2018 our group led the application and approval of an orphan drug designation for afatinib, to treat HNSCC in patients with FA (Montanuy, et al., 2020). After a high content screening, afatinib and gefitinib found to induce cancer specific lethality in tumor cell lines and to reduce FA HNSCC tumors size in mice with non-genotoxic effects (Montanuy, et al., 2020a and 2020b).

After the afatinib orphan drug designation, our group is committed to demonstrate the efficacy and safety of afatinib in FA patients with HNSCC through a repurposing, multicenter and international clinical trial, programmed to start shortly in Spain and German. In parallel, we seek to go one step further and find new therapeutic targets in AR FA HNSCCs. In this thesis, we developed AR sporadic (CAL 27, CAL 33), FA (VU 1131, VU 1365, VU 1604, OHSU 974), FA-edited (“fanconized” clones of CAL 27 and CAL33), and FA-corrected (corrected lines of VU 1131, VU 1365, VU 1604, and OHSU 974) HNSCC cell lines. Interestingly, FA HNSCC cell lines showed 20-50 times lower long-term AR capacity than sporadic HNSCC ones (20-45-50 nM vs 800-1,000 nM afatinib), what supports the relevance of the upcoming clinical trial. To note, VU 1604 cell line do not tolerate doses higher than 5 nM of afatinib (VU 1604 AR), but it was unstable and could not be maintained after 10 passages. Because of that, VU 1604 was discarded in the following experiments.

Although the development of resistance in the FA HNSCC cell lines was almost despicable in comparison with the sporadic tumors, we aimed to characterize these new AR cell lines. In this sense, all the AR cell lines were firstly compared with their parental cell line in SRB survival assays with increasing doses of afatinib (Figure 54). As expected, AR cell lines were resistant to the panERBB inhibitor, in comparison with non-resistant cell lines. Until now, it has been the first time that drug-resistant FA cell lines have been developed, what allows to other researchers to take these materials and them in future therapeutic research.

Considering that gefitinib and cetuximab are inhibitors against ERBB1, the evaluation the effect of the AR cell lines with these other drugs was also considered. As afatinib is a panERBB inhibitor, it made sense that cell lines which have developed some resistance mechanisms to this inhibitor, were also resistant to other ERBB inhibitors that act in the same pathway. Therefore, as shown in Figures 56 and 57, the resistance to gefitinib was similar to the resistance to afatinib, whereas the AR cell lines were more resistant to cetuximab. Cetuximab and gefitinib are both targeted therapies used in the treatment of certain types of cancer, but their mechanism of action is not the same. While the first one binds to the extracellular domain of the EGFR, preventing the receptor from being activated by its natural ligands, gefitinib inhibits the tyrosine kinase activity of EGFR by binding to the ATP-binding site of the receptor. However, both ways inhibit the downstream signaling pathways that promote cell proliferation and survival.

In addition, to unravel the mechanism of the different resistance-capacity between sporadic and FA cell lines, the activation status of 49 human RTKs was analyzed. Looking for promising candidates for potential second lines of therapy after afatinib, the array was firstly done with pools of cells, to search for different RTK activation between sporadic HNSCC (CAL 27 and CAL 33), FA HNSCC (VU 1131 and VU 1365), and AR cell lines (Figure 59). Some RTKs that were detected over-phosphorylated in FA HNSCC cell lines were [redacted] (Figure 59C), with literature support in the field of drug-resistance development in HNSCC cases. Due to the differences between groups, we tried to verify these results through flow cytometry, WB and immunoprecipitation against the tyrosine-kinase proteins that appeared activated in the array (data not shown). However, all the evaluated RTKs have many potential phosphorylation sites, which difficulted the task of the receptor's activation validation. As an additional approach, the RTK array kit was repeated with the independent cell lines, in this case. Thereby, each FA HNSCC cell line was compared against its corresponding AR FA HNSCC cell line. To note, OHSU 974 cell line was added later because it was not previously in our cell collection. Unfortunately, after months of work, the results of this second round of arrays did not validate the activation that was observed in the first round, as shown in Figure 60. The first experiment was done when AR cell lines were obtained, while second RTK experiment was done one year before, due to the previous mentioned additional validations. Moreover, when cells are subjected to treatment, the development of resistance is usually accompanied by mutations that can modify the initial characteristics of mentioned cells. Therefore, the passage of several months between both analyses and the evolution of the cell lines themselves, which were able to adapt to growth under these afatinib-conditions, could explain these different results.

In parallel, and during the research-stay in Dr. Juan Bueren's laboratory, surface expression of some markers that are currently being targeted in sporadic HNSCC by advanced CAR T-cell therapies was measured by flow cytometry. Therefore, ERBBs (Papa et al., 2015; Whilding & Maher, 2015), and NKG2D ligands (González et al., 2008; Tay et al., 2021) and CD44v6 (Haist et al., 2021; Ciulean et al., 2023) expression was compared between AR and non-resistant FA HNSCC. The expression of these markers was different depending on the studied cell line: CD44v6 expression was higher in OHSU 974 AR and lower in the other AR FA HNSCC cell lines; meanwhile the NKG2D-Ls expression was higher in all the AR FA HNSCC cell lines (Figures 62, 63). However, despite of the differences between cell lines, the levels of markers expression could make these AR cell lines susceptible for a potential CAR-T therapy targeted these receptors. Likewise, although ERBB2-4 expression was similar in all the samples, ERBB1 expression between FA HNSCC and AR FA HNSCC was significantly different depending on the cell line studied. As shown in Figure 61, VU 1131 cells did not show significant differences between AR and non-resistant cell lines. Whereas in VU 1365 and OHSU 974 cells, ERBB1 expression was significatively different depending on the AR/non-resistant status of the cell line. However, due to the high levels of expression detected in AR and non-resistant cell lines, these AR FA HNSCC cell lines would also be susceptible to a potential CAR-T therapy targeted these receptors.

Despite of the differential expression of ERBB receptors in the cell surface, no altered number of gene copies was observed by MLPA, as shown in Figure 64.

The development of alterations in the number of copies of some genes has been usually reported as a common resistance mechanism in cells under long-term treatment (Borg et al., 1994; Chen et al., 2000; Engelman et al., 2007). After the log-term treatment with afatinib, some of the cells could have been positive-selected by duplications in the number of *ERBB* genes, that would confer them resistance to afatinib. For this reason, and in order to validate if any of the cell lines had an alteration in the number of copies of the *ERBB* genes, MLPA targeting these 4 genes was performed. As shown in Figure 64, d 3 or 4 copies of *ERBB1* (instead of 2) were detected in all HNSCC cell lines except OHSU 974 and OHSU 974 AR. However, the number of copies of AR cell lines was not higher than the number of copies of the non-resistant cell lines. Therefore, we could not correlate this copy number with acquired resistance to afatinib indicating that the mechanism of afatinib resistance is not related to an increase in the number of ERBB genes copies.

Finally, to go further in cell lines characterization and its relationship with a potential second line of therapy, RNAseq analysis of AR and non-resistant, sporadic and FA HNSCC cell lines was performed. The results obtained of this study offered the opportunity to find interesting SL connections between EGFR and proteins that could be overexpressed as potential mechanisms of resistance in the studied cell lines. Surprisingly, a preliminary analysis showed more than 5,000 RNA transcripts that were significantly overexpressed in each AR cell line in comparison with non-resistant cell lines. From that point, the most interesting comparisons between cell line groups were established: FA HNSCC vs. sporadic HNSCC, afatinib resistant sporadic HNSCC vs. non-resistant sporadic HNSCC, and AR FA HNSCC vs. non-resistant FA HNSCC; focusing the attention on genes that were upregulated in AR FA HNSCC.

In accordance with the MLPA results, and contrarily to the studies published in 2022 in which *EGFR* copy number was shown increased in FA HNSCC in comparison to sporadic tumors (Jäwert et al., 2022; Roohollahi et al., 2022; Webster et al., 2022), our RNAseq results did not show a significant overexpression of *ERBB* genes in FA-derived cells. The comparison between *EGFR* CPMs in RNAseq (Figure 69A) with the EGFR expression detected in FA HNSCC cell lines membrane (Figure 61) supports our results. However, the expression of [redacted] was significantly upregulated, while the expression of [redacted] was significantly downregulated in FA HNSCC, in good agreement with gene amplification and deletion, respectively, observed in these publications (Figure 68).

After the comparison between AR and non-resistant sporadic HNSCC cell lines, up to 600 genes were detected significantly upregulated in both AR cell lines, CAL 27 AR, and CAL 33 AR (Appendix 2). However, the comparison of FA HNSCC cell lines in the same conditions resulted in the significantly upregulation of 89 genes in VU 1131 AR, VU 1365 AR and OHSU 974 AR simultaneously, compared to non-resistant FA HNSCC cell lines, as shown in Figure 67. After the study and selection of the up-expressed genes, we observed that most of the up-regulated genes are interconnected in the same interaction network, which interactions were shown in Figure 66, with [redacted] node located in the center of the network. In addition, some of these genes were published as upregulated in FA HNSCC, such as [redacted] (Figures 67-69), [redacted] Interestingly, our results show this gene overexpressed in AR cell lines.

[redacted]

[redacted].

Another gene upregulated in AR FA HNSCC cell lines was [redacted] (Figures 67, 68), that has been reported as a resistance mechanism in tumors [redacted]. In addition, the upregulation of this gene has been also related with poor prognosis in HNSCC [redacted], which could agree with AR tumors prognosis.

[redacted] Interestingly, the overactivation of [redacted] in the AR FA HNSCC samples analyzed was significative (Figures 67-69). Few studies correlate differential expression of [redacted] in resistant tumors. [redacted]

[redacted] According to that, data shown in Figures 67-69 suggests that the upregulation of [redacted] in AR FA HNSCC cell lines could be considered as a resistance mechanism to afatinib in these cell lines. This fact points [redacted] as a potential target to be inhibited in afatinib resistant tumors.

In addition to [redacted] is another interesting candidate to be inhibited in AR FA HNSCC cell lines. [redacted]

After comparing the abnormal regulated genes in all the HNSCC cell lines (sporadic and FA), 8 upregulated genes were detected in all AR cell lines (Figure 69C). Some of them, as [redacted] are not directly associated with HNSCC, but with other types of cancer development and progression. Also, there were upregulated genes as [redacted] which is implicated [redacted] has been documented by its potential contribution to tumorigenesis in various cancers, [redacted] (Figure 69C), [redacted]

[redacted] was also upregulated in our RNAseq analysis, as shown in Figure 69C. [redacted].

[redacted] The high expression of this protein was related with a poor prognostic factor in this type of tumors, [redacted] and were also observed in our HNSCC data (Figure 69C).

Finally, [redacted] was also upregulated in our cohort of AR cell lines, as shown in Figure 69C. [redacted] which highlights the relevance of this gene as a potential target in the HNSCC therapy.

As known, FA HNSCC are different from sporadic HNSCC cell lines in many terms, highlighting the potential limitations of our study. Although some of the differential expression genes in the data obtained from AR FA HNSCC were correlated with the documentation found about sporadic HNSCC or EGFR resistance, our aim with these data was to propose a potential second line of therapy in AR FA HNSCC tumors. Therefore, the upregulation of genes as [redacted] (Figure 69B), [redacted] Other potential lines that must be explored in this field are [redacted] Figure 69B); or [redacted] (Figure 69C) inhibition, [redacted]

Although the results obtained so far are promising, data validation with other techniques is warranted (qPCR, WB, cell cytometry) in order to verify the detected gene upregulation and the amount of the protein that is formed in each cell line. As it was mentioned before, the combined use of afatinib and [redacted] inhibitors to promote afatinib effects against AR FA HNSCC tumors could be a potential second line of treatment that should be explored. Taking that into consideration, additional experiments, as survival assays with these inhibitors, must be done to corroborate that hypothesis. Finally, the analysis of the samples from the patients who will participate in the afatinib clinical trial will involve another important milestone in FA HNSCC therapy, highlighting and supporting, moreover, the relevance of taking care of these type of patients.

Conclusions

6. Conclusions

In the first part of this thesis, regarding the "[redacted] developing inhibitors of DNA damage repair for cancer therapy", an extensive study of the contact surface [redacted] was performed before the start of this thesis. The importance of the [redacted] potential to bind specific small molecules was highlighted in the conclusions of Camps-Fajol's thesis (2022), whereof this is a continuation. The hit candidate's validation after the first and the second screening resulted in F27 and F2.14 as the most promising candidates. Four additional optimization rounds and one "*de novo"* screening have been done after that, with the following conclusions:

1. The capacity of the optimized hits to inhibit [redacted] was validated in U2OS and hFIB cell lines, being F3.6, F3.8, F3.10, F3.10A and F3.14 the best candidates of the first optimization round. F3.8, F3.10 and F3.10A also showed better affinity rates with the target.
2. F4.3 was the hit of the second optimization round with the best capacity to inhibit [redacted]y, and with the best affinity rate to the target.
3. F4.3 was also able to chemosensitize U2OS and hFIB cells [redacted] in clonogenic assays, and to inhibit [redacted].
4. F5.2, F5.4 and F5.6 were the hits of the third optimization round with better capacity to inhibit [redacted], and with better affinity rate to the target.
5. From the fourth optimization round, F6.1 was the hit with the best interaction with the target, inhibiting [redacted] without cell toxicity.
6. An additional "*de novo*" virtual screening was developed, and 2F17 was the hit with the best capacity to inhibit [redacted], without toxicity.

In the second part of this thesis, regarding the "Obtaining and characterization of AR HNSCC cell lines", the conclusions are:

1. FA HNSCC cell lines were less prone to acquire resistance to afatinib than sporadic HNSCC.
2. Afatinib-resistant cell lines are also resistant to other EGFR targeting drugs such as gefitinib and cetuximab.
3. Surface expression of ERBBs, NKG2D-Ls and CD44V6 in AR FA HNSCC cell lines makes them potential candidates for CAR T-cell therapy.
4. Afatinib resistance is not mediated by copy number amplification of *ERBBs* genes.
5. Fifteen of the 89 genes upregulated in AR FA HNSCC, have been reported by their dysregulation in tumor resistance and may be related with the acquired of resistance mechanism to afatinib
6. The upregulation of [redacted] in AR FA HNSCC must be further studied [redacted] potential use for the treatment of AR FA HNSCC.

References

7. References

Abdel-Magid, A. F. (2015). Inhibitors of the PD-1/PD-L1 Pathway Can Mobilize the Immune System: An Innovative Potential Therapy for Cancer and Chronic Infections. *ACS Medicinal Chemistry Letters*, *6*(5), 489–490. https://doi.org/10.1021/acsmedchemlett.5b00148

Actis, M. L., Ambaye, N. D., Evison, B. J., Shao, Y., Vanarotti, M., Inoue, A., McDonald, E. T., Kikuchi, S., Heath, R., Hara, K., Hashimoto, H., & Fujii, N. (2016). Identification of the first small-molecule inhibitor of the REV7 DNA repair protein interaction. *Bioorganic and Medicinal Chemistry*, *24*(18), 4339–4346. https://doi.org/10.1016/j.bmc.2016.07.026

Adar, S., Izhar, L., Hendel, A., Geacintov, N., & Livneh, Z. (2009). Repair of gaps opposite lesions by homologous recombination in mammalian cells. *Nucleic Acids Research*, *37*(17), 5737–5748. https://doi.org/10.1093/nar/gkp632

Alcón, P., Shakeel, S., Chen, Z. A., Rappsilber, J., Patel, K. J., & Passmore, L. A. (2020). FANCD2-FANCI is a clamp stabilized on DNA by monoubiquitination of FANCD2 during DNA repair. Nature structural & molecular biology, 27(3), 240–248. https://doi.org/10.1038/s41594-020-0380-1

Ali, R., Alabdullah, M., Algethami, M., Alblihy, A., Miligy, I., Shoqafi, A., Mesquita, K. A., Abdel-Fatah, T., Chan, S. Y., Chiang, P. W., Mongan, N. P., Rakha, E. A., Tomkinson, A. E., & Madhusudan, S. (2021). Ligase 1 is a predictor of platinum resistance and its blockade is synthetically lethal in XRCC1 deficient epithelial ovarian cancers. *Theranostics*, *11*(17), 8350–8361. https://doi.org/10.7150/thno.51456

Anscher, M. S., Chang, E., Gao, X., Gong, Y., Weinstock, C., Bloomquist, E., Adeniyi, O., Charlab, R., Zimmerman, S., Serlemitsos-Day, M., Ning, Y. M., Mayrosh, R., Fuller, B., Trentacosti, A. M., Gallagher, P., Bijwaard, K., Philip, R., Ghosh, S., Fahnbulleh, F., … Beaver, J. A. (2021). FDA Approval Summary: Rucaparib for the Treatment of Patients with Deleterious BRCA-Mutated Metastatic Castrate-Resistant Prostate Cancer. *Oncologist*, *26*(2), 139–146. https://doi.org/10.1002/onco.13585

Arvindh, S., Priyadarshini, M., Baba, A. B., Veeravarmal, V., Mishra, R., Dash, R., & Nagini, S. (2024). The Neem Limonoid Nimbolide Modulates Key Components of the DNA Damage Response Signalling in Cellular and Animal Models of Oral Squamous Cell Carcinoma. *Current Pharmaceutical Biotechnology*, *25*. https://doi.org/10.2174/0113892010291998240321074920

Atalay, G., Cardoso, F., Awada, A., & Piccart, M. J. (2003). Novel therapeutic strategies targeting the epidermal growth factor receptor (EGFR) family and its downstream effectors in breast cancer. *Annals of Oncology*, *14*(9), 1346–1363. https://doi.org/10.1093/annonc/mdg365

Atibalentja, D. F., Deutzmann, A., & Felsher, D. W. (2024). A big step for MYC-targeted therapies. *Trends in Cancer*. https://doi.org/10.1016/j.trecan.2024.03.009

Baell, J. B., & Nissink, J. W. M. (2018). Seven Year Itch: Pan-Assay Interference Compounds (PAINS) in 2017—Utility and Limitations. *ACS Chemical Biology*, *13*(1), 36–44. https://doi.org/10.1021/acschembio.7b00903

Bai, F., Morcos, F., Cheng, R. R., Jiang, H., & Onuchic, J. N. (2016). Elucidating the druggable interface of protein-protein interactions using fragment docking and coevolutionary analysis. *Proceedings of the National Academy of Sciences of the United States of America*, *113*(50), E8051–E8058. https://doi.org/10.1073/pnas.1615932113

Bebek, G., Orloff, M., & Eng, C. (2011). Microenvironmental genomic alterations reveal signaling networks for head and neck squamous cell carcinoma. *Journal of Clinical Bioinformatics*, *1*(1), 21. https://doi.org/10.1186/2043-9113-1-21

Bhargava, R., Onyango, D. O., & Stark, J. M. (2016). Regulation of Single-Strand Annealing and its Role in Genome Maintenance. In *Trends in Genetics* (Vol. 32, Issue 9, pp. 566–575). Elsevier Ltd. https://doi.org/10.1016/j.tig.2016.06.007

Bhattacharjee, S., & Nandi, S. (2017). DNA damage response and cancer therapeutics through the lens of the Fanconi Anemia DNA repair pathway. In *Cell Communication and Signaling* (Vol. 15, Issue 1). BioMed Central Ltd. https://doi.org/10.1186/s12964-017-0195-9

Billard, C. (2012). Development of Noxa-like BH3 Mimetics for Apoptosis-Based Therapeutic Strategy in Chronic Lymphocytic Leukemia. *Molecular Cancer Research*, *10*(6), 673–676. https://doi.org/10.1158/1541-7786.MCR-12-0015

Birkinshaw, R. W., Gong, J., Luo, C. S., Lio, D., White, C. A., Anderson, M. A., Blombery, P., Lessene, G., Majewski, I. J., Thijssen, R., Roberts, A. W., Huang, D. C. S., Colman, P. M., & Czabotar, P. E. (2019). Structures of BCL-2 in complex with venetoclax reveal the molecular basis of resistance mutations. *Nature Communications*, *10*(1), 2385. https://doi.org/10.1038/s41467-019-10363-1

Blasiak, J. (2021). Single-strand annealing in cancer. In *International Journal of Molecular Sciences* (Vol. 22, Issue 4, pp. 1–24). MDPI AG. https://doi.org/10.3390/ijms22042167

Bogliolo, M., Bluteau, D., Lespinasse, J., Pujol, R., Vasquez, N., D'Enghien, C. D., Stoppa-Lyonnet, D., Leblanc, T., Soulier, J., & Surrallés, J. (2018). Biallelic truncating FANCM mutations cause early-onset cancer but not Fanconi anemia. *Genetics in Medicine*, *20*(4), 458–463. https://doi.org/10.1038/gim.2017.124

Bogliolo, M., Lyakhovich, A., Callén, E., Castellà, M., Cappelli, E., Ramírez, M. J., Creus, A., Marcos, R., Kalb, R., Neveling, K., Schindler, D., & Surrallés, J. (2007). Histone H2AX and Fanconi anemia FANCD2 function in the same pathway to maintain chromosome stability. The EMBO journal, 26(5), 1340–1351. https://doi.org/10.1038/sj.emboj.7601574

Bogliolo, M., Schuster, B., Stoepker, C., Derkunt, B., Su, Y., Raams, A., Trujillo, J. P., Minguillón, J., Ramírez, M. J., Pujol, R., Casado, J. A., Baños, R., Rio, P., Knies, K., Zúñiga, S., Benítez, J., Bueren, J. A., Jaspers, N. G. J., Schärer, O. D., … Surrallés, J. (2013). Mutations in ERCC4, encoding the DNA-repair endonuclease XPF, cause Fanconi anemia. *American Journal of Human Genetics*, *92*(5), 800–806. https://doi.org/10.1016/j.ajhg.2013.04.002

Bogliolo, M., & Surrallés, J. (2015). Fanconi anemia: A model disease for studies on human genetics and advanced therapeutics. In *Current Opinion in Genetics and Development* (Vol. 33, pp. 32–40). Elsevier Ltd. https://doi.org/10.1016/j.gde.2015.07.002

Bogliolo, M., Pujol, R., Aza-Carmona, M., Muñoz-Subirana, N., Rodriguez-Santiago, B., Casado, J. A., Rio, P., Bauser, C., Reina-Castillón, J., Lopez-Sanchez, M., Gonzalez-Quereda, L., Gallano, P., Catalá, A., Ruiz-Llobet, A., Badell, I., Diaz-Heredia, C., Hladun, R., Senent, L., Argiles, B., Bergua Burgues, J. M., … Surralles, J. (2020). Optimised molecular genetic diagnostics of Fanconi anaemia by whole exome sequencing and functional studies. Journal of medical genetics, 57(4), 258–268. https://doi.org/10.1136/jmedgenet-2019-106249

Bojadzic, D., & Buchwald, P. (2018). Toward Small-Molecule Inhibition of Protein–Protein Interactions: General Aspects and Recent Progress in Targeting Costimulatory and Coinhibitory (Immune Checkpoint) Interactions. *Current Topics in Medicinal Chemistry*, *18*(8), 674–699. https://doi.org/10.2174/1568026618666180531092503

Borg, Å., Baldetorp, B., Fernö, M., Killander, D., Olsson, H., Ryden, S., & Sigurdsson, H. (1994). ERBB2 amplification is associated with tamoxifen resistance in steroid-receptor positive breast cancer. *Cancer Letters*, *81*(2), 137–144. https://doi.org/10.1016/0304-3835(94)90194-5

Bornstein, G., Ganoth, D., & Hershko, A. (2006). Regulation of neddylation and deneddylation of cullin1 in SCF ^{Skp2} ubiquitin ligase by F-box protein and substrate. *Proceedings of the National Academy of Sciences*, *103*(31), 11515–11520. https://doi.org/10.1073/pnas.0603921103

Brambati, A., Barry, R. M., & Sfeir, A. (2020). DNA polymerase theta (Polθ) – an error-prone polymerase necessary for genome stability. In *Current Opinion in Genetics and Development* (Vol. 60, pp. 119–126). Elsevier Ltd. https://doi.org/10.1016/j.gde.2020.02.017

Brochier, C., & Langley, B. (2013). Chromatin Modifications Associated with DNA Double-strand Breaks Repair as Potential Targets for Neurological Diseases. In *Neurotherapeutics* (Vol. 10, Issue 4, pp. 817–830). https://doi.org/10.1007/s13311-013-0210-9

Brown, J. S., O'Carrigan, B., Jackson, S. P., & Yap, T. A. (2017). Targeting DNA repair in cancer: Beyond PARP inhibitors. In *Cancer Discovery* (Vol. 7, Issue 1, pp. 20–37). American Association for Cancer Research Inc. https://doi.org/10.1158/2159-8290.CD-16-0860

Brunner, A., Li, Q., Fisicaro, S., Kourtesakis, A., Viiliäinen, J., Johansson, H. J., Pandey, V., Mayank, A. K., Lehtiö, J., Wohlschlegel, J. A., Spruck, C., Rantala, J. K., Orre, L. M., & Sangfelt, O. (2023). FBXL12 degrades FANCD2 to regulate replication recovery and promote cancer cell survival under conditions of replication stress. *Molecular Cell*, *83*(20), 3720-3739.e8. https://doi.org/10.1016/j.molcel.2023.07.026

Bryant, H. E., Schultz, N., Thomas, H. D., Parker, K. M., Flower, D., Lopez, E., Kyle, S., Meuth, M., Curtin, N. J., & Helleday, T. (2005). *Specific killing of BRCA2-deficient tumours with inhibitors of poly(ADP-ribose) polymerase*. www.nature.com/nature

Bueren, J. A., Guenechea, G., Casado, J. A., Lamana, M. L., & Segovia, J. C. (2003). Genetic modification of hematopoietic stem cells: Recent advances in the gene therapy of inherited diseases. In *Archives of Medical Research* (Vol. 34, Issue 6, pp. 589–599). Elsevier Inc. https://doi.org/10.1016/j.arcmed.2003.09.004

Burtness, B. (2005). The role of cetuximab in the treatment of squamous cell cancer of the head and neck. In *Expert Opinion on Biological Therapy* (Vol. 5, Issue 8, pp. 1085–1093). https://doi.org/10.1517/14712598.5.8.1085

Burtness, B., Harrington, K. J., Greil, R., Soulières, D., Tahara, M., de Castro, G., Psyrri, A., Basté, N., Neupane, P., Bratland, Å., Fuereder, T., Hughes, B. G. M., Mesía, R., Ngamphaiboon, N., Rordorf, T., Wan Ishak, W. Z., Hong, R.-L., González Mendoza, R., Roy, A., … Yorio, J. (2019). Pembrolizumab alone or with chemotherapy versus cetuximab with chemotherapy for recurrent or metastatic squamous cell carcinoma of the head and neck (KEYNOTE-048): a randomised, open-label, phase 3 study. *The Lancet*, *394*(10212), 1915–1928. https://doi.org/10.1016/S0140-6736(19)32591-7

Cai, M. Y., Dunn, C. E., Chen, W., Kochupurakkal, B. S., Nguyen, H., Moreau, L. A., Shapiro, G. I., Parmar, K., Kozono, D., & D'Andrea, A. D. (2020). Cooperation of the ATM and Fanconi Anemia/BRCA Pathways in Double-Strand Break End Resection. *Cell Reports*, *30*(7), 2402-2415.e5. https://doi.org/10.1016/j.celrep.2020.01.052

Cai, W.-Q., Zeng, L.-S., Wang, L.-F., Wang, Y.-Y., Cheng, J.-T., Zhang, Y., Han, Z.-W., Zhou, Y., Huang, S.-L., Wang, X.-W., Peng, X.-C., Xiang, Y., Ma, Z., Cui, S.-Z., & Xin, H.-W. (2020). The Latest Battles Between EGFR Monoclonal Antibodies and Resistant Tumor Cells. *Frontiers in Oncology*, *10*. https://doi.org/10.3389/fonc.2020.01249

Cai, X., Zhan, H., Ye, Y., Yang, J., Zhang, M., Li, J., & Zhuang, Y. (2021). Current Progress and Future Perspectives of Immune Checkpoint in Cancer and Infectious Diseases. *Frontiers in Genetics*, *12*. https://doi.org/10.3389/fgene.2021.785153

Callén, E., Casado, J. A., Tischkowitz, M. D., Bueren, J. A., Creus, A., Marcos, R., Dasí, A., Estella, J. M., Muñoz, A., Ortega, J. J., de Winter, J., Joenje, H., Schindler, D., Hanenberg, H., Hodgson, S. V., Mathew, C. G., & Surrallés, J. (2005). A common founder mutation in FANCA underlies the world's highest prevalence of Fanconi anemia in Gypsy families from Spain. Blood, 105(5), 1946–1949. https://doi.org/10.1182/blood-2004-07-2588

Camps-Fajol, C. (2022). Discovery of First-In-Class inhibitors of a DNA damage repair pathway (PhD thesis). https://www.tdx.cat/handle/10803/687563

Casado, J. A., Valeri, A., Sanchez-Dominguez, R., Vela, P., Lopez, A., Navarro, S., Alberquilla, O., Hanenberg, H., Pujol, R., Segovia, J. C., Minguillon, J., Surralles, J., De Heredia, C. D., Sevilla, J., Rio, P., & Bueren, J. A. (2022). Upregulation of NKG2D ligands impairs hematopoietic stem cell function in Fanconi anemia. *Journal of Clinical Investigation*, *132*(15). https://doi.org/10.1172/JCI142842

Chatterjee, N., & Walker, G. C. (2017). Mechanisms of DNA damage, repair, and mutagenesis. In *Environmental and Molecular Mutagenesis* (Vol. 58, Issue 5, pp. 235–263). John Wiley and Sons Inc. https://doi.org/10.1002/em.22087

Chaugule, V. K., Arkinson, C., Rennie, M. L., Kämäräinen, O., Toth, R., & Walden, H. (2020). Allosteric mechanism for site-specific ubiquitination of FANCD2. *Nature Chemical Biology*, *16*(3), 291–301. https://doi.org/10.1038/s41589-019-0426-z

Che, R., Zhang, J., Nepal, M., Han, B., & Fei, P. (2018). Multifaceted Fanconi Anemia Signaling. *Trends in Genetics*, *34*(3), 171–183. https://doi.org/10.1016/j.tig.2017.11.006

Checinska, A., Hoogeland, B. S. J., Rodriguez, J. A., Giaccone, G., & Kruyt, F. A. E. (2007). Role of XIAP in inhibiting cisplatin-induced caspase activation in non-small cell lung cancer cells: A small molecule Smac mimic sensitizes for chemotherapy-induced apoptosis by enhancing caspase-3 activation. *Experimental Cell Research*, *313*(6), 1215–1224. https://doi.org/10.1016/j.yexcr.2006.12.011

Chen, X., Cao, Y., Sedhom, W., Lu, L., Liu, Y., Wang, H., Oka, M., Bornstein, S., Said, S., Song, J., & Lu, S. (2020). Distinct roles of *PIK3CA* in the enrichment and maintenance of cancer stem cells in head and neck squamous cell carcinoma. *Molecular Oncology*, *14*(1), 139–158. https://doi.org/10.1002/1878-0261.12584

Chen, X., Chen, C., Luo, C., Liu, J., & Lin, Z. (2024). Discovery of UMI-77 as a novel Ku70/80 inhibitor sensitizing cancer cells to DNA damaging agents in vitro and in vivo. *European Journal of Pharmacology*, 176647. https://doi.org/10.1016/j.ejphar.2024.176647

Chen, X., Yeung, T. K., & Wang, Z. (2000). Enhanced Drug Resistance in Cells Coexpressing ERBB2 with EGF Receptor or ERBB3. *Biochemical and Biophysical Research Communications*, *277*(3), 757–763. https://doi.org/10.1006/bbrc.2000.3731

Chen, Y., Liu, X., Hu, Y., & Xia, L. (2024). Efficacy and safety of PD-1/PD-L1 immune checkpoint inhibitors in the treatment of recurrent ovarian cancer: A systematic review and meta-analysis. *Medicine*, *103*(18), e38019. https://doi.org/10.1097/MD.0000000000038019

Cheung, R. S., & Taniguchi, T. (2017). Recent insights into the molecular basis of Fanconi anemia: genes, modifiers, and drivers. *International Journal of Hematology*, *106*(3), 335–344. https://doi.org/10.1007/s12185-017-2283-4

Ciulean, I. S., Fischer, J., Quaiser, A., Bach, C., Abken, H., Tretbar, U. S., Fricke, S., Koehl, U., Schmiedel, D., & Grunwald, T. (2023). CD44v6 specific CAR-NK cells for targeted immunotherapy of head and neck squamous cell carcinoma. *Frontiers in Immunology*, *14*. https://doi.org/10.3389/fimmu.2023.1290488

Cole, A. R., Lewis, L. P. C., & Walden, H. (2010). The structure of the catalytic subunit FANCL of the Fanconi anemia core complex. *Nature Structural and Molecular Biology*, *17*(3), 294–298. https://doi.org/10.1038/nsmb.1759

Cornwell, M. J., Thomson, G. J., Coates, J., Belotserkovskaya, R., Waddell, I. D., Jackson, S. P., & Galanty, Y. (2019). Small-Molecule Inhibition of UBE2T/FANCL-Mediated Ubiquitylation in the Fanconi Anemia Pathway. *ACS Chemical Biology*, *14*(10), 2148–2154. https://doi.org/10.1021/acschembio.9b00570

de Lima, J. M., Morand, G. B., Macedo, C. C. S., Diesel, L., Hier, M. P., Mlynarek, A., Kowalski, L. P., Maschietto, M., Alaoui-Jamali, M. A., & da Silva, S. D. (2020). NDRG1 deficiency is associated with regional metastasis in oral cancer by inducing epithelial–mesenchymal transition. *Carcinogenesis*, *41*(6), 769–777. https://doi.org/10.1093/carcin/bgaa017

Deeks, E. D. (2015). Olaparib: First global approval. *Drugs*, *75*(2), 231–240. https://doi.org/10.1007/s40265-015-0345-6

Deng, J., Paulus, A., Fang, D. D., Manna, A., Wang, G., Wang, H., Zhu, S., Chen, J., Min, P., Yin, Y., Dutta, N., Halder, N., Ciccio, G., Copland, J. A., Miller, J., Han, B., Bai, L., Liu, L., Wang, M., … Zhai, Y. (2022). Lisaftoclax (APG-2575) Is a Novel BCL-2 Inhibitor with Robust Antitumor Activity in Preclinical Models of Hematologic Malignancy. *Clinical Cancer Research*, *28*(24), 5455–5468. https://doi.org/10.1158/1078-0432.CCR-21-4037

Deng, Z., Liao, W., Wei, W., Zhong, G., He, C., Zhang, H., Liu, Q., Xu, X., Liang, J., & Liu, Z. (2021). Anlotinib as a promising inhibitor on tumor growth of oral squamous cell carcinoma through cell apoptosis and mitotic catastrophe. *Cancer Cell International*, *21*(1), 37. https://doi.org/10.1186/s12935-020-01721-x

Dernovšek, J., & Tomašič, T. (2023). Following the design path of isoform-selective Hsp90 inhibitors: Small differences, great opportunities. *Pharmacology & Therapeutics*, *245*, 108396. https://doi.org/10.1016/j.pharmthera.2023.108396

Dorrell, C., Peters, A. M., Zhang, Q., Balaji, N., Baradar, K., Mochizuki-Kashio, M., Major, A., Finegold, M., Liu, C., Lu, K., & Grompe, M. (2024). Long-term combination therapy with metformin and oxymetholone in a Fanconi anemia mouse model. *Pediatric Blood & Cancer*. https://doi.org/10.1002/pbc.31030

Dou, H., Song, C., Wang, X., Feng, Z., Su, Y., & Wang, H. (2024). Integrated bioinformatics analysis of SEMA3C in tongue squamous cell carcinoma using machine-learning strategies. *Cancer Cell International*, *24*(1), 58. https://doi.org/10.1186/s12935-024-03247-y

Elmenoufy, A. H., Gentile, F., Jay, D., Karimi-Busheri, F., Yang, X., Soueidan, O. M., Mani, R. S., Ciniero, G., Tuszynski, J. A., Weinfeld, M., & West, F. G. (2020). Design, synthesis and in vitro cell-free/cell-based biological evaluations of novel ERCC1-XPF inhibitors targeting DNA repair pathway. *European Journal of Medicinal Chemistry*, *204*, 112658. https://doi.org/10.1016/j.ejmech.2020.112658

Elmenoufy, A. H., Gentile, F., Jay, D., Karimi-Busheri, F., Yang, X., Soueidan, O. M., Weilbeer, C., Mani, R. S., Barakat, K. H., Tuszynski, J. A., Weinfeld, M., & West, F. G. (2019). Targeting DNA Repair in Tumor Cells via Inhibition of ERCC1–XPF. *Journal of Medicinal Chemistry*, *62*(17), 7684–7696. https://doi.org/10.1021/acs.jmedchem.9b00326

Engelman, J. A., Zejnullahu, K., Mitsudomi, T., Song, Y., Hyland, C., Park, J. O., Lindeman, N., Gale, C.-M., Zhao, X., Christensen, J., Kosaka, T., Holmes, A. J., Rogers, A. M., Cappuzzo, F., Mok, T., Lee, C., Johnson, B. E., Cantley, L. C., & Jänne, P. A. (2007). *MET* Amplification Leads to Gefitinib Resistance in Lung Cancer by Activating ERBB3 Signaling. *Science*, *316*(5827), 1039–1043. https://doi.org/10.1126/science.1141478

Errazquin, R., Sieiro, E., Moreno, P., Ramirez, M. J., Lorz, C., Peral, J., Ortiz, J., Casado, J. A., Roman-Rodriguez, F. J., Hanenberg, H., Río, P., Surralles, J., Segrelles, C., & Garcia-Escudero, R. (2021). Generating new fanca-deficient hnscc cell lines by genomic editing recapitulates the cellular phenotypes of fanconi anemia. *Genes*, *12*(4). https://doi.org/10.3390/genes12040548

Fancelli, S., Petroni, G., Pillozzi, S., & Antonuzzo, L. (2024). Unconventional strategy could be the future: From target to KRAS broad range treatment. *Heliyon*, *10*(9), e29739. https://doi.org/10.1016/j.heliyon.2024.e29739

Gaillard, H., García-Muse, T., & Aguilera, A. (2015). Replication stress and cancer. In *Nature Reviews Cancer* (Vol. 15, Issue 5, pp. 276–280). Nature Publishing Group. https://doi.org/10.1038/nrc3916

Garner, K. M., Pletnev, A. A., & Eastman, A. (2009). Corrected structure of mirin, a small-molecule inhibitor of the Mre11–Rad50–Nbs1 complex. *Nature Chemical Biology*, *5*(3), 129–130. https://doi.org/10.1038/nchembio0309-129

Garralda, E., Beaulieu, M.-E., Moreno, V., Casacuberta-Serra, S., Martínez-Martín, S., Foradada, L., Alonso, G., Massó-Vallés, D., López-Estévez, S., Jauset, T., Corral de la Fuente, E., Doger, B., Hernández, T., Perez-Lopez, R., Arqués, O., Castillo Cano, V., Morales, J., Whitfield, J. R., Niewel, M., … Calvo, E. (2024). MYC targeting by OMO-103 in solid tumors: a phase 1 trial. *Nature Medicine*, *30*(3), 762–771. https://doi.org/10.1038/s41591-024-02805-1

Garrett, M. D., & Collins, I. (2011). Anticancer therapy with checkpoint inhibitors: What, where and when? In *Trends in Pharmacological Sciences* (Vol. 32, Issue 5, pp. 308–316). Elsevier Ltd. https://doi.org/10.1016/j.tips.2011.02.014

Genovese, G., Carugo, A., Tepper, J., Robinson, F. S., Li, L., Svelto, M., Nezi, L., Corti, D., Minelli, R., Pettazzoni, P., Gutschner, T., Wu, C.-C., Seth, S., Akdemir, K. C., Leo, E., Amin, S., Molin, M. D., Ying, H., Kwong, L. N., … Chin, L. (2017). Synthetic vulnerabilities of mesenchymal subpopulations in pancreatic cancer. *Nature*, *542*(7641), 362–366. https://doi.org/10.1038/nature21064

Gentile, F., Barakat, K., & Tuszynski, J. (2018). Computational Characterization of Small Molecules Binding to the Human XPF Active Site and Virtual Screening to Identify Potential New DNA Repair Inhibitors Targeting the ERCC1-XPF Endonuclease. *International Journal of Molecular Sciences*, *19*(5), 1328. https://doi.org/10.3390/ijms19051328

Glanzer, J. G., Liu, S., Wang, L., Mosel, A., Peng, A., & Oakley, G. G. (2014). RPA inhibition increases replication stress and suppresses tumor growth. Cancer research, 74(18), 5165–5172. https://doi.org/10.1158/0008-5472.CAN-14-0306

Goldstein, B., Coombs, D., He, X., Pineda, A. R., & Wofsy, C. (1999). The influence of transport on the kinetics of binding to surface receptors: application to cells and BIAcore. *Journal of Molecular Recognition*, *12*(5), 293–299. https://doi.org/10.1002/(SICI)1099-1352(199909/10)12:5<293::AID-JMR472>3.0.CO;2-M

González, S., López-Soto, A., Suarez-Alvarez, B., López-Vázquez, A., & López-Larrea, C. (2008). NKG2D ligands: key targets of the immune response. *Trends in Immunology*, *29*(8), 397–403. https://doi.org/10.1016/j.it.2008.04.007

Gou, Q., Gou, Q., Gan, X., & Xie, Y. (2024). Novel therapeutic strategies for rare mutations in non-small cell lung cancer. *Scientific Reports*, *14*(1), 10317. https://doi.org/10.1038/s41598-024-61087-2

Grandis, J. R., Chakraborty, A., Melhem, M. F., Zeng, Q., & Tweardy, D. J. (1997). *Inhibition of epidermal growth factor receptor gene expression and function decreases proliferation of head and neck squamous carcinoma but not normal mucosal epithelial cells*.

Grant, C., & Nagasaka, M. (2024). Neoadjuvant EGFR-TKI therapy in Non-Small cell lung cancer. *Cancer Treatment Reviews*, *126*, 102724. https://doi.org/10.1016/j.ctrv.2024.102724

Green, A. M., & Kupfer, G. M. (2009). Fanconi Anemia. In *Hematology/Oncology Clinics of North America* (Vol. 23, Issue 2, pp. 193–214). https://doi.org/10.1016/j.hoc.2009.01.008

Gu, L., Li, M., Li, C. M., Haratipour, P., Lingeman, R., Jossart, J., Gutova, M., Flores, L., Hyde, C., Kenjić, N., Li, H., Chung, V., Li, H., Lomenick, B., Von Hoff, D. D., Synold, T. W., Aboody, K. S., Liu, Y., Horne, D., … Malkas, L. H. (2023). Small molecule targeting of transcription-replication conflict for selective chemotherapy. *Cell Chemical Biology*, *30*(10), 1235-1247.e6. https://doi.org/10.1016/j.chembiol.2023.07.001

Guo, X.-Y., Zhang, J.-Y., Shi, X.-Z., Wang, Q., Shen, W.-L., Zhu, W.-W., & Liu, L.-K. (2020). Upregulation of CSF-1 is correlated with elevated TAM infiltration and poor prognosis in oral squamous cell carcinoma. *American Journal of Translational Research*, *12*(10), 6235–6249.

Ha, S.-D., Lewin, N., Li, S. S. C., & Kim, S.-O. (2021). HDAC8 Activates AKT through Upregulating PLCB1 and Suppressing DESC1 Expression in MEK1/2 Inhibition-Resistant Cells. *Cells*, *10*(5), 1101. https://doi.org/10.3390/cells10051101

Haist, C., Schulte, E., Bartels, N., Bister, A., Poschinski, Z., Ibach, T. C., Geipel, K., Wiek, C., Wagenmann, M., Monzel, C., Scheckenbach, K., & Hanenberg, H. (2021). CD44v6-targeted CAR T-cells specifically eliminate CD44 isoform 6 expressing head/neck squamous cell carcinoma cells. *Oral Oncology*, *116*, 105259. https://doi.org/10.1016/j.oraloncology.2021.105259

Herreros-Pomares, A., Llorens, C., Soriano, B., Bagan, L., Moreno, A., Calabuig-Fariñas, S., Jantus-Lewintre, E., & Bagan, J. (2021). Differentially methylated genes in proliferative verrucous leukoplakia reveal potential malignant biomarkers for oral squamous cell carcinoma. *Oral Oncology*, *116*, 105191. https://doi.org/10.1016/j.oraloncology.2021.105191

Hillig, R. C., Sautier, B., Schroeder, J., Moosmayer, D., Hilpmann, A., Stegmann, C. M., Werbeck, N. D., Briem, H., Boemer, U., Weiske, J., Badock, V., Mastouri, J., Petersen, K., Siemeister, G., Kahmann, J. D., Wegener, D., Böhnke, N., Eis, K., Graham, K., … Bader, B. (2019). Discovery of potent SOS1 inhibitors that block RAS activation via disruption of the RAS–SOS1 interaction. *Proceedings of the National Academy of Sciences*, *116*(7), 2551–2560. https://doi.org/10.1073/pnas.1812963116

Hodson, C., Cole, A. R., Lewis, L. P. C., Miles, J. A., Purkiss, A., & Walden, H. (2011). Structural analysis of human FANCL, the E3 ligase in the fanconi anemia pathway. *Journal of Biological Chemistry*, *286*(37), 32628–32637. https://doi.org/10.1074/jbc.M111.244632

Hodson, C., Purkiss, A., Miles, J. A., & Walden, H. (2014). Structure of the human FANCL RING-Ube2T complex reveals determinants of cognate E3-E2 selection. *Structure*, *22*(2), 337–344. https://doi.org/10.1016/j.str.2013.12.004

Hoeijmakers, J. H. J. (2001). *A plethora of damages in DNA The consequences of DNA injury Genome maintenance mechanisms for preventing cancer*. www.nature.com

Hou, J., Li, H., Ma, S., He, Z., Yang, S., Hao, L., Zhou, H., Zhang, Z., Han, J., Wang, L., & Wang, Q. (2022). EGFR exon 20 insertion mutations in advanced non-small-cell lung cancer: current status and perspectives. *Biomarker Research*, *10*(1), 21. https://doi.org/10.1186/s40364-022-00372-6

Hoy, S. M. (2018). Talazoparib: First Global Approval. *Drugs*, *78*(18), 1939–1946. https://doi.org/10.1007/s40265-018-1026-z

Hu, C., Liu, M., Li, Y., Zhao, Y., Sharma, A., Liu, H., & Schmidt-Wolf, I. G. H. (2023). Recent advances and future perspectives of CAR-T cell therapy in head and neck cancer. In *Frontiers in Immunology* (Vol. 14). Frontiers Media SA. https://doi.org/10.3389/fimmu.2023.1213716

Huang, F., Goyal, N., Sullivan, K., Hanamshet, K., Patel, M., Mazina, O. M., Wang, C. X., An, W. F., Spoonamore, J., Metkar, S., Emmitte, K. A., Cocklin, S., Skorski, T., & Mazin, A. V. (2016). Targeting BRCA1- and BRCA2-deficient cells with RAD52 small molecule inhibitors. *Nucleic Acids Research*, *44*(9), 4189–4199. https://doi.org/10.1093/nar/gkw087

Huang, L., Luo, E.-L., Xie, J., Gan, R.-H., Ding, L.-C., Su, B.-H., Zhao, Y., Lin, L.-S., Zheng, D.-L., & Lu, Y.-G. (2019). FZD2 regulates cell proliferation and invasion in tongue squamous cell carcinoma. *International Journal of Biological Sciences*, *15*(11), 2330–2339. https://doi.org/10.7150/ijbs.33881

Huang, R., & Zhou, P. K. (2021). DNA damage repair: historical perspectives, mechanistic pathways and clinical translation for targeted cancer therapy. In *Signal Transduction and Targeted Therapy* (Vol. 6, Issue 1). Springer Nature. https://doi.org/10.1038/s41392-021-00648-7

Huang, T., Bi, Y., Cui, Z., Guan, J., & Huang, Y. (2020). MUC1 confers radioresistance in head and neck squamous cell carcinoma (HNSCC) cells. *Bioengineered*, *11*(1), 769–778. https://doi.org/10.1080/21655979.2020.1791590

Huo, Z., Li, Y., Chen, B., Zhang, W., Yang, X., & Yang, X. (2023). Recent advances in surface plasmon resonance imaging and biological applications. *Talanta*, *255*, 124213. https://doi.org/10.1016/j.talanta.2022.124213

Ikram, S., Sayyah, E., & Durdagi, S. (2024). Identifying Potential SOS1 Inhibitors via Virtual Screening of Multiple Small Molecule Libraries against KRAS-SOS1 Interface. *ChemBioChem*. https://doi.org/10.1002/cbic.202400008

Islam, T., Rahman, R., Gov, E., Turanli, B., Gulfidan, G., Haque, A., Arga, K. Y., & Haque Mollah, N. (2018). Drug Targeting and Biomarkers in Head and Neck Cancers: Insights from Systems Biology Analyses. *OMICS: A Journal of Integrative Biology*, *22*(6), 422–436. https://doi.org/10.1089/omi.2018.0048

Jackson, S. P. (2009). The DNA-damage response: new molecular insights and new approaches to cancer therapy. *Biochemical Society Transactions*, *37*(3), 483–494. https://doi.org/10.1042/BST0370483

Jacquemont, C., Simon, J. A., D'Andrea, A. D., & Taniguchi, T. (2012). Non-specific chemical inhibition of the Fanconi anemia pathway sensitizes cancer cells to cisplatin. *Molecular Cancer*, *11*. https://doi.org/10.1186/1476-4598-11-26

Jang, S.-W., & Kim, J. M. (2022). The RPA inhibitor HAMNO sensitizes Fanconi anemia pathway-deficient cells. *Cell Cycle*, *21*(14), 1468–1478. https://doi.org/10.1080/15384101.2022.2074200

Jason-Moller, L., Murphy, M., & Bruno, J. (2006). Overview of Biacore Systems and Their Applications. *Current Protocols in Protein Science*, *45*(1). https://doi.org/10.1002/0471140864.ps1913s45

Jäwert, F., Fehr, A., Öhman, J., Stenman, G., & Kjeller, G. (2022). Recurrent copy number alterations involving <scp> *EGFR* </scp> , <scp> *CDKN2A* </scp> , and <scp> *CCND1* </scp> in oral premalignant lesions. *Journal of Oral Pathology & Medicine*, *51*(6), 546–552. https://doi.org/10.1111/jop.13303

Jeong, E., Lee, S. G., Kim, H. S., Yang, J., Shin, J., Kim, Y., Kim, J., Schärer, O. D., Kim, Y., Yeo, J. E., Kim, H. M., & Cho, Y. (2020). Structural basis of the fanconi anemia-associated mutations within the FANCA and FANCG complex. *Nucleic Acids Research*, *48*(6), 3328–3342. https://doi.org/10.1093/nar/gkaa062

Jordheim, L. P., Barakat, K. H., Heinrich-Balard, L., Matera, E.-L., Cros-Perrial, E., Bouledrak, K., El Sabeh, R., Perez-Pineiro, R., Wishart, D. S., Cohen, R., Tuszynski, J., & Dumontet, C. (2013). Small Molecule Inhibitors of ERCC1-XPF Protein-Protein Interaction Synergize Alkylating Agents in Cancer Cells. *Molecular Pharmacology*, *84*(1), 12–24. https://doi.org/10.1124/mol.112.082347

Kais, Z., Rondinelli, B., Holmes, A., O'Leary, C., Kozono, D., D'Andrea, A. D., & Ceccaldi, R. (2016). FANCD2 Maintains Fork Stability in BRCA1/2-Deficient Tumors and Promotes Alternative End-Joining DNA Repair. *Cell Reports*, *15*(11), 2488–2499. https://doi.org/10.1016/j.celrep.2016.05.031

Kaminski, G. A. (2008). Computational Studies of the X-Linked Inhibitor of Apoptosis Complex Formation with Caspase-9 and a Small Antagonist. *Journal of Chemical Theory and Computation*, *4*(5), 847–854. https://doi.org/10.1021/ct8000188

Kee, Y., & D'Andrea, A. D. (2012). Molecular pathogenesis and clinical management of Fanconi anemia. *Journal of Clinical Investigation*, *122*(11), 3799–3806. https://doi.org/10.1172/JCI58321

Kennedy, R. D., Chen, C. C., Stuckert, P., Archila, E. M., De La Vega, M. A., Moreau, L. A., Shimamura, A., & D'Andrea, A. D. (2007). Fanconi anemia pathway-deficient tumor cells are hypersensitive to inhibition of ataxia telangiectasia mutated. *Journal of Clinical Investigation*, *117*(5), 1440–1449. https://doi.org/10.1172/JCI31245

Khatib, J. B., Nicolae, C. M., & Moldovan, G. L. (2024). Role of Translesion DNA Synthesis in the Metabolism of Replication-associated Nascent Strand Gaps. In *Journal of Molecular Biology* (Vol. 436, Issue 1). Academic Press. https://doi.org/10.1016/j.jmb.2023.168275

Kim, H., Kim, Y., Bae, S., Kong, J. M., Choi, J., Jang, M., Choi, J., Hong, J., Hwang, Y., Kang, J. S., & Lee, W. J. (2015). Direct Interaction of CD40 on Tumor Cells with CD40L on T Cells Increases the Proliferation of Tumor Cells by Enhancing TGF-β Production and Th17 Differentiation. *PLOS ONE*, *10*(5), e0125742. https://doi.org/10.1371/journal.pone.0125742

Kim, Y. Y., Um, J., Shin, D. J., Jeong, D. J., Hong, Y. Bin, & Yun, J. (2021). p53-mediated regulation of mitochondrial dynamics plays a pivotal role in the senescence of various normal cells as well as cancer cells. *The FASEB Journal*, *35*(2). https://doi.org/10.1096/fj.202002007R

Kirsch, P., Hartman, A. M., Hirsch, A. K. H., & Empting, M. (2019). Concepts and Core Principles of Fragment-Based Drug Design. *Molecules*, *24*(23), 4309. https://doi.org/10.3390/molecules24234309

Kohl, Flach, Naumann, Brendel, Kleiner, Weiss, Seifarth, Nowak, Hofmann, Fabarius, & Popp. (2019). Antileukemic Efficacy in Vitro of Talazoparib and APE1 Inhibitor III Combined with Decitabine in Myeloid Malignancies. *Cancers*, *11*(10), 1493. https://doi.org/10.3390/cancers11101493

Kosaka, A., Ohkuri, T., & Okada, H. (2014). Combination of an agonistic anti-CD40 monoclonal antibody and the COX-2 inhibitor celecoxib induces anti-glioma effects by promotion of type-1 immunity in myeloid cells and T-cells. *Cancer Immunology, Immunotherapy*, *63*(8), 847–857. https://doi.org/10.1007/s00262-014-1561-8

Kottemann, M. C., & Smogorzewska, A. (2013). Fanconi anaemia and the repair of Watson and Crick DNA crosslinks. *Nature*, *493*(7432), 356–363. https://doi.org/10.1038/nature11863

Kozakiewicz, P., & Grzybowska-Szatkowska, L. (2018). Application of molecular targeted therapies in the treatment of head and neck squamous cell carcinoma (Review). *Oncology Letters*. https://doi.org/10.3892/ol.2018.8300

Kuster, A., Mozaffari, N. L., Wilkinson, O. J., Wojtaszek, J. L., Zurfluh, C., Przetocka, S., Zyla, D., von Aesch, C., Dillingham, M. S., Williams, R. S., & Sartori, A. A. (2021). A stapled peptide mimetic of the CtIP tetramerization motif interferes with double-strand break repair and replication fork protection. *Science Advances*, *7*(8). https://doi.org/10.1126/sciadv.abc6381

Langevin, F., Crossan, G. P., Rosado, I. V., Arends, M. J., & Patel, K. J. (2011). Fancd2 counteracts the toxic effects of naturally produced aldehydes in mice. Nature, 475(7354), 53–58. https://doi.org/10.1038/nature10192

Lawson, A. D. G., Maccoss, M., & Heer, J. P. (2018). Importance of Rigidity in Designing Small Molecule Drugs to Tackle Protein-Protein Interactions (PPIs) through Stabilization of Desired Conformers. In *Journal of Medicinal Chemistry* (Vol. 61, Issue 10, pp. 4383–4389). American Chemical Society. https://doi.org/10.1021/acs.jmedchem.7b01120

Lee, A. (2021). Fuzuloparib: First Approval. In *Drugs* (Vol. 81, Issue 10, pp. 1221–1226). Adis. https://doi.org/10.1007/s40265-021-01541-x

Lee, J.-C., Chung, L.-C., Chen, Y.-J., Feng, T.-H., & Juang, H.-H. (2014). N-myc downstream-regulated gene 1 downregulates cell proliferation, invasiveness, and tumorigenesis in human oral squamous cell carcinoma11Equal contributions. *Cancer Letters*, *355*(2), 242–252. https://doi.org/10.1016/j.canlet.2014.08.035

Lee, R. H., Kang, H., Yom, S. S., Smogorzewska, A., Johnson, D. E., & Grandis, J. R. (2021). Treatment of fanconi anemia–associated head and neck cancer: Opportunities to improve outcomes. In *Clinical Cancer Research* (Vol. 27, Issue 19, pp. OF1–OF20). American Association for Cancer Research Inc. https://doi.org/10.1158/1078-0432.CCR-21-1259

Lee, Y. S., Yu, J. E., Kim, K. C., Lee, D. H., Son, D. J., Lee, H. P., Jung, J., Kim, N. Du, Ham, Y. W., Yun, J., Han, S., & Hong, J. T. (2022). A small molecule targeting CHI3L1 inhibits lung metastasis by blocking IL-13Rα2-mediated JNK-AP-1 signals. *Molecular Oncology*, *16*(2), 508–526. https://doi.org/10.1002/1878-0261.13138

Lewis, L. M., Tang, A. L., Wise-Draper, T. M., Myers, K. C., Greenberger, J. S., & Takiar, V. (2020). Successful use of a therapeutic trial of graduated volume and dose escalation for postoperative head and neck radiotherapy in a Fanconi anemia patient. *Head and Neck*, *42*(10), E16–E22. https://doi.org/10.1002/hed.26395

Li, B., & Dewey, C. N. (2011). RSEM: accurate transcript quantification from RNA-Seq data with or without a reference genome. *BMC Bioinformatics*, *12*(1), 323. https://doi.org/10.1186/1471-2105-12-323

Liu, Q., Yu, S., Zhao, W., Qin, S., Chu, Q., & Wu, K. (2018). EGFR-TKIs resistance via EGFR-independent signaling pathways. *Molecular Cancer*, *17*(1), 53. https://doi.org/10.1186/s12943-018-0793-1

Liu, Y. L., & Weigelt, B. (2024). A tale of two pathways: Review of immune checkpoint inhibitors in DNA mismatch repair-deficient and microsatellite instability-high endometrial cancers. *Cancer*, *130*(10), 1733–1746. https://doi.org/10.1002/cncr.35267

Lombardi, A. J., Hoskins, E. E., Foglesong, G. D., Wikenheiser-Brokamp, K. A., Wiesmüller, L., Hanenberg, H., Andreassen, P. R., Jacobs, A. J., Olson, S. B., Keeble, W. W., Hays, L. E., & Wells, S. I. (2015). Acquisition of Relative Interstrand Crosslinker Resistance and PARP Inhibitor Sensitivity in Fanconi Anemia Head and Neck Cancers. *Clinical Cancer Research*, *21*(8), 1962–1972. https://doi.org/10.1158/1078-0432.CCR-14-2616

Longerich, S., Li, J., Xiong, Y., Sung, P., & Kupfer, G. M. (2014). Stress and DNA repair biology of the Fanconi anemia pathway. *Blood*, *124*(18), 2812–2819. https://doi.org/10.1182/blood-2014-04-526293

Lu, H., Zhou, Q., He, J., Jiang, Z., Peng, C., Tong, R., & Shi, J. (2020). Recent advances in the development of protein–protein interactions modulators: mechanisms and clinical trials. *Signal Transduction and Targeted Therapy*, *5*(1), 213. https://doi.org/10.1038/s41392-020-00315-3

Lu, Y., Yang, Y., Zhu, G., Zeng, H., Fan, Y., Guo, F., Xu, D., Wang, B., Chen, D., & Ge, G. (2023). Emerging Pharmacotherapeutic Strategies to Overcome Undruggable Proteins in Cancer. In *International Journal of Biological Sciences* (Vol. 19, Issue 11, pp. 3360–3382). Ivyspring International Publisher. https://doi.org/10.7150/ijbs.83026

Luo, L., Zheng, T., Wang, Q., Liao, Y., Zheng, X., Zhong, A., Huang, Z., & Luo, H. (2022). Virtual Screening Based on Machine Learning Explores Mangrove Natural Products as KRASG12C Inhibitors. *Pharmaceuticals*, *15*(5), 584. https://doi.org/10.3390/ph15050584

Ma, B., Akosman, B., Kamle, S., Lee, C.-M., He, C. H., Koo, J. S., Lee, C. G., & Elias, J. A. (2021). CHI3L1 regulates PD-L1 and anti–CHI3L1–PD-1 antibody elicits synergistic antitumor responses. *Journal of Clinical Investigation*, *131*(21). https://doi.org/10.1172/JCI137750

Ma, S., Li, X., Wang, X., Cheng, L., Li, Z., Zhang, C., Ye, Z., & Qian, Q. (2019). Current progress in car-t cell therapy for solid tumors. In *International Journal of Biological Sciences* (Vol. 15, Issue 12, pp. 2548–2560). Ivyspring International Publisher. https://doi.org/10.7150/ijbs.34213

Ma, X., Wu, S., Li, B., Zhang, Q., Zhang, J., Liu, W., Yan, H., Bernards, R., Qin, W., & Wang, C. (2022). EGFR blockade confers sensitivity to cabozantinib in hepatocellular carcinoma. *Cell Discovery*, *8*(1), 82. https://doi.org/10.1038/s41421-022-00425-y

Macalino, S. J. Y., Basith, S., Clavio, N. A. B., Chang, H., Kang, S., & Choi, S. (2018). Evolution of in silico strategies for protein-protein interaction drug discovery. In *Molecules* (Vol. 23, Issue 8). MDPI AG. https://doi.org/10.3390/molecules23081963

Markham, A. (2021). Pamiparib: First Approval. *Drugs*, *81*(11), 1343–1348. https://doi.org/10.1007/s40265-021-01552-8

Marret, G., Temam, S., Kamal, M., Even, C., Delord, J.-P., Hoffmann, C., Dolivet, G., Malard, O., Fayette, J., Capitain, O., Vergez, S., Geoffrois, L., Rolland, F., Zrounba, P., Laccourreye, L., Saada-Bouzid, E., Aide, N., Bénavent, V., Klijianenko, J., … Le Tourneau, C. (2023). Randomized phase II study of preoperative afatinib in untreated head and neck cancers: predictive and pharmacodynamic biomarkers of activity. *Scientific Reports*, *13*(1), 22524. https://doi.org/10.1038/s41598-023-49887-4

Martinelli, E., Morgillo, F., Troiani, T., & Ciardiello, F. (2017). Cancer resistance to therapies against the EGFR-RAS-RAF pathway: The role of MEK. *Cancer Treatment Reviews*, *53*, 61–69. https://doi.org/10.1016/j.ctrv.2016.12.001

Mateos-Gomez, P. A., Gong, F., Nair, N., Miller, K. M., Lazzerini-Denchi, E., & Sfeir, A. (2015). Mammalian polymerase θ promotes alternative NHEJ and suppresses recombination. *Nature*, *518*(7538), 254–257. https://doi.org/10.1038/nature14157

Matthews, T. P., Jones, A. M., & Collins, I. (2013). Structure-based design, discovery and development of checkpoint kinase inhibitors as potential anticancer therapies. In *Expert Opinion on Drug Discovery* (Vol. 8, Issue 6, pp. 621–640). https://doi.org/10.1517/17460441.2013.788496

Meador, C. B., Sequist, L. V., & Piotrowska, Z. (2021). Targeting *EGFR* Exon 20 Insertions in Non–Small Cell Lung Cancer: Recent Advances and Clinical Updates. *Cancer Discovery*, *11*(9), 2145–2157. https://doi.org/10.1158/2159-8290.CD-21-0226

Michl, J., Zimmer, J., Buffa, F. M., McDermott, U., & Tarsounas, M. (2016). FANCD2 limits replication stress and genome instability in cells lacking BRCA2. *Nature Structural & Molecular Biology*, *23*(8), 755–757. https://doi.org/10.1038/nsmb.3252

Miles, J. A., Frost, M. G., Carroll, E., Rowe, M. L., Howard, M. J., Sidhu, A., Chaugule, V. K., Alpi, A. F., & Walden, H. (2015). The Fanconi Anemia DNA repair pathway is regulated by an interaction between ubiquitin and the E2-like fold domain of FANCL. *Journal of Biological Chemistry*, *290*(34), 20995–21006. https://doi.org/10.1074/jbc.M115.675835

Minguillón, J., & Surrallés, J. (2018). Therapeutic research in the crystal chromosome disease Fanconi anemia. *Mutation Research - Genetic Toxicology and Environmental Mutagenesis*, *836*, 104–108. https://doi.org/10.1016/j.mrgentox.2018.05.012

Minko, I. G., Moellmer, S. A., Luzadder, M. M., Tomar, R., Stone, M. P., McCullough, A. K., & Stephen Lloyd, R. (2024). Interaction of mitoxantrone with abasic sites - DNA strand

cleavage and inhibition of apurinic/apyrimidinic endonuclease 1, APE1. *DNA Repair*, *133*, 103606. https://doi.org/10.1016/j.dnarep.2023.103606

Montanuy, H., Camps-Fajol, C., Camps-Fajol, C., Carreras-Puigvert, J., Carreras-Puigvert, J., Carreras-Puigvert, J., Häggblad, M., Häggblad, M., Lundgren, B., Aza-Carmona, M., Aza-Carmona, M., Helleday, T., Minguillón, J., Minguillón, J., Minguillón, J., Surrallés, J., Surrallés, J., Surrallés, J., & Surrallés, J. (2020). High content drug screening for Fanconi anemia therapeutics. *Orphanet Journal of Rare Diseases*, *15*(1). https://doi.org/10.1186/s13023-020-01437-1

Montanuy, H., Martínez-Barriocanal, A., Casado, J. A., Rovirosa, L., Ramírez, M. J., Nieto, R., Carrascoso-Rubio, C., Riera, P., Gonzalez, A., Lerma, E., Lasa, A., Carreras-Puigvert, J., Helleday, T., Bueren, J. A., Arango, D., Minguillon, J., & Surralles, J. (2020). Gefitinib and afatinib show potential efficacy for fanconi anemia-related head and neck cancer. *Clinical Cancer Research*, *26*(12), 3044–3057. https://doi.org/10.1158/1078-0432.CCR-19-1625

Moradi-Kalbolandi, S., Hosseinzade, A., Salehi, M., Merikhian, P., & Farahmand, L. (2018). Monoclonal antibody-based therapeutics, targeting the epidermal growth factor receptor family: from herceptin to Pan HER. *Journal of Pharmacy and Pharmacology*, *70*(7), 841–854. https://doi.org/10.1111/jphp.12911

Mourón, S., Rodriguez-Acebes, S., Martínez-Jiménez, M. I., García-Gómez, S., Chocrón, S., Blanco, L., & Méndez, J. (2013). Repriming of DNA synthesis at stalled replication forks by human PrimPol. *Nature Structural & Molecular Biology*, *20*(12), 1383–1389. https://doi.org/10.1038/nsmb.2719

Murai, J., Huang, S. Y. N., Das, B. B., Renaud, A., Zhang, Y., Doroshow, J. H., Ji, J., Takeda, S., & Pommier, Y. (2012). Trapping of PARP1 and PARP2 by clinical PARP inhibitors. *Cancer Research*, *72*(21), 5588–5599. https://doi.org/10.1158/0008-5472.CAN-12-2753

Nausch, N., & Cerwenka, A. (2008). NKG2D ligands in tumor immunity. *Oncogene*, *27*(45), 5944–5958. https://doi.org/10.1038/onc.2008.272

Nayak, S., Calvo, J. A., & Cantor, S. B. (2021). Targeting translesion synthesis (TLS) to expose replication gaps, a unique cancer vulnerability. In *Expert Opinion on Therapeutic Targets* (Vol. 25, Issue 1, pp. 27–36). Taylor and Francis Ltd. https://doi.org/10.1080/14728222.2021.1864321

Neelsen, K. J., & Lopes, M. (2015). Replication fork reversal in eukaryotes: from dead end to dynamic response. *Nature Reviews Molecular Cell Biology*, *16*(4), 207–220. https://doi.org/10.1038/nrm3935

Nero, T. L., Morton, C. J., Holien, J. K., Wielens, J., & Parker, M. W. (2014). Oncogenic protein interfaces: small molecules, big challenges. *Nature Reviews Cancer*, *14*(4), 248–262. https://doi.org/10.1038/nrc3690

Ngo, H. V., Thanh Le, T. T., Vu, H. N., Hoang, H., Ikenaga, H., Sato-Matsubara, M., Uchida-Kobayashi, S., Urushima, H., Van Nguyen, K., Nguyen, H. T., Shinkawa, H., Kubo, S., Ohtani, N., Enomoto, M., Tamori, A., & Kawada, N. (2024). Poorly Differentiated Hepatocellular Carcinoma Cells Avoid Apoptosis by Interacting with T Cells via CD40–CD40L Linkage. *The American Journal of Pathology*. https://doi.org/10.1016/j.ajpath.2024.03.004

Nguyen, H. H., Park, J., Kang, S., & Kim, M. (2015). Surface plasmon resonance: A versatile technique for biosensor applications. In *Sensors (Switzerland)* (Vol. 15, Issue 5, pp. 10481–10510). MDPI AG. https://doi.org/10.3390/s150510481

Niraj, J., Färkkilä, A., & D'Andrea, A. D. (2019). The Fanconi Anemia Pathway in Cancer. *Annual Review of Cancer Biology*, *3*(1), 457–478. https://doi.org/10.1146/annurev-cancerbio-030617-050422

Nijman, S. M., Huang, T. T., Dirac, A. M., Brummelkamp, T. R., Kerkhoven, R. M., D'Andrea, A. D., & Bernards, R. (2005). The deubiquitinating enzyme USP1 regulates the Fanconi anemia pathway. Molecular cell, 17(3), 331–339. https://doi.org/10.1016/j.molcel.2005.01.008

Olaru, A., Bala, C., Jaffrezic-Renault, N., & Aboul-Enein, H. Y. (2015). Surface Plasmon Resonance (SPR) Biosensors in Pharmaceutical Analysis. *Critical Reviews in Analytical Chemistry*, *45*(2), 97–105. https://doi.org/10.1080/10408347.2014.881250

Paluszczak, J., Kiwerska, K., & Mielcarek-Kuchta, D. (2018). Frequent methylation of DAB2, a Wnt pathway antagonist, in oral and oropharyngeal squamous cell carcinomas. *Pathology - Research and Practice*, *214*(2), 314–317. https://doi.org/10.1016/j.prp.2017.12.010

Pandey, M. S., Wang, C., Umlauf, S., & Lin, S. (2021). Simultaneous Inhibition of PD-1 and Stimulation of CD40 Signaling Pathways by Anti-PD-L1/CD40L Bispecific Fusion Protein Synergistically Activate Target and Effector Cells. *International Journal of Molecular Sciences*, *22*(21), 11302. https://doi.org/10.3390/ijms222111302

Papa, S., Adami, A., Metoudi, M., Beatson, R., George, M. S., Achkova, D., Williams, E., Arif, S., Reid, F., Elstad, M., Beckley-Hoelscher, N., Douri, A., Delord, M., Lyne, M., Shivapatham, D., Fisher, C., Hope, A., Gooljar, S., Mitra, A., … Maher, J. (2023). Intratumoral pan-ERBB targeted CAR-T for head and neck squamous cell carcinoma: interim analysis of the T4 immunotherapy study. *Journal for ImmunoTherapy of Cancer*, *11*(6). https://doi.org/10.1136/jitc-2023-007162

Papa, S., van Schalkwyk, M., & Maher, J. (2015). Clinical Evaluation of ERBB-Targeted CAR T-Cells, Following Intracavity Delivery in Patients with ERBB-Expressing Solid Tumors. *Methods in Molecular Biology (Clifton, N.J.)*, *1317*, 365–382. https://doi.org/10.1007/978-1-4939-2727-2_21

Park, Y. P., Jin, L., Bennett, K. B., Wang, D., Fredenburg, K. M., Tseng, J. E., Chang, L.-J., Huang, J., & Chan, E. K. L. (2018). CD70 as a target for chimeric antigen receptor T cells in head and neck squamous cell carcinoma. *Oral Oncology*, *78*, 145–150. https://doi.org/10.1016/j.oraloncology.2018.01.024

Patel, K. J., & Joenje, H. (2007). Fanconi anemia and DNA replication repair. *DNA Repair*, *6*(7), 885–890. https://doi.org/10.1016/j.dnarep.2007.02.002

Peake, J. D., Horne, K. I., Noguchi, C., Gilligan, J. P., & Noguchi, E. (2023). The p53 DNA damage response and Fanconi anemia DNA repair pathway protect against acetaldehyde-induced replication stress in esophageal keratinocytes. *Cell Cycle*, *22*(18), 2088–2096. https://doi.org/10.1080/15384101.2023.2261740

Peake, J. D., Noguchi, C., Lin, B., Theriault, A., O'Connor, M., Sheth, S., Tanaka, K., Nakagawa, H., & Noguchi, E. (2021). FANCD2 limits acetaldehyde-induced genomic instability during DNA replication in esophageal keratinocytes. *Molecular Oncology*, *15*(11), 3109–3124. https://doi.org/10.1002/1878-0261.13072

Peake, J. D., & Noguchi, E. (2022). Fanconi anemia: current insights regarding epidemiology, cancer, and DNA repair. *Human Genetics*, *141*(12), 1811–1836. https://doi.org/10.1007/s00439-022-02462-9

Perez, C., Soler, D., Soliva, R., & Guallar, V. (2020). FragPELE: Dynamic Ligand Growing within a Binding Site. A Novel Tool for Hit-To-Lead Drug Design. *Journal of Chemical Information and Modeling*, *60*(3), 1728–1736. https://doi.org/10.1021/acs.jcim.9b00938

Persico, I., Fiscarelli, I., Pelle, A., Faleschini, M., Pasini, B., Savoia, A., & Bottega, R. (2023). Phenotype reversion as "natural gene therapy" in Fanconi anemia by a gene conversion event. *Frontiers in Genetics*, *14*. https://doi.org/10.3389/fgene.2023.1240758

Piliarik, M., Vaisocherová, H., & Homola, J. (2009). *Surface Plasmon Resonance Biosensing* (pp. 65–88). https://doi.org/10.1007/978-1-60327-567-5_5

Pitu, F., Pasca, S., Popa, C., & Nadim, A. H. (2021). The importance of MLH1, MSH2, MSH6 and PMS2 in determining DNA damage response in digestive cancers. *Romanian Biotechnological Letters*, *26*(1), 2289–2294. https://doi.org/10.25083/rbl/26.1/2289.2294

Porta, C., Paglino, C., & Mosca, A. (2014). Targeting PI3K/Akt/mTOR signaling in cancer. In *Frontiers in Oncology: Vol. 4 APR*. Frontiers Research Foundation. https://doi.org/10.3389/fonc.2014.00064

Qiu, Y., Li, X., He, X., Pu, J., Zhang, J., & Lu, S. (2020). Computational methods-guided design of modulators targeting protein-protein interactions (PPIs). In *European Journal of Medicinal Chemistry* (Vol. 207). Elsevier Masson s.r.l. https://doi.org/10.1016/j.ejmech.2020.112764

Quinet, A., Lerner, L. K., Martins, D. J., & Menck, C. F. M. (2018). Filling gaps in translesion DNA synthesis in human cells. In *Mutation Research - Genetic Toxicology and Environmental Mutagenesis* (Vol. 836, pp. 127–142). Elsevier B.V. https://doi.org/10.1016/j.mrgentox.2018.02.004

Rahimian, E., Amini, A., Alikarami, F., Pezeshki, S. M. S., Saki, N., & Safa, M. (2020). DNA repair pathways as guardians of the genome: Therapeutic potential and possible prognostic role in hematologic neoplasms. In *DNA Repair* (Vol. 96). Elsevier B.V. https://doi.org/10.1016/j.dnarep.2020.102951

Rai, G., Vyjayanti, V. N., Dorjsuren, D., Simeonov, A., Jadhav, A., Wilson, D. M., & Maloney, D. J. (2012). Synthesis, Biological Evaluation, and Structure–Activity Relationships of a Novel Class of Apurinic/Apyrimidinic Endonuclease 1 Inhibitors. *Journal of Medicinal Chemistry*, *55*(7), 3101–3112. https://doi.org/10.1021/jm201537d

Ramírez, M. J., Minguillón, J., Loveless, S., Lake, K., Carrasco, E., Stjepanovic, N., Balmaña, J., Català, A., Mehta, P. A., & Surrallés, J. (2020). Chromosome fragility in the buccal epithelium in patients with Fanconi anemia. *Cancer Letters*, *472*, 1–7. https://doi.org/10.1016/j.canlet.2019.12.008

Ramírez, M. J., Pujol, R., Trujillo-Quintero, J. P., Minguillón, J., Bogliolo, M., Río, P., Navarro, S., Casado, J. A., Badell, I., Carrasco, E., Balmaña, J., Català, A., Sevilla, J., Beléndez, C., Argilés, B., López, M., Díaz de Heredia, C., Rao, G., Nicoletti, E., … Surrallés, J. (2021). Natural gene therapy by reverse mosaicism leads to improved hematology in <scp>Fanconi</scp> anemia patients. *American Journal of Hematology*, *96*(8), 989–999. https://doi.org/10.1002/ajh.26234

Ranjha, L., Howard, S. M., & Cejka, P. (2018). Main steps in DNA double-strand break repair: an introduction to homologous recombination and related processes. In *Chromosoma* (Vol. 127, Issue 2, pp. 187–214). Springer Science and Business Media Deutschland GmbH. https://doi.org/10.1007/s00412-017-0658-1

Rao, V. S., Srinivas, K., Sujini, G. N., & Kumar, G. N. S. (2014). Protein-Protein Interaction Detection: Methods and Analysis. *International Journal of Proteomics*, *2014*, 1–12. https://doi.org/10.1155/2014/147648

Río, P., Navarro, S., & Bueren, J. A. (2018). Advances in Gene Therapy for Fanconi Anemia. *Human Gene Therapy*, *29*(10), 1114–1123. https://doi.org/10.1089/hum.2018.124

Río, P., Navarro, S., Wang, W., Sánchez-Domínguez, R., Pujol, R. M., Segovia, J. C., Bogliolo, M., Merino, E., Wu, N., Salgado, R., Lamana, M. L., Yañez, R. M., Casado, J. A., Giménez, Y., Román-Rodríguez, F. J., Álvarez, L., Alberquilla, O., Raimbault, A., Guenechea, G., … Bueren, J. A. (2019). Successful engraftment of gene-corrected hematopoietic stem cells in non-conditioned patients with Fanconi anemia. *Nature Medicine*, *25*(9), 1396–1401. https://doi.org/10.1038/s41591-019-0550-z

Ritchie, M. E., Phipson, B., Wu, D., Hu, Y., Law, C. W., Shi, W., & Smyth, G. K. (2015). limma powers differential expression analyses for RNA-sequencing and microarray studies. *Nucleic Acids Research*, *43*(7), e47–e47. https://doi.org/10.1093/nar/gkv007

Roohollahi, K., de Jong, Y., Pai, G., Zaini, M. A., de Lint, K., Sie, D., Rooimans, M. A., Rockx, D., Hoskins, E. E., Ameziane, N., Wolthuis, R., Joenje, H., Wells, S. I., & Dorsman, J. (2022). BIRC2–BIRC3 amplification: a potentially druggable feature of a subset of head and neck cancers in patients with Fanconi anemia. *Scientific Reports*, *12*(1), 45. https://doi.org/10.1038/s41598-021-04042-9

Roslind, A., Johansen, J. S., Christensen, I. J., Kiss, K., Balslev, E., Nielsen, D. L., Bentzen, J., Price, P. A., & Andersen, E. (2008). High serum levels of YKL-40 in patients with squamous cell carcinoma of the head and neck are associated with short survival. *International Journal of Cancer*, *122*(4), 857–863. https://doi.org/10.1002/ijc.23152

Sajadian, M., Khademi, B., Moinzadeh, L., Ghaderi, A., Jafarzadeh, A., & Razmkhah, M. (2023). Modulation of semaphorin 3C & 4D expression in cancerous tissues from individuals with laryngeal squamous cell carcinoma. *Indian Journal of Medical Research*, *158*(4), 432. https://doi.org/10.4103/ijmr.ijmr_3148_21

Sale, J. E. (2012). Competition, collaboration and coordination - Determining how cells bypass DNA damage. *Journal of Cell Science*, *125*(7), 1633–1643. https://doi.org/10.1242/jcs.094748

Sanjiv, K., Hagenkort, A., Calderón-Montaño, J. M., Koolmeister, T., Reaper, P. M., Mortusewicz, O., Jacques, S. A., Kuiper, R. V., Schultz, N., Scobie, M., Charlton, P. A., Pollard, J. R., Berglund, U. W., Altun, M., & Helleday, T. (2016). Cancer-Specific Synthetic Lethality between ATR and CHK1 Kinase Activities. *Cell Reports*, *14*(2), 298–309. https://doi.org/10.1016/j.celrep.2015.12.032

Schwab, R. A., Nieminuszczy, J., Shah, F., Langton, J., Lopez Martinez, D., Liang, C. C., Cohn, M. A., Gibbons, R. J., Deans, A. J., & Niedzwiedz, W. (2015). The Fanconi Anemia Pathway Maintains Genome Stability by Coordinating Replication and Transcription. *Molecular Cell*, *60*(3), 351–361. https://doi.org/10.1016/j.molcel.2015.09.012

Scribner, J. A., Brown, J. G., Son, T., Chiechi, M., Li, P., Sharma, S., Li, H., De Costa, A., Li, Y., Chen, Y., Easton, A., Yee-Toy, N. C., Chen, F. Z., Gorlatov, S., Barat, B., Huang, L., Wolff, C. R., Hooley, J., Hotaling, T. E., … Loo, D. (2020). Preclinical Development of MGC018, a Duocarmycin-based Antibody–drug Conjugate Targeting B7-H3 for Solid Cancer. *Molecular Cancer Therapeutics*, *19*(11), 2235–2244. https://doi.org/10.1158/1535-7163.MCT-20-0116

Seltzsam, S., Ziemann, F., Dreffke, K., Preising, S., Arenz, A., Schötz, U., Engenhart-Cabillic, R., Dikomey, E., & Wittig, A. (2019). In HPV-Positive HNSCC Cells, Functional Restoration of the p53/p21 Pathway by Proteasome Inhibitor Bortezomib Does Not Affect Radio- or Chemosensitivity. *Translational Oncology*, *12*(3), 417–425. https://doi.org/10.1016/j.tranon.2018.11.013

Sevilla, J., Navarro, S., Rio, P., Sánchez-Domínguez, R., Zubicaray, J., Gálvez, E., Merino, E., Sebastián, E., Azqueta, C., Casado, J. A., Segovia, J. C., Alberquilla, O., Bogliolo, M., Román-Rodríguez, F. J., Giménez, Y., Larcher, L., Salgado, R., Pujol, R. M., Hladun, R., … Bueren, J. A. (2021). Improved collection of hematopoietic stem cells and progenitors from Fanconi anemia patients for gene therapy purposes. *Molecular Therapy - Methods and Clinical Development*, *22*, 66–75. https://doi.org/10.1016/j.omtm.2021.06.001

Shakeel, S., Rajendra, E., Alcón, P., O'Reilly, F., Chorev, D. S., Maslen, S., Degliesposti, G., Russo, C. J., He, S., Hill, C. H., Skehel, J. M., Scheres, S. H. W., Patel, K. J., Rappsilber, J., Robinson, C. V., & Passmore, L. A. (2019). Structure of the Fanconi anaemia monoubiquitin ligase complex. *Nature*, *575*(7781), 234–237. https://doi.org/10.1038/s41586-019-1703-4

Shangary, S., & Wang, S. (2009). Small-Molecule Inhibitors of the MDM2-p53 Protein-Protein Interaction to Reactivate p53 Function: A Novel Approach for Cancer Therapy. *Annual Review of Pharmacology and Toxicology*, *49*(1), 223–241. https://doi.org/10.1146/annurev.pharmtox.48.113006.094723

Sharp, M. F., Bythell-Douglas, R., Deans, A. J., & Crismani, W. (2021). The Fanconi anemia ubiquitin E3 ligase complex as an anti-cancer target. In *Molecular Cell* (Vol. 81, Issue 11, pp. 2278–2289). Cell Press. https://doi.org/10.1016/j.molcel.2021.04.023

Sharp, M. F., Murphy, V. J., Twest, S. Van, Tan, W., Lui, J., Simpson, K. J., Deans, A. J., & Crismani, W. (2020). Methodology for the identification of small molecule inhibitors of the Fanconi Anaemia ubiquitin E3 ligase complex. *Scientific Reports*, *10*(1). https://doi.org/10.1038/s41598-020-64868-7

Shinohara, K., Yoda, N., Takane, K., Watanabe, T., Fukuyo, M., Fujiwara, K., Kita, K., Nagase, H., Nemoto, T., & Kaneda, A. (2016). Inhibition of DNA Methylation at the *MLH1* Promoter Region Using Pyrrole–Imidazole Polyamide. *ACS Omega*, *1*(6), 1164–1172. https://doi.org/10.1021/acsomega.6b00229

Shinsato, Y., Furukawa, T., Yunoue, S., Yonezawa, H., Minami, K., Nishizawa, Y., Ikeda, R., Kawahara, K., Yamamoto, M., Hirano, H., Tokimura, H., & Arita, K. (2013). Reduction of

MLH1 and PMS2 confers temozolomide resistance and is associated with recurrence of glioblastoma. *Oncotarget*, *4*(12), 2261–2270. https://doi.org/10.18632/oncotarget.1302

Singh, A., Kumar, A., Kumar, P., Nayak, N., Bhardwaj, T., Giri, R., & Garg, N. (2021). A novel inhibitor L755507 efficiently blocks c-Myc–MAX heterodimerization and induces apoptosis in cancer cells. *Journal of Biological Chemistry*, *297*(1), 100903. https://doi.org/10.1016/j.jbc.2021.100903

Singh, A., Sharma, S., Kumar, P., & Garg, N. (2022). *Cellular experiments to study the inhibition of c-Myc/MAX heterodimerization* (pp. 193–205). https://doi.org/10.1016/bs.mie.2022.07.009

Skwarczynska, M., & Ottmann, C. (2015). Protein-protein interactions as drug targets. In *Future Medicinal Chemistry* (Vol. 7, Issue 16, pp. 2195–2219). Future Science Ltd. https://doi.org/10.4155/fmc.15.138

Song, C., Zhang, S., & Huang, H. (2015). Choosing a suitable method for the identification of replication origins in microbial genomes. *Frontiers in MICROBIOLOGY*, *6*. https://doi.org/10.3389/fmicb.2015.01049

Sparkes, R. S. (1996). Molecular insights into Fanconi anemia. *Journal of Clinical Investigation*, *97*(4), 897–898. https://doi.org/10.1172/JCI118510

Srivastava, M., Nambiar, M., Sharma, S., Karki, S. S., Goldsmith, G., Hegde, M., Kumar, S., Pandey, M., Singh, R. K., Ray, P., Natarajan, R., Kelkar, M., De, A., Choudhary, B., & Raghavan, S. C. (2012). An Inhibitor of Nonhomologous End-Joining Abrogates Double-Strand Break Repair and Impedes Cancer Progression. *Cell*, *151*(7), 1474–1487. https://doi.org/10.1016/j.cell.2012.11.054

Sterner, R. C., & Sterner, R. M. (2021). CAR-T cell therapy: current limitations and potential strategies. In *Blood Cancer Journal* (Vol. 11, Issue 4). Springer Nature. https://doi.org/10.1038/s41408-021-00459-7

Stickler, S., Rath, B., & Hamilton, G. (2024). Targeting KRAS in pancreatic cancer. *Oncology Research*, *32*(5), 799–805. https://doi.org/10.32604/or.2024.045356

Strohm, L., Daiber, A., Ubbens, H., Krishnankutty, R., Oelze, M., Kuntic, M., Hahad, O., Klein, V., Hoefer, I. E., von Kriegsheim, A., Kleinert, H., Atzler, D., Lurz, P., Weber, C., Wild, P. S., Münzel, T., Knosalla, C., Lutgens, E., & Daub, S. (2024). Role of inflammatory signaling pathways involving the CD40–CD40L–TRAF cascade in diabetes and hypertension—insights from animal and human studies. *Basic Research in Cardiology*. https://doi.org/10.1007/s00395-024-01045-1

Sullivan, K., Cramer-Morales, K., McElroy, D. L., Ostrov, D., Haas, K., Nieborowska-Skorska, M., Childers, W., Mazin, A., Hromas, R. A., Pomerantz, R., & Skorski, T. (2015). Identification of a Small Molecule Inhibitor of RAD52 to Induce Synthetic Lethality in BRCA-Deficient Leukemias. *Blood*, *126*(23), 4434–4434. https://doi.org/10.1182/blood.V126.23.4434.4434

Sun, H., Nikolovska-Coleska, Z., Yang, C.-Y., Xu, L., Tomita, Y., Krajewski, K., Roller, P. P., & Wang, S. (2004). Structure-Based Design, Synthesis, and Evaluation of Conformationally Constrained Mimetics of the Second Mitochondria-Derived Activator of Caspase That Target the X-Linked Inhibitor of Apoptosis Protein/Caspase-9 Interaction Site. *Journal of Medicinal Chemistry*, *47*(17), 4147–4150. https://doi.org/10.1021/jm0499108

Sun Jung, H., oo Byun, G.-W., Lee, K.-E., Chul Mun, Y., Hyun Nam, S., Mi Kwon, J., Nae Lee, S., Im, S.-A., Seong, C.-M., & Nam Lee, S. (2005). G efitinib T rial in a Fanconi's A nem ia Patient w ith M ultiple Squam ous C ell C arcinom as and H epatocellular C arcinom a. In *Cancer Res Treat* (Vol. 37, Issue 6).

Syamsu, S. A., Faruk, M., Smaradania, N., Sampepajung, E., Pranoto, A. S., Irsandy, F., & Tammasse, I. F. U. (2024). PD-1/PD-L1 pathway: Current research in breast cancer. *Breast Disease*, *43*(1), 79–92. https://doi.org/10.3233/BD-249006

Tan, J., Sun, X., Zhao, H., Guan, H., Gao, S., & Zhou, P. (2023). Double-strand DNA break repair: molecular mechanisms and therapeutic targets. *MedComm*, *4*(5). https://doi.org/10.1002/mco2.388

Tan, W., Murphy, V. J., Charron, A., van Twest, S., Sharp, M., Constantinou, A., Parker, M. W., Crismani, W., Bythell-Douglas, R., & Deans, A. J. (2020). Preparation and purification of mono-ubiquitinated proteins using Avi-tagged ubiquitin. *PLOS ONE*, *15*(2), e0229000. https://doi.org/10.1371/journal.pone.0229000

Tan, W., van Twest, S., Leis, A., Bythell-Douglas, R., Murphy, V. J., Sharp, M., Parker, M. W., Crismani, W. M., & Deans, A. J. (2020). Monoubiquitination by the human Fanconi Anemia core complex clamps FANCI: FANCD2 on DNA in filamentous arrays. *ELife*, *9*. https://doi.org/10.7554/eLife.54128

Tang, X., Chang, C., Mosallaei, D., Woodley, D. T., Schönthal, A. H., Chen, M., & Li, W. (2022). Heterogeneous Responses and Isoform Compensation Dim the Therapeutic Window of Hsp90 ATP-Binding Inhibitors in Cancer. *Molecular and Cellular Biology*, *42*(2). https://doi.org/10.1128/mcb.00459-21

Tathineni, P., Joshi, N., & Jelinek, M. J. (2023). Current State and Future Directions of EGFR-Directed Therapy in Head and Neck Cancer. *Current Treatment Options in Oncology*, *24*(6), 680–692. https://doi.org/10.1007/s11864-023-01080-5

Tay, J. C. K., Wang, J., Du, Z., Ng, Y. Y., Li, Z., Ren, Y., Zhang, C., Zhu, J., Xu, X. H., & Wang, S. (2021). Manufacturing NKG2D CAR-T cells with piggyBac transposon vectors and K562 artificial antigen-presenting cells. *Molecular Therapy - Methods & Clinical Development*, *21*, 107–120. https://doi.org/10.1016/j.omtm.2021.02.023

Taylor, S. J., Arends, M. J., & Langdon, S. P. (2020). Inhibitors of the Fanconi anaemia pathway as potential antitumour agents for ovarian cancer. In *Exploration of Targeted Anti-tumor Therapy* (Vol. 1, Issue 1, pp. 26–52). Open Exploration Publishing Inc. https://doi.org/10.37349/etat.2020.00003

Tian, S., Wang, Y., Wan, J., Yang, M., & Fu, Z. (2024). Co-stimulators CD40-CD40L, a potential immune-therapy target for atherosclerosis: A review. *Medicine*, *103*(14), e37718. https://doi.org/10.1097/MD.0000000000037718

Tisato, V., Voltan, R., Gonelli, A., Secchiero, P., & Zauli, G. (2017). MDM2/X inhibitors under clinical evaluation: perspectives for the management of hematological malignancies and pediatric cancer. *Journal of Hematology & Oncology*, *10*(1), 133. https://doi.org/10.1186/s13045-017-0500-5

Titeca, K., Lemmens, I., Tavernier, J., & Eyckerman, S. (2019). Discovering cellular protein-protein interactions: Technological strategies and opportunities. *Mass Spectrometry Reviews*, *38*(1), 79–111. https://doi.org/10.1002/mas.21574

Toulany, M., Dittmann, K., Krüger, M., Baumann, M., & Rodemann, H. P. (2005). Radioresistance of K-Ras mutated human tumor cells is mediated through EGFR-dependent activation of PI3K-AKT pathway. *Radiotherapy and Oncology*, *76*(2), 143–150. https://doi.org/10.1016/j.radonc.2005.06.024

Tozaki, Y., Aoki, H., Kato, R., Toriuchi, K., Arame, S., Inoue, Y., Hayashi, H., Kubota, E., Kataoka, H., & Aoyama, M. (2023). The Combination of ATM and Chk1 Inhibitors Induces Synthetic Lethality in Colorectal Cancer Cells. *Cancers*, *15*(3). https://doi.org/10.3390/cancers15030735

Tseng, H.-M., Shum, D., Bhinder, B., Escobar, S., Veomett, N. J., Tomkinson, A. E., Gin, D. Y., Djaballah, H., & Scheinberg, D. A. (2012). A High-Throughput Scintillation Proximity-Based Assay for Human DNA Ligase IV. *ASSAY and Drug Development Technologies*, *10*(3), 235–249. https://doi.org/10.1089/adt.2011.0404

van Zeeburg, H. J. T., Snijders, P. J. F., Pals, G., Hermsen, M. A. J. A., Rooimans, M. A., Bagby, G., Soulier, J., Gluckman, E., Wennerberg, J., Leemans, C. R., Joenje, H., & Brakenhoff, R. H. (2005). Generation and Molecular Characterization of Head and Neck Squamous Cell Lines of Fanconi Anemia Patients. *Cancer Research*, *65*(4), 1271–1276. https://doi.org/10.1158/0008-5472.CAN-04-3665

Vermersch, P., Granziera, C., Mao-Draayer, Y., Cutter, G., Kalbus, O., Staikov, I., Dufek, M., Saubadu, S., Bejuit, R., Truffinet, P., Djukic, B., Wallstroem, E., & Giovannoni, G. (2024). Inhibition of CD40L with Frexalimab in Multiple Sclerosis. *New England Journal of Medicine*, *390*(7), 589–600. https://doi.org/10.1056/NEJMoa2309439

Vichai, V., & Kirtikara, K. (2006). Sulforhodamine B colorimetric assay for cytotoxicity screening. *Nature Protocols*, *1*(3), 1112–1116. https://doi.org/10.1038/nprot.2006.179

Vu, T. Van, Das, S., Nguyen, C. C., Kim, J., & Kim, J. (2022). Single-strand annealing: Molecular mechanisms and potential applications in CRISPR-Cas-based precision genome editing. *Biotechnology Journal*, *17*(7). https://doi.org/10.1002/biot.202100413

Wang, H. Q., Fu, R., Man, Q. W., Yang, G., Liu, B., & Bu, L. L. (2023). Advances in CAR-T Cell Therapy in Head and Neck Squamous Cell Carcinoma. In *Journal of Clinical Medicine* (Vol. 12, Issue 6). Multidisciplinary Digital Publishing Institute (MDPI). https://doi.org/10.3390/jcm12062173

Wang, H., Teriete, P., Hu, A., Raveendra-Panickar, D., Pendelton, K., Lazo, J. S., Eiseman, J., Holien, T., Misund, K., Oliynyk, G., Arsenian-Henriksson, M., Cosford, N. D. P., Sundan, A., & Prochownik, E. V. (2015). Direct inhibition of c-Myc-Max heterodimers by celastrol and celastrol-inspired triterpenoids. *Oncotarget*, *6*(32), 32380–32395. https://doi.org/10.18632/oncotarget.6116

Wang, H.-Q., Fu, R., Man, Q.-W., Yang, G., Liu, B., & Bu, L.-L. (2023). Advances in CAR-T Cell Therapy in Head and Neck Squamous Cell Carcinoma. *Journal of Clinical Medicine*, *12*(6), 2173. https://doi.org/10.3390/jcm12062173

Wang, L., Kumar, R., Winblad, B., & Pavlov, P. F. (2024). Structure-based discovery of small molecule inhibitors of FKBP51-Hsp90 protein-protein interaction. *European Journal of Medicinal Chemistry*, *270*, 116356. https://doi.org/10.1016/j.ejmech.2024.116356

Wang, M., Brandt, L. T. L., Wang, X., Russell, H., Mitchell, E., Kamimae-Lanning, A. N., Brown, J. M., Dingler, F. A., Garaycoechea, J. I., Isobe, T., Kinston, S. J., Gu, M., Vassiliou, G. S., Wilson, N. K., Göttgens, B., & Patel, K. J. (2023). Genotoxic aldehyde stress prematurely ages hematopoietic stem cells in a p53-driven manner. *Molecular Cell*, *83*(14), 2417-2433.e7. https://doi.org/10.1016/j.molcel.2023.05.035

Wang, M., Chen, S., & Ao, D. (2021). Targeting DNA repair pathway in cancer: Mechanisms and clinical application. In *MedComm* (Vol. 2, Issue 4, pp. 654–691). John Wiley and Sons Inc. https://doi.org/10.1002/mco2.103

Warta, R., & Herold-Mende, C. (2017). Helping EGFR inhibition to block cancer. In *Nature Neuroscience* (Vol. 20, Issue 8, pp. 1035–1037). Nature Publishing Group. https://doi.org/10.1038/nn.4605

Webster, A. L. H., Sanders, M. A., Patel, K., Dietrich, R., Noonan, R. J., Lach, F. P., White, R. R., Goldfarb, A., Hadi, K., Edwards, M. M., Donovan, F. X., Hoogenboezem, R. M., Jung, M., Sridhar, S., Wiley, T. F., Fedrigo, O., Tian, H., Rosiene, J., Heineman, T., … Smogorzewska, A. (2022). Genomic signature of Fanconi anaemia DNA repair pathway deficiency in cancer. *Nature*, *612*(7940), 495–502. https://doi.org/10.1038/s41586-022-05253-4

Whilding, L. M., & Maher, J. (2015). ERBB-targeted CAR T-cell immunotherapy of cancer. In *Immunotherapy* (Vol. 7, Issue 3, pp. 229–241). Future Medicine Ltd. https://doi.org/10.2217/imt.14.120

Wickham, H. (2009). *ggplot2*. Springer New York. https://doi.org/10.1007/978-0-387-98141-3

Wieduwilt, M. J., & Moasser, M. M. (2008). The epidermal growth factor receptor family: Biology driving targeted therapeutics. *Cellular and Molecular Life Sciences*, *65*(10), 1566–1584. https://doi.org/10.1007/s00018-008-7440-8

Wing, A., Fajardo, C. A., Posey, A. D., Shaw, C., Da, T., Young, R. M., Alemany, R., June, C. H., & Guedan, S. (2018). Improving CART-Cell Therapy of Solid Tumors with Oncolytic Virus–Driven Production of a Bispecific T-cell Engager. *Cancer Immunology Research*, *6*(5), 605–616. https://doi.org/10.1158/2326-6066.CIR-17-0314

Wright, W. D., Shah, S. S., & Heyer, W. D. (2018). Homologous recombination and the repair of DNA double-strand breaks. In *Journal of Biological Chemistry* (Vol. 293, Issue 27, pp. 10524–10535). American Society for Biochemistry and Molecular Biology Inc. https://doi.org/10.1074/jbc.TM118.000372

Wu, J., Su, H., Yu, Z., Xi, S., Guo, C., Hu, Z., Qu, Y., Cai, H., Zhao, Y., Zhao, H., Chen, F., Huang, Y., To, S. T., Feng, B., Sai, K., Chen, Z., & Wang, J. (2020). Skp2 modulates proliferation, senescence and tumorigenesis of glioma. *Cancer Cell International*, *20*(1), 71. https://doi.org/10.1186/s12935-020-1144-z

Xie, L., Liao, J., Liu, W., Wang, R., Li, X., Li, W., & Zhou, Z. (2023). Gastrodin overcomes chemoresistance via inhibiting Skp2-mediated glycolysis. *Cell Death Discovery*, *9*(1), 364. https://doi.org/10.1038/s41420-023-01648-y

Xu, T., Yu, C., Sun, J., Liu, Y., Wang, X., Pi, L., Tian, Y., & Zhang, X. (2011). Bone Morphogenetic Protein-4-induced Epithelial-Mesenchymal Transition and Invasiveness Through Smad1-mediated Signal Pathway in Squamous Cell Carcinoma of the Head and Neck. *Archives of Medical Research*, *42*(2), 128–137. https://doi.org/10.1016/j.arcmed.2011.03.003

Yamashita, G., Okamoto, I., Ito, T., Tokashiki, K., Okada, T., & Tsukahara, K. (2023). Efficacy of Nivolumab and Pembrolizumab in Platinum-sensitive Recurrent or Metastatic Head and Neck Squamous Cell Carcinoma. *Anticancer Research*, *43*(8), 3679–3683. https://doi.org/10.21873/anticanres.16550

Yang, F., Hu, Z., & Guo, Z. (2022). Small-Molecule Inhibitors Targeting FEN1 for Cancer Therapy. *Biomolecules*, *12*(7), 1007. https://doi.org/10.3390/biom12071007

Yang, W.-H., Lan, H.-Y., Tai, S.-K., & Yang, M.-H. (2013). Repression of bone morphogenetic protein 4 by let-7i attenuates mesenchymal migration of head and neck cancer cells. *Biochemical and Biophysical Research Communications*, *433*(1), 24–30. https://doi.org/10.1016/j.bbrc.2013.02.076

Yao, R., Zhang, M., Zhou, J., Liu, L., Zhang, Y., Gao, J., & Xu, K. (2022). Novel dual-targeting c-Myc inhibitor D347-2761 represses myeloma growth via blocking c-Myc/Max heterodimerization and disturbing its stability. *Cell Communication and Signaling*, *20*(1), 73. https://doi.org/10.1186/s12964-022-00868-6

Yata, K., & Esashi, F. (2009). Dual role of CDKs in DNA repair: To be, or not to be. In *DNA Repair* (Vol. 8, Issue 1, pp. 6–18). https://doi.org/10.1016/j.dnarep.2008.09.002

Yearley, J. H., Gibson, C., Yu, N., Moon, C., Murphy, E., Juco, J., Lunceford, J., Cheng, J., Chow, L. Q. M., Seiwert, T. Y., Handa, M., Tomassini, J. E., & McClanahan, T. (2017). PD-L2 expression in human tumors: Relevance to anti-PD-1 therapy in cancer. *Clinical Cancer Research*, *23*(12), 3158–3167. https://doi.org/10.1158/1078-0432.CCR-16-1761

Yin, J., & Ren, P. (2024). New advances in the treatment of chondrosarcoma under the PD-1/PD-L1 pathway. *Journal of Cancer Research and Therapeutics*, *20*(2), 522–530. https://doi.org/10.4103/jcrt.jcrt_2269_23

Yokota, T., Homma, A., Kiyota, N., Tahara, M., Hanai, N., Asakage, T., Matsuura, K., Ogawa, T., Saito, Y., Sano, D., Kodaira, T., Motegi, A., Yasuda, K., Takahashi, S., Tanaka, K., Onoe, T., Okano, S., Imamura, Y., Ariizumi, Y., & Hayashi, R. (2020a). Immunotherapy for squamous cell carcinoma of the head and neck. *Japanese Journal of Clinical Oncology*, *50*(10), 1089–1096. https://doi.org/10.1093/jjco/hyaa139

Yokota, T., Homma, A., Kiyota, N., Tahara, M., Hanai, N., Asakage, T., Matsuura, K., Ogawa, T., Saito, Y., Sano, D., Kodaira, T., Motegi, A., Yasuda, K., Takahashi, S., Tanaka, K., Onoe, T., Okano, S., Imamura, Y., Ariizumi, Y., & Hayashi, R. (2020b). Immunotherapy for squamous cell carcinoma of the head and neck. In *Japanese Journal of Clinical Oncology* (Vol. 50, Issue 10, pp. 1089–1096). Oxford University Press. https://doi.org/10.1093/jjco/hyaa139

Yoon, J. Y., Roth, J. J., Rushton, C. A., Morrissette, J. J. D., Nathanson, K. L., Cohen, R. B., & Rosenbaum, J. N. (2023). Homologous recombination pathway gene variants identified by tumor-only sequencing assays in lung carcinoma patients. *Translational Lung Cancer Research*, *12*(6). https://doi.org/10.21037/tlcr-22-749

Yoshimura, C., Nagatoishi, S., Kuroda, D., Kodama, Y., Uno, T., Kitade, M., Chong-Takata, K., Oshiumi, H., Muraoka, H., Yamashita, S., Kawai, Y., Ohkubo, S., & Tsumoto, K. (2021). Thermodynamic Dissection of Potency and Selectivity of Cytosolic Hsp90 Inhibitors. *Journal of Medicinal Chemistry*, *64*(5), 2669–2677. https://doi.org/10.1021/acs.jmedchem.0c01715

Yu, S., Qin, D., Shangary, S., Chen, J., Wang, G., Ding, K., McEachern, D., Qiu, S., Nikolovska-Coleska, Z., Miller, R., Kang, S., Yang, D., & Wang, S. (2009). Potent and Orally Active Small-Molecule Inhibitors of the MDM2−p53 Interaction. *Journal of Medicinal Chemistry*, *52*(24), 7970–7973. https://doi.org/10.1021/jm901400z

Zatreanu, D., Robinson, H. M. R., Alkhatib, O., Boursier, M., Finch, H., Geo, L., Grande, D., Grinkevich, V., Heald, R. A., Langdon, S., Majithiya, J., McWhirter, C., Martin, N. M. B., Moore, S., Neves, J., Rajendra, E., Ranzani, M., Schaedler, T., Stockley, M., … Lord, C. J. (2021). Polθ inhibitors elicit BRCA-gene synthetic lethality and target PARP inhibitor resistance. *Nature Communications*, *12*(1). https://doi.org/10.1038/s41467-021-23463-8

Zeman, M. K., & Cimprich, K. A. (2014). *R E V I E W Causes and consequences of replication stress*.

Zhang, H., & Fu, L. (2021). The role of ALDH2 in tumorigenesis and tumor progression: Targeting ALDH2 as a potential cancer treatment. Acta pharmaceutica Sinica. B, 11(6), 1400–1411. https://doi.org/10.1016/j.apsb.2021.02.008

Zhang, H., Zhong, A., & Chen, J. (2023). Immune checkpoint inhibitors in advanced cutaneous squamous cell carcinoma: A systemic review and meta-analysis. *Skin Research and Technology*, *29*(1). https://doi.org/10.1111/srt.13229

Zhang, S., Yan, Z., Li, Y., Gong, Y., Lyu, X., Lou, J., Zhang, D., Meng, X., & Zhao, Y. (2022). Structure-Based Discovery of MDM2/4 Dual Inhibitors that Exert Antitumor Activities against MDM4-Overexpressing Cancer Cells. *Journal of Medicinal Chemistry*, *65*(8), 6207–6230. https://doi.org/10.1021/acs.jmedchem.2c00095

Zhang, S., Zheng, M., Nie, D., Xu, L., Tian, H., Wang, M., Liu, W., Feng, Z., & Han, F. (2022). Efficacy of cetuximab plus PD-1 inhibitor differs by HPV status in head and neck squamous cell carcinoma: a systematic review and meta-analysis. *Journal for ImmunoTherapy of Cancer*, *10*(10). https://doi.org/10.1136/jitc-2022-005158

Zhang, X., Zhu, L., Zhang, H., Chen, S., & Xiao, Y. (2022). CAR-T Cell Therapy in Hematological Malignancies: Current Opportunities and Challenges. In *Frontiers in Immunology* (Vol. 13). Frontiers Media S.A. https://doi.org/10.3389/fimmu.2022.927153

Zhao, Y., Thomas, H. D., Batey, M. A., Cowell, I. G., Richardson, C. J., Griffin, R. J., Calvert, A. H., Newell, D. R., Smith, G. C. M., & Curtin, N. J. (2006). Preclinical evaluation of a potent novel DNA-dependent protein kinase inhibitor NU7441. *Cancer Research*, *66*(10), 5354–5362. https://doi.org/10.1158/0008-5472.CAN-05-4275

Zhi, W., Li, S., Wan, Y., Wu, F., & Hong, L. (2022). Short-term starvation synergistically enhances cytotoxicity of Niraparib via Akt/mTOR signaling pathway in ovarian cancer therapy. *Cancer Cell International*, *22*(1). https://doi.org/10.1186/s12935-022-02447-8

Zhou, M., Boulos, J. C., Omer, E. A., Klauck, S. M., & Efferth, T. (2023). Modes of Action of a Novel c-MYC Inhibiting 1,2,4-Oxadiazole Derivative in Leukemia and Breast Cancer Cells. *Molecules*, *28*(15), 5658. https://doi.org/10.3390/molecules28155658

Zhou, M., Li, Q., & Wang, R. (2016). Current Experimental Methods for Characterizing Protein–Protein Interactions. *ChemMedChem*, *11*(8), 738–756. https://doi.org/10.1002/cmdc.201500495

Zhou, R. M., Li, Y., Wang, N., Niu, C. X., Huang, X., Cao, S. R., & Huo, X. R. (2020). PARP1 Gene Polymorphisms and the Prognosis of Esophageal Cancer Patients from Cixian High-Incidence Region in Northern China. *Asian Pacific Journal of Cancer Prevention*, *21*(10), 2987–2992. https://doi.org/10.31557/APJCP.2020.21.10.2987

Zhu, C., Xu, Z., Zhang, T., Qian, L., Xiao, W., Wei, H., Jin, T., & Zhou, Y. (2021). Updates of pathogenesis, diagnostic and therapeutic perspectives for ovarian clear cell carcinoma. In *Journal of Cancer* (Vol. 12, Issue 8, pp. 2295–2316). Ivyspring International Publisher. https://doi.org/10.7150/jca.53395

Zhu, H., Wei, M., Xu, J., Hua, J., Liang, C., Meng, Q., Zhang, Y., Liu, J., Zhang, B., Yu, X., & Shi, S. (2020). PARP inhibitors in pancreatic cancer: Molecular mechanisms and clinical applications. In *Molecular Cancer* (Vol. 19, Issue 1). BioMed Central Ltd. https://doi.org/10.1186/s12943-020-01167-9

Zhu, T., Zheng, J. Y., Huang, L. L., Wang, Y. H., Yao, D. F., & Dai, H. Bin. (2023). Human PARP1 substrates and regulators of its catalytic activity: An updated overview. In *Frontiers in Pharmacology* (Vol. 14). Frontiers Media S.A. https://doi.org/10.3389/fphar.2023.1137151

Zibelman, M., & Mehra, R. (2016). Overview of Current Treatment Options and Investigational Targeted Therapies for Locally Advanced Squamous Cell Carcinoma of the Head and Neck. In *American Journal of Clinical Oncology: Cancer Clinical Trials* (Vol. 39, Issue 4, pp. 396–406). Lippincott Williams and Wilkins. https://doi.org/10.1097/COC.0000000000000283

Zimmermann, A., Zenke, F. T., Chiu, L. Y., Dahmen, H., Pehl, U., Fuchss, T., Grombacher, T., Blume, B., Vassilev, L. T., & Blaukat, A. (2022). A New Class of Selective ATM Inhibitors as Combination Partners of DNA Double-Strand Break Inducing Cancer Therapies. *Molecular Cancer Therapeutics*, *21*(6), 859–870. https://doi.org/10.1158/1535-7163.MCT-21-0934

Zimmermann, M., Bernier, C., Kaiser, B., Fournier, S., Li, L., Desjardins, J., Skeldon, A., Rimkunas, V., Veloso, A., Young, J. T. F., Roulston, A., & Zinda, M. (2022). Guiding ATR and PARP inhibitor combinationswith chemogenomic screens. *Cell Reports*, *40*(2). https://doi.org/10.1016/j.celrep.2022.111081

Zinovyev, A., Kuperstein, I., Barillot, E., & Heyer, W. D. (2013). Synthetic Lethality between Gene Defects Affecting a Single Non-essential Molecular Pathway with Reversible Steps. *PLoS Computational Biology*, *9*(4). https://doi.org/10.1371/journal.pcbi.1003016

Zuo, C., Lv, X., Liu, T., Yang, L., Yang, Z., Yu, C., & Chen, H. (2022). Polymorphisms in ERCC4 and ERCC5 and risk of cancers: Systematic research synopsis, meta-analysis, and epidemiological evidence. *Frontiers in Oncology*, *12*. https://doi.org/10.3389/fonc.2022.951193

Zuo, N., Ma, L., Hu, W., Deng, Y., Wei, L., & Liu, Q. (2022). Detection of Alternative End-Joining in HNSC Cell Lines Using DNA Double-Strand Break Reporter Assays. *Bio-Protocol*, *12*(17). https://doi.org/10.21769/BioProtoc.4506

Zwick, E., Bange, J., & Ullrich, A. (2001). Receptor tyrosine kinase signalling as a target for cancer intervention strategies. In *Endocrine-Related Cancer* (Vol. 8). http://www.endocrinology.org

Supplementary data

8. Supplementary data

8.1. Appendix 1



Figure A1. [redacted] inhibition by F27 and F2.14 at 50 and 100 µM during 6-18h (ON) in hFIB cells.



Figure A2. [redacted] inhibition by F1 and F32 at 20 and 50 µM during 18h in hFIB cells.



Figure A3. [redacted] inhibition by F3.4 and F3.6 at 10, 20 and 50 µM during 18h in U2OS cells.



Figure A4. [redacted] inhibition by F3.8 and F3.14 at 10, 20 and 50 µM during 18h in U2OS cells.



Figure A5. [redacted] inhibition by F3.5 and F3.10 at 10, 20 and 50 μM during 18h in U2OS cells.



Figure A6. [redacted] inhibition by F3.10A and F3.19 at 10, 20 and 50 μM during 18h in U2OS cells.



Figure A7. [redacted] inhibition by F3.7 and F3.21 at 10, 20 and 50 μM during 18h in U2OS cells.



Figure A8. [redacted] inhibition by F3.24 and F3.24A at 10, 20 and 50 μM during 18h in U2OS cells.



Figure A9. [redacted] inhibition by F3.20 at 10, 20 and 50 μM during 18h in U2OS cells.



Figure A10. [redacted] inhibition by F3.4 and F3.6 at 10, 20 and 50 μM during 18h in hFIB cells.



Figure A11. [redacted] inhibition by F3.8 and F3.14 at 10, 20 and 50 μM during 18h in hFIB cells.



Figure A12. [redacted] inhibition by F3.5 and F3.10 at 10, 20 and 50 μM during 18h in hFIB cells.



Figure A13. [redacted] inhibition by F3.10A and F3.19 at 10, 20 and 50 μM during 18h in hFIB cells.



Figure A14. [redacted] inhibition by F3.7 and F3.21 at 10, 20 and 50 μM during 18h in hFIB cells.



Figure A15. [redacted] inhibition by F3.24 and F3.24A at 10, 20 and 50 µM during 18h in hFIB cells.



Figure A16. [redacted] inhibition by F3.20 at 10, 20 and 50 µM during 18h in hFIB cells.



Figure A17. [redacted] inhibition by F4.1 and F4.2 at 10, 20 and 50 µM during 18h in U2OS cells.



Figure A18. [redacted] inhibition by F4.3 at 10, 15 and 20 µM during 6h, and 1 and 5 µM during 18h (ON) in U2OS cells.



Figure A19. [redacted] inhibition by F4.4 at 10, 20 and 50 µM during 18h in U2OS cells.



Figure A20. [redacted] inhibition by F4.5 at 10, 20 and 50 µM during 18h in U2OS cells.



Figure A21. [redacted] inhibition by F4.1 and F4.2 at 10, 20 and 50 µM during 18h in hFIB cells.



Figure A22. [redacted] inhibition by F4.3 at 10, 15 and 20 µM during 6h, and 1, 5 ad 10 µM during 18h in hFIB cells.



Figure A23. [redacted] inhibition by F4.4 at 10, 20 and 50 µM during 18h in hFIB cells.



Figure A24. [redacted] inhibition by F4.5 at 10, 20, 50, 100 and 200 µM during 18h in hFIB cells.



Figure A25. [redacted] inhibition by F5.1 and F5.2 at 1, 5 and 10 µM during 6h in U2OS cells.



Figure A26. [redacted] inhibition by F5.3 and F5.4 at 1, 5 and 10 µM during 6h in U2OS cells.



Figure A27. [redacted] inhibition by F5.5 and F5.6 at 1, 5 and 10 µM during 6h in U2OS cells.



Figure A28. [redacted] inhibition by F5.7 and F5.8 at 1, 5 and 10 μM during 6h in U2OS cells.



Figure A29. [redacted] inhibition by F5.9 and F5.10 at 1, 5 and 10 μM during 6h in U2OS cells.



Figure A30. [redacted] inhibition by F5.11 at 1, 5 and 10 μM during 6h in U2OS cells.



Figure A31. [redacted] inhibition by F5.1 and F5.2 at 1, 5 and 10 μM during 18h in U2OS cells.



Figure A32. [redacted] inhibition by F5.3 and F5.4 at 1, 5 and 10 μM during 18h in U2OS cells.



Figure A33. [redacted] inhibition by F5.5 and F5.6 at 1, 5 and 10 µM during 18h in U2OS cells.



Figure A34. [redacted] inhibition by F5.7 and F5.8 at 1, 5 and 10 µM during 18h in U2OS cells.



Figure A35. [redacted] inhibition by F5.9 and F5.10 at 1, 5 and 10 µM during 18h in U2OS cells.



Figure A36. [redacted] inhibition by F5.11 at 1, 5 and 10 µM during 18h in U2OS cells.



Figure A37. [redacted] inhibition by F5.1 and F5.2 at 1, 5 and 10 µM during 6h in hFIB cells.



Figure A38. [redacted] inhibition by F5.3 and F5.4 at 1, 5 and 10 µM during 6h in hFIB cells.



Figure A39. [redacted] inhibition by F5.5 and F5.6 at 1, 5 and 10 µM during 6h in hFIB cells.



Figure A40. [redacted] inhibition by F5.7 and F5.8 at 1, 5 and 10 µM during 6h in hFIB cells.



Figure A41. [redacted] inhibition by F5.9 and F5.10 at 1, 5 and 10 µM during 6h in hFIB cells.



Figure A42. [redacted] inhibition by F5.11 at 1, 5 and 10 µM during 6h in hFIB cells.



Figure A43. [redacted] inhibition by F5.1 and F5.2 at 1, 5 and 10 µM during 18h in hFIB cells.



Figure A44. [redacted] inhibition by F5.3 and F5.4 at 1, 5 and 10 µM during 18h in hFIB cells.



Figure A45. [redacted] inhibition by F5.5 and F5.6 at 1, 5 and 10 µM during 18h in hFIB cells.



Figure A46. [redacted] inhibition by F5.7 and F5.8 at 1, 5 and 10 µM during 18h in hFIB cells.



Figure A47. [redacted] inhibition by F5.9 and F5.10 at 1, 5 and 10 µM during 18h in hFIB cells.



Figure A48. [redacted] inhibition by F5.11 at 1, 5 and 10 µM during 18h in hFIB cells.



Figure A49. [redacted] inhibition by 2F1 and 2F2 at 1, 5 and 10 µM during 18h in U2OS cells.



Figure A50. [redacted] inhibition by 2F3 and 2F4 at 1, 5 and 10 µM during 18h in U2OS cells.



Figure A51. [redacted] inhibition by 2F5 and 2F6 at 1, 5 and 10 µM during 18h in U2OS cells.

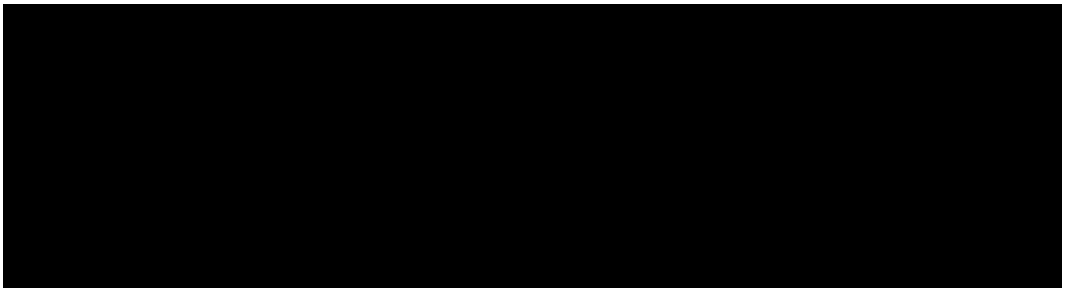


Figure A52. [redacted] inhibition by 2F7 and 2F8 at 1, 5 and 10 µM during 18h in U2OS cells.



Figure A53. [redacted] inhibition by 2F9 and 2F10 at 1, 5 and 10 µM during 18h in U2OS cells.



Figure A54. [redacted] inhibition by 2F11 and 2F12 at 1, 5 and 10 µM during 18h in U2OS cells.



Figure A55. [redacted] inhibition by 2F13 and 2F14 at 1, 5 and 10 µM during 18h in U2OS cells.



Figure A56. [redacted] inhibition by F6.1 and 2F15 at 1, 5 and 10 µM during 18h in U2OS cells.



Figure A57. [redacted] inhibition by 2F16 and 2F17 at 1, 5 and 10 µM during 18h in U2OS cells.



Figure A58. [redacted] inhibition by 2F18 and F6.2 at 1, 5 and 10 µM during 18h in U2OS cells.



Figure A59. [redacted] inhibition by 2F20 and 2F21 at 1, 5 and 10 µM during 18h in U2OS cells.



Figure A60. [redacted] inhibition by 2F19 and F6.3 at 1, 5 and 10 µM during 18h in U2OS cells.



Figure A61. [redacted] inhibition by F6.4 and F6.5 at 1, 5 and 10 µM during 18h in U2OS cells.



Figure A62. [redacted] inhibition by F6.6 and 2F22 at 1, 5 and 10 µM during 18h in U2OS cells.



Figure A63. [redacted] inhibition by 2F23 and F6.7 at 1, 5 and 10 µM during 18h in U2OS cells.



Figure A64. [redacted] inhibition by F6.8 and F6.9 at 1, 5 and 10 µM during 18h in U2OS cells.



Figure A65. [redacted] inhibition by F6.10 and 2F24 at 1, 5 and 10 µM during 18h in U2OS cells.



Figure A66. [redacted] inhibition by 2F25 and 2F26 at 1, 5 and 10 μM during 18h in U2OS cells.



Figure A67. [redacted] inhibition by 2F1, 2F2 and 2F3 at 20 and 50 μM during 18h in U2OS cells.



Figure A68. [redacted] inhibition by 2F4, 2F5 and 2F6 at 20 and 50 μM during 18h in U2OS cells.



Figure A69. [redacted] inhibition by 2F7, 2F8 and 2F9 at 20 and 50 μM during 18h in U2OS cells.



Figure A70. [redacted] inhibition by 2F10, 2F11 and 2F12 at 20 and 50 µM during 18h in U2OS cells.



Figure A71. [redacted] inhibition by 2F13, 2F14 and F6.1 at 20 and 50 µM during 18h in U2OS cells.



Figure A72. [redacted] inhibition by 2F15, 2F16 and 2F17 at 20 and 50 µM during 18h in U2OS cells.



Figure A73. [redacted] inhibition by 2F18, F6.2 and 2F19 at 20 and 50 µM during 18h in U2OS cells.



Figure A74. [redacted] inhibition by 2F20, 2F21 and F6.3 at 20 and 50 µM during 18h in U2OS cells.



Figure A75. [redacted] inhibition by F6.4, F6.5 and F6.6 at 20 and 50 µM during 18h in U2OS cells.



Figure A76. [redacted] inhibition by 2F22, 2F23 and F6.7 at 20 and 50 µM during 18h in U2OS cells.



Figure A77. [redacted] inhibition by F6.8, F6.9 and F6.10 at 20 and 50 µM during 18h in U2OS cells.



Figure A78. [redacted] inhibition by 2F24, 2F25 and 2F26 at 20 and 50 µM during 18h in U2OS cells.



Figure A79. [redacted] inhibition by 2F1 and 2F2 at 1, 5 and 10 µM during 18h in hFIB cells.



Figure A80. [redacted] inhibition by 2F3 and 2F4 at 1, 5 and 10 µM during 18h in hFIB cells.



Figure A81. [redacted] inhibition by 2F5 and 2F6 at 1, 5 and 10 µM during 18h in hFIB cells.



Figure A82. [redacted] inhibition by 2F7 and 2F8 at 1, 5 and 10 µM during 18h in hFIB cells.



Figure A83. [redacted] inhibition by 2F9 and 2F10 at 1, 5 and 10 µM during 18h in hFIB cells.



Figure A84. [redacted] inhibition by 2F11 and 2F12 at 1, 5 and 10 µM during 18h in hFIB cells.



Figure A85. [redacted] inhibition by 2F22 and 2F23 at 1, 5 and 10 µM during 18h in hFIB cells.



Figure A86. [redacted] inhibition by F6.1 and F6.2 at 1, 5 and 10 µM during 18h in hFIB cells.



Figure A87. [redacted] inhibition by 2F16 and 2F17 at 1, 5 and 10 µM during 18h in hFIB cells.



Figure A88. [redacted] inhibition by F6.2 and F6.6 at 1, 5 and 10 µM during 18h in hFIB cells.



Figure A89. [redacted] inhibition by 2F21 and F6.3 at 1, 5 and 10 µM during 18h in hFIB cells.



Figure A90. [redacted] inhibition by 2F23 and F6.7 at 1, 5 and 10 µM during 18h in hFIB cells.



Figure A91. [redacted] inhibition by F6.8 and F6.9 at 1, 5 and 10 µM during 18h in hFIB cells.



Figure A92. [redacted] inhibition by F6.9 and F6.10 at 1, 5 and 10 µM during 18h in hFIB cells.



Figure A93. [redacted] inhibition by 2F25 and 2F26 at 1, 5 and 10 µM during 18h in hFIB cells.



Figure A94. [redacted] inhibition by 2F1, 2F2 and 2F3 at 20 and 50 µM during 18h in hFIB cells.



Figure A95. [redacted] inhibition by 2F4, 2F5 and 2F6 at 20 and 50 µM during 18h in hFIB cells.



Figure A96. [redacted] inhibition by 2F7, 2F8 and 2F9 at 20 and 50 µM during 18h in hFIB cells.

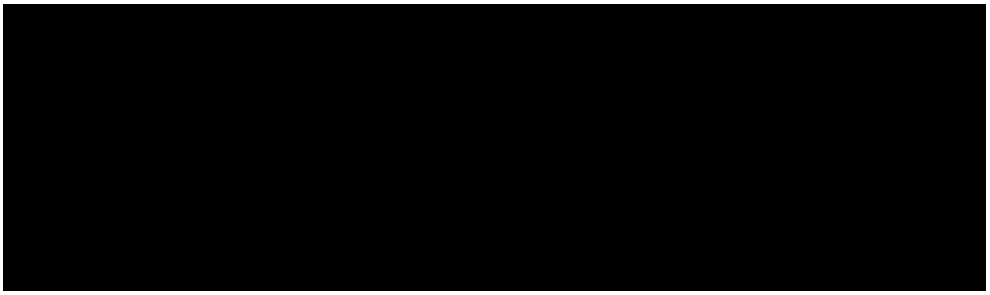


Figure A97. [redacted] inhibition by 2F10, 2F11 and 2F12 at 20 and 50 µM during 18h in hFIB cells.



Figure A98. [redacted] inhibition by 2F13, 2F14 and F6.1 at 20 and 50 µM during 18h in hFIB cells.



Figure A99. [redacted] inhibition by 2F15, 2F16 and 2F17 at 20 and 50 µM during 18h in hFIB cells.

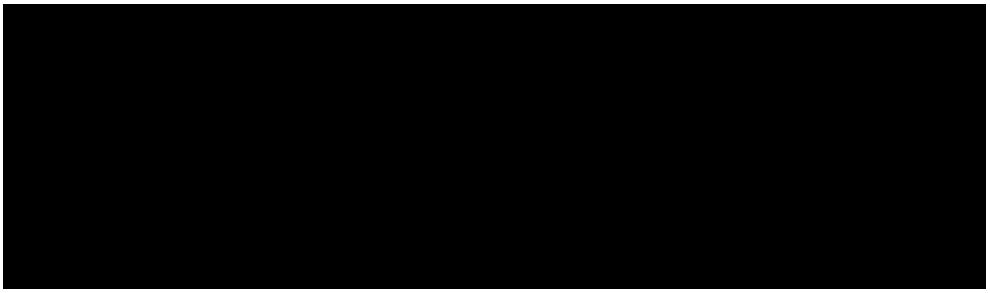


Figure A100. [redacted] inhibition by 2F18, F6.2 and 2F19 at 20 and 50 µM during 18h in hFIB cells.



Figure A101. [redacted] inhibition by 2F20, 2F21 and F6.3 at 20 and 50 µM during 18h in hFIB cells.



Figure A102. [redacted] inhibition by F6.4, F6.5 and F6.6 at 20 and 50 µM during 18h in hFIB cells.

		In vitro inhibition (µM)			K_D (SPR, µM)		Docking	FQ Prop.	Toxicity (µM)
		U2OS (6h)	U2OS (24h)	hFib (24h)	Mean	SD	Gscore	LogS	
[redacted]	**F1**	[redacted]			30.4	2.1	-6.98	-4.01	>50(6h)/ >40(24h)
	F27				17.8	1.5	-7.42	-5.35	>50(6h)/ >20(24h)
	F32				24.3	0.6	-8.75	-3.17	>50(6h)/ >40(24h)
	F2.14				8.23	-	-5.50	-4.62	>100(24h)

Figure A103. Best candidates of Fx and F2.x rounds: chemical formulation, *in vitro* validation, biochemical validation data and toxicity.

				K_D (SPR, µM)		Docking	FQ Prop.	Toxicity (µM)
		U2OS (24h)	hFib (24h)	Mean	SD	Gscore	LogS	
[redacted]	**F3.4**	[redacted]	[redacted]	X	X	-2.72	-	NO
	F3.5			47.0	54.7	-3.38	-	NO
	F3.6			X	X	-2.95	-	>50(24h) (vacuoles)
	F3.7			45.8	80.5	-3.4	-	NO
	F3.8			17.1	0.09	-3.15	-	NO
	F3.10			4.3	0.07	-3.07	-	NO (cristalls)
	F3.10 A			32.3	6.4	-	-	NO (cristalls)
	F3.14			148.2	-	-3.24	-	NO
	F3.19			27.1	3.3	-2.55	-	NO
	F3.20			27.5	18	-3.24	-	NO
	F3.21			137.7	-	-4.01	-	NO
	F3.24			116.6	93.5	-	-	NO
	F3.24 A			72.5	53.8	-	-	NO

Figure A104. Best candidates of F3.x round: chemical formulation, *in vitro* validation, biochemical validation data and toxicity.

	In vitro inhibition (μM)				K_D (SPR, μM)		Docking	FQ Prop.	Toxicity (μM)
	U2OS (6h)	U2OS (24h)	hFib (6h)	hFib (24h)	Mean	SD	Gscore	LogS	
F4.1	[redacted]				3	4	-	-	NO
F4.2					1348	211	-	-	>50(24h)
F4.3					3	2	-	-	>10(6h)/ >5(24h)
F4.4					X	X	-	-	NO (cristalls)
F4.5					332	235	-	-	NO

Figure A105. Best candidates of F4.x round: chemical formulation, *in vitro* validation, biochemical validation data and toxicity.

	In vitro inhibition (μM)				K_D (SPR, μM)		Docking	FQ Prop.	Toxicity (μM)
	U2OS (6h)	U2OS (24h)	hFib (6h)	hFib (24h)	Mean	SD	Gscore	LogS	
F5.1	[redacted]				X	-	-5.50	-4.62	NO
F5.2					2.5 (↓solub)	1.1	-3.10	5.4	NO
F5.3					93.4	7.0	-	-	>10(24h)
F5.4					37.0	43.9	-	-	>10(24h)
F5.5					44.0	20.9	-3.36	6.8	NO
F5.6					7.2 (↓solub)	7.4	-3.06	-5.7	>10(6h)/ >10(24h)
F5.7					X (↑solub)	-	-	-	NO
F5.8					34.1	16.0	-	-	>10(24h)
F5.9					58.3	3.4	-	-	>10(24h)
F5.10					29.7	10.4	-3.23	-6.7	>10(24h)
F5.11					81.9	20.9	-	-	NO

Figure A106. Best candidates of F5.x round: chemical formulation, *in vitro* validation, biochemical validation data and toxicity.

				K_D (SPR, µM)		Docking	FQ Prop.	Toxicity (µM)
		U2OS (24h)	hFib (24h)	Mean	SD	Gscore	LogS	
[redacted]	**F6.1**	[redacted]	[redacted]	199.2	89.2	-4.80	-	NO
	F6.2			↑	-	-4.94	-4.141	NO
	F6.3			↑	-	-	-	NO
	F6.4			↑	-	-4.35	-3.01	NO
	F6.5			X	X	-4.82	-3.19	NO
	F6.6			81.5	111.0	-	-	NO
	F6.7			88.4	79.6	-5.03	-3.85	NO
	F6.8			30.1	-	-	-	NO
	F6.9			↑	-	-	-	NO
	F6.10			357.4	366.8	-4.28	-4.04	>50(24h)

Figure A107. Best candidates of F6.x round: chemical formulation, *in vitro* validation, biochemical validation data and toxicity.

				K_D (SPR, µM)		Docking	FQ Prop.	Toxicity (µM)
		U2OS (24h)	hFib (24h)	Mean	SD	Gscore	LogS	
[redacted]	**2F1**	[redacted]	[redacted]	X	X	-6.15	-	NO
	2F2			X	X	-6.25	-	NO
	2F3			X	X	-6.19	-	NO
	2F4			X	X	-6.65	-	NO
	2F5			↑	-	-6.31	-	NO
	2F6			X	X	-6.10	-	NO
	2F7			X	X	-6.08	-	NO
	2F8			X	X	-6.00	-	NO
	2F9			↑	-	-6.41	-	NO
	2F10			X	X	-6.53	-	NO
	2F11			227.7	5.5	-6.72	-	NO
	2F12			X	X	-6.38	-	NO

Figure A108. Best candidates of 2Fx round: chemical formulation, *in vitro* validation, biochemical validation data and toxicity. Candidates from 2F1 to 2F12.

				K_D (SPR, µM)		Docking	FQ Prop.	Toxicity (µM)
		U2OS (24h)	hFib (24h)	Mean	SD	Gscore	LogS	
[redacted]	**2F13**	[redacted]	[redacted]	X	X	-6.12	-	NO
	2F14			X	-	-6.57	-	NO
	2F15			29.7	34.1	-6.09	-	NO
	2F16			10.0	1.6	-6.36	-	NO
	2F17			126.3	120.9	-6.82	-	NO
	2F18			X	X	-6.33	-	NO
	2F19			94.2	32.8	-6.34	-	NO
	2F20			241.0	14.5	-6.25	-	NO
	2F21			257.4	159.2	-6.22	-	NO
	2F22			X	X	-6.54	-	NO
	2F23			X	-	-6.49	-	NO
	2F24			X	X	-6.37	-	NO
	2F25			X	X	-6.31	-	NO
	2F26			X	-	-6.01	-	NO

Figure A109. Best candidates of 2Fx round: chemical formulation, *in vitro* validation, biochemical validation data and toxicity. Candidates from 2F13 to 2F26.

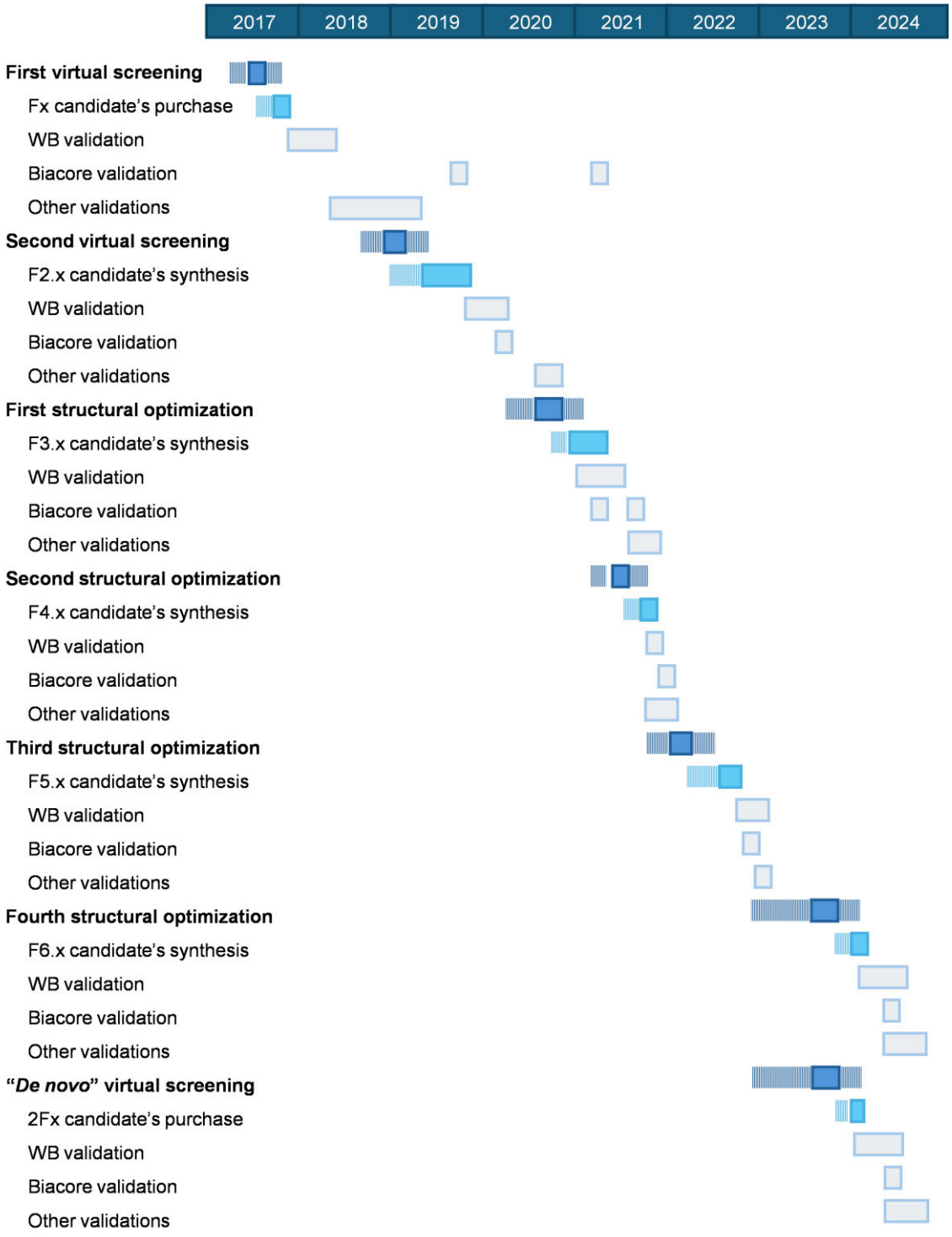


Figure A109. Time organization in Fanconinib project.

8.2. Appendix 2

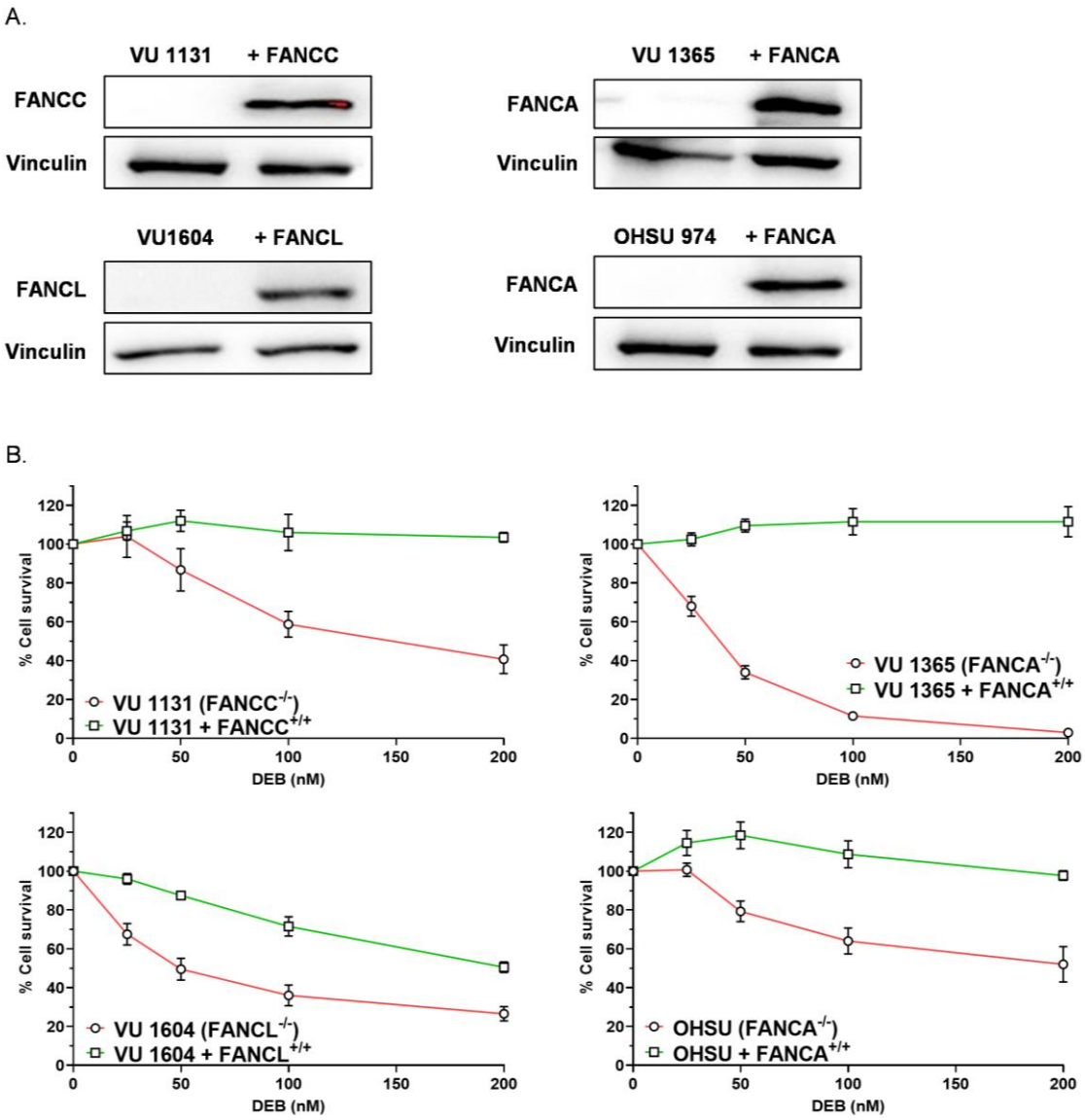


Figure A108. FA HNSCC and FA-corrected cell lines confirmation. A. Western blot of Fanconi proteins FANCA, FANCC and FANCL to confirm the deficient and corrected cell lines. **B**. DEB survival assays for the validation of the corrected cell lines. Graphs show mean +/- SEM of 3-5 experiments with similar results.

Table 1A. AR sporadic HNSCC overexpressed common genes.

Gene	Coding	logFC CAL 27	adj.P.Val CAL 27	logFC CAL 33	adj.P.Val CAL 33
[redacted]	protein coding	0.619954561	0.021257088	2.430653489	2.78163E-09
	protein coding	1.951042867	1.9877E-13	4.167745142	5.78084E-11
	protein coding	1.561818683	1.10248E-09	1.678831079	5.2631E-06
	protein coding	1.004013887	9.81222E-12	0.70445779	5.32846E-09
	protein coding	1.124478624	0.003043063	1.306171353	0.007111157
	protein coding	3.346357987	1.52061E-09	4.955110315	4.72827E-13
	protein coding	2.758512682	1.47822E-11	3.055824188	1.27518E-10
	protein coding	0.828538646	0.004314	3.47644404	4.91094E-07
	protein coding	1.385750816	5.48582E-11	1.332763299	8.48154E-06
	protein coding	1.543739807	0.000700108	2.5229873	2.83272E-08
	protein coding	0.7380387	0.048792391	2.630223763	7.74283E-07
	protein coding	0.591504023	4.82717E-07	0.946075645	1.91222E-10
	protein coding	5.163924427	6.84252E-12	2.497166601	0.002625945
	protein coding	3.746672795	7.98502E-05	4.589270993	4.77891E-05
	protein coding	0.679561638	9.38633E-06	0.834316842	2.38291E-07
	protein coding	0.905717611	1.63588E-07	1.22026921	2.39438E-09
	protein coding	1.309958725	4.70775E-12	2.326494315	1.76722E-08
	protein coding	6.056755969	3.56412E-08	2.939008366	0.011406397
	protein coding	2.07963179	1.28988E-05	1.006924514	0.010279969
	protein coding	1.160118417	3.79088E-12	1.216194598	3.74606E-12
	protein coding	0.735613329	0.047467892	1.827389761	0.00050477
	protein coding	1.670766181	6.79286E-11	0.859113334	9.16435E-07
	protein coding	3.037809902	3.03999E-09	1.822935209	2.41302E-05
	protein coding	2.228648179	0.001857447	2.703719009	0.00255599
	protein coding	1.330269373	2.0753E-05	1.523590318	2.08242E-06
	protein coding	0.743098276	0.049753542	1.05201001	0.006003893
	protein coding	0.935520888	3.44989E-08	0.873939011	4.81573E-07

[redacted]	protein coding	0.985066687	0.000290963	3.536061224	8.66546E-06
	protein coding	2.245613545	3.48436E-13	1.531001422	3.43318E-08
	protein coding	3.383299415	1.28103E-16	2.159254567	1.97752E-08
	protein coding	1.179557932	2.50527E-05	2.104140901	8.01113E-12
	protein coding	0.625996927	0.005547845	5.009806442	8.79924E-09
	protein coding	1.620384375	1.54192E-13	1.008599991	1.40415E-08
	protein coding	0.655707527	1.54629E-06	1.138343018	7.05182E-07
	protein coding	0.633325243	0.003499036	3.249025321	1.40226E-08
	lncRNA	0.761910805	0.004409943	1.156504863	0.001370317
	protein coding	1.491469175	1.09908E-05	0.61961342	0.043044266
	protein coding	0.894638283	1.9312E-11	0.98576919	5.31702E-12
	protein coding	0.616103747	0.001563679	0.600293034	0.000360504
	lncRNA	0.673347795	0.020910641	1.443319362	0.000913172
	protein coding	0.592870868	4.68587E-09	0.599856984	6.57528E-09
	protein coding	3.554714494	2.69972E-07	2.032619014	0.007535775
	protein coding	0.977445991	2.45944E-05	0.724807241	0.000843021
	protein coding	4.006872137	6.62331E-10	2.029446292	0.007726768
	protein coding	2.689333471	8.87739E-12	2.042225375	1.7124E-09
	protein coding	1.607636938	4.17695E-05	1.184003076	0.000344898
	protein coding	1.87235846	1.35847E-07	3.596336539	2.43857E-09
	protein coding	1.095870965	0.001247974	2.340745843	0.002467788
	protein coding	0.842463916	1.95544E-06	0.970075989	3.04232E-07
	protein coding	0.773732161	7.9197E-10	1.727569172	3.27364E-14
	protein coding	0.806132872	9.96391E-06	4.608519346	5.86948E-13
	protein coding	0.912567682	6.70009E-07	2.951213178	5.20431E-11
	protein coding	1.982387049	5.02404E-07	2.884661636	1.75697E-07
	protein coding	2.492198552	6.39169E-08	1.397250008	0.000977986
	lncRNA	0.810643542	9.34472E-06	1.36810036	6.2279E-06
	protein coding	2.256194302	9.33279E-05	2.457202363	0.004071861
	protein coding	1.123306455	0.000339053	4.476830793	1.97355E-06

[redacted]	protein coding	0.882361846	0.000164145	0.784411395	0.000160879
	protein coding	1.048163422	0.002417679	6.899566846	7.54011E-06
	lncRNA	0.704030635	7.64627E-07	0.70480914	2.84846E-05
	protein coding	1.77541671	7.15433E-10	1.356310482	6.34868E-08
	protein coding	0.950591236	0.000485754	1.319664694	1.02992E-06
	protein coding	3.835536635	8.85634E-06	5.03503846	1.05312E-07
	protein coding	1.707751617	2.78263E-10	1.191553685	6.27442E-06
	protein coding	1.205053149	0.005942322	2.720784604	0.003191304
	protein coding	2.875677058	2.92026E-08	1.687403758	0.000790063
	protein coding	1.012087385	8.1741E-09	0.948876442	6.77297E-07
	protein coding	1.09908113	1.40918E-06	1.700629339	4.04831E-06
	protein coding	1.289519864	2.07258E-09	4.022187478	1.03533E-13
	protein coding	0.794372089	0.003077838	4.826239556	0.014010426
	protein coding	1.56829409	1.98069E-09	3.099105911	1.0858E-14
	protein coding	0.814253843	0.000197169	1.039068331	1.46728E-05
	protein coding	0.624848975	0.000426523	0.859801681	1.54182E-05
	protein coding	5.367597447	9.1557E-19	12.38309238	2.08326E-15
	lncRNA	3.614156975	4.28048E-10	2.237814456	0.004266658
	protein coding	1.648281679	3.55932E-09	3.301230167	9.19302E-07
	protein coding	2.189985947	1.02441E-12	2.300199728	7.94605E-08
	protein coding	1.370222799	2.91448E-07	1.771050522	3.76242E-08
	protein coding	1.582837887	2.37234E-12	0.773508157	2.80875E-07
	protein coding	1.42597577	1.10065E-10	1.044035041	1.7157E-08
	protein coding	1.352273246	4.14199E-11	2.179463747	9.45539E-10
	protein coding	0.734400925	3.45793E-05	1.034211138	5.68722E-07
	protein coding	1.131317737	0.000906485	1.307781192	5.26156E-05
	protein coding	0.750107976	4.66652E-05	7.088036374	6.52448E-09
	protein coding	4.074593087	8.66094E-12	4.420670567	0.00016767
	protein coding	2.004580432	0.006050881	4.026164455	0.001357444
	protein coding	0.769888046	0.000299952	1.201712972	2.2155E-06

[redacted]					
	protein coding	2.199343941	5.84491E-06	2.174058853	5.78974E-07
	protein coding	2.416224055	3.16548E-07	3.717207934	2.93926E-08
	protein coding	0.635349546	0.003056651	0.920704742	7.15676E-05
	protein coding	0.632004087	0.001083491	0.902198431	2.8869E-05
	protein coding	1.00235738	0.01938869	2.435616088	6.19736E-05
	protein coding	1.126664978	1.09035E-08	0.689651097	1.09976E-05
	protein coding	0.935124992	7.64159E-08	0.93973762	1.45953E-08
	protein coding	0.832918352	1.56069E-06	0.594864307	0.000173864
	protein coding	4.865347239	2.41767E-05	2.863915052	0.016948288
	protein coding	1.251026663	9.16867E-05	1.021305255	9.57531E-05
	protein coding	1.624848478	5.44838E-11	2.342625564	6.47882E-14
	protein coding	0.580242379	4.66017E-06	0.902878733	1.42237E-08
	protein coding	1.004210619	3.70851E-06	0.710538433	0.000392912
	protein coding	0.763764482	2.31478E-07	0.703443242	1.13538E-06
	protein coding	0.918088606	3.52073E-06	1.001605666	1.21375E-08
	protein coding	0.892284599	0.004449924	4.914321291	3.998E-08
	protein coding	2.274731994	3.36393E-14	0.637223416	9.65907E-06
	protein coding	1.155802982	2.77749E-09	1.497871442	6.32107E-11
	protein coding	0.928156265	4.78445E-06	1.239560868	9.04197E-08
	protein coding	1.299160254	5.03987E-05	2.448096851	1.27968E-08
	protein coding	0.989545332	0.001857795	3.257650086	1.88013E-05
	protein coding	2.14266086	2.01983E-09	1.060493897	0.000100308
	protein coding	1.736583925	2.39158E-05	1.120880358	0.003440944
	protein coding	0.792059697	0.000808854	1.075741144	9.72748E-05
	protein coding	0.626718016	0.009405514	0.648336001	0.005550272
	lncRNA	1.172301617	0.014473271	1.230925019	0.018618171
	protein coding	0.923886544	1.31529E-09	1.324500783	1.12035E-08
	protein coding	2.173265171	4.7558E-18	0.918775728	7.47621E-09
	protein coding	1.715015013	1.13535E-06	5.019242612	1.53152E-09
	protein coding	1.943350641	1.46656E-08	3.15202868	1.69155E-10

[redacted]	protein coding	0.928703172	0.025420565	2.884005537	5.87722E-06
	protein coding	5.51356546	1.46424E-11	6.507606203	4.44062E-07
	protein coding	2.17127261	0.000108425	3.696113022	0.000812675
	protein coding	0.721127874	5.51005E-08	0.665774416	1.69915E-07
	protein coding	0.904173762	0.002476501	5.301476118	6.05697E-09
	protein coding	1.119745997	3.45833E-07	5.363208305	3.49718E-14
	protein coding	2.829505618	0.007231923	4.655797319	0.000726314
	protein coding	3.523402155	0.000503072	4.758475121	0.000376731
	protein coding	3.675431796	1.82816E-05	2.438403357	8.21176E-06
	protein coding	0.658282996	4.05687E-06	0.865795003	2.59479E-07
	protein coding	1.819695075	1.22156E-11	1.686156163	3.82643E-07
	protein coding	0.858390876	1.76471E-08	0.67231292	5.13934E-08
	protein coding	2.369999559	1.84478E-08	2.337894762	6.36774E-08
	protein coding	0.654050975	5.01464E-06	0.744819505	7.74283E-07
	protein coding	4.53790368	1.10298E-11	1.955167523	0.000239
	protein coding	0.655231334	0.000416026	1.030451323	1.92655E-06
	protein coding	0.964508987	3.42322E-06	0.737705698	1.05284E-05
	protein coding	1.602659837	6.85911E-07	1.407299557	0.004014331
	protein coding	4.440711535	2.29032E-11	2.889879095	5.15707E-10
	lncRNA	0.702250524	0.000807939	1.538768402	1.27816E-05
	protein coding	0.804302656	9.51877E-05	2.035565331	6.67682E-09
	protein coding	3.158203531	8.66094E-12	1.885289527	0.002357552
	protein coding	2.593766816	1.61069E-08	2.034826169	2.89445E-05
	protein coding	1.1247274	4.12645E-06	2.635238284	5.09092E-09
	protein coding	0.787522602	0.003871934	0.64530176	0.03551776
	protein coding	1.998647798	3.7557E-11	2.564591554	1.81619E-13
	protein coding	1.348345712	1.38142E-08	1.263324089	3.08601E-07
	protein coding	1.62663073	4.78851E-09	1.454515987	0.000364628
	protein coding	0.618150084	2.49192E-09	1.156518935	1.65073E-14
	protein coding	1.749187146	3.54809E-13	2.758636002	5.2697E-13

[redacted]	protein coding	3.818573413	1.23971E-14	1.595866019	4.97656E-08
	protein coding	2.134476059	1.09324E-08	1.495269396	4.19059E-07
	protein coding	0.777498611	0.000232604	1.078848508	5.61753E-06
	protein coding	0.619595018	1.69315E-06	0.734363336	3.73963E-08
	protein coding	1.929138831	6.22797E-07	1.874542728	0.000135287
	lncRNA	0.995647084	1.50912E-05	1.046053746	0.000101915
	protein coding	0.668850443	0.001608103	1.142527622	8.86101E-06
	protein coding	2.870195765	1.03578E-05	2.123954144	1.30173E-06
	processed pseudogene	1.469385249	0.002281783	2.400831177	2.64856E-06
	lncRNA	5.025680008	2.93146E-08	6.504871942	8.57145E-09
	lncRNA	2.019266604	0.014277474	2.657979067	0.020078065
	protein coding	2.372616756	0.000291181	7.188916896	8.50565E-08
	lncRNA	1.564493616	1.86284E-06	1.111450467	1.08329E-05
	lncRNA	1.395521162	0.001936334	2.252753604	0.000226691
	lncRNA	4.193594634	6.25774E-11	2.117991993	0.01055876
	lncRNA	0.813705772	0.016458991	1.069342252	0.024657352
	lncRNA	1.565912008	3.53367E-06	2.30954715	2.50132E-06
	transcribed processed pseudogene	0.839539968	0.000365259	0.588955545	0.038081638
	lncRNA	3.299173182	0.000139558	1.85491959	0.016850791
	lncRNA	1.234673037	1.17698E-07	0.619851828	0.006491708
	lncRNA	0.695775861	0.013907381	1.19106347	0.001094423
	lncRNA	2.282394214	9.21969E-05	2.299521678	0.000142579
	lncRNA	0.80641331	2.22657E-08	3.615363431	3.90855E-13
	lncRNA	1.980821378	1.10657E-07	2.423879778	4.56043E-07
	TEC	0.855178416	0.002753756	0.592214702	0.022249878
	TEC	0.960793013	0.001038753	1.060010694	0.00046679
	TEC	1.419701064	0.000162535	2.282114198	1.88354E-07
	TEC	1.060892982	0.000362654	1.060865461	0.000276578
	lncRNA	2.244050926	0.001142774	3.038444395	0.001169824

[redacted]	lncRNA	1.02616741	0.002213798	0.661407288	0.024069584
	lncRNA	1.903423597	0.001475928	1.311564363	0.038616486
	protein coding	1.596729106	0.003733468	8.440389813	5.45066E-07
	lncRNA	5.61603578	4.94681E-09	3.569974908	0.000426593
	lncRNA	0.834938931	0.002341094	0.616414195	0.020232091
	lncRNA	1.412119843	0.000343295	0.78554184	0.000310742
	lncRNA	4.882857065	2.77692E-08	3.64600043	0.00175306
	lncRNA	1.489983917	1.91114E-06	1.337546163	0.02456322
	lncRNA	1.2107165	0.001282744	1.536113175	0.03291462
	lncRNA	1.590821059	1.97081E-05	2.184719254	0.003148832
	lncRNA	1.62549504	2.08402E-06	2.82808046	6.99261E-08
	protein coding	1.6670493	0.008482031	2.139206461	0.028980726
	lncRNA	1.003614437	0.001294147	0.947833583	0.014313699
	lncRNA	5.995733989	9.88412E-08	5.023953257	1.05713E-08
	lncRNA	0.613436108	0.034940764	0.668059549	0.001358648
	lncRNA	1.047337953	0.000268363	3.658922722	3.03594E-06
	lncRNA	4.696605154	1.32544E-08	4.076015033	0.000121975
	lncRNA	3.424477243	8.52392E-11	1.296857886	0.000162208
	lncRNA	1.482138746	1.4089E-05	1.053691879	1.23882E-05
	lncRNA	1.405520548	8.18249E-07	1.346375164	3.38379E-06
	lncRNA	0.918419249	7.69795E-05	1.157892838	6.38567E-07
	lncRNA	0.972644503	0.000777648	2.304993017	1.40403E-06
	lncRNA	0.987076729	7.35443E-05	1.316554008	0.000607684
	lncRNA	1.48304816	3.09606E-05	1.335337196	0.000594473
	lncRNA	1.505868675	0.008099915	2.493402883	0.002457528
	lncRNA	1.330830477	5.37271E-06	1.733194628	0.000120866
	lncRNA	2.274211296	8.44065E-15	0.876394011	0.000733054
	protein coding	2.402557056	0.002442441	2.285066559	0.035428402
	protein coding	0.975310491	5.30048E-08	0.696749319	1.2436E-05
	protein coding	0.763211964	0.003343959	1.197545264	0.000114817

[redacted]					
	protein coding	0.84400887	1.18362E-07	0.85689557	1.87988E-07
	protein coding	0.824363619	2.1961E-08	1.088534329	2.61379E-10
	protein coding	0.86838569	0.002391576	1.13634475	1.77623E-06
	protein coding	1.335845131	5.22289E-08	1.583772655	1.22642E-08
	protein coding	1.683177578	4.78656E-09	0.933617311	0.00053816
	protein coding	2.575309996	4.26422E-08	1.185012962	3.81457E-06
	protein coding	3.680167634	5.58474E-14	1.618608201	6.18635E-07
	protein coding	2.198673035	1.13163E-08	1.345976431	4.06059E-06
	protein coding	5.095404948	8.54017E-12	1.203827303	2.74948E-05
	protein coding	5.404135804	5.82268E-06	4.470875804	0.000107134
	protein coding	4.113814143	6.01477E-09	2.947754083	2.51107E-06
	protein coding	0.915358386	0.004774179	0.984812535	0.00364145
	protein coding	0.628008347	0.00052745	3.48147381	8.28672E-11
	protein coding	1.258531807	9.92192E-08	3.568028082	1.43401E-12
	protein coding	0.897026802	4.17517E-10	0.680289636	2.31743E-07
	protein coding	1.46582613	3.30779E-09	1.512761378	1.13721E-06
	protein coding	2.542587541	2.05748E-13	1.655289668	4.35595E-11
	protein coding	0.707276285	3.47389E-06	4.969817505	3.75668E-10
	processed pseudogene	2.402103612	0.000317058	2.164219196	3.14263E-05
	protein coding	0.673424811	0.004539967	1.431423118	4.87706E-05
	protein coding	1.040337645	2.11116E-05	2.434736256	7.28317E-08
	lncRNA	1.123158824	0.000110514	0.618407161	0.028542696
	protein coding	0.85000591	3.70558E-09	0.883553687	4.07379E-08
	protein coding	0.736093872	0.000104995	0.779821233	2.48222E-05
	protein coding	0.668503808	0.00388967	0.944040641	9.36318E-05
	protein coding	0.71190777	0.002122103	0.811483421	0.000484659
	protein coding	1.409823452	1.19746E-05	0.581301487	0.006564171
	lncRNA	1.146796928	2.35226E-07	0.886872846	6.8783E-05
	protein coding	0.963879008	9.45558E-09	1.156934052	1.56875E-08
	protein coding	1.121173204	1.84573E-05	0.58595023	0.029121911

[redacted]	protein coding	0.617262758	0.024101582	0.885692836	0.009949462
	lncRNA	4.854812052	3.7657E-16	7.183149695	1.23785E-12
	protein coding	0.780777612	0.028975378	2.545689338	5.95826E-06
	protein coding	1.357366714	9.68583E-06	2.075845482	5.32827E-12
	protein coding	0.854121944	3.9945E-07	1.735312736	9.28423E-06
	protein coding	1.795906423	0.030115012	3.269861825	0.000284397
	protein coding	3.550953751	1.0459E-12	1.069275532	8.75294E-07
	protein coding	2.025386593	0.001026079	2.174717709	1.77959E-05
	protein coding	0.662119008	1.21094E-05	0.892660322	2.33023E-07
	protein coding	0.630868565	0.002373955	0.744134625	0.000357957
	protein coding	4.118123741	9.40083E-06	5.570611417	4.65842E-11
	protein coding	1.386322495	7.97187E-08	3.335156273	2.61723E-12
	protein coding	3.761520996	3.73753E-16	2.633642829	3.38152E-12
	protein coding	0.722245769	7.18153E-08	1.193778733	1.28688E-11
	protein coding	2.626610869	9.17596E-09	1.560410553	4.83259E-08
	protein coding	3.062331438	6.20521E-11	5.087542511	1.14821E-09
	protein coding	1.213034334	6.04914E-06	2.316289244	4.317E-10
	protein coding	1.676974039	1.3298E-07	0.600788312	0.026947666
	protein coding	1.613917303	1.40621E-13	1.136067129	5.81473E-10
	protein coding	3.299319053	7.87443E-09	0.783380459	0.010587161
	protein coding	2.357999267	5.61579E-06	2.838425204	0.000236291
	protein coding	1.061574004	3.24517E-12	2.190611656	5.60682E-18
	processed pseudogene	0.910050167	0.015915562	1.450833219	0.011632574
	protein coding	0.789695005	1.33178E-08	1.804194203	4.3041E-15
	protein coding	1.072978388	2.93303E-08	0.853736883	1.3958E-06
	protein coding	2.154033791	5.81921E-12	1.398561389	7.28317E-08
	lncRNA	1.255876576	0.003159884	1.881784689	0.005803814
	protein coding	1.664422867	1.0464E-05	1.67164446	0.000199639
	protein coding	1.86572789	1.3221E-08	1.543104773	0.029838853
	protein coding	0.869725937	1.58455E-10	1.154159067	7.66771E-09

[redacted]	protein coding	1.307207449	1.224E-09	0.640068023	0.000709686
	protein coding	1.033183142	3.4381E-07	2.198354485	3.34201E-11
	protein coding	1.236678153	1.00206E-08	0.993477057	0.000325645
	lncRNA	1.475018695	0.003707952	0.599090661	0.049995117
	protein coding	1.62763834	0.014723943	3.175029405	0.000781455
	protein coding	2.341726009	1.88439E-15	3.324000657	4.36998E-15
	protein coding	4.174549349	8.49417E-06	5.068832891	1.70386E-09
	protein coding	1.30230568	9.34192E-14	0.861622738	2.92379E-10
	protein coding	1.114287585	1.457E-07	3.300234055	1.50169E-12
	protein coding	1.964561283	5.85765E-09	1.100348498	0.000281131
	protein coding	1.374433263	2.75514E-05	0.760047336	0.000410918
	protein coding	1.843487519	0.015247371	2.525423156	0.001712539
	protein coding	0.623674058	5.56901E-08	1.268452025	3.02192E-13
	lncRNA	0.844093707	0.000223127	1.767774808	4.31235E-11
	lncRNA	1.654090106	0.017566936	1.398440362	0.024185569
	protein coding	0.790461916	4.68587E-09	0.71516379	2.07215E-07
	protein coding	1.070781114	0.000346899	2.520000204	9.14628E-05
	protein coding	1.283404494	2.16849E-06	1.751827356	3.49597E-08
	protein coding	0.633505051	0.002846735	1.075408776	4.82786E-05
	lncRNA	1.049446843	0.004177649	0.893883582	0.036123782
	protein coding	1.020366075	1.61535E-06	0.65251994	0.000587081
	protein coding	0.838066521	3.45793E-05	0.616070117	0.001277943
	lncRNA	0.696208334	0.03068384	1.719335819	0.000224115
	protein coding	2.149730391	0.00057273	1.89534739	0.022118492
	protein coding	0.851680013	0.000200012	2.320807304	6.27481E-09
	protein coding	1.069214519	1.16368E-06	5.2475622	6.91472E-05
	protein coding	1.157175926	1.0473E-07	0.593691497	0.001160999
	protein coding	0.926418376	1.18153E-09	0.678915948	2.04749E-07
	protein coding	0.932133223	3.32956E-10	0.940862593	3.85454E-10
	protein coding	0.941307717	5.07825E-06	1.738150855	7.51757E-10
	protein coding	1.425474825	2.18434E-09	5.525343169	9.0874E-13

[redacted]	protein coding	1.635855239	2.70063E-05	0.930844617	0.002354476
	protein coding	0.751339797	3.19436E-07	2.193758087	1.0378E-13
	protein coding	2.176526439	0.003285026	3.544843103	2.24457E-07
	protein coding	2.945039589	5.22138E-08	1.037660105	0.000885369
	protein coding	2.079721904	0.000123899	2.001895517	0.031577817
	protein coding	1.568475193	6.63746E-08	5.780442976	6.95282E-15
	protein coding	2.625847761	4.17935E-10	9.677454193	2.3011E-09
	protein coding	1.01500912	7.0688E-10	0.781672051	8.5932E-08
	protein coding	4.130896863	2.63976E-11	2.116833377	9.72446E-08
	protein coding	2.292668421	6.32185E-14	2.263302874	3.85043E-13
	protein coding	1.491711472	3.26052E-05	4.792690702	4.84217E-08
	protein coding	3.840149503	4.04072E-13	2.070834587	0.027424762
	protein coding	2.975348186	1.35316E-05	3.22179853	1.6573E-05
	protein coding	1.015971878	0.001458371	0.744496365	0.024853193
	protein coding	2.316609684	5.85052E-15	1.06033655	2.20184E-05
	lncRNA	0.714626313	0.005046466	1.020362178	0.001832971
	protein coding	3.058682517	5.50643E-05	4.03649628	7.79089E-06
	protein coding	3.230907096	5.25702E-08	4.888371508	4.44E-06
	lncRNA	1.145757479	0.005911819	2.212877321	0.000328971
	protein coding	2.286768371	6.67565E-15	1.749616765	1.51124E-10
	protein coding	2.0918689	1.83747E-10	3.43887972	1.55487E-06
	protein coding	0.790362379	0.001116528	1.421447355	3.36638E-07
	protein coding	1.044834043	0.000375903	2.728266357	6.05766E-06
	protein coding	0.867621974	0.011016258	0.943692975	0.000356672
	protein coding	0.828923649	0.000534555	1.584448353	0.002226421
	protein coding	2.89807623	6.82534E-10	1.541128627	8.5594E-08
	protein coding	1.302975467	1.13247E-07	1.371781091	8.22034E-08
	lncRNA	0.65148925	0.00099287	0.991430289	0.000285712
	protein coding	0.674452587	0.002575275	0.968945955	8.61891E-05
	protein coding	0.710241344	8.56984E-05	0.616184285	0.000843971

[redacted]	protein coding	2.345201559	4.97058E-07	2.011300633	3.52526E-05
	protein coding	1.138997439	1.62714E-10	0.939576016	1.15551E-07
	protein coding	1.192190495	0.00402551	0.979613147	0.008032795
	protein coding	1.202364512	6.19039E-12	1.982044694	1.85812E-15
	protein coding	1.501156246	3.44604E-07	1.647326063	1.20204E-05
	protein coding	1.744661398	3.21302E-08	2.494322289	1.27933E-06
	protein coding	2.402424968	1.04843E-05	6.796277719	5.54611E-08
	protein coding	3.466659587	5.03793E-06	6.314135884	6.45701E-09
	protein coding	0.721235871	0.000567984	0.725765461	0.000516818
	lncRNA	1.234755732	0.01021681	2.704268159	0.004169178
	protein coding	1.972734789	2.18356E-07	0.820130923	0.008054767
	protein coding	1.236095407	2.03817E-05	1.425091483	9.0164E-06
	processed pseudogene	2.557927327	6.45858E-09	0.846595441	0.029949869
	protein coding	3.912548318	1.14626E-05	5.932091392	8.56805E-07
	protein coding	1.699469412	5.13903E-07	3.766907435	3.17809E-08
	protein coding	1.487501107	1.70795E-13	0.938090008	9.19206E-10
	protein coding	0.987727465	4.80984E-12	0.676698832	7.39328E-09
	protein coding	1.716506136	3.70912E-11	5.136944503	1.05087E-08
	protein coding	0.791827966	1.63847E-05	1.022156283	1.99907E-07
	protein coding	1.02209139	2.37891E-11	0.654235296	8.22985E-08
	protein coding	1.210037828	5.85123E-09	0.665423299	5.10443E-05
	protein coding	0.794515666	1.31597E-06	0.661529849	2.56057E-05
	protein coding	1.547749814	1.55445E-07	3.328037816	5.31834E-06
	protein coding	1.08997258	0.000757012	2.644172703	7.16081E-10
	protein coding	1.174842884	0.000128179	0.753964346	0.004854404
	protein coding	1.354215883	2.26832E-08	1.961869542	3.39728E-10
	lncRNA	1.381809165	0.000132095	1.936106722	4.00726E-06
	protein coding	2.093475496	1.44293E-05	2.201455331	0.004310613
	protein coding	2.231620708	6.82126E-14	4.498709182	1.16883E-14
	protein coding	1.239223123	1.80959E-09	0.628112521	0.000410743
	lncRNA	1.032849977	0.00268129	1.860371142	0.000546743

lncRNA	2.751114916	4.13764E-05	1.531391426	0.005525579
lncRNA	0.838609585	6.07451E-06	0.69871349	0.000487579
lncRNA	2.143906677	1.52675E-09	1.242721031	0.000277327
lncRNA	1.049528288	0.035647877	4.809653018	1.4359E-08
lncRNA	1.076647637	0.036208661	2.586211185	0.000880671
lncRNA	0.831096654	0.02061025	2.285712093	2.53821E-06
lncRNA	1.512992156	0.000955948	1.655989913	0.003258319
lncRNA	1.572461137	2.46172E-06	4.329201186	1.49194E-07
lncRNA	4.446991084	9.46703E-09	1.682769199	0.000235359
lncRNA	0.617549619	8.52044E-06	0.901283303	7.37658E-08
lncRNA	1.770143378	0.00119207	1.212845526	0.023572412
lncRNA	1.795177275	0.000457611	1.992197551	0.004952042
lncRNA	3.828289816	2.34872E-06	1.723474853	0.001187192
lncRNA	0.673949131	7.02968E-05	0.813703572	0.001448654
lncRNA	1.747323982	1.00478E-05	0.962994773	0.044033943
lncRNA	3.929289238	4.0583E-08	2.253000327	0.007329352
lncRNA	1.755188846	0.001064643	2.843707798	0.001194244
lncRNA	0.71092068	2.01715E-05	6.654744104	2.79859E-12
lncRNA	1.430787763	7.76659E-06	0.992340518	0.027841185
protein coding	0.614476967	2.77692E-08	0.71147955	2.88533E-09
protein coding	0.686294353	4.84858E-06	0.973378826	7.84292E-08
protein coding	0.913196773	3.30364E-06	1.74418574	9.06075E-10
protein coding	0.717716407	7.75509E-05	0.797066267	7.35506E-05
protein coding	1.827687326	3.11802E-13	1.874725311	1.05741E-09
protein coding	1.240038544	0.0169371	1.894470807	0.021303348
protein coding	2.36693049	2.63502E-13	2.065254509	3.43198E-11
protein coding	1.988748065	9.58466E-16	1.329889084	1.23785E-12
protein coding	0.872333272	4.47951E-06	1.844478157	2.72219E-08
protein coding	2.410782306	1.90526E-11	5.305984537	4.94293E-10
protein coding	1.082533635	1.38142E-08	3.144817613	3.90933E-13
protein coding	0.690313802	2.42909E-07	0.602598628	1.89244E-05
protein coding	0.686493387	7.22579E-06	0.630685893	4.07605E-06
protein coding	1.073173451	0.009405514	3.834236066	1.15313E-05
lncRNA	0.60104662	0.034717435	1.317382593	0.000658664
protein coding	0.594643014	1.5636E-07	0.833495405	1.11971E-09

[redacted]	protein coding	1.517878509	2.90058E-14	0.707423893	4.45371E-08
	protein coding	1.309580028	7.07641E-05	2.065484132	0.000133551
	protein coding	0.689363398	3.0192E-06	0.990350656	1.16384E-08
	protein coding	0.935120814	0.000220969	1.879986505	2.06948E-05
	protein coding	2.073501784	1.49046E-08	0.651784447	0.00854367
	protein coding	1.786105304	1.14575E-10	0.932703248	2.83671E-05
	lncRNA	0.644904888	0.033179974	0.747994636	0.011884139
	protein coding	0.892570748	0.003340942	1.924068098	0.000108969
	lncRNA	5.496590042	8.28653E-07	0.930739589	0.016905978
	lncRNA	0.910230091	0.000800351	6.615903293	2.92858E-09
	protein coding	1.734285474	2.94121E-13	1.928814583	1.30169E-12
	protein coding	0.956663669	0.000256174	1.099952043	0.00656042
	protein coding	0.786571837	2.27836E-07	1.006648263	8.11918E-09
	protein coding	0.932272318	2.57397E-05	0.618993918	0.002911781
	protein coding	1.144023399	7.22579E-06	1.109524215	0.000108159
	protein coding	1.282624395	0.00925986	0.924451737	0.004162187
	protein coding	1.374259266	5.30048E-08	1.559410794	2.0283E-08
	protein coding	1.41320228	0.000921413	5.557764073	1.69755E-05
	protein coding	2.22724639	4.27719E-07	0.650666963	0.01674426
	transcribed unitary pseudogene	2.236718503	0.006276922	1.819503934	0.002817381
	protein coding	3.85993908	1.90526E-11	1.11695078	0.022344694
	protein coding	1.561405326	3.70361E-09	0.786527317	0.000240394
	protein coding	4.178808839	4.54582E-06	1.220165957	0.003206383
	protein coding	1.288217123	0.000412007	1.372213993	0.004694272
	protein coding	3.239468735	1.12482E-09	1.46703874	0.00908125
	protein coding	1.502685339	0.001003452	2.276334288	2.16113E-07
	lncRNA	2.049268726	1.20871E-09	1.271974888	0.000210399
	protein coding	0.647314214	0.001453478	0.92166255	4.77891E-05
	protein coding	1.250574069	3.84412E-12	0.837782291	7.93001E-09
	protein coding	1.445897258	1.23867E-12	1.510816341	1.41826E-12

[redacted]					
	protein coding	0.687493824	5.28594E-06	0.858976599	3.17526E-07
	protein coding	0.631234617	5.21355E-05	0.888165551	6.16354E-07
	protein coding	1.381785034	0.000585293	0.919155913	0.015663106
	protein coding	1.850228282	1.73379E-06	3.600675806	6.85727E-07
	protein coding	2.352543516	2.86786E-18	2.956941909	8.23457E-19
	protein coding	0.631822887	7.47199E-06	1.756195734	1.76869E-12
	protein coding	0.74087825	1.69804E-05	1.827937499	4.18328E-11
	protein coding	1.050094251	3.60417E-06	0.67744159	0.001194244
	protein coding	3.437801591	2.09112E-08	1.782050394	1.08657E-05
	protein coding	1.325335977	5.48582E-11	1.122754874	7.60093E-08
	protein coding	5.423663871	8.86098E-10	2.11718474	0.037626775
	protein coding	0.854436402	8.49353E-07	2.007358789	3.02192E-13
	protein coding	0.636330333	1.76051E-07	0.588783853	5.55476E-07
	protein coding	2.315481684	1.21944E-08	1.588361047	2.01678E-08
	protein coding	0.679347701	7.03694E-07	0.950699404	7.05366E-07
	lncRNA	1.616306569	0.004368615	1.635305787	0.001113898
	protein coding	0.746778135	3.81363E-05	0.638582511	0.000629664
	protein coding	2.472910395	5.87156E-12	2.483888335	0.00507287
	protein coding	1.662360119	5.41693E-13	1.024757356	5.58467E-09
	protein coding	0.994908842	1.13467E-05	4.727834661	5.44516E-15
	protein coding	0.925555942	2.47187E-09	0.621143561	2.27876E-06
	protein coding	0.811945516	5.37129E-05	1.165325488	4.91292E-07
	protein coding	1.034325422	0.003576288	0.897682192	0.011981476
	protein coding	1.177939484	0.006393764	1.645095879	0.008890694
	protein coding	1.541385626	4.35257E-05	2.870753396	0.004379526
	protein coding	0.75590897	2.34389E-05	0.952768873	1.60956E-05
	protein coding	1.148687022	4.95727E-08	0.824166811	6.1482E-06
	protein coding	1.317509645	6.99529E-06	3.283506206	2.63686E-09
	protein coding	1.021013788	0.002187493	2.282748191	3.48342E-08
	protein coding	0.750883264	0.013634332	2.873689089	5.42789E-06

[redacted]	protein coding	0.595797773	2.82776E-10	1.033849605	1.16883E-14
	protein coding	1.21779201	4.10575E-07	0.872752953	0.000206128
	lncRNA	3.12402232	7.48039E-05	3.470841787	0.001236389
	protein coding	1.317495458	5.55802E-06	2.066764988	2.70573E-09
	protein coding	0.70395261	7.28197E-06	0.791125734	3.51588E-06
	protein coding	1.209470744	1.59595E-08	1.479832788	6.30763E-12
	protein coding	2.45707027	4.23891E-07	3.182812214	5.01198E-10
	protein coding	2.11068228	0.013968754	5.171019437	6.06043E-06
	protein coding	2.22897412	2.42911E-09	3.381525383	1.36046E-08
	protein coding	2.79611914	1.39315E-08	2.760599104	3.76357E-08
	protein coding	0.733844287	5.90376E-11	1.213601674	5.56916E-15
	protein coding	0.748721154	1.00834E-07	0.618303377	1.99405E-07
	protein coding	0.841511794	8.46457E-08	1.744339307	6.79019E-12
	protein coding	1.263851314	0.019438067	4.741352125	5.48278E-07
	protein coding	0.905958311	0.003586445	0.823863042	0.035664954
	protein coding	0.770109483	9.98853E-05	0.968848489	7.62107E-06
	protein coding	0.617581394	7.2581E-05	0.877554576	2.34983E-07
	protein coding	1.630022551	2.03326E-11	0.828485933	1.11424E-05
	protein coding	1.093379976	4.18988E-07	2.132693818	4.34302E-12
	protein coding	1.037441213	5.40117E-08	1.296996171	0.005142171
	protein coding	0.644237109	6.06939E-06	0.669726187	1.88679E-05
	protein coding	0.614371566	0.009974107	0.76229064	0.002372047
	protein coding	1.054192826	1.11816E-08	1.733776382	1.58011E-12
	protein coding	1.320641469	4.07551E-06	0.730626493	0.000850681
	protein coding	3.070277894	1.66737E-10	1.074832816	2.4315E-05
	lncRNA	1.114932652	4.28043E-05	1.752518033	1.19385E-06
	protein coding	0.808398548	0.0039158	0.596500597	0.032363774
	protein coding	0.742588823	1.09437E-07	0.937796657	2.56818E-09
	protein coding	0.767413229	1.0666E-08	1.143753645	4.84359E-11
	protein coding	1.808245181	4.29005E-05	2.18761437	0.000406788

[redacted]	protein coding	0.585872742	0.006849569	0.773285536	0.001205443
	lncRNA	0.909952184	1.28029E-07	0.963516039	1.17161E-06
	lncRNA	1.135853423	0.014572748	2.869237752	0.000239074
	protein coding	1.587134488	5.83339E-06	1.491119419	4.7321E-07
	protein coding	0.9836228	3.74264E-05	1.296544997	4.04863E-06
	protein coding	1.0167046	8.53899E-10	0.608547498	8.21136E-06
	protein coding	0.762862917	0.000819003	0.628589291	0.002247655
	protein coding	1.216637833	8.64604E-05	3.132218837	9.40125E-09
	protein coding	2.259026013	7.5428E-14	1.750922511	3.65151E-11
	protein coding	1.223002314	8.99734E-10	6.84024291	8.93424E-14
	protein coding	0.687790943	2.46256E-06	1.147643536	7.31062E-10
	protein coding	0.673652059	1.3045E-05	0.842200976	7.97341E-07
	protein coding	3.398344113	1.27615E-12	5.285578049	6.77495E-12
	protein coding	2.536413401	1.24384E-11	3.597511702	1.86026E-20
	protein coding	0.645098744	9.86233E-07	0.910136853	5.2847E-09
	protein coding	0.965969148	3.53318E-07	1.567554131	1.30094E-07
	protein coding	3.088010812	0.000257544	3.334916511	6.55367E-07
	protein coding	1.269010944	1.24384E-11	0.736647725	2.24545E-07
	lncRNA	1.289805746	0.000432417	0.765330205	0.01134877
	protein coding	2.232159808	2.02811E-14	0.607662391	8.22399E-05
	protein coding	0.663057681	2.16056E-09	0.581828067	2.64389E-08
	protein coding	1.504508706	0.007583012	2.383891671	0.009357786
	protein coding	0.700348585	1.21641E-07	0.811864994	9.8896E-09
	protein coding	1.03154896	1.33604E-08	1.711342238	1.10981E-08
	protein coding	1.913144439	3.04058E-17	1.875505683	5.85819E-08
	protein coding	0.952748467	1.38142E-08	0.674392221	2.25016E-06
	protein coding	1.065959349	1.86329E-05	3.322305617	2.94795E-07
	protein coding	3.462236316	1.04301E-06	2.960570444	0.003550133
	protein coding	1.248735464	6.60923E-16	0.90491815	4.50669E-13
	protein coding	0.935568516	0.006741243	3.221106579	4.44364E-08

[redacted]	protein coding	0.969342667	1.43366E-08	1.210489269	8.62145E-09
	protein coding	0.857514462	6.26013E-05	2.553995779	5.77438E-08
	protein coding	0.644403027	0.000583373	0.873822134	1.39447E-06
	protein coding	1.70487177	1.67396E-11	1.718049377	0.000138231
	protein coding	1.618178855	1.05841E-07	1.313876568	0.003579219
	protein coding	0.65176941	2.85217E-06	1.288641675	8.19833E-11
	protein coding	1.522425143	1.87719E-07	0.849360019	7.8204E-05
	protein coding	0.668895092	2.94258E-08	0.717839646	1.11609E-09
	protein coding	2.6930293	4.61948E-14	1.877467771	0.018884784
	protein coding	2.069737545	2.32266E-08	2.244630837	8.22497E-06
	protein coding	0.675372081	0.016830512	0.609400364	0.026292961
	protein coding	2.959139189	2.91535E-06	0.63575581	0.044521171
	protein coding	4.802569726	5.20085E-08	3.956330268	7.00721E-06
	protein coding	0.843601254	6.30679E-07	1.48749433	1.0398E-08
	protein coding	1.371926623	1.43636E-07	1.498501602	5.71339E-06
	protein coding	2.107159587	0.002947146	3.573565547	0.000250019
	protein coding	1.781238238	2.258E-10	1.949924684	0.004372256
	protein coding	0.793865301	4.51538E-06	2.252405675	6.13287E-12
	protein coding	0.904254455	8.01755E-07	7.282383248	2.43951E-13
	protein coding	1.730105112	8.13252E-09	1.454190402	2.11572E-07
	protein coding	1.602371938	1.51012E-15	1.350268788	1.90856E-13
	protein coding	0.947232999	0.000381374	0.639636196	0.010742003
	protein coding	0.930633595	1.09874E-09	1.063222479	1.34599E-10
	protein coding	0.822584792	0.041823952	2.195645698	1.3693E-05
	protein coding	1.068567179	6.74933E-06	1.217533445	9.75629E-07
	protein coding	0.971888002	0.000527957	1.55398268	1.13886E-05
	protein coding	1.650699727	6.23712E-06	2.032956711	7.44497E-06
	lncRNA	2.544455069	0.016204794	7.047290433	8.12244E-09
	protein coding	0.827377132	0.000375503	3.639840043	4.0127E-07
	protein coding	0.598801633	0.001619836	1.260260163	3.10517E-06

[redacted]

lncRNA	4.435958109	6.4489E-06	3.630071987	1.66463E-07
protein coding	1.27080759	2.64495E-11	0.812713147	3.51729E-08
protein coding	1.02931679	0.045785673	2.496316558	0.000769142
protein coding	4.359769206	5.21693E-11	1.74002458	0.019669828
protein coding	4.597481221	4.39138E-14	3.023772201	3.24768E-06
protein coding	0.935662163	0.000461743	2.594690028	6.61022E-08
protein coding	0.826457588	1.23342E-06	0.778069207	3.53604E-06
protein coding	0.607600099	6.19855E-06	1.225093505	1.86696E-10
protein coding	3.086544072	7.54148E-10	0.856912795	0.032919891
protein coding	2.158614217	4.63754E-13	1.770783035	1.77096E-10
protein coding	1.90902055	1.01679E-06	0.83744674	0.005055972
lncRNA	1.251050274	0.001956089	1.841108	0.002518088
protein coding	0.760386005	1.63263E-09	0.710142921	1.46767E-08
protein coding	1.311970076	1.64411E-07	1.128322559	2.54822E-07
protein coding	1.051870756	0.000806151	2.826312655	2.64389E-08
lncRNA	2.441674179	2.20773E-06	5.100835799	8.77085E-07
protein coding	1.337211568	3.39112E-08	4.655571642	7.16772E-11
protein coding	0.651765817	0.000920591	0.912605111	2.2155E-06
protein coding	2.529407669	1.67974E-14	3.608545495	6.46161E-14
protein coding	1.306510099	2.71283E-05	1.487584513	4.18075E-05
protein coding	1.499287516	4.31326E-13	1.012649645	2.31326E-10
protein coding	1.416167165	1.67376E-06	2.223990392	0.000993267
protein coding	1.729293837	3.48576E-09	2.253737561	2.34996E-11
lncRNA	1.580684112	0.003631458	3.322266174	0.000513044
protein coding	2.783902059	9.10477E-07	1.58823401	2.4173E-05
protein coding	1.198869646	0.005141973	1.455961921	0.032610392
protein coding	1.416843817	0.000447695	2.097067762	2.84723E-06
protein coding	0.606613488	2.14927E-05	1.189044746	1.4359E-08
protein coding	3.81413482	2.09001E-12	2.525489213	3.43198E-11
protein coding	1.822150282	8.84375E-05	2.426813987	2.51033E-06

[redacted]	protein coding	1.216465558	0.002865241	1.030197021	0.002431295
	lncRNA	0.895781628	7.48048E-05	0.625055774	0.006581006
	protein coding	0.791470717	0.000129389	2.491690994	6.43507E-10
	protein coding	0.882491667	8.51323E-07	2.07464883	1.04952E-07
	protein coding	1.829616439	5.61438E-09	1.462298447	5.05567E-07
	protein coding	1.307623486	0.003163717	1.404040098	0.000124513
	protein coding	1.710015142	1.1715E-15	3.495928245	2.38232E-21
	protein coding	1.638059384	1.08738E-09	1.996392937	2.12092E-11
	protein coding	1.070204544	2.67843E-10	0.608977281	7.92049E-06
	protein coding	3.475203711	4.21033E-11	0.984247721	0.00071707
	protein coding	0.637933284	3.47308E-07	0.81225835	1.76317E-08
	unprocessed pseudogene	0.715856983	0.002403984	0.647855303	0.001933407
	protein coding	0.815297653	0.001227322	0.595141751	0.000998136
	protein coding	1.481831873	5.09331E-12	4.369389337	4.66614E-07
	lncRNA	0.697470382	0.014102093	1.597575582	8.75076E-05
	protein coding	2.774592282	2.76817E-11	1.028605299	0.010468888
	lncRNA	4.31451654	5.73272E-12	9.152138998	1.58011E-12
	protein coding	0.692111827	7.59758E-09	0.860728298	9.06075E-10
	protein coding	0.904975241	0.001548413	3.600758843	2.91722E-07
	protein coding	0.729860798	1.70362E-07	0.748132129	1.52216E-07
	lncRNA	1.006082887	1.85574E-07	1.466761312	3.78466E-09
	protein coding	0.770063766	1.57939E-09	0.673205948	5.47241E-09
	protein coding	3.011666405	4.71594E-11	2.641126792	0.001574791
	protein coding	1.112413756	1.92593E-06	1.406518077	7.88192E-07
	protein coding	5.005482493	1.38367E-12	2.470494469	7.55595E-10
	protein coding	5.27661138	5.07352E-06	2.96242443	0.006038988
	protein coding	0.804713685	0.039994089	1.391442202	7.31373E-05
	protein coding	1.379600527	0.003292005	1.731030371	0.001134475
	protein coding	0.84262566	0.016887413	3.128499208	3.52933E-07
	protein coding	0.674991768	4.80441E-09	0.736224809	4.36905E-09
	protein coding	2.05900056	8.47749E-12	0.598333238	0.007446502

[redacted]	protein coding	0.929301445	1.22077E-07	1.469277502	5.20118E-12
	protein coding	0.655640274	9.40318E-06	2.149393026	2.34996E-11
	protein coding	1.43200236	2.07739E-13	0.758498632	3.56612E-08
	protein coding	1.43227507	0.000695836	2.737880035	2.30662E-06
	lncRNA	1.376385083	0.002701337	3.012846373	6.80889E-06
	protein coding	2.786085758	2.03712E-13	6.682145922	4.06214E-09
	protein coding	1.786480196	0.000223545	2.128807125	0.00994258
	protein coding	2.769977871	1.46171E-06	1.42638183	0.004192133
	lncRNA	3.102108271	4.14342E-09	2.074931227	0.000566534
	protein coding	1.754455703	1.22526E-15	0.831066491	6.90244E-08
	protein coding	2.278285206	6.87202E-20	2.701989226	9.66769E-19
	protein coding	1.033764639	2.79849E-09	0.663088523	4.8653E-06
	protein coding	1.580641327	0.005050759	1.080284377	0.020429344
	protein coding	2.058430752	5.74654E-11	2.075794158	2.03851E-08
	protein coding	3.005680814	0.009202949	4.204347042	0.000806213
	protein coding	1.618865069	0.00010004	2.2279167	0.002274037
	protein coding	1.211660187	2.31398E-07	2.05220236	2.69963E-05
	protein coding	3.792814852	3.06194E-18	3.692588004	3.32911E-05
	protein coding	0.830567793	5.98674E-05	1.553071438	2.16535E-08
	protein coding	1.410729097	1.01194E-11	0.604566436	1.00963E-05
	lncRNA	1.066378025	2.78736E-06	0.915241142	5.40218E-06
	protein coding	3.33215378	6.76176E-08	1.837217745	0.000913775
	protein coding	1.048686477	0.000162919	3.173987825	0.003856347
	protein coding	1.398374913	2.10489E-07	2.523175504	9.5989E-08
	protein coding	2.814803439	2.258E-10	3.589479085	1.83781E-11
	protein coding	1.254051	0.037120836	2.319118942	0.000534576
	protein coding	0.788385224	6.3629E-09	0.794654875	7.39328E-09
	protein coding	0.977326129	0.004052252	0.850826623	0.004133922
	protein coding	0.899373721	8.21662E-09	1.37738749	6.34999E-11
	protein coding	0.728410005	4.13242E-07	0.687184039	3.15578E-07

[redacted]	protein coding	1.84769854	4.78865E-08	3.699187443	6.42988E-07
	protein coding	0.792480874	0.00015479	1.21959892	3.73875E-05
	protein coding	2.109616216	2.34642E-12	0.598586307	0.000626903
	protein coding	0.991572966	2.60527E-05	1.216199129	5.59951E-07
	protein coding	1.64552818	5.45277E-09	3.950307656	0.000171483
	protein coding	0.973694865	4.92466E-06	1.282159526	3.18458E-07
	protein coding	1.991999746	0.020850837	3.00357456	7.74517E-06
	protein coding	0.684391214	0.033179974	0.730351887	0.001939021
	protein coding	0.583554063	9.59103E-05	0.715874818	6.10374E-05
	protein coding	1.831910621	0.017081205	1.959962929	0.014442515
	protein coding	1.918898853	1.57336E-12	1.742228318	1.79661E-07
	protein coding	2.113941967	0.000766459	1.654923487	0.001615618
	protein coding	1.35798148	1.01999E-06	1.07783304	0.002244304
	protein coding	0.618321691	1.70005E-06	0.745708976	6.14719E-06
	protein coding	1.459617244	1.23666E-08	0.780755371	0.00022904
	protein coding	2.069749275	8.68605E-11	1.159712558	4.22319E-08
	protein coding	2.926234335	9.75194E-05	5.061551746	0.031456473
	protein coding	1.138319278	2.51401E-05	0.584487159	0.015643618
	lncRNA	1.10247166	0.000376002	3.814456227	8.66145E-07
	protein coding	0.853501414	1.31149E-09	1.816857617	4.5611E-15
	protein coding	3.878026057	2.17671E-08	3.312800411	1.45357E-06
	protein coding	0.647761891	9.58139E-08	0.647949302	1.40367E-07
	lncRNA	3.298618987	3.54018E-08	0.84392863	0.013915122
	protein coding	0.634283453	0.000172916	1.436843853	2.18403E-09
	protein coding	1.358007426	1.44845E-10	1.051854978	1.88911E-08
	protein coding	3.7039359	2.11051E-12	1.172876877	9.72446E-08
	protein coding	4.085666956	0.000289384	4.355111197	1.19296E-05
	lncRNA	2.327557448	0.000189959	3.081032218	2.22341E-07
	protein coding	1.221626359	4.49764E-06	5.615136885	2.16905E-08
	protein coding	1.099130212	1.09177E-08	1.748319983	1.05865E-07
	protein coding	3.143603527	8.23156E-05	5.770231084	2.24184E-05

[redacted]					
	protein coding	0.901957801	1.66628E-08	0.805016023	1.75109E-07
	protein coding	3.794779982	3.47308E-07	5.35108565	3.54116E-11
	protein coding	1.021598404	4.94836E-07	0.650595669	0.000109623
	protein coding	0.617943049	4.39154E-05	0.864058923	6.73004E-07
	protein coding	0.857271339	2.41401E-05	1.276213664	8.9583E-08
	protein coding	0.678145528	1.03364E-06	0.870967289	2.81279E-08
	protein coding	1.027075683	2.29032E-11	2.222247436	3.02062E-06
	protein coding	0.605978065	0.045444507	0.893503232	0.000259562
	protein coding	1.357769593	6.70516E-10	0.745365502	1.22038E-05
	protein coding	2.108293568	1.23489E-08	2.434658049	2.24196E-06
	protein coding	0.929884414	8.14358E-10	1.022337087	1.24251E-09
	protein coding	0.602380881	2.99102E-08	0.629669398	1.37914E-08
	transcribed processed pseudogene	1.040202639	0.001354608	0.819934226	7.22905E-06
	protein coding	0.591177172	2.16567E-05	1.073753832	4.27803E-09
	protein coding	1.26801665	7.05908E-07	1.136827444	9.68526E-06
	lncRNA	1.281118013	1.21599E-05	0.644540952	0.00216319

Table 2A. AR Fanconi anemia HNSCC overexpressed common genes.

Gene	Coding	logFC VU 1131	adj.P.Val VU 1131	logFC VU 1365	adj.P.Val VU 1365	logFC OHSU 974	adj.P.Val OHSU 974
[redacted]	protein coding	1.406652468	3.34017E-12	0.98661915	7.243E-11	1.131621364	1.16755E-11
	protein coding	0.847874881	0.03349257	1.508086959	1.20301E-05	3.339734569	0.014950903
	protein coding	3.199589284	9.67443E-14	2.707152161	1.18253E-14	1.807649019	8.25178E-12
	protein coding	1.54241061	1.27984E-06	1.154406745	0.004148398	0.753147968	0.018763789
	protein coding	2.11079149	0.000755212	3.018759268	7.4308E-07	2.319470028	1.07504E-10
	protein coding	1.228445619	3.26108E-05	0.743402204	0.011589073	0.614709408	0.005760668
	protein coding	1.423979309	5.32831E-05	4.727823442	2.56066E-09	0.723627758	0.026442905
	protein coding	0.993622059	5.24406E-05	1.036614628	6.34177E-07	1.211674296	0.000453365
	protein coding	0.907423991	0.018742161	0.825304488	0.00262441	1.097656054	0.000232473
	protein coding	1.108737376	1.71794E-12	0.916296162	7.85397E-12	1.119158026	1.85541E-14
	protein coding	1.048133001	0.001496053	1.712662 9	0.002553871	1.171494333	0.034565764
	protein coding	1.264789941	1.62394E-07	2.127376992	1.82938E-11	0.919166911	0.006433011
	protein coding	1.273627001	2.3724E-05	0.771560326	0.000749175	4.647369361	2.88963E-12
	protein coding	2.777041356	0.000714775	2.679826334	0.007285043	5.965787533	8.92644E-09
	protein coding	1.471180353	0.001397348	0.75650689	0.00688016	1.753450914	0.0326364
	protein coding	1.319856542	0.000160397	0.926110722	0.041424089	1.031694216	0.001102526
	protein coding	1.649255503	7.42001E-09	0.700550129	0.000730084	3.758333562	3.55569E-15
	protein coding	1.093738744	0.002937874	0.869892616	0.019955283	1.372511466	0.0369034 2
	protein coding	3.126071518	8.28305E-10	1.753073191	0.009054173	1.790674659	8.0719E-11
	protein coding	1.726856478	9.50564E-09	1.595381546	2.33891E-08	0.855123845	0.000279488
	protein coding	0.821928537	0.00609727	1.345031142	0.000155021	4.575306533	6.67913E-05
	protein coding	1.418920669	0.006168257	1.427732786	5.3351E-10	2.760114145	7.51297E-09
	protein coding	1.864782395	1.06226E-07	1.878207509	5.30646E-09	3.291256566	1.39704E-12
	protein coding	0.624107976	0.000114146	0.609768526	0.000203432	0.619985545	0.000267457
	protein coding	0.652538649	0.000455272	1.338712135	1.6407E-09	2.125457301	4.95194E-09
	protein coding	4.390786983	9.54326E-11	1.009322845	0.044087427	2.337320237	3.42938E-08
	protein coding	0.673288955	0.000230755	3.191009857	0.000369075	1.440495502	0.000464462

[redacted]	protein coding	0.664472036	0.047204491	2.027224201	0.043932675	2.895972575	3.7605E-06
	protein coding	1.004559243	0.012072523	0.678428673	0.022136796	5.049259096	1.71313E-11
	protein coding	1.510048801	1.5308E-06	2.39483556	1.04776E-09	3.955828574	4.99131E-13
	lncRNA	2.59293902	2.60369E-08	0.968406682	5.82276E-05	1.365558569	0.00569681
	lncRNA	0.595673145	0.027015539	2.261530098	3.49525E-10	0.813769996	0.040035932
	lncRNA	2.07465534	0.011103485	0.693597656	0.007331863	0.940783934	0.002702536
	lncRNA	1.718237266	0.018907079	1.428471088	1.8849E-07	4.234628567	6.52176E-08
	lncRNA	1.096254029	0.000419026	1.36477777	0.001411699	4.080665894	8.7374E-07
	lncRNA	0.607214703	0.009737572	1.218445885	0.002647374	5.25489903	4.74486E-08
	protein coding	1.362701589	0.015134591	2.911643842	0.004894076	9.098269375	8.82365E-13
	protein coding	1.21561135	1.58993E-05	3.014500485	5.25708E-12	1.371719483	3.28419E-08
	protein coding	0.633974481	0.00772955	1.305892321	1.56893E-05	0.813127583	3.45552E-05
	protein coding	2.74100536	1.12115E-09	3.179382666	1.70379E-14	2.312000171	2.44209E-12
	protein coding	0.946231606	1.70545E-09	0.654320079	4.72983E-07	1.583475142	3.6076E-14
	process. pseudo.	1.211330272	0.013262056	1.465200823	0.00165832	2.956158571	0.001298068
	protein coding	1.137012846	0.002455529	2.183820337	5.31911E-07	1.79805895	2.95321E-10
	protein coding	1.188138496	4.25383E-07	0.587883505	0.002177728	7.074264669	2.44317E-17
	lncRNA	2.013284252	0.004692337	3.692760865	1.78402E-05	0.726119405	0.024502606
	protein coding	1.437340659	0.000994881	5.238458084	3.07007E-11	1.074194554	0.01702767
	protein coding	0.971781299	7.88012E-05	0.875690521	6.81856E-07	1.135974763	0.004911974
	protein coding	1.667133129	2.1316E-07	2.390397747	1.92357E-10	1.877465389	3.27503E-06
	protein coding	0.980870509	0.006484797	1.390678117	8.35092E-10	1.207032345	0.004616358
	protein coding	2.419697872	0.022574224	10.7361234	3.58973E-12	4.038074396	8.12908E-13
	protein coding	2.546080639	5.9873E-11	0.95480259	0.000149717	1.54888591	1.58844E-07
	protein coding	1.477864206	0.001098831	2.232284483	4.97498E-07	1.114121329	2.23715E-05
	protein coding	1.459509003	2.5141E-07	1.561470373	1.36141E-09	0.903002447	1.58991E-07
	protein coding	0.669225818	0.00409618	1.142497515	0.033393045	1.230794076	0.000588813
	protein coding	1.042552429	1.25198E-05	1.712004572	2.89861E-06	2.191761897	3.05871E-08
	protein coding	0.781156795	0.011025875	2.674373894	0.019652727	2.35373214	4.96204E-10

[redacted]	protein coding	0.948321472	0.005552469	2.718650397	0.000971364	1.699423989	0.028958748
	protein coding	0.7914721	0.018657775	2.170569175	4.42282E-10	1.736848834	1.39543E-09
	protein coding	1.791705418	4.07842E-07	1.022838612	0.002513634	1.076838332	5.43441E-07
	protein coding	1.845909613	2.25391E-08	2.682085958	7.17079E-05	1.367159475	0.01008566
	protein coding	1.897216865	0.000173745	3.092150948	0.004786815	5.363577496	1.78194E-07
	protein coding	0.907751687	8.03715E-08	0.937443055	2.24544E-06	4.011234847	1.58653E-06
	protein coding	0.868736952	0.042619161	1.100928489	0.003131 39	0.728611142	0.005079444
	protein coding	1.425168217	2.85439E-05	0.980764855	1.35476E-06	1.804644459	1.4128E-07
	protein coding	1.178867455	9.30029E-06	1.223655018	0.000123712	6.265324044	6.47137E-20
	protein coding	1.651535195	0.013371031	1.661594129	0.013340949	2.681580612	3.34042E-09
	protein coding	2.087715099	0.003028112	0.968314291	6.62116E-05	3.533726178	0.001892354
	protein coding	2.076523343	2.69514E-07	1.179110497	5.58497E-11	0.699230306	8.60394E-06
	protein coding	1.51375174	1.05923E-06	1.369574923	2.45023E-07	0.932419618	0.000321224
	protein coding	0.934446066	8.36209E-09	0.867545514	1.19117E-08	1.329235086	1.376E-09
	protein coding	1.392963432	0.009212052	1.095921774	0.041878918	2.048780956	5.40111E-08
	protein coding	1.761751246	4.23305E-05	4.172739929	4.20298E-07	1.227834545	0.023055132
	protein coding	1.512060263	1.53274E-08	0.769876419	0.000158595	0.895715115	3.18787E-05
	protein coding	0.706925987	0.012326317	0.712386873	0.004264758	0.831478299	0.001156823
	protein coding	0.802332046	0.000910072	0.855045097	0.000928743	0.62832559	0.005773199
	protein coding	0.985059029	0.015696116	3.476068395	1.59513E-07	2.133803268	0.000165659
	protein coding	0.79414466	8.34372E-05	0.685401116	0.000146019	0.624384899	0.001279044
	protein coding	1.577115689	0.000401756	1.215923804	0.008390898	0.771638507	0.002628155
	protein coding	1.15011301	0.004723299	0.658038434	0.033194806	0.967670195	0.000310377
	protein coding	1.15319487	1.32436E-08	0.765203337	4.50535E-06	1.316526185	9.69692E-10
	protein coding	0.819202826	2.01939E-06	1.496414682	1.21999E-11	1.536086753	1.04001E-10
	lncRNA	0.855954469	0.001191257	0.729095254	7.85952E-05	1.344356502	2.15108E-09
	protein coding	0.66735015	0.027225139	1.760659934	2.36091E-05	1.204215361	0.048680257
	protein coding	0.833419767	1.03111E-05	2.050293287	6.83605E-15	0.732783511	0.028720258
	protein coding	1.919487366	4.41693E-12	3.891512658	7.1379E-08	3.036399913	2.37908E-17
	protein coding	1.064052463	0.016896649	2.042336793	0.000414455	1.273008688	0.001225586

[redacted]	protein coding	0.804587329	0.000291078	1.20812831	1.49588E-06	0.589605852	0.006347103
	protein coding	0.598380732	0.029029405	2.160072564	0.048284877	1.25818578	2.45866E-08
	protein coding	2.548647272	1.97481E-09	0.706923917	0.008545761	2.598598498	3.33028E-05

Table 3A. AR sporadic and Fanconi anemia HNSCC overexpressed common genes.

Gene	logFC VU 1131	adj. P.Val VU 1131	logFC VU 1365	adj. P.Val VU 1365	logFC OHSU 974	adj. P.Val OHSU 974	logFC CAL 27	adj. P.Val CAL 27	logFC CAL 33	adj. P.Val CAL 33
[redacted]	2.11079149	0.000755521	3.018759275	7.43E-07	2.31947003	1.08E-10	1.98238705	5.02E-07	2.88466164	1.76E-07
	1.8647824	1.06E-07	1.87820751	5.31E-09	3.29125657	1.40E-12	1.94335064	1.47E-08	3.15202868	1.69E-10
	0.65253865	0.000045527	1.33871214	1.64E-09	2.1254573	4.95E-09	1.81969508	1.22E-11	1.68615616	3.83E-07
	0.66447204	0.04720449	2.0272242	0.04393268	2.89597258	3.76E-06	2.59376682	1.61E-08	2.03482617	2.89E-05
	0.94623161	1.71E-09	0.65432008	4.73E-07	1.58347514	3.61E-14	0.78969501	1.33E-08	1.8041942	4.30E-15
	2.54608064	5.99E-11	0.95480259	0.00014972	1.54888591	1.59E-07	1.28340449	2.17E-06	1.75182736	3.50E-08
	1.51206026	1.53E-08	0.76987642	0.0001586	0.89571512	3.19E-05	1.06856718	6.75E-06	1.21753345	9.76E-07
	2.54864727	1.97E-09	0.70692392	0.00854576	2.5985985	3.33E-05	3.79477998	3.47E-07	5.35108565	3.54E-11

But in the end, it's only a passing thing, this shadow.

Even darkness must pass.

A new day will come.

And when the sun shines, it'll shine out the clearer.

Samwise Gamgee